Non-perturbative and finite N corrections on matrix holography

Dissertation

zur Erlangung des Doktorgrades
der Naturwissenschaften (Dr. rer. nat.)
der Fakultät für Physik
der Universität Regensburg

vorgelegt von

Efstratios Pateloudis

aus Griechenland

im Jahr 2022

Promotionsgesuch eingereicht am: 11. Mai 2022

Die Arbeit wurde angeleitet von: Dr. Norbert Bodendorfer

To my family

Ιθάκη

Σὰ βγεῖς στὸν πηγαιμὸ γιὰ τὴν Ἰθάκη,
νὰ εὔχεσαι νά ῾ναι μακρὺς ὁ δρόμος,
γεμάτος περιπέτειες, γεμάτος γνώσεις....

...῾Η Ἰθάκη σ᾽ ἔδωσε τ᾽ ὡραῖο ταξίδι.
Χωρὶς αὐτὴν δὲν θά ῾βγαινες στὸν δρόμο.
Ἄλλα δὲν ἔχει νὰ σὲ δώσει πιά.

Κι ἂν πτωχικὴ τὴν βρεῖς, ἡ Ἰθάκη δὲν σὲ γέλασε.
Ἔτσι σοφὸς ποὺ ἔγινες, μὲ τόση πεῖρα,
ἤδη θὰ τὸ κατάλαβες οἱ Ἰθάκες τὶ σημαίνουν.

Κωνσταντίνος Καβάφης

Ithaka

Once you set out for Ithaka
hope your road to be long,
full of adventures, full of knowledge...

...Ithaka gave you the beautiful journey.
Without her you wouldn't have set out
there's nothing else to give you anymore.

And if you find her poor, Ithaka hasn't fooled you.
Now that you became wise with so much experience,
you should have already understood what Ithakas mean.

Constantine P. Cavafy

Author declaration and publications

The work done during the PhD period is based on some published and unpublished work while cooperation with collaborators is indicated below. In particular, some of the contents of the dissertation are and will be presented in https://arXiv.org.

Specifically, the author declares that:

(1) The work presented in this dissertation has been done without the impermissible help of third parties, without the use of resources other than those indicated. Data and concepts stemming directly or indirectly from other sources are indicated with citations to the literature.

(2) No further persons were involved with the creation of the contents of the dissertation presented. In particular, the author has *not* made use of the assistance of a doctoral consultant or other person in return for payment. No-one has received payment in kind either directly or indirectly for work which is associated with the content of the dissertation submitted.

(3) The dissertation has not been submitted in the same or similar form to another examining authority, neither in Germany nor abroad.

This thesis is based on:

[1] G. Bergner, N. Bodendorfer, M. Hanada, S. Pateloudis, E. Rinaldi, A. Schäfer, P. Vranas, H. Watanabe, "*Confinement/deconfinement transition in the D0-brane matrix model – A signature of M-theory?*", *JHEP* **2021** arXiv:hep-th/2110.01312.

[2] S. Pateloudis, G. Bergner, N. Bodendorfer, M. Hanada, E. Rinaldi, A. Schäfer, "*Nonperturbative test of the Maldacena-Milekhin conjecture for the BMN matrix model*", **2022** arXiv:hep-th/2205.06098.

[3] G. Bergner, N. Bodendorfer, M. Hanada, S. Pateloudis, E. Rinaldi, A. Schäfer, "*Testing the gauge/gravity duality at low temperatures using the BMN matrix model*", *to appear* **2022**

Other projects during the PhD period:

[1] F. M. Mele, J. Münch, S. Pateloudis "*Quantum Corrected Polymer Black Hole Thermodynamics: Mass Relations and Logarithmic Entropy Correction*", *JCAP* **2021** arXiv:gr-qc/2102.04788.

Stratos Pateloudis

How to read this thesis

Even though it is not usual, it would not be so illogical to provide guidance to the reader regarding the tools one needs to follow the topic. Most of this thesis is devoted to string theory matrix models, and therefore, to understand the logic, analysis, and results in their core, one should have some pre-existing exposure to string theory.

To be self-consistent, the thesis is organised into six parts, beginning from the very basics. The first part contains the main stimuli and a general introduction to the topic of the dissertation, and where it might be helpful and applicable. This is indeed one of the parts that most readers should go through carefully. Part two is an elementary introduction to, both conceptual and concrete, string theory and matrix models. This information contains the foundations one needs to follow the thesis. Readers familiar with both topics could skip directly to part three at first read.

The third part contains all new results and developments from the Monte Carlo simulations performed in a supercomputer starting with some basic introduction also. This is one of the genuine parts of the topic and experts could directly start with this. At the end of each section of this part, we include also a small table addressing the most important points, in the view of the author, of each work and the scientific contribution in the high-energy and gravity communities. The fourth part, on the other hand, is as genuine as it is abstract. It examines a non-established connection, if it exists by any means, between matrix models emanating from string theory and specific coarse-grained spin networks from loop quantum gravity. Readers not familiar with ideas of loop quantum gravity could skip it at first read.

Part five contains the synopsis of the dissertation and how its contents might benefit the scientific community. It also contains some future directions that could potentially be investigated using the results presented here. In the final part, we supplement the reader with miscellaneous results concerning some important points that have been used in the main body of the thesis.

We hope the reader finds the exposure to the above topics as enjoyable as the author found their embedding and construction into this thesis.

List of abbreviations and symbols

Here we provide a list with some abbreviations and symbols that will play an important role.

BFSS	The D0-brane model suggested by Banks, Fishcler, Susskind, Shenker
BMN	The massive deformation of BFSS proposed by Berestein, Maldacena, Nastase
w.r.t	With respect to
LHS	Left hand side
RHS	Right hand side
QFT	Quantum field theory
CFT	Conformal field theory
N	The degrees of freedom, number of D0-branes, and the size of the matrix
S	The lattice spacing
T	Temperature (dimensionfull)
μ	The mass of BMN model
λ	The 't Hooft coupling
H	The Hamiltonian
$\mathcal{H}$	The Hilbert space
ℓ_s	The string length
ℓ_P	The Planck length
α'	ℓ_s^2
$\mathbf{g}_s$	The string coupling
$\mathbf{g}_{YM}$	The Yang-Mills coupling
UV	Ultraviolet
IR	Infrared

Contents

Part I

Prolegomena

1

Introduction and motivation

Αρχή σοφίας της αγνοίας η γνώσις

Socrates

The unification of all forces of nature has haunted theoretical physicists since the birth of the celebrated standard model which unifies electrodynamics, the weak and strong interactions of the nuclei of fundamental particles. Even though this unified theory describes particle physics very well, it certainly cannot describe gravitational systems. Even before that, Einstein, the father of the current gravitational theory, spent a big part of his life trying to unify all physics. The same theory instructs us that one should not consider gravity as a force, since Einstein's equation makes clear that one can think of matter entirely as a geometrical entity. In a very precise way, gravity is equivalent to geometry in this theory and it does not seem to combine very well with the above particle theories. The underlying characteristic of the so-called standard model unifying the forces above is their quantum nature. This is not so unexpected, since the (known) particles contained in nature are different modes of the fields which subject to quantum mechanical laws in their fundamental nature. Therefore, if someone insists on the unification idea one should better describe gravity as a quantum theory, namely a theory of quantum gravity.

Interestingly, the quantum nature of gravity is treated on equal footing by communities that do not believe in a unified theory, but rather try to understand in a mathematically rigorous way quantum aspects of gravity in Planck scales. At these scales where, speaking in geometrical terms, the curvature is very large, we expect that the gravitational theory will be dominated by quantum effects. This indeed instructs us to treat spacetime as a quantum geometry at these scales, leading to a physical marriage of the two pillars of nature. Independent of the approach, the study of the behaviour of gravity in micro scales as well as its interaction with other theories which contain matter is one of the most interesting problems in the branch of theoretical physics.

Quantum gravity has one very important characteristic that makes it unique, it has to

be non-local. This is in stark contrast to what most physicists are used to because the most successful theory that describes nature at the quantum level is the quantum field theory (QFT) which is certainly local. However, taking a skeptical point of view, it is not entirely clear whether the latter theory is a fundamental aspect of nature or just an analytic tool that is carefully constructed to describe nature. Nevertheless, tool or not, the important point is that indeed one can perform analytic calculations in a local theory and compare with the experimental data with an outstanding accuracy [1].

On the other hand, for a theory of quantum gravity, we do not have concrete experiments, at least not in the usual sense. Instead, we have every theoretical physicist's favourite experiment, the so-called Gedanken (thought) experiments. Such an experiment reveals the non-local nature of a theory of quantum gravity when one takes into account the holographic principle [2, 3]. Before performing this Gedankenexperiment, let us point out that after the work of Hawking [4, 5] a temperature was assigned to the event horizon of the black hole and later the four laws for black hole mechanics were constructed [6] per the four laws of thermodynamics. Having a temperature, the black hole should also have energy as well as entropy. The interpretation of the entropy as information initially appeared even before the work of Hawking in [7], where Bekenstein conjectured a natural bound which claims that a black hole stores information according to one bit per Planck area patch (ℓ_P^2) on the black hole event horizon. This is the minimal, physically allowed bound mainly for two reasons: first of all, we do not have length scales smaller than Planks' length, and secondly, we do not know what is happening inside the event horizon. Since the inside of a black hole cannot communicate with the region outside, a compromise has to be made in order to access the information of a black hole. The compromise is to put all the black hole information on the surface of the horizon respecting Bekenstein's bound in such a way that an outside observer could potentially access it. In other words, if someone would throw this thesis into the black hole then the information contained in this thesis would probably remain on the black hole event horizon but it would be inaccessible for an external observer since one would see that the information contained in the thesis would be lost because the "information" emitted from the black hole as radiation would depend only on the mass, the angular momentum and the charge of the black hole due to the no-hair theorem. Let us pause this discussion here because it leads to the black hole information paradox and will just make the situation more complicated. At the same time, the event horizon has the right characteristics to store information (as entropy) since every time we throw something into the black hole, its horizon increases [8]. The entropy of the black hole scales as

$$S_{BH} = \frac{k_B A}{4\ell_P^2}, \quad \ell_P = \sqrt{\frac{G\hbar}{c^3}}. \tag{1.1}$$

In theoretical physics, it is quite common to put all constants, such as the speed of light (c), the gravitational constant (G), $\hbar$, and the Boltzmann constant (k_B) to unity. A is the area of the black hole horizon, which indicates that the information we can store in a black hole, scales like the area in accordance with Bekenstein's bound.

Let us now switch to a QFT description in flat spacetime and perform the Gedankenexperiment. Let us consider an imaginary cube that encloses a region of space and let us suppose that we want to store information in this region. To this end, we may discretise the cube in a three-dimensional lattice using minimal discretization length, namely the Planck length, and consider N cites where we can place one degree of freedom per site by Bekenstein's bound.

Then, it should be clear that the information we can put into this three-dimensional cube, expressed as the entropy, should scale as

$$S_{\text{cube}} \sim \frac{N^3}{\ell_P^3}, \tag{1.2}$$

or, in other words, should scale like the volume of this cube V. Therefore, we see that a local QFT theory predicts storage information scaling like the volume, while a gravitational theory considers a scaling of the entropy like the horizon area surface. Note that at constant time slices, both the black hole and the cube are indeed three-dimensional objects. Hence, a quantum theory of gravity should have a non-local profile.

Every approach to quantum gravity tries to reproduce this interesting black hole behaviour from a statistical point of view. Recalling that thermodynamics is actually the large number of degrees of freedom of a statistical system, one can revert the logic and try to find what the microstates of the black hole are [9–44].

This interesting behaviour led to the proposal of the so-called holographic principle [2] where a lower-dimensional surface (actually a co-dimension 2 surface such as the black hole horizon) stores information for higher-dimensional objects. Let us not forget, after all, that in a four-dimensional spacetime the black hole remains to be three-dimensional (at constant time slices) and hence the information for this three-dimensional black hole is entirely given by a two-dimensional surface, its horizon. The actual term, holography, emanates from the more familiar situation of real-world holograms.

The first concrete example of such holography is proposed in [45] in the context of string theory, where a d-dimensional gauge theory is conjectured to be equivalent to a $(d+1)$-gravitational theory. Both the field theory and the gravity theory in this example were specific, but later this was generalised to the celebrated gauge/gravity duality [46–50].

One of the most important ingredients of the duality is a large number of degrees of freedom N since in this case, the gravity theory becomes classical, in particular a supergravity theory. Another valuable ingredient is the kind of Dp-branes that appear. These, after the second superstring revolution, became genuine contents of a superstring theory and are objects extending in p spatial dimensions of the superstring's ten-dimensional spacetime. They are dynamical, non-perturbative objects in their nature and host the endpoints of the string [51, 52].

The original example of such a duality [45] considers $p = 3$. At this specific value, the gauge theory defined on the worldvolume of N coincident D3-branes becomes a four-dimensional conformal field theory (CFT_4) since the 't Hooft coupling becomes dimensionless. On the other side, the gravitational theory lives in a hyperbolic, five-dimensional spacetime and has negative curvature, namely, it is a five-dimensional anti-de-Sitter spacetime (AdS_5).

This dissertation, considers exclusively the case $p = 0$ that corresponds to zero-dimensional D-branes whose dynamics create a worldline. In this particular case, there is *not* a CFT_1, since the 't Hooft coupling becomes dimensionful. Instead, we have a one-dimensional quantum mechanical matrix model having a $U(N)$ gauge symmetry. The rank of this group gives the number of degrees of freedom which is also the size of the matrices appearing in the matrix model. Hence it is not necessary to look for an AdS_2 spacetime. On the other hand, the gravitational dual of this one-dimensional quantum mechanical matrix model is a black zero-brane geometry. This geometry lives in the ten-dimensional spacetime of the type IIA supergravity and, in addition, is asymptotically flat. The number of D0-branes

gives the degrees of freedom in the gravitational theory such that N has a dual description. Interestingly, a one-dimensional matrix model living on a worldline is the gauge dual of a ten-dimensional gravitational theory in the large N limit. This unconventional holography defines the matrix holography, or more rarely the worldline holography for such one-dimensional quantum mechanical systems.

The authors of [53] pushed the duality a step forward and they claimed that this one-dimensional matrix model can describe the contents of M-theory! This might not be so surprising if one already knows that the latter theory is the underlying theory that connects all five superstring theories [54]. However, this connection is a bit more subtle than the conventional holography. Specifically, as we will see the type IIA superstring theory (and supergravity) is defined as M-theory compactified on a spatial dimension. The idea of [53] was to perform a boost along this spatial circle and uplift the ten-dimensional contents on the eleven-dimensional spacetime where M-theory lives. This boosting procedure corresponds essentially to the large N limit of the theory as we shall see when we will discuss precisely this problem. At the same time, this procedure is still subtle because having a black hole in eleven dimensions and boosting along one spatial dimension raises the question of what happens to the black hole under the boost. If Lorentz contracts, such as normal objects do, this would lead to a violation of the second law of thermodynamics because its horizon would contract and be assigned to entropy then the entropy would decrease! Fortunately, black holes do not Lorentz contract under a boost. On the other hand, examining the boost carefully, one is led to the interesting question of what happens to the Bekenstein bound if the boosting procedure corresponds to the large N limit. The degrees of freedom increase but the black hole cannot accommodate them without violating Bekenstein's bound. This leads to the notion of strong holography which in the case of matrix models states that black holes should expand under a boost [37].

The matrix character of the one dimensional model makes analytic gauge theory calculations intractable. On the other hand, one can employ numerical results in the gauge theory and compare with the gravitational calculations which in the large N limit are tractable. Keeping $\lambda = g_{YM}^2 N$ finite, the large N limit corresponds to a classical gravitational theory, namely a supergravity because this limit corresponds also to the planar limit of superstring theory (surfaces of genus zero). Quantum corrections, or effects characterizing a theory of quantum gravity, are considered for finite N. That is because $1/N^a$ corrections correspond to g_s^a expansions which are corrections in a-loops of a supergravity theory. In matrix models, this situation is depicted from keeping finite the size of the matrices. At the same time, finite N calculations for supergravity corrections become intractable so one always has to make a compromise between them.

The best possible compromise at this current level is to use simulations for the matrix model while taking the large N limit and comparing it with supergravity. In this way, the gauge/gravity duality could be put in more precise and concrete tests and potentially be verified or falsified. The non-perturbative nature of D-branes allows also for a non-perturbative cross check for the already developed perturbative intuition for the gauge/gravity duality. Upon careful treatment, one can exploit this powerful tool and examine various interesting phenomena, both in the gauge theory and the gravity side such as the confinement/deconfinement transition, black hole physics, Hawking radiation, topology changes, and the behaviour of the systems in specific parameter limits.

In particular, in the forthcoming chapters, we shall see that these matrix models can be used beyond the scope of string theory. Indeed, they can be generalised to a spacetime having an arbitrary dimensionality and describe (gauge) theories consisting of partons. Whether these gauge theories have a gravitational dual is not known, but we examine an interesting comparison at first level. Leaving the arbitrary spacetime dimensionality and moving to the ten-dimensional setting, we study a more concrete gauge/gravity example. In particular, a one-dimensional matrix model is dual to ten-dimensional supergravity. In this particular project, we show that the large N limit of the matrix model indeed follows the predicted gravity behaviour, while finite N corrections corresponding to quantum effects show a small discrepancy. One of the most exciting characteristics of this project is the fact that a parameter region not accessible in the past was examined using the D0-matrix models upon careful treatment. Specifically, we studied a theory considered to be out of reach until now with the current resources available. In other words, we have promising indications that we just entered the M-theory region by an interesting topology change of the gravitational system.

Another interesting direction was to push this duality in a parameter region where the temperatures are small. Even though this project is currently under examination and construction we have strong hints that the supergravity results are reproduced by matrix model numerics while a precision test requires more resources. The significance of this project is that going to smaller temperatures, α' corrections of string theory become negligible because the gravity theory is dominated by classical non-stringy supergravity and analytic results are available. At the same parameter region, we can study better the above transition between string theory and M-theory.

In the same parameter region, we can test equally appealing phenomena. In particular, the gauge constraint responsible for the gauge/gravity correspondence is examined according to a recent conjecture which states that it is not that important for the duality at low temperatures. We tested this for our matrix models and indeed we can verify that the partition functions of the gauged and ungauged models are exponentially close to each other at small temperatures. Apart from the genuine physical motivation, one further interest goes to the development of the quantum computer, where physical models which do not have a gauge symmetry are easier to realise and thus simulate.

A last and equally interesting topic discussed is a possible connection between matrix models with a different branch of quantum gravity physics emanating from loop quantum gravity. The underlying structure appearing in these two models is the fuzzy sphere. The latter is related to polyhedra in the language of coarse-grained spin networks of loop quantum gravity. Based on work built in this direction we discuss possible uses of matrix models to relate and eventually study those specific spin networks by using matrix models from string theory.

The non-perturbative, matrix character of these models allows a deep, not accesible in the past, examination of physical systems where all the relevant information is contained in these $N \times N$ matrices. In the large N limit we probe classical physics which is the analogue of the thermodynamic limit, while, on the other hand, finite N corrections correspond to the quantum character of the system. In this dissertation, we use these D0-matrix models to describe different physical systems, and via the gauge/gravity correspondence we study classical and quantum gravity.

Part II

Introduction to string theory and matrix models

2

String theory

Ετεή δε ουδέν ίδμεν. Εν βυθώ γαρ η αλήθεια

Democritus

This chapter is aiming for a brief introduction to string theory [55–62]. Being such a vast topic, string theory cannot be deeply understood by any brief introduction, instead, we are going to provide as much intuition and details, as we think, are sufficient to follow the explanations and the importance of the main ideas we are going to present later on. As an introduction, it cannot be considered by any means a complete description of the topic and we advise the interested reader to consult the standard references above. We shall begin very elementarily, keeping the fundamental ideas at the core of the discussion, and gradually change gears towards the ingredients that are important for the contents of this thesis. But before presenting the materials let us comment on some important historical remarks.

Let us begin by stating that even though string theory today is believed to be also a theory of quantum gravity, the original idea had nothing to do with gravity. However, we shall see how gravity appears from string theory. It was in quantum chromodynamics where firstly, the usage of a string described strong interactions between quarks. The Veneziano amplitude (describing the S-matrix) of strong interactions between fundamental particles, was given a physical interpretation. The nuclear forces between them could be described as one-dimensional strings! Later this concept, leaving the dimensionality of spacetime abstract, was formulated in a different context and created string theory.

One peculiar thing about string theory is the need for extra dimensions. This is what makes it so popular, so exciting and so controversial at the same time. But, in physics, we know that we should not add extra structure if it is not needed. After general relativity, the dimensions of spacetime were always considered to be four. However, as we will see later, mathematical consistency required from Lorentz invariant of the theory forces extra dimensions in our theory. In particular, demanding invariance under the Lorentz group of

the earliest bosonic string theory made the spacetime have 26 dimensions, while the later fermionic supersymmetric string theory lowered them down to 10 spacetime dimensions.

It was only when the discovery of a mode of the string spectrum that was named the graviton came into the game and made things even more fascinating. The graviton is expected to be massless because the gravitational force has a very long range, and appears to propagate at the speed of light. In addition, it must be a spin-2 boson because the source of gravitation is the stress–energy tensor, a second-order tensor. Additionally, it can be shown that any massless spin-2 field would give rise to a force indistinguishable from gravitation, because a massless spin-2 field would couple to the stress–energy tensor in the same way that gravitational interactions do, so if a massless spin-2 boson particle is to be discovered it has to be a graviton [55, 61]. People started believing that string theory could unify all the fundamental interactions since gravity[1] also appeared quite naturally. After that, many researchers started working on string theory leading to several discoveries.

The first superstring revolution, began in 1984 when this scientific community realized that string theory could describe all elementary particles and interactions between each other. Intense research leads to five different string theories one year later: type I, two types II (IIA and IIB), and two heterotic ($SO(32)$ and $E_8 \times E_8$). The second superstring revolution consisted of one extra dimension and some interesting objects appearing in the theories. In particular, after the work of [54] the community realised that the above types of string theories could be imagined as different limits of one more fundamental theory living in eleven dimensions though! This new theory comes with a new name and some new objects. It was baptised as M-theory, with M being undetermined while the most worthy meaning was *M for mysterious* because we do not know (up to now) what exactly this theory is. We would like to motivate, later on, that the name changed *M for matrix* as we will see in Sec. 3.2.1 and Sec. 4.3. Moreover, the second revolution introduces some new objects, called D-branes [63,64] where the endpoints of the (open) string can live. These objects were obtained as solutions to the low energy limit of ten-dimensional supergravity and they seem to provide a non-perturbative study of string theory [65]. However, there is no complete understanding of what they are and how to think about them. Let us also notice that M-theory is not a string theory since it does not contain strings, but the fundamental objects are the supergraviton, the membrane, and the five-brane. For a more precise analysis we shall refer to Sec. 2.7.

2.1 Conceptual analysis

2.1.1 World-volume and spacetime descriptions

Let us consider a spatially extended classical and p-dimensional object (relativistic or not) - a p-brane which propagates in a spacetime $\mathcal{M}$ with coordinates $x^\mu = (t, x^i)$. Such an object however is not rigid but it can change by bending, wiggling such that it has it's own dynamics.

A p-brane can be fundamental or not. There are two aspects in which a brane can be fundamental or not:

- the brane is an assembly of lower-dimensional branes bound together by some force

[1] Here by gravity we mean the hypothetical carrier of the gravity force, the graviton, and we shall give a more precise meaning later on.

- the fact that it appears to be p-dimensional can be an approximation by forgetting about some dimensions if those are not observable (In the same spirit, a two-dimensional brane on a flatland could be a projection of a three-dimensional object of a three-dimensional world. Thus, species living in the flatland and being able to only observe two-dimensions would never detect the extra dimension and the true nature of the three-dimensional brane)

On the other hand, a fundamental object cannot be decomposed in terms of lower-dimensional elements nor can any structure be found in it. However, a brane can split into several other objects. Moreover, fundamental objects of the same type are indistinguishable (at the quantum level) by definition: they can be in different quantum states but their nature is identical. This can be summarised as:

Some ontological aspects

The string and the particle are different in their existential aspects. A fundamental particle is ontologically one and cannot be divided: it can decay in several other particles but the latter cannot be seen as being part of the first one. Simply imagine decays of particles. This is because for an observer there is a clear notion of a particle, defined as the intersection between its equal-time surfaces and the worldline of the particle. This is not the case for the string: any set of strings that have interacted together do not have an independent existence, and only the full world-sheet has an ontological property.
This is related to the non-locality of the string interactions, implying that the two observers cannot agree on the question "when does the string cease to exist?" A more intuitive picture is that a string can be cut into pieces, and these pieces do not acquire some new property making them "different" than the initial one. Nonetheless one cannot say that the original string is made out of pieces with some glue tying them together since it can be separated at any point (due to the non-locality), and the above reasoning would imply that the string is not fundamental.

For example, one can imagine that a 0-brane is a point, and thus any particle falls in this category. A 1-brane is all kinds of strings, a 2-brane is any kind of surface, etc. A violin string is not fundamental because it is made out of many atoms which are made out of fundamental particles (0-branes). This is (one) of the differences between a string of string theory and a string of a string theory.

2.1.2 Dynamical classical variables

The history of a p-brane[2] is called the world-volume $\mathcal{W}$ and it is parameterized in terms of coordinates $\sigma^a (a = 0, \cdots, p)$. The dynamics can be described in two different fashions, depending on the variables chosen and the way they relate the object to the spacetime:

- Worldvolume (or σ-model) approach: the spacetime position of the object $X^\mu(\sigma^a)$ given as functions of the worldvolume coordinates are the dynamical variables. They

[2]History requires a time of course, and here we mean the time evolution of the p-brane and its spatial locations.

are mapped describing the embedding of the p-brane worldvolume in spacetime (they can be viewed as a field *on* the worldvolume)

- Spacetime (or field) approach: the object position is encoded in a field $\Psi[X^\mu(\text{shape})]$ which is a function(al) of the object spacetime coordinates (giving a p-dimensional shape). The simplest instance being the density field.

At the conceptual level, both descriptions are *fully* equivalent, but they differ as computational tools since some calculations (if at all possible) are simpler in one of them. Of course, there are advantages and disadvantages that we will address later on. This means that we will briefly review both of them.

Other descriptions do not rely at all on a Lagrangian such as the conformal bootstrap and scattering amplitude programs. However, we will not review these here

The goal of an action is to describe the dynamics of a system by making extremal one of its properties. Given a geometric object, it is natural to consider its shape, hence the simplest action for a brane is the worldvolume

$$S = -T \int_{\mathcal{W}} \mathrm{d}Vol, \tag{2.1}$$

where T is the tension of the brane and gives the correct units to the RHS and $\mathcal{W}$ is the worldvolume. Then, introducing the embedding maps $X^\mu(\sigma)$, one can rewrite the above action as

$$S = -T \int \mathrm{d}^{p+1}\sigma \sqrt{-\det h}, \tag{2.2}$$

where h is the induced metric on the brane

$$h_{ab} = \eta_{\mu\nu} \frac{\partial X^\mu}{\partial \sigma^a} \frac{\partial X^\nu}{\partial \sigma^b}, \tag{2.3}$$

from the spacetime Minkowski metric $\eta_{\mu\nu}$ with signature $(-1, 1, \cdots, 1)$. Introducing an independent metric $g_{ab}(\sigma)$ on the worldvolume, one can rewrite the above action as

$$S = -\frac{T}{2} \int \mathrm{d}^{p+1}\sigma \sqrt{-\det g} \eta_{\mu\nu} g^{ab} \partial_a X^\mu \partial_b X^\nu + \frac{p-1}{2} T \int \mathrm{d}^{p+1}\sigma \sqrt{-\det g}, \tag{2.4}$$

where the classical equations of motion yield a proportionality between g_{ab} and h_{ab}

The above action is problematic for $p > 1$ because it describes too many degrees of freedom. The worldvolume itself should not have intrinsic dynamics, which corresponds to g_{ab} having no degrees of freedom. To get rid of them, one can only impose diffeomorphisms and possibly Weyl invariance (local rescalings of the metric). This gives in total $p + 2$ constraints for an object which has $\frac{(p+2)(p+1)}{2}$ degrees of freedom. The worldvolume metric can be fixed only for $p = 0$ (with diffeomorphisms) and $p = 1$ (with diffeomorphisms and Weyl invariance). That the string $p = 1$ has Weyl invariance it is a special case since for a generic p-brane we have

$$\sqrt{-h} h^{ab} \to \Omega^{\frac{p-1}{2}} \sqrt{-h} h^{ab}. \tag{2.5}$$

In the worldvolume description, nothing should depend on the parameterization of the surface: the worldvolume coordinates σ^a are merely internal labels that indicate how to read off the corresponding spacetime position from the dynamical variable (the same applies to the maps $X^\mu(\sigma^a)$ or the metric $g_{ab}(\sigma)$ which are just tools to describe a physical object). This leads to the existence of a gauge symmetry that can be fixed, for example by equating some of the parameters with some spacetime coordinates. In particular, it is natural to set the proper-time $\tau \equiv \sigma^0$ equal to the time $\tau = t$ when there is a foliation of the spacetime in spatial slices. We also note that the gauge symmetry for a relativistic system leads to constraints among the canonical momenta, which in turn implies that the (worldvolume) energy-momentum tensor vanishes, including the Hamiltonian

$$H_{\mathcal{W}} = 0. \tag{2.6}$$

These constraints are equivalent to the on-shell condition for the brane: as a consequence, the tools available in QFT (renormalization, analyticity, etc) which rely on an off-shell formulation and which ensure the consistency of the theory (gauge invariance, divergences, unitarity, causality) are not available in the worldsheet formulation.

The spacetime action is found by introducing some fields given by the functional $\Psi[X^\mu(\text{shape})]$[3] and the free action is quadratic in the fields

$$S = \int \mathrm{d}X^\mu(\text{shape})\Psi K\Psi, \tag{2.7}$$

with K being an adapted kinetic operator. For the example of a particle, one has $K = \partial^2 + m^2$.

2.1.3 Some quantum aspects

Depending on the framework one is working on, the canonical quantization, which replaces the dynamical variables by operators, leads to different descriptions:

- First-quantization (worldvolume): the spacetime positions of each object become operators $\hat{X}^\mu(\sigma)$ (in the Schrödinger picture). The evolution is given in terms of a (one-brane) wave-function $\psi_p[X^\mu(\sigma), \tau]$ satisfying the Schrödinger equation with time τ and p denoting collectively eigenvalues. Multi-brane states are found by solving the Schrödinger equation for the (anti-)symmetrized tensor product of one-brane wave functions.

- Second-quantization (spacetime): the field is promoted to an operator $\hat{\Psi}[X^\mu(\text{shape})]$ which can be decomposed in terms of annihilation and creation operators $\hat{a}_p$ and $\hat{a}_p^\dagger$ with first-quantized wave functions as coefficients

$$\hat{\Psi}[X^\mu(shape)] = \sum_p \left(\hat{a}_p \psi_p[X^\mu(\text{shape})] + \hat{a}_p^\dagger \psi_p[X^\mu(\text{shape})]^* \right). \tag{2.8}$$

  These operators build the Fock space (multi-brane states) by acting on the vacuum $|0\rangle$ which is the no-brane state.

The second quantization can also be viewed (for a single-brane system) as reinterpreting the first-quantized wave function as a classical spacetime field, which is then quantized (the proper-time dependence is absent due to the gauge symmetry).

[3] It is a functional since the position depends on the shape of the object.

Even if multi-brane systems can be considered in the first quantization, the resulting description is much more complicated than with a field. For example, if the wave-function of one brane has K degrees of freedom (and generically is $K = \infty$, due to the spacetime dependence), then an N-brane wave-function would have K^N components. On the other hand, a field always has K components.

2.1.4 Interactions

Also, the interactions of strings are handled differently in the two formalisms:

- In the worldvolume picture amplitudes are computed by a path integral, which is weighted by the free action of one brane, with a sum over all possible processes

$$\langle \mathcal{O}_1 \cdots \mathcal{O}_n \rangle \sim \sum_{\mathcal{W}} \lambda^{\#(\mathcal{W})} e^{-S[\mathcal{W}]}. \tag{2.9}$$

  The sum is over all worldvolumes $\mathcal{W}$ with the external states as to boundary conditions. The interaction vertices with the corresponding coupling constant λ are added *by hand* and determine all possible topologies. Note that for simplicity we have introduced only one coupling constant, but in general, each vertex comes with its own coupling.

- In the spacetime picture the interaction between n fields is described by adding a monomial of order n in the fields in the action

$$S_{int} = \int \mathrm{d}X^\mu(\text{shape}) \Psi^n[X^\mu(\text{shape})], \tag{2.10}$$

  and then the scattering amplitudes are built from the Feynman graphs, which are themselves uniquely fixed by the action

$$\langle \mathcal{O}_1 \cdots \mathcal{O}_n \rangle \sim \int \mathrm{d}X^\mu(\text{shape}) e^{-S_{\text{free}}[\Psi] - S_{\text{int}}[\Psi]} \mathcal{O}_1 \cdots \mathcal{O}_n. \tag{2.11}$$

Typically the scattering amplitudes diverge and as always there are UV and IR divergences. The former originate from the high-energy region in loop diagrams, and they are removed by renormalizing with counterterms. The latter arise when an internal particle is forced to be on-shell, either as a part of a massless particle tadpole of a propagator on an external leg or of an internal propagator. Physically they correspond to quantum effects which shift the vacuum and the masses. Both problems are cured by renormalizing. In addition to these physical divergences, there are also non-physical ones coming from the fact of a bad parameterization of the amplitudes.

Renormalization is an intrinsically off-shell procedure and thus it can be employed only with difficulties in the worldvolume formalism. Moreover, since the masses of the states are shifted due to quantum effects, only (quantum) amplitudes for protected states can be computed. We note that a protected state is a state whose mass is not renormalized due to some symmetry (gauge, supersymmetry, etc) or because of representation symmetry.

Comparison of two formalisms

This brings us to a brief comparison between the two formalisms. In particular, we will just state the disadvantages of the worldvolume formalism over the field theory.

Firstly, the worldvolume approach *cannot* describe interactions since the path integral is weighted with the action of a single brane, and its Hilbert space does not include multi-brane states. The arbitrariness in the worldvolume approach complicates highly the models when several particles can interact in many different ways. Also, the worldvolume formulation is perturbative since the sum over the topologies is perturbative. On the other hand, a field theory can probe non-perturbative features of the system since the partition function is not given as a series in the coupling constant.

The rest of the disadvantages have been implicitly or explicitly stated before, but we collect them in the following list:

Caveats of the worldvolume formalism

- No natural description of multi-particle states
- On-shell states
- Lack of renormalization
- Infrared divergences
- Hard to check consistency (unitarity, causality, etc)
- Scattering amplitudes only for protected states
- Absence of non-perturbative processes

Some of these problems can be avoided with some prescriptions - or even in some cases they turn out to have some positive outcomes (such case is when scattering amplitudes in the worldvolume formalism can be computed with CFT methods)- but ultimately we should have a unified and systematic prescription, which is to be found in the field theory description.

Vocabulary of strings

In this subsection, we shall give some properties of the strings that we will use throughout the whole chapter. Thus we will collect the most obvious properties here.

String tension

If we consider a static non-relativistic string, then to describe it we need three parameters. The mass per unit of length μ, the tension T and the rest length l_0. If one wishes to stretch the string to a length l, its potential energy is given by $V = T(l-l_0)^2/2$ and the mass-energy $\mu l_0 c^2$. The minimal energy is for $l = l_0$.

The tension is independent of the parameters. To see this, we consider a spring with stiffness k_1. Then the force we have to give to the spring to modify its length by Δl is given as $F = k\Delta l$ by Hookes' law. Next, we replace the original spring with two springs of half the size of the first one but made from the same material. Applying the same force, the total change of the length is still Δl and it splits equally between the two springs, so $\Delta l_2 = \frac{\Delta l_1}{2}$. The force that applies on the two springs is $F = k_2 \Delta l_2$, yielding $k_2 = 2k_1$. From this, we see that the stiffness is inversely proportional to the length. Now, if we consider a string to be a series of many such springs, upon integration one obtains the tension as this coefficient of proportionality. Then it is understood that tension is energy per unit length or in other words it is a force.

Next, we consider a relativistic string with tension T defined in the rest frame and attach it such that its length is l. Then its energy is given as $E = Tl$ and is equal to the potential energy due to the stretching. From special relativity we know that the energy is the sum of the rest mass and the potential energy, implying that the string is massless. However, we can associate an *effective mass* (per unit length) due to the tension through $\mu c^2 = E/l = T$. Hence, in contrast to the non-relativistic case, mass and tension are not independent parameters.

Taking into account quantum effects, the string cannot shrink without limit due to the uncertainty relation

$$l \cdot p \geq \frac{\hbar}{2}, \tag{2.12}$$

since doing so would require infinite momentum. To find the natural string length, we do the following. We consider the center of the mass to have momentum p which can be related to energy as

$$p = \frac{E}{c} = \frac{\mu c^2 l}{c} = \frac{Tl}{c}, \tag{2.13}$$

since the center of the mass behaves like a massless particle with $p^\mu = (E, -E/c)$. Then taking the equality in the uncertainty relation yields

$$l \sim \sqrt{\frac{\hbar c}{2T}}. \tag{2.14}$$

The string length is defined with an additional factor[4] of π

$$\ell_s = \sqrt{\frac{\hbar c}{2\pi T}} \Rightarrow T = \frac{\hbar c}{2\pi \ell_s}. \tag{2.15}$$

Note that this is the only length one can create on the dimensional ground using just the tension and the fundamental constants. Since it arises from a quantum argument one may expect it to be close to the Planck length.

This means that any string which is not attached to something will spontaneously shrink. In particular, closed strings cannot be attached to anything and will tend to be very tiny, of the order of l_s, and thus just a few orders of magnitude above the Planck length. Note

[4]The precise relation between the energy and the tension depends on the details of the system. For example a rotating string has $E = \frac{\pi}{2}T$, so the precise factor defining ℓ_s is a matter of convention. Moreover the length is often parametrized to range from 0 to 2π: since the action is proportional to T, it is convenient to rewrite them in terms of ℓ_s^2 such that the spatial integral is normalized by 2π.

that the size of the string depends on its energy, and thus on its momentum and vibrational mode.

At the classical level, the lowest energy of string is obtained when the string shrinks to a point. But one can consider classical configurations where the string is of finite length even if it is not attached to anything. This is explained by the conservation of energy: the length of the string is fixed as an initial condition and the energy cannot change because one considers an isolated free string.

The last parameter to be introduced is the Regge slop α', defined by the relation

$$\frac{J}{\hbar} = \alpha' E^2, \tag{2.16}$$

where J is the angular momentum. Considering a rotating string gives the relation

$$T = \frac{1}{2\pi\hbar c\alpha'} \quad , \quad \ell_s = \hbar c\sqrt{\alpha'}. \tag{2.17}$$

Finally, it makes sense to speak about the string tension or the string length because one considers only one type of string. In fact, there will be two types of strings, closed and open, but unitarity requires them to have the same elementary properties, only their shapes differ.

Spectrum

Let us give some intuition about the states described by a *closed* string. One can start by choosing the gauge $g_{ab} = \eta_{ab}$ and after imposing the equations of motion, write the Fourier expansion of the fields X^μ as

$$X^\mu(\tau,\sigma) \sim x^\mu + p^\mu\tau + \frac{i}{\sqrt{2}}\sum_{n\in\mathbb{Z}^*}\frac{1}{n}\left(\alpha_n^\mu e^{-in(\tau-\sigma)} + \bar{\alpha}_n^\mu e^{-in(\tau+\sigma)}\right), \tag{2.18}$$

where x^μ is the *center-of-mass* of the string and p^μ its momentum, satisfying the usual commutation relation

$$[x^\mu, p^\nu] = i\eta^{\mu\nu}. \tag{2.19}$$

This differs from the expansion for a point-particle due to the third term. The later introduces an infinite number of oscillators α_n^μ and $\bar{\alpha}_n^\mu$ which satisfy canonical commutation relations for creation ($n < 0$) and annihilation operators ($n > 0$)

$$[\alpha_k^\mu, \alpha_l^\nu] = \eta^{\mu\nu}\delta_{k+l,0}. \tag{2.20}$$

For the case of opens strings, we just have to set $\alpha_n = \bar{\alpha}_n$. The Hamiltonian for the closed and open strings is respectively

$$H_{\text{closed}} = -\frac{m^2}{2} + N + \bar{N} - 2 \tag{2.21}$$

$$H_{\text{open}} = -m^2 + N - 1, \tag{2.22}$$

where $m^2 = -p^\mu p_\mu$ is the mass of the state in Planck units, N and $\bar{N}$ count the numbers N_n and $\bar{N}_n$ of oscillators α_n and $\bar{\alpha}_n$ weighted by their mode index n

$$N = \frac{1}{n}\sum_{n\in\mathbb{N}} nN_n, \quad N_n = \alpha_{-n}\cdot\alpha_n, \tag{2.23}$$

$$N = \frac{1}{n}\sum_{n\in\mathbb{N}} n\bar{N}_n, \quad \bar{N}_n = \bar{\alpha}_{-n}\cdot\bar{\alpha}_n. \tag{2.24}$$

Knowing these, one can construct the Hilbert space of the string theory. Recalling that invariance under reparametrization implies that the Hamiltonian vanishes, translates to

$$H\left|\psi\right\rangle = 0, \tag{2.25}$$

for any physical state. Another constraint for the closed string is the so-called level matching condition

$$(N - \bar{N})\left|\psi\right\rangle = 0. \tag{2.26}$$

The ground state $|p\rangle$ with momentum p is defined to be the eigenstate of momentum operator which does not contain any oscillator

$$\forall n > 0 : \alpha_n^\mu \left|p\right\rangle = 0. \tag{2.27}$$

Then it is understood that one can built an arbitrary excited state by applying successively creation operators

$$\left|\psi\right\rangle = \prod_{n>0}\prod_{\mu=0}^{d}\left(\alpha_{-n}^\mu\right)^{N_{n,\mu}}\left|p\right\rangle, \tag{2.28}$$

where $N_{n,\mu} \in \mathbb{N}$ counts how many times the oscillator α_{-n}^μ appears. For the moment we will focus on the first two levels of states.

The ground state is a *tachyon* because the Hamiltonian constraint shows that it has negative mass

$$\text{closed} : m^2 = -4, \tag{2.29}$$

$$\text{open} : m^2 = -1. \tag{2.30}$$

The first excited state of the *open string* is found by applying α_{-1}

$$\alpha_{-1}^\mu \left|p\right\rangle, \tag{2.31}$$

one finds that it is massless and since it transforms as a Lorentz vector (spin 1), it is identified with a $U(1)$ gauge boson. In fact, one can write a superposition of such states as

$$\left|A\right\rangle = \int d^D p A_\mu(p)\alpha_{-1}^\mu \left|p\right\rangle, \tag{2.32}$$

and the coefficient $A_\mu(p)$ of the Fourier expansion is interpreted as the spacetime field for the gauge boson. Reparametrization invariance is equivalent to the equation of motion

$$p^2 A_\mu = 0. \tag{2.33}$$

Furthermore, one can prove that the field obeys the Lorentz gauge condition

$$p^\mu A_\mu = 0, \tag{2.34}$$

which results from gauge fixing the $U(1)$ gauge invariance

$$A_\mu \to A_\mu + p_\mu \lambda. \tag{2.35}$$

It is interesting also (and can be checked) that the low energy action reproduces the Maxwell action.

The first level of a *closed string* is obtained by applying both α^μ_{-1} and $\bar{\alpha}^\mu_{-1}$ (which is the only way to match N and $\bar{N}$ at this level)

$$\alpha^\mu_{-1}\bar{\alpha}^\nu_{-1}\left|p\right\rangle, \tag{2.36}$$

and the corresponding states are massless as well. Furthermore, these states can be decomposed into irreducible representations of the Lorentz group

$$\left(\alpha^\mu_{-1}\bar{\alpha}^\nu_{-1}+\alpha^\nu_{-1}\bar{\alpha}^\mu_{-1}-\frac{1}{D}\eta^{\mu\nu}\alpha_{-1}\cdot\bar{\alpha}_{-1}\right)\left|p\right\rangle,$$
$$\left(\alpha^\mu_{-1}\bar{\alpha}^\nu_{-1}-\alpha^\nu_{-1}\bar{\alpha}^\mu_{-1}\right)\left|p\right\rangle, \quad \frac{1}{D}\eta_{\mu\nu}\alpha^\mu_{-1}\bar{\alpha}^\nu_{-1}\left|p\right\rangle.$$

These are respectively associated to the spacetime fields $G_{\mu\nu}$ (metric, spin 2), $B_{\mu\nu}$ (Kalb-Ramond 2-form, spin 1) and Φ (dilaton, spin 0). The appearance of a massless spin 2 particle is a key result that raised interest in string theory. This is because the low energy action of this particle is the Einstein-Hilbert action.

Reparametrization invariance leads to other constraints than $H = 0$. In particular, it implies that the massless fields have the correct gauge invariance and hence the correct degrees of freedom. Note that, after taking into account these constraints, the remaining modes correspond to excitations of the string in the directions transverse to it.

Each vibrational mode (harmonic) of the string corresponds to a spacetime field for a point-particle. Linear superpositions of these modes can describe several fields. Thus, this is how string theory is supposed to unify different theories since each field of every theory can be expressed as a superposition of the excitation of the modes of a single string. The spin and other properties of the particles are provided by the internal structure of the string and in particular its vibrational mode.

One disadvantage of the bosonic string theory is the fact that the spectrum contains tachyons. While the interpretation for open strings is the fact that they tend to form closed strings and stabilize the situation for closed strings is more subtle. In a sense, it indicates that spacetime itself is unstable and tends to decay! Since our lack of understanding is manifest, we remove the problem by introducing supersymmetry, and then the spectrum does not contain any tachyon and the dimension of the spacetime is lowered to 10.

2.2 Main analysis

2.2.1 Worldsheet Theory

The string worldsheet is a Riemannian surface $\mathcal{W} = \Sigma_n$ of genus n; the genus counts the number of holes or handles. The wordlsheet itself is the object on which all the string theory information is encoded. Coordinates on this two-dimensional worldsheet are denoted as $\sigma^a = (\tau, \sigma)$. Whenever there is no risk of confusion, σ will be used to denote collectively both. Let us furthermore consider the case of closed strings (the treatment of open strings is analogous) and hence the topology of the worldsheet will be a cylinder with a spatial direction being a circle $\mathcal{S}^1$ of unit radius, such that

$$\sigma \in [0, 2\pi) \quad , \quad \sigma \sim \sigma + 2\pi. \tag{2.37}$$

Then the string itself is embedded in arbitrary dimensional (D) spacetimes $\mathcal{M}$ with metric $G_{\mu\nu}$ via the embedding maps

$$X^\mu(\sigma^a) \quad : \quad \mathcal{W} \to \mathcal{M} \quad , \quad \mu = 0, \cdots, D-1. \tag{2.38}$$

These are the dynamical variables we saw at the beginning of the chapter in the section on conceptual analysis. The Nambu-Goto action is the starting point of the worldsheet description

$$S_{NG}[X^\mu] = \frac{1}{2\pi\alpha'} \int \mathrm{d}^2\sigma \sqrt{\det G_{\mu\nu}(X) \frac{\partial X^\mu}{\partial \sigma^a} \frac{\partial X^\nu}{\partial \sigma^b}}. \tag{2.39}$$

Quantizing this action turns to be difficult because it is highly non-linear. One way out is to introduce a Lagrange multiplier to remove the square root by introducing an auxiliary field that corresponds to an intrinsic worldsheet metric $g_{ab}(\sigma)$. Then the dynamical behaviour of the worldsheet is described by the Polyakov action

$$S_P[g, X^\mu] = \frac{1}{4\pi\alpha'} \int \mathrm{d}^2\sigma \sqrt{g} g^{ab} G_{\mu\nu}(X) \frac{\partial X^\mu}{\partial \sigma^a} \frac{\partial X^\nu}{\partial \sigma^b}, \tag{2.40}$$

which classically is equivalent to the Nambu-Goto action. The embeddings X^μ characterize the string theory under consideration in two ways: firstly their number gives the dimensionality of spacetime in which the strings propagate. More generally, they describe properties of the spacetime. Secondly, they describe the internal degrees of freedom of the string (i.e the vibration modes which are constrained by the spacetime).

However, one can use more general matter to describe a different spacetime or different degrees of freedom. For example in Polyakov's formalism, the worldsheet geometry is equipped with a metric $g_{ab}(\sigma)$ together with a set of fields living on it. The scalar fields $X^\mu(\sigma)$ can be described by a general sigma model which encodes the embedding of the string in D non-compact dimensions, and other fields can be added, for example, to describe compact dimensions or spin. Thus, different sets of fields and actions correspond to different string theories. Yet, to describe the other possibilities, one has to first understand the constraints on the worldsheet theories and introduce conformal field theories.

One important topological invariant is the *Euler characteristic*. This is computed by integrating the Riemann curvature $\mathcal{R}$ of the metric g_{ab} over the surface Σ_n

$$\chi := 2 - 2n = \frac{1}{4\pi} \int_{\Sigma_n} \mathrm{d}^2\sigma \sqrt{g} R, \tag{2.41}$$

with n being the genus of the surface. Note that oriented Riemann surfaces without boundaries are completely classified topologically by χ or equivalently n.

To describe a proper string theory the metric should *not* be dynamical: this corresponds to the worldsheet not having intrinsic dynamics and that no supplementary degrees of freedom are introduced when parametrizing the worldsheet with a metric. If any, a way to remove these degrees of freedom is by introducing gauge symmetries with the number of the gauge parameters to be equal to the number of degrees of freedom. Since the worldsheet theory is effectively a QFT coupled to gravity, it makes sense to ask invariance under diffeomorphisms. Physically this means that the choice of space parameter σ and the time parameter τ of the worldsheet is arbitrary. However, this invariance is not sufficient to completely fix the metric. Another natural candidate is Weyl invariance corresponding to *local* rescalings of the metric.

Having a diffeomorphism $\varphi \in \mathrm{Diff}(\Sigma_n)$ it acts on the fields as

$$\sigma'^a = \varphi^a(\sigma^b) \quad , \quad g'(\sigma') = \varphi^* g(\sigma) \quad , \quad \Psi'(\sigma') = \varphi^* \Psi(\sigma), \tag{2.42}$$

where $*$ denotes the pullback by φ, and by Ψ we denote collectively the matter fields. In coordinate notation, the metric and the scalar fields transform precisely as

$$g'_{ab}(\sigma') = \frac{\partial \sigma^c}{\partial \sigma'^a} \frac{\partial \sigma^d}{\partial \sigma'^b} g_{cd}(\sigma) \quad , \quad X'^\mu(\sigma') = X^\mu(\sigma). \tag{2.43}$$

The index μ here is redundant and not affected since from the worldsheet point of view it just labels a collection of worldsheet scalar fields and it is thus a target spacetime index. The infinitesimal analogues are generated by vector fields on Σ_n

$$\delta_\xi \sigma^a = \xi^a \quad , \quad \delta_\xi \Psi = \mathcal{L}_\xi \Psi \quad , \quad \delta_\xi g_{ab} = \mathcal{L}_\xi g_{ab}, \tag{2.44}$$

with $\mathcal{L}_\xi$ denoting the Lie derivative with respect to the vector field $\xi \in \mathfrak{diff}(\Sigma_n) \simeq T\Sigma_n$. The Lie derivative of the metric is

$$\mathcal{L}_\xi g_{ab} = \xi^c \partial_c g_{ab} + g_{ac} \partial_b \xi^c + g_{bc} \partial_a \xi^c = \nabla_a \xi_b + \nabla_b \xi_a. \tag{2.45}$$

The Lie algebra generates only transformations in the connected component $\mathrm{Diff}_0(\Sigma_n)$ of the diffeomorphism group which contains the identity. The rest of transformations not contained in $\mathrm{Diff}_0(\Sigma)$ are called large diffeomorphisms (e.g reflections). By taking the quotient of the two groups, one obtains the modular group

$$\mathfrak{G}_g := \frac{\mathrm{Diff}(\Sigma_n)}{\mathrm{Diff}_0(\Sigma_n)}, \tag{2.46}$$

which depends only on the genus of the Riemann surface and not on the metric. For $g \geq 1$ it is an infinite discrete group and in particular $\mathfrak{G}_1 = SL(2, \mathbb{Z})$.

On the other hand a Weyl transformation $e^{2\omega} \in \mathrm{Weyl}(\Sigma_n)$ corresponds to a local rescaling of the metric and leaves the other fields unaffected

$$g'_{ab}(\sigma) = e^{2\omega(\sigma)} g_{ab}(\sigma) \quad , \quad \Psi'(\sigma) = \Psi(\sigma). \tag{2.47}$$

This implicitly excludes fermionic fields which do not transform under a Weyl transformation. In addition, the exponentiation is in direct analogy with the fact that e^ω and not ω is an element of the group. Infinitesimally one has

$$\delta_\omega g_{ab} = 2\omega g_{ab} \quad , \quad \delta_\omega \Psi = 0, \tag{2.48}$$

where $\omega \in \mathfrak{weyl}(\Sigma) \simeq \mathcal{F}(\Sigma_n)$ is a function on the manifold. Two metrics are said to be conformally equivalent if they are related in this way. The conformal structure of Riemann surface is defined by

$$\mathrm{Conf}(\Sigma_n) := \frac{\mathrm{Met}(\Sigma_n)}{\mathrm{Weyl}(\Sigma_n)}, \tag{2.49}$$

where $\mathrm{Met}(\Sigma_n)$ denotes the space of all metrics on Σ_n.

Diffeomorphisms have two components ξ^a while Weyl transformations just one ω. It is therefore sufficient to locally fix the three components of the metric (using a symmetric matrix) and the total gauge group of the theory is the semi-direct product

$$G := \mathrm{Diff}(\Sigma_n) \ltimes \mathrm{Weyl}(\Sigma_n). \tag{2.50}$$

Similarly, the component connected to the identity is

$$G_0 := \mathrm{Diff}_0(\Sigma_n) \ltimes \mathrm{Weyl}_0(\Sigma_n). \tag{2.51}$$

The semi-direct character is because the Weyl parameter is not inert under diffeomorphisms. This is shown by the combination of the two transformations

$$g' = \varphi^*(e^{2\omega} g) = e^{2\varphi^* \omega} \varphi^* g, \tag{2.52}$$

since the diffeomorphism acts also on the conformal factor. Such combinations for the transformations can be chosen to fix the metric in a convenient gauge. For example the conformal gauge is

$$g_{ab}(\sigma) = e^{2\phi(\sigma)} \bar{g}_{ab}(\sigma), \tag{2.53}$$

where $\bar{g}_{ab}$ is some fixed background metric and $\phi(\sigma)$ the conformal factor. Note that this is also called *Liouville field*, a field that plays an important role in two-dimensional quantum gravity. Fixing only diffeomorphisms amounts to keep ϕ arbitrary, while this can be fixed with a Weyl transformation. As an example, one can use the conformally flat gauge

$$\bar{g}_{ab} = \delta_{ab} \quad , \quad \phi \quad \text{arbitrary} \tag{2.54}$$

with a diffeomorphism and then reach the flat gauge

$$\bar{g}_{ab} = \delta_{ab} \quad , \quad \phi = 0 \tag{2.55}$$

with a Weyl transformation.

Active and passive transformations

Symmetries are usually described by active transformations, which means that the field seems to change under transformations. At the same time, gauge fixing is seen as a passive transformation where the field is expressed in terms of other fields (e.g different parametrization). These are mathematically equivalent since both cases correspond to inverse elements, and one can choose the most convenient representation.

Topology and gauge choices

While it is always possible to adopt the flat gauge (2.55) locally it is not always possible to extend it globally. The sign of the curvature is given by $1 - n$ but the curvature of the flat metric is zero, meaning that curvature must be localized somewhere on the surface and this prevents from using just one coordinate patch.

All in all the system is described by an action $S_m[g, \psi]$ which has the following properties

- local in the fields
- renormalizable
- non-linear sigma models for a subset of the fields
- invariant under diffeomorphisms

- invariant under Weyl transformations

The last two conditions are summarized as

$$S_m[\varphi^* g, \varphi^* \Psi] = S_m[g, \Psi], \quad S_m[e^{2\omega} g, \Psi] = S_m[g, \Psi]. \tag{2.56}$$

The invariance under diffeomorphisms is straightforward to enforce by focusing only on covariant objects. The non-linear sigma model condition means that there is a spacetime interpretation for the string: the sigma model fields and the target manifold are respectively the spacetime coordinates and the manifold. The isometries of the target manifold metric become global symmetries of S_m.

To make the action consistent with the topology of the worldsheet, the fields must satisfy appropriate boundary conditions. In the simplest case, the bosonic fields should be periodic

$$X^\mu(\tau, \sigma) \sim X^\mu(\tau, \sigma + 2\pi). \tag{2.57}$$

2D gravity (see also Sec. 3.1)

The ingredients in two-dimensional gravity are similar, except that the system has, in general, no Weyl invariance. As a consequence, one component of the metric, which is usually taken to be the Liouville mode remains unconstrained. In the conformal gauge (2.53), only $\bar{g}$ is fixed.

The symmetries (2.56) imply that the matter is conformally invariant on flat space $g_{ab} = \delta_{ab}$. A conformal field theory (CFT) is characterized by a *central charge* c (see Sec. 2.3) which roughly measures the quantum degrees of freedom. In addition, is additive for decoupled sectors and in particular, the scalar fields X^μ contribute as the spacetime dimension D and it is useful to define a perpendicular CFT with central charge $c_\perp$ as matter which does not describe the non-compact space:

$$c = D + c_\perp. \tag{2.58}$$

In general the energy-momentum tensor is defined via

$$T_{ab} := -\frac{4\pi}{\sqrt{g}} \frac{\delta S}{\delta g^{ab}}. \tag{2.59}$$

The variation of the action under transformations (2.44) vanishes *on-shell* if the energy-momentum tensor is conserved

$$\nabla^a T_{ab} = 0. \tag{2.60}$$

On the other hand, variation under (2.48) vanishes *off-shell* if the energy-momentum tensor is traceless:

$$g^{ab} T_{ab} = 0. \tag{2.61}$$

The respective conserved charges generates worldsheet translations

$$P^a := \int \mathrm{d}\sigma T^{0a}. \tag{2.62}$$

The first component is identified with the worldsheet Hamiltonian $P^0 = H$ and generates time translations while the second component generates spatial translations.

Traceless and curvature

The trace of the energy-momentum tensor is proportional to the curvature

$$g^{ab}T_{ab} \propto \mathcal{R}. \tag{2.63}$$

Then, the equations of motion are invariant since the integral of $\mathcal{R}$ is a topological invariant. The theory is invariant even if the action is not. For example, this happens for fields at the quantum level (Weyl anomaly) and in the Liouville theory.

2.2.2 Path integral

One among the different ways to quantize the system is by considering the path integral which is achieved via the partition function

$$Z_n := \int \frac{[\mathrm{d}_n g_{ab}]}{\Omega_{\text{gauge}}[n]} Z_m[n] \quad , \quad Z_m[n] = \int [\mathrm{d}_n \Psi] e^{-S_m[g,\psi]}, \tag{2.64}$$

of fixed genus n. The integration over g_{ab} is performed over all metrics (geometries) of the surface Σ_n! The factor $\Omega_{\text{gauge}} \in \text{Met}(\Sigma_n)$ is a normalization inserted to make the integral finite and it depends on the metric. Usually it is the volume of the gauge group of the theory. That it depends on the metric explains (mathematically) why it is placed after the integral. Its value is determined by requiring the cancellation of the infinities due to gauge parameters, and of course, the latter is sensitive to the theory under consideration. This partition function corresponds to $n-$loop expansion, similarly to the case of Feynman diagrams in the usual quantum field theory, but here the expansion is over different topologies. This program is considered in the case of calculation of amplitudes and it is something that we will not need in this thesis and not explain further.

In order to proceed with gauge fixing and handle the path integral (2.64), one has to define an integration measure over the fields. That the space is infinite-dimensional makes the difficulty of the problem obvious, and one possibility is to define the measure implicitly through Gaussian integration over the field tangent space. Because a Gaussian integration involves a quadratic form, which is an inner product and equivalently a metric on the field space. However, to reduce the freedom in the definition of the inner product it is insightful to introduce three natural assumptions:

- *Ultralocality*: the measure is invariant under reparametrizations and defined point-wise, which implies that it can depend on the fields but not on their derivatives
- *Invariance*: the measure for the matter transforms trivially under any symmetry of the matter theory which is achieved by contracting indices with appropriate tensors
- *Free-field*: for fields other than the worldsheet metric and matter (e.g ghost fields, Killing vectors, etc), the measure is the one of a free field.

Thus, the inner product is obtained by contracting worldsheet indices of the fields with a tensor built only from the worldsheet metric, by contracting other indices (like the spacetime) with some invariant tensor (like the spacetime metric) and integrating over the worldsheet.

We also wish to distinguish the matter fields from those appearing in the gauge fixing procedure. The matter fields live in the representation of some group under which the

inner product is invariant. In other words, it is not possible to define each field measure independently if the exponential of the inner products does not factorize. For example in a curved background one has $[\mathrm{d}X] \neq \prod_\mu \mathrm{d}X^\mu$. However, these data are not needed if we already know that the matter is a CFT, this suffices to gauge fix the theory. In this procedure, different types of fields appear which do not carry indices beyond the worldsheet metric. Therefore under the third condition ensuring free-field measures we define measures of those single fields.

Let us consider the finite elements $\delta\Phi_1$ and $\delta\Phi_2$ of tangent space at the point Φ of the state of fields. Then the inner product and the associated norm are written as

$$(\delta\Phi_1, \delta\Phi_2)_g = \int \mathrm{d}^2\sigma\sqrt{g} h_g \left(\delta\Phi_1, \delta\Phi_2\right) \quad , \quad |\delta\Phi|_g^2 = (\delta\Phi, \delta\Phi)_g \,, \tag{2.65}$$

where h_g is the metric on the $\delta\Phi$ (tangent space). It is taken to be flat for all fields except for the metric. In principle one requires that these inner-product are ultralocal in a sense that h depends only on g_{ab} but not on its derivatives. Moreover the dependence of the flat metric h on g reflects the diffeomorphism invariant of the inner product which in turn will lead to a metric-dependent but nevertheless diffeomorphism invariant measure. The functional measure is then normalised via a Gaussian integral

$$\int [\mathrm{d}_g\delta\Phi] e^{-\frac{1}{2}(\delta\Phi,\delta\Phi)_g} = \frac{1}{\sqrt{\det h_g}}. \tag{2.66}$$

This, will lead to a measure on the field space itself

$$\int [\mathrm{d}\Phi] \sqrt{\det h_g} \tag{2.67}$$

on the tangent space. The determinant can be absorbed in the measure such that

$$\int [\mathrm{d}_g\delta\Phi] e^{-\frac{1}{2}(\delta\Phi,\delta\Phi)_g} = 1. \tag{2.68}$$

This normalization and the definition of the inner product is ambiguous, but the ultralocality condition fixes uniquely [66]

$$\sqrt{\det h_g} = e^{-\mu_h S_\mu[g]} \quad , \quad \mu_h \in \mathbb{R}, \tag{2.69}$$

since S_μ is the only renormalizable covariant functional depending on the metric but not on its derivative. The effect is to redefine the cosmological constant which is responsible for the Weyl anomaly.

Weyl anomaly

The Weyl anomaly is equivalent to a non-zero trace of the quantum energy-momentum tensor

$$\langle g^{\mu\nu} T_{\mu\nu} \rangle = \frac{c}{12}\mathcal{R}, \tag{2.70}$$

where c is the central charge and $\mathcal{R}$ the Ricci scalar. The Weyl anomaly can be equivalent traded for a gravitational anomaly which translates to broken diffeomorphisms at quantum level [67].

Fadeed-Popov method

At first sight the integration over the space of metrics $\mathrm{Met}(\Sigma_n)$ of all metrics Σ_n at fixed genus n leads to divergence of the functional integral since equivalent configurations

$$(\varphi^* g, \varphi^* \Psi) \sim (g, \Psi) \quad , \quad (e^{2\omega} g, \Psi) \sim (g, \Psi) \tag{2.71}$$

contribute in the same way to the integral. Since this redundancy is infinite, the integral diverges, and because the multiple counting is generated by the gauge group, the infinite contribution corresponds to the volume of this gauge group.

The Fadeed-Popov procedure is a mechanism to extract this volume by separating the integration over the gauge and physical degrees of freedom, schematically

$$\mathrm{d}(\text{fields}) = \text{Jacobian} \times \mathrm{d}(\text{gauge}) \times \mathrm{d}(\text{physical}). \tag{2.72}$$

The space of fields denoted by (g, Ψ) is divided into equivalent classes and one integrates over only one representative of each class, i.e over a gauge slice. This change of variables introduces a Jacobian factor which can be represented by a partition function with ghost fields, which are fields with negative norm.

> Mathematically, the Faddeev-Popov procedure consists in identifying the orbits (class of equivalent metrics) under the gauge group G and writing the integral in terms of G-invariant objects (orbits instead of individual metrics). This can be done by decomposing the tangent space into variations generated by G and its complement. Then, one can define a foliation of the field space which equips it with a fiber bundle structure: the base is the push forward of the complement and the fiber corresponds to the gauge orbits. The integral is then defined by selecting a section of this bundle.

2.3 Conformal Field Theories

In this section, we explain some basic ideas about conformal field theories (CFT) that we will refer later on. We do not need all the ingredients, nor will we perform strict computations using its tools but its simplicity instructs us to mention a few words for completeness. Conformal field theories are called the theories that are invariant under conformal transformations. This is quite general, as it is the fact that conformal transformations are called those that leave the angle between two vectors invariant. Since the aim of this thesis does not involve conformal field theories much we will rather present the basic ideas while details and more advanced topics will be omitted. Hence we will start with the conformal analysis in arbitrary D dimensions and then we will conclude with the CFT on the string worldsheet.

2.3.1 The conformal group in D dimensions

Let us start with an arbitrary D dimensional manifold $\mathcal{M}$ equipped with a metric g with signature (p, q), such that $p + q = D$. In a components notation, a conformal transformation is one that leaves the angle $g_{\mu\nu} u^\mu v^\nu / \sqrt{u^2 v^2}$ invariant. More precisely, the group of conformal

transformations is the subgroup of coordinate transformations $\phi : \mathcal{M} \to \mathcal{M}$ which leave the metric invariant up to a (spacetime depended) scale factor, such that

$$\phi : g \mapsto g' = \phi^* g := \Omega g \quad , \quad \Omega \in \mathcal{F}(\mathcal{M}), \tag{2.73}$$

where Ω is the scale factor and $\mathcal{F}(\mathcal{M})$ is the space of functions on $\mathcal{M}$. One can write the above transformation in components

$$g_{\mu\nu}(x) \longmapsto g'_{\mu\nu}(x') = \Omega(x) g_{\mu\nu}(x). \tag{2.74}$$

Note that this rescaling of the metric should not be confused with the Weyl transformations on the metric which do not act on the coordinates. In fact, conformal transformations are a subgroup of diffeomorphisms.

One important point is that in conformal field theories it is the angles that matter and not length scales since the latter are absent. In addition, the interpretation of (2.74) depends on whether or not the metric is kept dynamical. When it is dynamical, the conformal transformations are local and hence they are treated as a gauge symmetry. On the other hand, when the metric is fixed, the transformation corresponds to a global symmetry and one usually expects to have conserved currents associated with this.

Since in most CFT treatments the metric is flat we will also follow this recipe such that $g_{\mu\nu} = \eta_{\mu\nu}$, and therefore the manifold $\mathcal{M}$ will be identified with $\mathbb{R}^{p,q}$. Recalling the transformation law of the metric under a coordinate transformation

$$x^\mu \longmapsto x'^\mu = x^\mu(x), \tag{2.75}$$

we have

$$g_{\mu\nu}(x) \longmapsto g'_{\mu\nu}(x') = \frac{\partial x^\rho}{\partial x'^\mu} \frac{\partial x^\sigma}{\partial x'^\nu} g_{\rho\sigma}(x). \tag{2.76}$$

Comparing now with (2.74) and for the case of flat metric one gets

$$\Omega(x) \eta_{\mu\nu} = \frac{\partial x^\rho}{\partial x'^\mu} \frac{\partial x^\sigma}{\partial x'^\nu} \eta_{\rho\sigma}. \tag{2.77}$$

For the case of flat metric, the Poincaré group and hence the Lorentz group are subgroups of the conformal transformations with $\Omega(x) = 1$.

We shall examine the generators of these transformations. Let us then consider an infinitesimal coordinate transformation such that

$$x^\mu \longmapsto x'^\mu = x^\mu + \epsilon \mu(x) + \mathcal{O}(\epsilon^2) \quad , \quad \epsilon(x) \ll 1. \tag{2.78}$$

Then from (2.77) one finds that

$$\eta_{\rho\sigma} \partial_\mu (x^\rho + \epsilon^\rho(x) + \mathcal{O}(\epsilon^2)) \partial_\nu (x^\sigma + \epsilon^\sigma(x) + \mathcal{O}(\epsilon^2)) = \eta_{\mu\nu} + (\partial_\mu \epsilon_\nu + \partial_\nu \epsilon_\mu) + \mathcal{O}(\epsilon^2). \tag{2.79}$$

In order to have a conformal transformation the last expression should be a scaling factor of the metric, i.e

$$\partial_\mu \epsilon_\nu + \partial_\nu \epsilon_\mu = \mathcal{K}(x) \eta_{\mu\nu}, \tag{2.80}$$

such that from (2.76) infinitesimally we must have

$$\Omega(x) \eta_{\mu\nu} := (1 + \mathcal{K}(x)) \eta_{\mu\nu}. \tag{2.81}$$

Concretely we have to find this scaling factor $\mathcal{K}(x)$ for these transformations. In order to do this, we can take the trace of (2.80) yielding

$$\mathcal{K}(x) = \frac{2}{D}\partial_\mu \epsilon^\mu, \tag{2.82}$$

such that we find the scaling factor

$$\Omega(x) = 1 + \frac{2}{D}(\partial \cdot \epsilon) + \mathcal{O}(\epsilon^2). \tag{2.83}$$

This is on fact the conformal Killing equation in flat spacetime

Conformal Killing equation in flat spacetime

$$\partial_\mu \epsilon_\nu + \partial_\nu \epsilon_\mu = \mathcal{K}(x)\eta_{\mu\nu} \quad , \quad \mathcal{K}(x) = \frac{2}{D}\partial_\mu \epsilon^\mu. \tag{2.84}$$

Note that in the general non-flat case one has to use the Lie derivative

Conformal Killing equation in curved spacetime

A conformal Killing vector is defined as a vector field $\epsilon \in \mathfrak{X}(\mathcal{M})$ on the manifold $\mathcal{M}$ such that when the metric is transported along the curves generated by ϵ its Lie derivative is proportional to itself

$$\mathcal{L}_\epsilon g = \mathcal{K} g, \tag{2.85}$$

for some scalar field $\mathcal{K} = \mathcal{K}(x), x \in \mathcal{M}$.

Physically speaking the meaning of equation (2.85) is that as the metric is transported along some curve, or some congruence of curves its change is given by $\mathcal{K}$. In case $\mathcal{K}$ is an arbitrary function, it could be different along the manifold and vary. Contrary it could be that it is either zero, representing the familiar Killing equation resulting in a genuine invariance of the metric or it could be a constant that scales the metric along the curves. Such an example could be the dilatations where the killing vector is characterized as homothetic.

Returning in the flat case we can write interesting constraints for ϵ such that it allows conformal transformations. If we differentiate twice both sides of the flat Killing equation with respect to (w.r.t) x we get

$$\begin{aligned} \partial_\nu \partial^\rho \left(\partial_\mu \epsilon_\rho + \partial_\rho \epsilon_\mu\right) =& \partial_\nu \partial^\rho \left[\frac{2}{D}(\partial \cdot \epsilon)\eta_{\mu\rho}\right] \\ \partial_\nu \partial_\mu (\partial \cdot \epsilon) + \Box \partial_\nu \epsilon_\mu =& \frac{2}{D}\partial_\nu \partial_\mu (\partial \cdot \epsilon) \quad , \quad \Box := \partial^\rho \partial_\rho. \end{aligned} \tag{2.86}$$

We can add now $\partial_\mu \partial_\nu (\partial \cdot \epsilon) + \Box \partial_\mu \epsilon_\nu = (2/D)\partial_\mu \partial_\nu (\partial \cdot \epsilon)$ to the previous equation (note that it is the same equation with $\mu \leftrightarrow \nu$ exchanged) such that

$$\begin{aligned} 2\partial_\mu \partial_\nu (\partial \cdot \epsilon) + \Box \left(\partial_\mu \epsilon_\nu + \partial_\nu \epsilon_\mu\right) =& \frac{4}{D}\partial_\mu \partial_\nu (\partial \cdot \epsilon), \\ \left[\eta_{\mu\nu}\Box + (D-2)\partial_\mu \partial_\nu\right](\partial \cdot \epsilon) =& 0, \end{aligned} \tag{2.87}$$

where we have used the flat conformal Killing equation. We can furthermore contract with $\eta^{\mu\nu}$ yielding

$$2(D-1)\Box(\partial\cdot\epsilon)=0. \tag{2.88}$$

This is the constraint that ϵ has to satisfy such that it can generate conformal transformations. It is also obvious that the cases $D=1$ and $D=2$ are special and this will be the topic of the next subsection. Before going to this discussion however it would be illustrative to classify the possible conformal transformations. Let us consider the case $D>2$ and since the operator $\eta_{\mu\nu}\Box+(D-2)\partial_\mu\partial_\nu$ is non-degenerate it follows that $\partial\cdot\epsilon$ can be at most linear in x^μ. Therefore, one can propose a general ansatz

$$\epsilon_\mu(x)=a_\mu+b_{\mu\nu}x^\nu+c_{\mu\nu\rho}x^\nu x^\rho. \tag{2.89}$$

Each term in the r.h.s of the above equation gives rise to a conformal transformation in D dimensions. Explicitly we have the following possibilities

- For $\epsilon_\mu(x)=a_\mu$ and infinitesimally

$$x'^\mu=x^\mu+a^\mu, \tag{2.90}$$

  which are translations generated by $\mathcal{P}_\mu=-i\partial_\mu$.

- If $\epsilon_\mu(x)=b_{\mu\nu}x^\nu$, we have scaling transformations and rotations. Indeed the conformal flat Killing equation gives

$$b_{\mu\nu}+b_{\nu\mu}=\frac{2}{D}(\eta^{\rho\sigma}b_{\rho\sigma})\eta_{\mu\nu}, \tag{2.91}$$

  implying that the symmetric part of $b_{\mu\nu}\sim\eta_{\mu\nu}$. By decomposing into symmetric and antisymmetric parts we have

$$b_{\mu\nu}=\lambda\eta_{\mu\nu}+\omega_{\mu\nu}\quad,\quad\omega_{\mu\nu}=-\omega_{\nu\mu}. \tag{2.92}$$

  Focusing on the symmetric part, it yields

$$\epsilon^\mu=\lambda\eta^{\mu\nu}x_\nu\longrightarrow x'^\mu=x^\mu+\epsilon^\mu(x)=(1+\lambda)x^\mu, \tag{2.93}$$

  which are infinitesimal scaling transformations generated by the Liouville vector field $\mathcal{D}=-ix^\mu\partial_\mu$. Focusing instead on the antisymmetric part, we have infinitesimal rotations

$$x'^\mu=x^\mu+\omega^\mu_\nu x^\nu=\left(\delta^\mu_\nu+\omega^\mu_\nu\right)x^\nu, \tag{2.94}$$

  which are generated by the operators $\mathcal{J}_{\mu\nu}=i\left(x_\mu\partial_\nu-x_\nu\partial_\mu\right)$.

- The last case $\epsilon_\mu(x)=c_{\mu\nu\rho}x^\nu x^\rho$, corresponds to special conformal transformations. Let us differentiate the conformal flat Killing equation w.r.t x

$$\partial_\rho\partial_\nu\epsilon_\mu+\partial_\rho\partial_\mu\epsilon_\nu=\frac{2}{D}\partial_\rho(\partial\cdot\epsilon)\eta_{\mu\nu}. \tag{2.95}$$

Let us furthermore consider cyclic permutations of the indices of the above equation

$$\partial_\nu\partial_\mu\epsilon_\rho + \partial_\mu\partial_\nu\epsilon_\rho = \frac{2}{D}\partial_\mu(\partial\cdot\epsilon)\eta_{\nu\rho}, \tag{2.96}$$

$$\partial_\mu\partial_\rho\epsilon_\nu + \partial_\nu\partial_\rho\epsilon_\mu = \frac{2}{D}\partial_\nu(\partial\cdot\epsilon)\eta_{\rho\mu}. \tag{2.97}$$

Then, we have that (2.96)+(2.97)-(2.95) yields

$$\partial_\mu\partial_\nu\epsilon_\rho = \frac{1}{D}\left(\eta_{\nu\rho}\partial_\mu + \eta_{\rho\mu}\partial_\nu - \eta_{\mu\nu}\partial_\rho\right)(\partial\cdot\epsilon), \tag{2.98}$$

which furthermore using $\epsilon_\rho(x) = c_{\rho\sigma\gamma}x^\sigma x^\gamma$ gives

$$c_{\rho\mu\nu} = \eta_{\nu\rho}b_\mu + \eta_{\rho\mu}b_\nu - \eta_{\mu\nu}b_\rho, \tag{2.99}$$

where we have defined $b := \frac{1}{D}c^\sigma_{\sigma\mu}$. Therefore, infinitesimally one has

$$\begin{aligned} x'^\rho =& x^\rho + c^\rho{}_{\mu\nu}x^\mu x^\nu \\ =& x^\rho + \delta^\rho_\mu b_\nu x^\mu x^\nu + \delta^\rho_\nu b_\mu x^\mu x^\nu - \eta_{\mu\nu}b^\rho x^\mu x^\nu \\ =& x^\rho + 2(x\cdot b)x^\rho - x^2 b^\rho. \end{aligned} \tag{2.100}$$

This corresponds to an inversion, followed by a translation and then again an inversion. Let us show this,

$$x^\rho \mapsto \frac{1}{x^\rho} = \frac{x^\rho}{x^2} \tag{2.101}$$

$$\mapsto \frac{x^\rho}{x^2} - b^\rho = \frac{x^\rho - b^\rho - x^2}{x^2} \tag{2.102}$$

$$\mapsto \frac{(x^\rho - b^\rho x^2)x^2}{(x^\rho - b^\rho x^2)^2} = \frac{x^\rho - b^\rho x^2}{1 - 2(x\cdot b) + b^2x^2} \tag{2.103}$$

$$\begin{aligned} &\approx \left[\left(1 + 2(x\cdot b) - b^2x^2\right)\right]\left(x^\rho - b^\rho x^2\right) \quad , \quad b \ll 1 \\ &= x^\rho + 2(x\cdot b)x^\rho - x^2 b^\rho + \mathcal{O}(b^2) \end{aligned} \tag{2.104}$$

In the first line, we have an inversion, in the second line a translation while in the third line again an inversion. The generator for these special conformal transformations is $\mathcal{K}_\mu = -i\left(2x_\mu x^\nu\partial_\nu - x^2\partial_\mu\right)$.

We summarise all the transformations in the following table.

Conformal transformations in D dimensions

transformations	$\mathbf{\Omega(x)}$	**generators**	**# generators**
translations	1	$\mathcal{P}_\mu = -i\partial_\mu$	D
$x'^\mu = x^\mu + a^\mu$			
rotations	1	$\mathcal{J}_{\mu\nu} = i(x_\mu\partial_\nu - x_\nu\partial_\mu)$	$\frac{1}{2}D(D-1)$
$x'^\mu = (\delta^\mu_\nu + \omega^\mu_\nu)x^\nu$			
dilatations	$\frac{1}{\lambda^2}$	$\mathcal{D} = -ix^\mu\partial_\mu$	1
$x'^\mu = \lambda x^\mu$			
special conformal	$(1 + 2b\cdot x + {}^2\, x^2)^2$	$\mathcal{K}_\mu = -i(2x_\mu\cdot\partial - x^2\partial_\mu)$	D
$x'^\mu = \frac{x^\mu + b^\mu x^2}{1+2b\cdot x + b^2x^2}$			

The corresponding algebra is the one generated by the above generators whose total number is

$$\#\text{ generators} = \frac{1}{2}(d+1)(d+2) = \frac{1}{2}(p+q+1)(p+q+2), \tag{2.105}$$

while their commutation relations are

$$\begin{aligned}
[\mathcal{J}_{\mu\nu}, \mathcal{P}_\rho] =& -i(\eta_{\mu\rho}\mathcal{P}_\nu - \eta_{\nu\rho}\mathcal{P}_\mu),\\
[\mathcal{P}_\mu, \mathcal{K}_\nu] =& 2i\left(J_{\mu\nu} - \eta_{\mu\nu}\mathcal{D}\right),\\
[\mathcal{J}_{\mu\nu}, \mathcal{J}_{\rho\sigma}] =& -i\left(\eta_{\mu\rho}\mathcal{J}_{\nu\sigma} - \eta_{\mu\sigma}J_{\nu\rho} - \eta_{\nu\rho}\mathcal{J}_{\mu\sigma} + \eta_{\nu\sigma}\mathcal{J}_{\mu\rho}\right),\\
[\mathcal{J}_{\mu\nu}, \mathcal{K}_\rho] =& -i\left(\eta_{\mu\rho}\mathcal{K}_\nu - \eta_{\nu\rho}\mathcal{K}_\mu\right),\\
[\mathcal{D}, \mathcal{K}_\mu] =& i\mathcal{K}_\mu, \quad [\mathcal{D}, \mathcal{P}_\mu] = -i\mathcal{P}_\mu, \quad [\mathcal{J}_{\mu\nu}, \mathcal{D}] = 0.
\end{aligned}$$

In a space with signature (p, q) the Lorentz group is $SO(p, q)$. The above algebra is locally isomorphic to $SO(p+1, q+1)$. In fact, one can collect the generators in a group defined by an antisymmetric $(D+2)\times(D+2)$ matrix, which creates rotations in $(D+2)-$dimensions. Therefore, the number of generators of the conformal group in D dimensions is the same as for the group of rotations in $(D+2)-$dimensions.

2.3.2 The special case of two dimensions

The case of $D = 2$ is more special as we will see. The Killing flat conformal equation becomes

$$\partial_\mu\epsilon_\nu + \partial_\nu\epsilon_\mu = (\partial\cdot\epsilon)\eta_{\mu\nu}, \tag{2.106}$$

and considering the case of a Euclidean two-dimensional metric $g_{\mu\nu} = \delta_{\mu\nu}$ the only non-vanishing components are

$$\partial_1\epsilon_1 = \partial_2\epsilon_2, \tag{2.107}$$

$$\partial_1\epsilon_2 = -\partial_2\epsilon_1. \tag{2.108}$$

We recognize the Cauchy-Riemann conditions for a function to be holomorphic. This means that indeed we can construct a complex function

$$f : A \subset \mathbb{C} \longrightarrow \mathbb{C} : f(x_1 + ix_2) = \epsilon_1 + i\epsilon_2 \quad \text{holomoprhic} \Leftrightarrow \frac{\partial \epsilon_1}{\partial x_1} = \frac{\partial \epsilon_2}{\partial x_2} \ , \ \frac{\partial \epsilon_1}{\partial x_2} = -\frac{\partial \epsilon_2}{\partial x_1}.$$

In our case we can think of ϵ_1 and ϵ_2 as the real and imaginary part of a holomorphic function

$$\epsilon(z) = \epsilon_1 + i\epsilon_2 \quad \text{with} \quad z = x_1 + ix_2, \tag{2.109}$$

and similarly the real and imaginary part of an anti-holomorphic function

$$\bar{\epsilon}(\bar{z}) = \bar{\epsilon}_1 - i\bar{\epsilon_2} \quad \text{with} \quad \bar{z} = x_1 - ix_2. \tag{2.110}$$

This characterises conformal transformations in the two dimensional plane as analytic coordinate transformations on the complex plane

$$z \to f(z) \quad \text{and} \quad \bar{z} \to \bar{f}(\bar{z}). \tag{2.111}$$

Since there is an infinite number of coordinate transformations, the conformal algebra is infinite dimensional as well. The infinitesimal transformations can be written as

$$z \longmapsto z' = z + \epsilon(z) \quad , \quad \bar{z} \longmapsto \bar{z}' = \bar{z} + \bar{\epsilon}(\bar{z}) \tag{2.112}$$

where $\epsilon(z)$ can be expanded in infinite series as

$$\epsilon(z) = -\sum_n a_n z^{n+1} \quad , \quad \bar{\epsilon}(\bar{z}) = -\sum_n \bar{a}_n \bar{z}^{n+1}, \tag{2.113}$$

whilst the relevant generators are

$$\xi_n = iz^{n+1}\partial_z \quad , \quad \bar{\xi}_n = i\bar{z}^{n+1}\bar{\partial}_z, \tag{2.114}$$

that is ξ_n and $\bar{\xi}_n$ generate the coordinate transformations with $\epsilon = -z^{n+1}$ and $\bar{\epsilon} = -\bar{z}^{n+1}$ respectively. These generators close an algebra, identified by

$$[\xi_m, \xi_n] = (m-n)\xi_{m+n} \quad , \quad [\bar{\xi}_m, \bar{\xi}_n] = (m-n)\bar{\xi}_{m+n} \quad , \quad [\xi_m, \bar{\xi}_n] = 0, \tag{2.115}$$

and can be proven by applying the commutator on an arbitrary $f(z)$ function.

Conformal algebra in two dimensions

The classical (local) form of the conformal algebra in two dimensions is

$$\begin{aligned} [\xi_m, \xi_n] &= (m-n)\xi_{m+n}, \\ [\bar{\xi}_m, \bar{\xi}_n] &= (m-n)\bar{\xi}_{m+n}. \\ [\xi_m, \bar{\xi}_n] &= 0. \end{aligned}$$

This algebra is isomorphic to the classical Virasoro algebra or Witt algebra.

Despite the fact that the two-dimensional conformal algebra is infinite-dimensional, there exists a finite subgroup generated by $\xi_0, \xi_{\pm 1}$ and $\bar{\xi}_0, \bar{\xi}_{\pm 1}$. These generators are the only ones who are well defined on the whole Riemann sphere $S^2 = \mathbb{C} \cup \infty$ and they generate the following transformations

Generator	**Infinitesimal**	**Finite**	**Type**
ξ_{-1}	$z \to z - \epsilon$	$z \to z + \alpha$	translations
ξ_0	$z \to z - \epsilon z$	$z \to \lambda z$	scaling
ξ_1	$z \to z - \epsilon z^2$	$z \to \frac{z}{1-\beta z}$	special conformal

One can use combinations between ξ's and $\bar{\xi}$'s such that $i(\xi_0 - \bar{\xi}_0)$ generates a rescaling of the phase or, in other words, rotations on the $z-$plane. Dilatations are generated by $\xi_0 + \bar{\xi}_0$.

$SL(2,\mathbb{C})$ subgroup

The group $SL(2,\mathbb{C})$ is generated by the $\xi, \bar{\xi}$ generators upon inserted in the Virasoro algebra and the transformations they generate are summarised as

$$z \longmapsto \frac{az+b}{cz+d} \quad , \quad \bar{z} \longmapsto \frac{\bar{a}\bar{z}+\bar{b}}{\bar{c}\bar{z}+\bar{d}} \quad \text{with} \quad a,b,c,d \in \mathbb{C} \quad \text{and} \quad ad - bc = 1. \tag{2.116}$$

This is the group $SL(2,\mathbb{C})$ and when we quotient $\mathbb{Z}_2$, reflecting the invariance of the transformations by replacing a, b, c, d with their negatives, we get

$$PSL(2,\mathbb{C}) \cong SL(2,\mathbb{C})/\mathbb{Z}_2 \cong SO(3,1), \tag{2.117}$$

which is known as the group of projective conformal transformations in Euclidean dimensions. In the Lorentzian case, it gets replaced by

$$SO(2,2) \cong SL(2,\mathbb{R}) \times SL(2,\mathbb{R}), \tag{2.118}$$

where one factor pertains to left-movers and the other to right-movers.

This is the global conformal group in two dimensions and this apparent difference between the local and global case is a pathology of the two-dimensional case because in $D > 2$ only the global conformal group exists. In fact, the true conformal group in two dimensions is $SO(3,1)$ because the remaining conformal transformations do not admit global inverse on the Riemannian sphere S^2.

A CFT on the worldsheet

At this point, we have all information we need to make direct conduct with the worldsheet of string theory. One last bit of information will be the lightcone coordinates defined as

$$X^{\pm} = \frac{1}{\sqrt{2}} \left(X^0 \pm X^{D-1} \right), \tag{2.119}$$

generically. We recall the construction of the worldsheet energy-momentum tensor T_{ab} in equation (2.59). As a consequence of Weyl symmetry, in lightcone gauge the vanishing of

energy-momentum tensor becomes $T_{-+} = T_{+-} = 0$, and

$$T_{--} = 2\ell_s^2 \sum_{m=-\infty}^{\infty} \Xi_m e^{-2im(\tau-\sigma)} \tag{2.120}$$

$$T_{++} = 2\ell_s^2 \sum_{m=-\infty}^{\infty} \bar{\Xi}_m e^{-2im(\tau+\sigma)}, \tag{2.121}$$

where the Fourier coefficients are the Virasoro generators

$$\Xi_m = \frac{1}{2} \sum_{n=-\infty}^{\infty} \alpha_{m-n} \cdot \alpha_n \quad \text{and} \quad \bar{\Xi}_m = \frac{1}{2} \sum_{n=-\infty}^{\infty} \bar{\alpha}_{m-n} \cdot \bar{\alpha}_n \tag{2.122}$$

Requiring vanishing of the energy-momentum tensor results in

$$\Xi_m = 0 = \bar{\Xi}_m \quad \text{for} \quad m \in \mathbb{Z}. \tag{2.123}$$

In the quantum theory, to overcome the issue of singularities (note that we are evaluating the product of two operators $\partial_z \partial_z X(z)$ of the same spacetime point z) these operators are defined to be normal-ordered, that is,

$$\Xi_m := \frac{1}{2} \sum_{n=-\infty}^{\infty} : \alpha_{m-n} \cdot \alpha_n : . \tag{2.124}$$

These operators generate a quantum version of the Virasoro algebra

Quantum Virasoro algebra

In the quantum case, the Virasoro algebra can acquire a central extension, or the so-called conformal anomaly, with central charge c, in which case it takes the following form

$$[\Xi_m, \Xi_n] = (m-n)\Xi_{m+n} + \frac{c}{12} m(m^2-1)\delta_{m+n,0}. \tag{2.125}$$

In a two-dimensional CFT, the Virasoro operators are the modes of the energy-momentum tensor, which therefore is the operator generating conformal transformations. The term central extension means that the constant term can be understood to multiply the unit operator which furthermore is adjoined to the Lie algebra. In addition, the conformal anomaly can be interpreted, in certain cases, as breaking the conformal character of the theory at the quantum mechanical level, a feature that happens whenever there exists a central charge in the quantum algebra.
According to the usual convention of the normal-ordering prescription, the lowering operators always appear to the right of the raising operators. In particular, Ξ_0 becomes

$$\Xi_0 = \frac{1}{2}\alpha_0^2 + \sum_{n=1}^{\infty} \alpha_{-n} \cdot \alpha_n. \tag{2.126}$$

Since the worldsheet theory has translation symmetry, this tensor is also conserved as we saw

$$\partial^a T_{ab} = 0. \tag{2.127}$$

Now, after Wick rotation the lightcone indices $\pm$ are replaced by $(z, \bar{z})$ such that the non-vanishing components are $T_{zz} = T(z)$ and $T_{\bar{z}\bar{z}} = \tilde{T}(z)$. As we mentioned before, the Virasoro generators are the modes of the energy-momentum tensor. When we set $\ell_s = \sqrt{2\alpha'} = 1$, and we recall the expansion (2.18) we can treat separately left-movers and right-movers as

$$X_R^\mu(\sigma,\tau) \to X_R^\mu(z) = \frac{1}{2}x^\mu - \frac{i}{4}p^\mu \ln z + \frac{i}{2}\sum_n \frac{1}{n}\alpha_n^\mu z^{-n}, \tag{2.128}$$

$$X_L^\mu(\sigma,\tau) \to X_L^\mu(\bar{z}) = \frac{1}{2}x^\mu - \frac{i}{4}p^\mu \ln \bar{z} + \frac{i}{2}\sum_n \frac{1}{n}\bar{\alpha}_n^\mu \bar{z}^{-n}. \tag{2.129}$$

The holomorphic derivatives are respectively

$$\partial X^\mu(z,\bar{z}) = -\frac{i}{2}\sum_{n=-\infty}^{\infty} \alpha_n^\mu z^{-n-1}, \tag{2.130}$$

$$\bar{\partial} X^\mu(z,\bar{z}) = -\frac{i}{2}\sum_{n=-\infty}^{\infty} \bar{\alpha}_n^\mu \bar{z}^{-n-1}, \tag{2.131}$$

and therefore we can compute the energy-momentum tensor

$$T(z) = -2 : \partial X \cdot \partial X := \sum_{n=-\infty}^{\infty} \frac{\Xi_n}{z^{n+2}}. \tag{2.132}$$

Similarly

$$\bar{T}(\bar{z}) = -2 : \bar{\partial} X \cdot \bar{\partial} X := \sum_{n=-\infty}^{\infty} \frac{\bar{\Xi}_n}{\bar{z}^{n+2}}. \tag{2.133}$$

Since the two-dimensional conformal algebra is infinite-dimensional, there is an infinite number of conserved charges, namely the Virasoro generators. For an infinitesimal conformal transformation

$$\delta z = \epsilon(x) \quad \text{and} \quad \delta\bar{z} = \bar{\epsilon}(\bar{z}), \tag{2.134}$$

the associated conserved charge that generates this transformation is

$$Q = Q_\epsilon + Q_{\bar{\epsilon}} = \frac{1}{2\pi i}\oint \left[T(z)\epsilon(z)\,\mathrm{d}z + \bar{T}(\bar{z})\bar{\epsilon}(z)\,\mathrm{d}\bar{z}\right], \tag{2.135}$$

where the integral is performed over a circle of fixed radius.

A conformal field theory is characterised by a set of composite fields, or operators called $\mathcal{O}(z,\bar{z})$. The variation of this field/operator under a conformal transformation is given by

$$\delta_\epsilon \mathcal{O}(z,\bar{z}) = [Q_\epsilon, \mathcal{O}(z,\bar{z})] \quad \text{and} \quad \delta_{\bar{\epsilon}}\mathcal{O}(z,\bar{z}) = [Q_{\bar{\epsilon}}, \mathcal{O}(z,\bar{z})]. \tag{2.136}$$

The fields/operators of a CFT are characterised by their conformal dimensions, which specify how they transform under scale transformations.

Primary fields

- Primary operator:

$$\forall\ w \text{ meromorphic } : \qquad \mathcal{O}(z,\bar{z}) = \left(\frac{\partial w}{\partial z}\right)^{h} \left(\frac{\partial \bar{w}}{\partial \bar{z}}\right)^{\bar{h}} \mathcal{O}(w(z),\bar{w}(\bar{z})) \tag{2.137}$$

- Quasi-primary (or $SL(2,\mathbb{C})$ primary) operator:

$$\forall\ w\ \in PSL(2,\mathbb{C})\ : \qquad \mathcal{O}(z,\bar{z}) = \left(\frac{\partial w}{\partial z}\right)^{h} \left(\frac{\partial \bar{w}}{\partial \bar{z}}\right)^{\bar{h}} \mathcal{O}(w(z),\bar{w}(\bar{z})). \tag{2.138}$$

The parameters $(h,\bar{h})$ are the conformal weights of the operator $\mathcal{O}$ and independent of each other. They combine together such that they give the conformal dimension Δ and spin s of the operator/state $\mathcal{O}$

$$\Delta := h + \bar{h} \quad , \quad s := h - \bar{h}. \tag{2.139}$$

From another point of view, the $(h,\bar{h})$ differential

$$\mathcal{O}(z,\bar{z})(dz)^{h}(d\bar{z})^{\bar{h}} \tag{2.140}$$

is invariant under local/global conformal transformations.

Another ingredient that characterises a CFT is the operator product expansion (OPE) and specifically the OPE coefficients. It simply means that when two local operators come close to each other it is possible to replace their product by a sum of local operators

$$\mathcal{O}_i(z_i,\bar{z}_i)\mathcal{O}_j(z_j,\bar{z}_j) = \sum_k \frac{c_{ij}^k}{z_{ij}^{h_i+h_j-h_k}\,\bar{z}_{ij}^{\bar{h}_i+\bar{h}_j-\bar{h}_k}} \mathcal{O}_k(z_j,\bar{z}_j), \tag{2.141}$$

where the OPE coefficients c_{ij}^k are some constants and their sum runs over all operators. In the case where $\mathcal{O}_k$ is a primary operator, the coefficients are related to the structure constants and the field metric as

$$C_{ijk} = g_{kl}c_{ij}^l. \tag{2.142}$$

For a generic primary operator $\mathcal{O}(w)$, one finds the OPE of with stress-energy tensor to be

$$T(z)\mathcal{O}(w) = \frac{h\mathcal{O}(w)}{(z-w)^2} + \frac{\partial\mathcal{O}(w)}{z-w} + \cdots, \tag{2.143}$$

where h is the conformal weight of the operator. One of the most important OPE's is the one of energy-momentum tensor with itself. In fact, this gives the central charge of a CFT, the latter found as the coefficient of the z^{-4} term in the expansion

$$T(z)T(w) = \frac{c/2}{(z-w)^4} + \frac{2T(w)}{(z-w)^2} + \frac{\partial T(w)}{z-w} + \cdots. \tag{2.144}$$

From this one deduces that the conformal weight for the energy-momentum tensor is $h = 2$ analogously $\bar{h} = 2$. In addition one realises that the central charge gives the spacetime dimensions D of the theory. This central charge appearing here is the same c as in the quantum Virasoro algebra (2.125). That this is the case one can motivate as follows: from

the definition of the components of stress energy tensor from equations (2.132),(2.133) one can write the expression in the $z \to w$ limit, meaning locality

$$: \partial X^\mu(z)\partial x^\nu(z) := \lim_{z\to w}\left(\partial_z X^\mu(z)\partial_w X^\nu(w) + \frac{\eta^{\mu\nu}}{4(w-z)^2}\right). \tag{2.145}$$

Then each scalar field gives a contribution one to the conformal anomaly c. Therefore in D dimensions the X^μ coordinates give $c = \bar{c} = D$. It is rather obvious to note that in order for the energy-momentum tensor to be a conformal field it should be the case such that $c = 0$, hence another motivation of conformal anomaly.

Under a finite conformal transformation $z \to w(z)$ the energy-momentum tensor transforms as

$$(\partial_w)^2 T'(w) = T(z) - \frac{c}{12}S(w,z), \tag{2.146}$$

with $S(w,z)$ being the so-called Schwarzian derivative

$$S(w,z) = \frac{2(\partial w)(\partial^3 w) - 3(\partial^2 w)^2}{2(\partial w)^2}. \tag{2.147}$$

At this point, we have all the ingredients needed to completely describe a CFT. Independent of the dimensions one needs the conformal weights of the operators and the OPE coefficients. The worldsheet of a closed string propagating in spacetime is locally topologically equivalent to a cylinder $\mathbb{R}\times\mathbf{S}^1$ of circumference L. We will show that the cylinder can be mapped to the complex plane and thus to the Riemann sphere (after removing the poles) on which all the analysis that took place above can be applied. We note that this is insensitive to string theory interpretation and generically one can define two-dimensional models on the cylinder. The compactification $\mathbb{R} \to \mathbf{S}^1$ cures the infrared divergences, and in addition, it leads to a convenient definition of the "time" component and thus a Hamiltonian in the Euclidean case.

Let us start by denoting the worldsheet coordinates in Lorentzian signature by (t,σ) with

$$t \in \mathbb{R} \quad , \quad \sigma \in [0, L) \quad , \quad \sigma = \sigma + L. \tag{2.148}$$

The metric yields

$$\mathrm{d}s^2 = -\,\mathrm{d}t^2 + \mathrm{d}\sigma^2 = -\,\mathrm{d}\sigma^+\,\mathrm{d}\sigma^-, \tag{2.149}$$

where we have introduced the light-cone coordinates

$$\mathrm{d}\sigma^\pm = \mathrm{d}t \pm \mathrm{d}\sigma. \tag{2.150}$$

Then by performing a Wick rotation $\tau = it$, the metric becomes

$$\mathrm{d}s^2 = \mathrm{d}\tau^2 + \mathrm{d}\sigma^2. \tag{2.151}$$

In addition we introduce complex coordinates

$$w = \tau + i\sigma \quad , \quad \bar{w} = \tau - i\sigma, \tag{2.152}$$

for which the metric becomes

$$\mathrm{d}s^2 = \mathrm{d}w\,\mathrm{d}\bar{w}, \tag{2.153}$$

while the relation to Lorentzian light-cone coordinates is

$$w = i(t+\sigma) = i\sigma^+ \quad , \quad \bar{w} = i(t-\sigma) = -i\sigma^-. \tag{2.154}$$

Therefore, a(n) (anti)-holomorphic function of $w(\bar{w})$ depends only on $\sigma^+(\sigma^-)$ before Wick rotating and this leads to the identification on the left-and right-movers with the holomorphic and anti-holomorphic parts of the theory.
The cylinder can be mapped to the complex plane through

$$z = e^{2\pi w/L} \quad , \quad \bar{z} = e^{2\pi \bar{w}/L}, \tag{2.155}$$

while the corresponding metric is

$$\mathrm{d}s^2 = \left(\frac{L}{2\pi}\right)^2 \frac{\mathrm{d}z\,\mathrm{d}\bar{z}}{|z|^2}. \tag{2.156}$$

A conformal transformation can bring this metric to the flat one

$$\mathrm{d}s^2 = \mathrm{d}x^2 + \mathrm{d}y^2 = \mathrm{d}z\,\mathrm{d}\bar{z}. \tag{2.157}$$

The map from the cylinder works by sending the bottom end (infinite past) of the cylinder to the origin of the complex plane and the top end (infinite future) to infinity. Since the cylinder has two boundaries (its ends) in the complex plane one has to exclude these points corresponding to the $z = 0$ and $z = \infty$, obtaining in this way the space $\mathbb{C}^*$. This space consequently can be mapped to the Riemann two-sphere $\Sigma_{0,2}$.

The physical meaning for the difference of Σ_0 and $\Sigma_{0,2}$ is quite interesting. Since one considers the propagation of a closed string, it means that in a sense the worldsheet itself corresponds to an amplitude with two external states, which are then mapped to the sphere as punctures on the north and south poles. Removing the external states, yielding in this way the tree-level vacuum amplitude, corresponds to gluing a half-sphere at each end of the cylinder (i.e gluing the upper and lower hemispheres). Then, it can be mapped to the Riemann sphere without the punctures and as a consequence, the properties of tree-level string theory are found by studying the matter and ghost CFTs on the Riemann sphere.

Why extra dimensions?

Finally, we close the CFT analysis with some remarks regarding the dimensionality of spacetime of string theory. For simplicity, we shall consider the bosonic string theory where the spacetime dimensions turn out to be $D = 26$. We shall also not pursue all the analysis here because this is done in standard string theory textbooks [55,57,59] but we shall state the two common ways to obtain this:

- The Lorentz symmetry in string theory is not satisfied trivially, in a sense that the theory is not constructed as manifestly Lorentz invariant. In fact, neither the spacetime dimensionality (i.e the dimensions of target space) is specified. Then, defining the Lorentz generators one computes the algebra and demanding closure sets $D = 26$ [55]. Another intuitive way to grasp the idea is the following: the analysis of spin for massive and massless states is different. For a massive particle, one goes to the rest frame $p^\mu = (m, 0, \cdots, 0)$ and then the internal states form a representation of the spatial rotation group $SO(D-1)$. For the case of a massless particle there is no rest frame, hence what one does is to choose for example the frame $p^\mu = (E, E, 0, \cdots, 0)$. Now the $SO(D-2)$ acting on the transverse directions leaves p^μ invariant, and then the internal states form a representation of this smaller group. Similarly, in D dimensions,

a massive vector particle thus has $D-1$ spin states while a massless vector needs to have only $D-2$ states. This is the generalization of the familiar case of $D=4$ where spin states are labeled by representations of $SO(3)$ giving $2j+1$ states, while massless particles are labeled by their helicity λ, which represents the eigenvalue of the single generator of $SO(2)$. Lorentz invariance alone thus requires only one state, while CPT symmetry takes λ to $-\lambda$ and so requires two states for $\lambda \neq 0$. Thus, in the light-cone gauge of bosonic string theory $D-2$ transverse degrees of freedom produce oscillators $a_n^i, i = 1, \cdots, D-2$. The squared mass of the string in an arbitrary spacetime is given by the total number of all the harmonic oscillators

$$M^2 = \sum_{n\in\mathbb{Z}^+,i} a_{-n}^i a_n^i. \tag{2.158}$$

In addition each normal operator of the harmonic oscillator is normalised as $\sqrt{n}\cdot a$ turning the zero point energy of string theory to (see eq. (2.126))

$$\frac{1}{2}\sum_{i=1}^{D-2} : a_{-0}^i a_0^i : + \frac{D-2}{2}\sum_{m=1}^{\infty} n \underbrace{\equiv}_{a_0^i|0\rangle=0} E_0 = \frac{D-2}{2}\sum_{n=1}^{\infty} n. \tag{2.159}$$

The first excited state, gets excited by a_{-1}^i and considering the harmonic oscillator picture and remembering that the total energy is given by the total sum over the harmonic oscillators will add unity to the total energy as

$$a_{-1}\left|0\right\rangle = 1\cdot\left|0\right\rangle. \tag{2.160}$$

This is a level one ($n=1$) state and it is a spacetime (bosonic) vector. Therefore it has $D-2$ components rather than $D-1$ components, so it must correspond to a massless state. This leads to

$$\frac{D-2}{2}\left(-\frac{1}{12}\right) + 1 \overset{!}{=} 0. \tag{2.161}$$

This leads to $D=26$ upon using the famous result

$$\sum_{n=1}^{\infty} n = \zeta(-1) = -\frac{1}{12}, \tag{2.162}$$

with $\zeta(s)$ being the Riemann ζ function.

- Another common, but more advanced, way is the BRST quantization of the string. BRST stands for the *Becchi-Rouet-Stora-Tyupin* transformations and the formalism itself is essentially a way to handle the ghosts introduced in the theory. With the introduction of ghosts in the action for gauge-fixing, the theory is no more invariant under the original gauge symmetry. The BRST symmetry is an extension of the original symmetry, which remains intact. Therefore, all physical states must be BRST invariant. The introduction of ghost fields results, at the quantum level, to a further extension of the original Virasoro algebra (2.125) as

$$[\Xi_m, \Xi_n] = (m-n)\Xi_{m+n} + A(m)\delta_{m+n}, \tag{2.163}$$

with

$$A(m) = \frac{c}{12}m(m^2-1) + \frac{1}{6}(m-13m^3) + 2am, \tag{2.164}$$

and the last constant term is due to normal ordering of Ξ_0 in (2.126). We see that this extension vanishes if $c = D = 26$ and $a = 1$.

2.4 Gravity from string theory

Being a potential theory of unification, string theory should also contain gravity. In fact, statement simply means that Einstein's equation should be present somehow in string theory. One could fairly argue that since the topic of string theory is so vast there should be somewhere there. However, we will see Einstein's equation arising by demanding the theory on the worldsheet to be conformal invariant and in particular Weyl invariant. In a usual QFT conformal invariance implies scale invariance while it is not known yet if the inverse is true. On the other hand, likely for a two-dimensional unitary QFT with one compact dimension (i.e for closed strings) scale invariance means conformal invariance. Possible deviations from scale invariance are captured by the so-called beta function which describes the change of the coupling constant concerning a specific energy scale.

Let us then start by recalling the Polyakov action (2.40)

$$S_P[g, X^\mu] = \frac{1}{4\pi\alpha'} \int \mathrm{d}^2\sigma \sqrt{g} g^{ab} G_{\mu\nu}(X) \partial_a X^\mu \partial_b X^\nu, \tag{2.165}$$

by introducing the notation $\partial_a := \partial/\partial\sigma^a$. This worldsheet theory is and interacting theory, the so-called non-linear sigma model in contrast to propagation of the string in flat space which is a free theory. To see the interacting part it is convenient to expand the fields as

$$X^\mu(\sigma) = x^\mu + \sqrt{\alpha'} Y^\mu(\sigma). \tag{2.166}$$

This simply means that we consider the mean position of the string to be located at a point x^μ and $Y^\mu(\sigma)$ are the dynamical, yet small fluctuations around this point. In addition $\sqrt{\alpha'}$ serves as a dimensional regulator and has dimensions of [length]. We can furthermore expand the spacetime metric such that the Lagrangian becomes

$$G_{\mu\nu}(X)\partial_a X^\mu \partial_b X^\nu = \alpha' \left(G_{\mu\nu}(x) + \sqrt{\alpha'} \partial_\rho G_{\mu\nu}(x) Y^\rho + \frac{\alpha'}{2} \partial_\rho \partial_\delta G_{\mu\nu}(x) Y^\rho Y^\delta + \cdots \right) \partial_a X^\mu \partial_b X^\nu, \tag{2.167}$$

This expansion leads to two obvious facts: 1) the coupling constants are derivatives of the metric; 2) there is an infinite number of those. Moreover, classically the Polyakov action is conformal invariant but this is not true anymore in the quantum level due to the Weyl anomaly. To begin, let us use the Riemann normal coordinates such that the expansion of $X^\mu(\sigma) = x^\mu + \sqrt{\alpha'} Y^\mu(\sigma)$ will give

$$G_{\mu\nu}(x) = \delta_{\mu\nu} - \frac{\alpha'}{3} R_{\mu\lambda\nu\kappa}(x) Y^\lambda Y^\kappa + \mathcal{O}\left(Y^\alpha Y^\beta Y^\gamma\right), \tag{2.168}$$

which plugging it back into the action (2.165) yields

$$S_P[g, X^\mu] = \frac{1}{4\pi} \int \mathrm{d}^2\sigma \sqrt{g} \left(\partial^a Y^\mu \partial_a Y^\nu \delta_{\mu\nu} - \frac{\alpha'}{3} R_{\mu\lambda\nu\kappa} Y^\lambda Y^\kappa \partial^a Y^\mu \partial_a Y^\nu + \cdots \right). \tag{2.169}$$

We can treat this action as a QFT in two dimensions and immediately we recognize a diagrammatic expansion. The quartic interaction gives a cross vertex consisting of four lines as it can be seen in the left panel of Fig. 2.1, while in momentum space derivatives become the momenta k^μ_σ. Now it remains to compute the beta function of this theory and one easy way to do so is by curing the divergences occurring from the one-loop diagram of the right panel of Fig. 2.1. In position space, the propagator of a scalar field is given by

$$\langle Y^\lambda(\sigma) Y^\kappa(\sigma) \rangle = -\frac{1}{2} \delta^{\lambda\kappa} \ln\left(|\sigma - \sigma'|^2\right). \tag{2.170}$$

The scalar field running in the loop reach the same location after a 2π rotation yielding a divergence reflecting in this way the ultraviolet divergence that we would see in the momentum integral around the loop. We can choose a dimensional regularization to cure this divergence as $d = 2 - \epsilon$. The propagator in momentum space then takes the form

$$\langle Y^\lambda(\sigma) Y^\kappa(\sigma)\rangle = 2\pi\delta^{\lambda\kappa}\int \frac{\mathrm{d}^d k}{(2\pi)^d}\frac{e^{ik(\sigma-\sigma')}}{k^2}, \tag{2.171}$$

and in the limit $\sigma \to \sigma'$ it becomes

$$\begin{aligned}\lim_{\sigma\to\sigma'}\langle Y^\lambda(\sigma) Y^\kappa(\sigma)\rangle =& 2\pi\delta^{\lambda\kappa}\int \frac{\mathrm{d}^d k}{(2\pi)^d}\frac{1}{k^2}\\ =& 2\pi\delta^{\lambda\kappa}\pi^{d/2}\Gamma\left(2-\frac{d}{2}\right)\\ =& 2\pi^{-\epsilon/2}\delta^{\lambda\kappa}\left(\frac{2}{\epsilon}-\gamma+\mathcal{O}(\epsilon)\right).\end{aligned} \tag{2.172}$$

To go to the second line we have used the formula

$$\int \frac{\mathrm{d}^d k}{(2\pi)^d}\frac{1}{(k^2+a^2)^r} = \pi^{d/2}a^{d-2r}\frac{\Gamma\left(r-d/2\right)}{\Gamma(r)}, \tag{2.173}$$

while for the next line we have expanded the gamma function around ϵ. At the end, we are interested in the limit $\epsilon \to 0$ and it is obvious from the expression that we have truncated linear and higher orders in ϵ since in this limit the first term diverges. In addition $\gamma \approx 0.5772$ is the Euler-Mascheroni constant. Let us then schematically write the propagator in the limit $\epsilon \to 0$ as

$$\lim_{\epsilon\to 0}\langle Y^\lambda Y^\kappa\rangle \longrightarrow \frac{\delta^{\lambda\kappa}}{\epsilon}. \tag{2.174}$$

This divergence coming from the first (one loop) correction of the second term in the action (2.169) is obvious when we substitute $Y^\lambda Y^\kappa$ with $\langle Y^\lambda Y^\kappa\rangle$ resulting in a term

$$-\frac{1}{\epsilon}R_{\mu\nu}\partial^a Y^\mu \partial_a Y^\nu. \tag{2.175}$$

We can absorb this divergence if we add the following counter term

$$R_{\mu\lambda\nu\kappa}Y^\lambda Y^\kappa \partial^a Y^\mu \partial_a Y^\nu \to R_{\mu\lambda\nu\kappa}Y^\lambda Y^\kappa \partial^a Y^\mu \partial_a Y^\nu - \frac{1}{\epsilon}R_{\mu\nu}\partial^a Y^\mu \partial_a Y^\nu. \tag{2.176}$$

Moreover, this can be absorbed by a wave function renormalization $Y^\mu \to Y^\mu - (\alpha'/6\epsilon)R^\mu{}_\nu Y^\nu$ accompanied with the renormalization of the coupling constant

$$G_{\mu\nu} \to G_{\mu\nu} + \frac{\alpha'}{\epsilon}R_{\mu\nu}. \tag{2.177}$$

This specifies the value of the beta function at one loop to be

$$\beta(G) = \alpha' R_{\mu\nu} \tag{2.178}$$

and demanding scale invariance yields

$$\beta(G) = 0 \Rightarrow R_{\mu\nu} = 0. \tag{2.179}$$

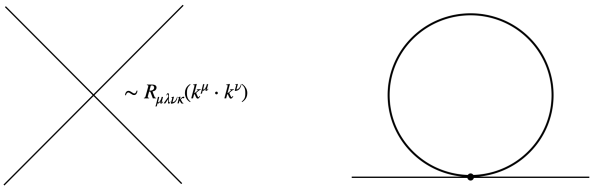

Figure 2.1: [Left]: The Feynman diagram representation of the quartic vertex interaction. [Right]: The one-loop diagram.

One recognizes Einstein's equation in vacuum with zero cosmological constant. Remember that this analysis has been done for Polyakov action, at the level of the worldsheet, and demanding scale invariance of the theory yields Einstein's vacuum equation! This means that the string propagates in Einstein vacuum backgrounds.

Gravity in string theory

General relativity in string theory is not implemented in any way. On the contrary, one starts with arbitrary string interactions on a Riemann surface, and demanding scale invariance of the worldsheet theory gives vacuum Einstein's equations

$$R_{\mu\nu} = 0. \tag{2.180}$$

In other words, we get gravity as an output and not as an input of the theory.

The problems with bosonic string theory

We see that the idea of string theory is fairly simple. The fundamental object is the string itself, usually called the fundamental string and each vibrational mode of this string corresponds to a spacetime field for a point-particle, while linear superpositions of modes can describe several fields. This idea is at the core of a unified theory, in which all contents of the theory, such as all possible fields in the standard model and gravity are produced by a single string. These fields correspond to the lowest excitation modes since the higher massive modes are too heavy to be observed at low energy.

On the other hand, bosonic string theory contains tachyons! Therefore we see that the price one has to pay with the unification idea, is a theory that at first sight seems to have no contact with the physical world whatsoever. This makes the theory unstable since the ground state of the theory itself is a tachyon resulting in negative masses, $m^2 = -4$ for closed strings and $m^2 = -1$ for open strings in units where $\alpha' = 1$ as we saw earlier in this chapter. While the instability of open strings can be naturally explained as decaying-and condensing-to closed strings the instability of the latter is much more worrisome. Being assigned to gravity and spacetime, instability of closed strings rather suggests that somehow spacetime itself should decay! To avoid this unfortunate event, one then is forced to introduce supersymmetry which indeed removes the tachyons from the spectrum of string theory.

2.5 Superstring theories and their classification

So far we have discussed the bosonic string theory, yet the most interesting theories are the ones that contain supersymmetry. The interest emerges from the hope that by adding supersymmetry in a string theory, one can actually obtain the particles, and perhaps matter that construct or are contained in our physical world, a feature that is not possible in a purely bosonic theory.

The idea of supersymmetry achieves a two-fold goal at once. On one hand, the (perturbatively) bosonic spectrum is enriched with spacetime fermions making the standard model goal appear more plausible, and on the other hand, the spacetime dimensionality becomes $D = 10$. The ultimate goal is to reproduce the standard model and the dimensionality of our spacetime $D = 4$, therefore one could argue along these lines that the compactification procedure might be easier. Indeed at first sight it seems that removing 6 dimensions would be more straightforward yet the different choices one could compactify a supersymmetric string theory are given by the classification of the compactification manifolds, the so-called Calabi-Yau manifolds whose counting still grows with the latest counting been $\mathcal{O}(10^{272000})$ [68].

The worldsheet field theory of closed strings in fact contains two sectors, the so-called left- and right-moving sectors (what we encountered earlier as α_n and $\bar{\alpha}_n$ modes). An important feature is that despite they being treated symmetrically in the simplest modes, the two sectors are in fact independent up to the zero-mode, and in principle, the corresponding CFT can be chosen to be distinct.

The action of supersymmetry associates to each boson a fermion, and conversely, through the action of a supercharge Q as

$$|\text{boson}\rangle = Q\,|\text{fermion}\rangle\,. \tag{2.181}$$

One can generalize this by considering N such supercharges which build up a class of several bosonic and fermionic partners. In $D = 4$ each, supercharge increases the spin by $1/2$, and hence there is an upper limit for the number of supersymmetries. This feature is only true in interacting theories with a finite number of fields in order to keep the spin of a class in the range where consistent actions exist, while for a free-and higher spin- theories this bound is absent. Therefore we have the following first classification

- $N_{\max} = 4$ without gravity ($-1 \leq \text{spin} \leq 1$),
- $N_{\max} = 8$ with gravity ($-2 \leq \text{spin} \leq 2$).

This classification serves as a basis to determine the maximal number of supersymmetries in other dimensions by relating them through dimensional reductions. However, we will only be interested in the worldsheet theory and the supersymmetries equipped with it. Since the CFT's of the closed-left and right-moving sectors are in principle different, we can also equip them with a different number of supercharges which we will call N_L and N_R for left and right movers respectively.

Type II superstrings have $(N_L, N_R) = (1, 1)$ and come into two classes called type IIA and type IIB according to the spacetime gravitini chiralities. This results in a distinction of the kind of Dp-branes each theory can host with p being an even number for IIA and an odd number for IIB. On the other hand, a theory is called heterotic if $N_L > N_R$ and contains only closed strings since open strings require $N_L = N_R$. For the case $N_L \neq N_R$ the two sectors

give different critical dimensions[5] and hence one has to use gauge symmetries to get rid of the additional dimensions of one of the sectors.

Gauge groups G associated with spacetime gauge bosons appear in two different ways in string theory. Firstly, as we discussed in heterotic models to balance the critical dimensions of the left-and right-moving sectors. Another possibility is to add degrees of freedom, known as the Chan-Paton indices at the ends of open strings. One of them transforms in the fundamental representation, while the other one in the anti-fundamental. This results in the modes of the open string residing in the adjoint representation, and the massless spin-1 particles become the gauge bosons of non-Abelian gauge symmetry.

One last point is the orientation of strings. Since an oriented string possesses an internal direction, there is a difference between going from left to right for open strings, or circling clockwise or anti-clockwise for closed strings. This orientation is inherited globally to the spacetime history of all strings either with interactions or not. The un-oriented string can be obtained by the $\mathbb{Z}_2$ worldsheet parity, which exchanges the left-and right-moving sectors.

We report all the supersymmetric theories and the relevant information in table 2.5. Only the bosonic string theory contains the tachyon, while all the rest supersymmetric theories are tachyon-free.

Classification of superstring theories and their content

	worldsheet susy	D	spacetime susy	gauge group	open string	oriented
bosonic	$(0,0)$	26	0	any	yes	yes/no
type I	$(1,1)$	10	$(1,0)$	SO(32)	yes	no
type IIA	$(1,1)$	10	$(1,1)$	U(1)	yes	yes
type IIB	$(1,1)$	10	$(2,0)$	none	yes	yes
heterotic SO(32)	$(1,0)$	10	$(1,0)$	SO(32)	no	yes
heterotic E_8	$(1,0)$	10	$(1,0)$	$E_8 \times E_8$	no	yes
heterotic SO(16)	$(1,0)$	10	$(0,0)$	SO(16)×SO(16)	no	yes

Table 2.3: Classification of all supertsting theories and their relevant condent

We may also make some remarks regarding the above table. Strictly speaking, the type II theories do not have an open string in their vacuum, in fact, they require a D-brane background. This might be expected if one knows that there is no gauge multiplet in $D = 10$ with $(1,1)$ or $(2,0)$ supergravities since the D-brane solutions break half of the supersymmetry. In addition, we included the bosonic case for comparison and the ultraviolet divergences beyond the tachyon which are interpreted as closed string dilaton tadpoles, cancel only for the unoriented plus closed strings with gauge group $SO(2^{13}) = SO(8192)$.

[5] Remember that the critical dimension depends on the number of supersymmetries and as we saw $D(N = 0) = 26, D(N = 1) = 10$

2.6 The simplest example of Kaluza-Klein reduction

In this brief section, we shall discuss the simplest example of Kaluza [69] and Klein [70] compactification (KK) while suppressing more sophisticated and advanced ideas to be discussed for the dimensional reduction of super Yang-Mill theory to obtain the BFSS model in Sec. 3.2.2.

As we will demonstrate, one can think of this procedure in its simplest form, as a mechanism that produces mass in a lower-dimensional spacetime by compactifying massless modes in spatial dimensions of a higher dimensional spacetime. This can be easily illustrated in three dimensions considering for example a spacetime of topology $\mathbb{R}^{1,2}$ where propagation of a massless scalar field ϕ takes place. The question we want to answer is how does this massless field appears in a two-dimensional spacetime when we compactify one spatial dimension. Therefore, we will consider a compact dimension of the topology of a circle $\mathbf{S}^1$ leading to an isomorphism $\mathbb{R}^{1,2} \cong \mathbb{R}^{1,1} \times \mathbf{S}^1$. Let us then write the Klein-Gordon equation in the non-compact space for a massless scalar field

$$\Box_3 \phi = 0 \quad , \quad \Box := \partial^a \cdot \partial_a \quad , \quad a = 1, 2, 3. \tag{2.182}$$

Under compactification, we expand the field in Fourier modes taking advantage of the symmetries associated with the topology as

$$\phi = \sum_{n=-\infty}^{\infty} \phi_n e^{ikx}, \tag{2.183}$$

with $k := n/R$. $n \in \mathbb{Z}^+$ indicates the number of (longitudinal) momentum modes running in the compact circle whose radius is given by R. In other words, each time the massless field goes around the compact circle gives one unit of momenta. Using properties of the derivative $\Box_3 = \Box_2 + \Box_{\mathbf{S}^1}$ the Klein-Gordon equation results in

$$\left(\Box_2 - \frac{n^2}{R^2} \right) \phi_n = 0. \tag{2.184}$$

We see that we started with a massless field in three dimensions and after compactifying one spatial dimension leads to a massive Klein-Gordon equation in two dimensions for the two-dimensional field ϕ_n! The mass parameter is given as the momenta $m := k = n/R$, and keeping fixed the units of momenta it is obvious that light modes and massive modes correspond to large and small R respectively.

We shall see in what follows that this simple idea is at the heart of the idea of uplifting the five 10-dimensional string theories to eleven dimensions.

2.7 Introduction to M-theory and its contents

Inevitably, superstring theories are defined only as divergent asymptotic power series in the string coupling constant g_s, which is related to the expectation value of the massless dilaton field ϕ appearing in the effective supergravity theory, $g_s = e^{\langle \phi \rangle}$. This is one of the reasons why superstring theory fails to be truly considered as a unified theory. The other reason discussed previously, is that there exist five of them. A true theory of unification should be at least unique by all means and defined non-perturbatively. M-theory is a candidate of such a theory as we shall see, yet the mystery that governs it justifies its name. The idea goes back to the work of [71] where the construction of supergravity in eleven dimensions is

discussed along the lines of Kaluza-Klein compactifications. However, this program faced two difficulties: the non-renormalizability of $D = 11$ supergravity and its failure to admit chiral compactifications. Both problems were resolved by superstring theory but the price that had to be paid was the reduction to $D = 10$ dimensions.

The fact that type IIA supergravity is the dimensional reduction of $D = 11$ supergravity [72], offered hope of a possible role for $D = 11$. In fact, since string theories were defined perturbatively in g_s the hope was that somehow the eleventh dimension was not shown in this perturbation but it should be present in a non-perturbative way. We shall see in a while how but before doing so, let us discuss how the contents of type IIA and M-theory are related. Whereas the two-form potential for $D = 10$ supergravity theories is naturally associated with a string, the three-form potential of $D = 11$ supergravity is naturally associated with a membrane [73]. Several works along this line led to the construction of $D = 11$ supermembrane action and the interpretation of $D = 11$ supergravity as an effective field theory of a hypothetical supermembrane theory [73, 74]. By simultaneous dimensional reduction of the worldvolume and the spacetime in [75] it was suggested the interpretation of the type IIA superstring as a membrane wrapped around the circular eleventh dimension. This was strengthened even more by the subsequent works [76,77] where the construction of an extreme membrane solution of $D = 11$ supergravity, reduces in $D = 10$ to the extreme string solution of type IIA supergravity. A further important development was the construction of the fivebrane solution of $D = 11$ supergravity [78] which was shown to be geodesically complete [79]. In a sense, the fivebrane is the "magnetic" dual of the "electric" membrane in $D = 11$, in agreement with the general prescription [80] that the dual of a $p-$brane is a $(D - p - 4)$-brane.

The connections between $D = 10$ and $D = 11$ supergravities still being at the classical level, it was still seemed impossible that the quantum type IIA superstring theory, with $D = 10$ as its critical dimension, could be eleven-dimensional. On the other hand, it was noted that the inclusion of wrapping modes of the fivebrane and membrane led to a spectrum of solitons identical to that of type IIA superstring if the latter includes the wrapping modes of the $D = 10$ $p-$branes carrying Ramond-Ramond charges [81].

Because of the connection between the dilaton and the string coupling, it was obvious that an improved understanding of the role of the dilaton would be crucial to any advance in non-perturbative string theory. In addition, because the type IIA supergravity is the dimensional reduction of $D = 11$ supergravity led to a Kaluza-Klein interpretation of the dilaton as a measure of the radius of the eleventh circle R_{11}

$$R_{11} = g_s\sqrt{\alpha'}. \tag{2.185}$$

This clearly demonstrates that perturbative analysis in string theory corresponds to an expansion around $R_{11} = 0$ such that the eleventh dimension is absent in perturbation theory. The correct interpretation of the tension of the supermembrane includes a factor of R_{11} only in $D = 11$ dimensions while in $D = 10$ this is absent, while at the same time the $D0-$brane mass is proportional to $1/R_{11}$ as required for its KK interpretation. We shall return to this point with more precise details when we will discuss the connection of M-theory with type IIA superstring theory.

In the strong coupling limit, where $R_{11} \to \infty$, the vacuum of the theory is eleven-dimensional Minkowski and the effective field theory is $D = 11$ supergravity. This special

moduli space of vacua is known as M-theory and if a true theory of unification exists, it should be realized in this limit where M-theory and superstring theory are realized as approximations of this unified theory.

11-dimensional supergravity

Being itself a theory of gravity there should be a graviton state, which is realized as a symmetric traceless tensor of $SO(D-2)$, the little group of a massless particle. The number of independent components of a symmetric $(D-2)\times(D-2)$ matrix is given as $\frac{1}{2}(D-1)(D-2)$ while due to tracelessness we have to subtract one state. This will result in

$$\frac{1}{2}(D-2)\times(D-2)-1=\frac{1}{2}D(D-3)=44 \tag{2.186}$$

physical degrees of freedom counting the polarization states. That this theory contains fermions, demands the usage of the vielbein formalism where one can represent the graviton with a vielbein field e_M^a. Since we are in eleven dimensions we can call it an elfbein [6]. The capital indices M run over the base-space (curved) vectors in eleven dimensions while the small indices a are used for tangent-space (flat) vectors. While the former transform non-trivially under general coordinate transformations, the latter transform non-trivially under *local* Lorentz transformations.

Being the theory itself supersymmetric, the gauge field for local supersymmetry is the gravitino field Ψ_M, which has an implicit spinor index in addition to its explicit vector index. In other words, for each index I the gravitino is a 32-component Majorana spinor. When in addition spinors are included, the little group becomes the covering of $SO(9)$, which is $Spin(9)$. From the point of view of group theory, the $Spin(9)$ Kronecker product of a vector and a spinor is $\mathbf{9}\times\mathbf{16}=\mathbf{128}+\mathbf{16}$. The construction in four dimensions gives spins $3/2$ and $1/2$ while the analysis for a free vector-spinor field carried out by Rarita and Schwinger [82], showed that there is a local gauge invariance of the form $\delta\Psi_M=\partial_M\varepsilon$ which precisely cancels the spin $1/2$ degrees of freedom giving pure spin $3/2$. This can be deduced from the fact that the kinetic term of a gravitino field Ψ_M in any dimension has the structure

$$S_{\Psi_i}\sim\int \mathrm{d}^D x\bar{\Psi}_M\Gamma^{MNP}\partial_N\Psi_P. \tag{2.187}$$

Because of the antisymmetry of the Dirac matrices Γ^{MNP}, for $\delta\Psi_I=\partial_I\varepsilon$ the kinetic term will be invariant up to a total derivative.

Similarly, the physical states for the eleven-dimensional free theory due to this local symmetry are **128**, while in the interacting case this local symmetry is identified as local supersymmetry. This amount of supersymmetry gives 32 conserved charges which form a Majorana spinor. Indeed, this is the dimension of the minimal spinor in eleven dimensions, so there could not be less supersymmetry than that in a Lorentz invariant vacuum. On the other hand, if there were more supersymmetry, the representation theory of the algebra would require the existence of massless states with spin greater than two. However, it is believed to be impossible to construct states with higher spins in Minkowski spacetime and this would require for example to find non-trivial supersymmetric theories for $D>11$.

So far we have 44 bosonic and 128 fermionic degrees of freedom. In order to be considered a successful supersymmetric theory, supergravity should somehow contain 84 more bosonic

[6] For the curious reader viel means many in German while elf means eleven.

degrees of freedom. The missing bosonic polarization states come from a rank-3 antisymmetric tensor, A_{MNP}, which can be represented as a three-form A_3. Recalling from conventional electromagnetism which contains the one-form (gauge field) A_1 these theories are invariant under gauge transformations

$$A_n \to A_n + \mathrm{d}\Lambda_{n-1}, \tag{2.188}$$

where Λ_{n-1} is a $(n-1)-$form. As it also happens in the case of electromagnetism, for antisymmetric tensor gauge fields, the gauge invariance ensures that the indices for the independent physical polarizations are transverse. In particular, in the case of a three-form in eleven dimensions one has precisely $9 \cdot 8 \cdot 7/3! = 84$ such polarizations, the ones needed to match the gravitino degrees of freedom, which is the only Fermi field of the theory.

Local Lorentz invariance, invariance under A_3 gauge transformations, and general coordinate invariance assign a lot of constraints on the form of the action. Even though we will not need the fermionic content of the action as it is common in all supergravity theories, dimensional analysis determines the latter as the constraint: the number of derivatives plus half of the number of Fermi fields equals two. Requiring also local supersymmetry as we argued previously along the lines of superstring theory, gives us $D = 11$. Then the ambiguity of the action drops to a few numerical coefficients depending on normalization and conventions. That still one can write an action taking into account all the above requirements is quite phenomenal.

The bosonic part of the eleven-dimensional supergravity action is given as

$$S_{11} = \frac{1}{16\pi G_{11}} \int \mathrm{d}^{11}x \sqrt{-G_{MN}} \left(R - \frac{1}{2}|C_4|^2 \right) - \frac{1}{6} \int A_3 \wedge C_4 \wedge C_4, \tag{2.189}$$

where R is the scalar curvature, $C_4 = \mathrm{d}A_3$ is the field strength associated with the potential A_3 and G_{11} is the eleven-dimensional Newton's constant related with Planck's length via

$$16\pi G_{11} = \frac{1}{2\pi} \left(2\pi \ell_p\right)^9 . \tag{2.190}$$

It is furthermore possible to reformulate the action in terms of the elfbein, where the part of the action (2.189) that will depend on it, is only the first term because of the structure of the metric

$$G_{MN} = \eta_{AB} e^A_M e^B_N, \tag{2.191}$$

while the last term of (2.189) which has a Chern-Simons structure is independent of the elfbein. Lastly the quantity $|C_4|^2$ is defined by the general rule

$$|C_4|^2 = \frac{1}{n!} G^{M_1 N_1} G^{M_2 N_2} \cdots G^{M_n N_n} C_{M1M2\cdots M_n} C_{N_1 N_2 \cdots N_n}. \tag{2.192}$$

M-branes

Another ingredient of M-theory is the presence of M-branes. The only accessible action we have is the one of eleven-dimensional supergravity (2.189), yet its content reveals the presence of more objects. The 3-form A_3 appearing in the action couples electrically to a two-brane and magnetically to a five-brane. The former we will be calling the membrane while the latter as the fivebrane, yet there is not available an action describing them. If their tension saturates the BPS bound (as they do), these turn out to be stable supersymmetric branes

whose tensions can be computed exactly. Thus, by focusing on BPS M-branes, it is possible to learn various facts about M-theory that go beyond the low-energy effective action expansion.

The only available scaling in M-theory is the eleven-dimensional Plank length ℓ_p. Therefore, the M-brane tensions can be determined, up to numerical coefficients by doing dimensional analysis. The exact results that relate the M-branes also with the IIA superstring theories which are furthermore confirmed by dualities are determined as

$$T_{M2} = 2\pi \left(2\pi \ell_p\right)^{-3} \quad , \quad T_{M5} = 2\pi \left(2\pi \ell_p\right)^{-6} . \tag{2.193}$$

As with all BPS branes, a M-brane can also be excited so that it is no longer a BPS, but it would be unstable and radiate until reaching the minimal BPS energy density as in (2.193).

The full eleven-dimensional supertranslation algebra that generates the above contents of M-theory is [83]

$$\{Q_\alpha, Q_\beta\} = \left(C\Gamma^M\right)_{\alpha\beta} P_M + \left(C\Gamma_{MN}\right)_{\alpha\beta} Z^{MN}_{(2)} + \left(C\Gamma_{MNPOK}\right)_{\alpha\beta} Z^{MNPOK}_{(5)}, \tag{2.194}$$

where $C = \Gamma^0$, under the choice of real Dirac matrices. The three types of charge appearing on the right-hand side are those associated with the supergraviton, the membrane, and the fivebrane, which are the three basic ingredients of M-theory. In this sense, it would be natural to regard (2.194) as the M-theory superalgebra. The total number of algebraically independent charges that could appear on the right-hand side is

$$11 + 55 + 462 = 528, \tag{2.195}$$

so that the algebra is also maximally extended.

Contents of M-theory

One can write the action of eleven-dimensional supergravity (2.189) which is the low energy limit of M-theory. The contents of the M-theory are

- the supergraviton[a],
- the membrane,
- the fivebrane,

generated by the algebra (2.194). The supergraviton is in a sense a local object while the membrane and the fivebrane are extended non-local objects with dimensionality two and five respectively. M-theory is *conjectured* to be realized as an ultraviolet completion of the effective low energy supergravity theory.

[a] In literature, the entire 256-dimensional supermultiplet is referred to as the *supergraviton*, a notion that we will adopt in what follows.

M-theory/type IIA superstring correspondence

We shall demonstrate the explicit connection, or if the reader prefers construction, of the action of ten-dimensional supergravity from eleven-dimensional supergravity. Then the conjecture in the high energy limit is that M-theory will be dual to type IIA superstring theory. Note however that there is still not a clear proof (to all orders) of the above such that it

remains a conjecture, since the high energy profile of M-theory is unknown, as it is the one of type IIA superstring while the latter is constructed also perturbatively. The difficulty is because the high energy limit of superstring theory is constructed perturbatively with perturbation parameter g_s. We recall (also below) that this parameter also controls the size of the eleventh compact dimension.

The procedure of connecting the supergravities is fairly easy, and in fact, it is one of the most straightforward connections of superstring theories and M-theory and the only relevant for this thesis. It heavily relies on the idea of dimensional reduction (KK), demonstrated in its simplest form above, in Sec. 2.6. Dimensional reduction is not equivalent to compactification, since the in the latter case one keeps all the modes in the Fourier expansions of the various fields, while in the former only the zero modes are kept in the lower dimensional theory. The compact circle has a radius given by

$$R_{11} = g_s \ell_s. \tag{2.196}$$

Then we shall demonstrate how the different eleven-dimensional field contents appear in ten dimensions.

We start with a qualitative discussion of fermionic fields. The massless fermions of type IIA supergravity consist of two Majorana-Weyl gravitinos of opposite chirality and two Majorana-Weyl dilatinos of opposite chirality. These can be obtained by taking a 32-component eleven-dimensional Majorana gravitino and dimensionally reducing it to ten dimensions. This will result in a pair of 16-component Majorana-Weyl spinors of opposite chirality. Then, the first ten components of these give the two ten-dimensional gravitinos while the eleventh component Ψ_{11} will give the two ten-dimensional dilatinos. Each type IIA dilatino has eight physical degrees of freedom because the Dirac equation implies that half of the 16 components describe independent propagating modes. Then, to match the original polarization states it is clear that each gravitino should have 56 degrees of freedom. This is indeed the dimension of the irreducible representation of $Spin(8)$, so the above discussion could be interpreted as the splitting of **128** representation of $Spin(9)$ to irreducible representations of $Spin(8)$. The preservation of physical degrees of freedom is a general feature of dimensional reduction on compact manifolds such as circles or tori.

Let us then continue with a quantitative discussion of dimensional reduction of bosonic fields, the metric and the three-form A_3. One index choice we can do here is to denote small Greek letters μ, ν referring to first ten components of the eleven-dimensional indices denoted by $M, N = 0, \cdots, 9, 11$ skipping the 10th compact dimension. The metric is decomposed as

$$G_{MN} = e^{-\frac{2\Phi}{3}} \begin{pmatrix} g_{\mu\nu} + e^{2\Phi} A_\mu A_\nu & e^{2\Phi} A_\mu \\ e^{2\Phi} A_\nu & e^{2\Phi} \end{pmatrix}, \tag{2.197}$$

where the dependence of the fields is exclusively on ten-dimensional spacetime. This decomposition allows a ten-dimensional metric $g_{\mu\nu}$, a $U(1)$ gauge field A_μ and a scalar dilaton field Φ, while the exponential factors are introduced for convenience. In addition we can write the decomposition in the following form

$$\mathrm{d}s_{11}^2 = G_{MN}\, \mathrm{d}x^M\, \mathrm{d}x^N = e^{-\frac{2\Phi}{3}} g_{\mu\nu}\, \mathrm{d}x^\mu\, \mathrm{d}x^\nu + e^{\frac{4\Phi}{3}} \left(\mathrm{d}x^{11} + A_\mu\, \mathrm{d}x^\mu\right)^2, \tag{2.198}$$

that is, given either a ten dimensional or eleven dimensional metric we can immediately either uplift it to eleven dimensions or reduce it to ten dimensions respectively.

One can also rewrite this metric decomposition in the vielbein formalism, something that we will not demonstrate here because we will not need it. In addition, the three-form in $D = 11$ decomposes to a three-form and a two-form in ten dimensions

$$A^{(11)}_{\mu\nu\rho} = A_{\mu\nu\rho}, \tag{2.199}$$

$$A^{(11)}_{\mu\nu 11} = B_{\mu\nu}, \tag{2.200}$$

with corresponding field strengths given by

$$C^{(11)}_{\mu\nu\rho\lambda} = e^{\frac{4\Phi}{3}} \left(C_{\mu\nu\rho\lambda} + 4A_{[\mu} H_{\nu\rho\lambda]} \right) = e^{\frac{4\Phi}{3}} \tilde{C}_{\mu\nu\rho\lambda}, \tag{2.201}$$

$$C^{(11)}_{\mu\nu\rho 11} = e^{\frac{\Phi}{3}} H_{\mu\nu\rho}, \tag{2.202}$$

such that upon dimensional reduction, the eleven-dimensional field strength is a combination of a four-form and a three-form field strength

$$\mathbf{C}^{(4)} = e^{\frac{4\Phi}{3}} \tilde{\mathbf{C}}(4) + e^{\frac{\Phi}{3}} \mathbf{H}^{(3)} \Gamma_{11}, \tag{2.203}$$

with Γ_{11} being the ten-dimensional chirality operator, and the forms defined by

$$\mathbf{C}^{(4)} = \frac{1}{4!} C_{MNPO} \Gamma^{MNPO}. \tag{2.204}$$

In a differential form notation the rescaled field strength is written as

$$\tilde{C}_4 = \mathrm{d}A_3 + A_1 \wedge H_3, \tag{2.205}$$

and invariance of $\tilde{C}_4$ under the $U(1)$ gauge transformation $\delta A_1 = \mathrm{d}\Lambda$ yields that the three-form potential should transform as

$$\delta A_3 = \mathrm{d}\Lambda \wedge B. \tag{2.206}$$

Then

$$\delta \tilde{C}_4 = \mathrm{d}\left(\mathrm{d}\Lambda \wedge B\right) + \mathrm{d}\Lambda \wedge H_3 = 0. \tag{2.207}$$

In addition to the above, an interesting ingredient that we will need later is the relation between the eleven-dimensional and ten-dimensional Newton's constants. To define those we need to know the string coupling, which for the case of type IIA supergravity is given as the vacuum expectation value of the dilaton

$$g_s := e^{\langle \Phi \rangle}. \tag{2.208}$$

In eleven dimensions the only length scale is the Planck length. From the metric (2.198) we can deduce that if we set a scale in the ten-dimensional theory, in a sense that if a distance in the ten-dimensional case in string units is $\mathrm{d}s_{10} = 1$ then in eleven dimensions and in Planck units is

$$\mathrm{d}s_{11} = \left(e^{-\frac{2\Phi}{3}} ds^2_{10} \right)^{\frac{1}{2}} = g_s^{-\frac{1}{3}}. \tag{2.209}$$

So we immediately see that if the string coupling is small, the Planck length is smaller than the string length. In other words, if g_s is small, the Planck length measured in eleven-dimensions is $g_s^{\frac{1}{3}}$ times smaller than the string length such that generically we have

$$\ell_p = g_s^{\frac{1}{3}} \ell_s \quad \text{with} \quad \ell_s = \sqrt{\alpha'}. \tag{2.210}$$

In ten dimensions, g_s and ℓ_s combine to give Newtons constant as

$$16\pi G_{10} = \frac{1}{2\pi}(2\pi\ell_s)^8 g_s^2. \tag{2.211}$$

Then dimensional reduction on a circle of radius R_{11} gives a relation between Newtons constant in ten and eleven dimensions

$$G_{11} = 2\pi R_{11} G_{10}. \tag{2.212}$$

We can use (2.190) with (2.211) to get a relation of R_{11} in terms of g_s

$$R_{11} = g_s^{2/3}\ell_p = g_s\ell_s. \tag{2.213}$$

The ten-dimensional bosonic action for type IIA supergravity can be obtained by integrating (2.189) over the compact coordinate. The result yields three distinct pieces for the action, a Neveu-Schwarz term, a Ramond term, and a Cern-Simons term denoted respectively as

$$S_{sugra} = S_{NS} + S_R + S_{CS}. \tag{2.214}$$

The first term has the form

$$S_{NS} = \frac{1}{2\kappa^2}\int \mathrm{d}^{10}x\sqrt{-g}e^{-2\Phi}\left(\mathcal{R} + 3\partial_\mu\Phi\partial^\mu\Phi - \frac{1}{2}|H_3|^2\right), \tag{2.215}$$

where we have defined $2\kappa^2 := (2\pi\ell_s)^8/2\pi$. This string-frame action is characterised by the exponential dependence of the dilaton in front of the curvature scalar $\mathcal{R}$. Note that we can use the relations above to show that the S_{NS} itself does not have a string coupling dependence.

The remaining two terms in the action, involve the R-R fields and are given by

$$S_R = -\frac{1}{4\kappa^2}\int \mathrm{d}^{10}x\sqrt{-g}\left(|C_2|^2 + |\tilde{C}_4|^2\right), \tag{2.216}$$

$$S_{CS} = -\frac{1}{4\kappa^2}\int B_2 \wedge C_4 \wedge C_4. \tag{2.217}$$

Let us remark on the structure of the various terms appearing in S_{sugra}. It is a general rule, that a worldsheet of Euler characteristic χ gives a contribution with a dilaton dependence $e^{\chi\Phi}$, which leads to the correct dependence on the string coupling constant. Therefore, all terms in (2.214) correspond to a spherical worldsheet with Euler characteristic $\chi = -2$. Now, this is obvious only in the first term S_{NS} while for the terms S_R and S_{CS} this can be easily achieved by doing a field redefinition with appropriate exponential powers of $e^{-\Phi}$ such that we have an overall $e^{-2\Phi}$ factor in front of the whole action S_{sugra}. Since this field redefinition is not usually adopted in the literature we shall leave the action as it is.

The low energy regimes of the two theories are related via the respective supergravities as we demonstrated above. Yet, the full correspondence should also contain the high energy limits. However, this is particularly challenging since there is no action description available in the high energy limits of both theories. The difficulty in type IIA, relies on the fact that this limit is only defined perturbatively in g_s. Therefore, one should exploit non-perturbative tools to explore this regime and make the connection with M-theory slightly more precise. D-branes are such non-perturbative objects and the lowest dimensional ones are the D0-branes. Their mass, in string frame, is given as $(\ell_s g_s)^{-1}$, so in perturbation theory around $g_s \approx 0$ it blows up.

The claim is that the mass of the D0-branes can be related with supergraviton KK modes compactified on a circle of radius R_{11}. This goes along the lines of the simple idea we demonstrated in Sec. 2.6 as we shall see. Before we continue, let us remind that the entire 256-dimensional supermultiplet is referred to as the supergraviton.

Let us then consider eleven-dimensional supergravity (or low energy M-theory), compactified on a circle. The mass of the supergraviton in eleven dimensions is zero

$$M_{11}^2 = -p_M p^M = 0 \quad , \quad M = 0, 1, \cdots, 9, 11, \tag{2.218}$$

while in ten dimensions it takes the form

$$M_{10}^2 = -p_\mu p^\mu = p_{11}^2 \quad , \quad \mu = 0, 1, \cdots, 9. \tag{2.219}$$

The momentum on the compact dimension is quantized $p_{11} = N/R_{11}$ and hence the spectrum of the ten-dimensional masses is

$$M_N^2 = \left(\frac{N}{R_{11}}\right)^2 \quad , \quad N \in \mathbb{Z}, \tag{2.220}$$

representing a tower of Kaluza-Klein modes. These states also form a short 256-dimensional supermultiplet, such that they are all BPS states, and carry N units of a conserved charge of $U(1)$ type. For $N = 1$, the correspondence with the mass of a single D0-brane requires

$$R_{11} = \ell_s g_s, \tag{2.221}$$

in agreement with the claim presented repetitively in this chapter. Indeed, this is a non-perturbative correspondence independent of the values of g_s. On the other hand, the value of g_s encodes the perturbative regime of type IIA theory. In particular, the weak coupling regime is given as $g_s \to 0$ which via (2.221) corresponds to $R_{11} \to 0$, while the strong coupling regime corresponds to the inverse limit, namely $g_s \to \infty$ which results in $R_{11} \to \infty$. The former limit corresponds strictly to a ten-dimensional theory (type IIA), while the latter to an eleven-dimensional one (M-theory). The latter is true since the compact circle opens up and all the ten spatial dimensions are treated on equal footing.

In fact, this argument can be also used to argue for the existence of bound states of D0-branes. More precisely, the N-th Kaluza-Klein excitation gives a multiplet of stable particles in ten dimensions that have N units of charge. Therefore, this multiplet can be regarded as a bound state consisting of N D0-branes, which in addition has zero-binding energy. Indeed, there is no room for any binding energy, since these states saturate a BPS bound, which means that they are as light as they are allowed to be for a state with N units of D0-brane charge. It also means that the formula (2.220) is exact to all orders in g_s.

These bound states can be related to higher dimensional structures with which they couple electrically and magnetically [65]. One important example is that D0-branes couple with a three-form forming a D2-brane consisting of D0-branes via the well-known Myers effect [84].

We close this chapter with the correspondence between contents of M-theory and contents of type IIA superstring theory given as:

M-theory/type IIA superstring correspondence

M-theory	type IIA superstring
KK photon (g_{M11})	RR gauge field A_μ
supergraviton with $p_{11} = 1/R_{11}$	D0-brane
wrapped membrane	IIA fundamental string
unwrapped membrane	IIA D2-brane
wrapped fivebrane	IIA D4-brane
unwrapped fivebrane	IIA NS5-brane

3

Matrix models and gravity

Φύσις κρύπτεσθαι φιλεί.

Heraclitus

Matrix models in string theory play an important role. Some specific models can be used to describe quantum gravity in two dimensions [85–87] (see also [88]). We will not pursue a relevant analysis here but we will say a few words about two-dimensional quantum gravity and we will focus on setting the ground such that the reader will understand the matrix models that will play a major role for this thesis. We will also spend some time on a particular matrix model that describes (and regularizes) the membrane in eleven dimensions as well as its quantization. This will be the key ingredient to proceed to the following constructions. Then we shall move to the D0-brane matrix model [53] which we will use throughout this dissertation. We shall discuss it's construction from dimensional reduction, as well as its massive deformation presented by Berestein-Maldacena-Nastase [89]. Proceeding, we shall also discuss their geometric, i.e gravity interpretation using holography and explain the parameters that control the gauge and the gravity systems as well as their interpretation in both cases.

3.1 Quantum gravity in two dimensions

It is quite well known that in the first quantization of string theory, summation over string trajectories reduces to a two-dimensional quantum gravity on the worldsheet [57, 58]. The full string action includes the Einstein-Hilbert term and a cosmological constant Λ for the wordlsheet metric. Then, this action defines a theory of D scalar fields X^μ coupled minimally[1] to the world sheet metric h_{ab}. The Euclidean action is

$$S = \int d^2\sigma \sqrt{h} \left(\frac{1}{4\pi\alpha'} h^{ab} \partial_a X^\mu \partial_b X_\mu + \frac{\phi}{4\pi} R + \Lambda \right). \tag{3.1}$$

[1] This means that we consider the partial derivative in the action.

In two dimensions, the Einstein-Hilbert action is a topological term and equals the Euler character

$$\chi = \int d^2\sigma\sqrt{h}\left(\frac{R}{4\pi}\right) = 2 - 2n, \tag{3.2}$$

with n being the genus of the worldsheet surface $\mathcal{M}_n$ which in this case is a sphere $\mathbf{S}^2$ with n handles. The parameter ϕ is related to the expectation value of the dilaton field and thus it is determined by the string coupling

$$e^{\langle\phi\rangle} = g_s. \tag{3.3}$$

Moreover, the partition function is given by

$$\mathcal{Z} = \sum_n g_s^{2n-2}\int [dX^\mu][dh_{ab}]\exp\left(-\int_{\mathcal{M}_n} d^2\sigma\sqrt{h}\left(\frac{1}{4\pi\alpha'}h^{ab}\partial_a X^\mu\partial_b X_\mu + \Lambda\right)\right). \tag{3.4}$$

There exists a lattice-like regularisation of this theory in discretising the worldsheet geometries by dynamical triangulations, meaning the replacement of the integration over the worldsheet metrics by a summation over wordlsheet triangulations [90–93]. Another approach is to collectively gauge fix and use the Fadeev-Popov method such that the description of string coordinates and the metric is given by Liouville theory [66, 94] but we will not discuss it further here and we shall demonstrate the first choice because in an analogy with field theory it does not require gauge fixing.

The easiest example to consider is the $D = 0$ theory. The latter is an empty theory of surfaces with no conformal matter and the partition function is given as

$$\mathcal{Z} = \sum_n g_s^{2n-2}\int [\mathrm{d}h_{ab}]e^{\left(-\int_{\mathcal{M}_n} d^2\sigma\sqrt{h}\Lambda\right)}. \tag{3.5}$$

This model describes fluctuations of the internal metric and topology of the zero-dimensional wordlsheet. The essence of dynamical surface triangulation is the approximation of the surface of genus n by a combination of equilateral triangles. On the plane, at each vertex i there are $N_i = 6$ such triangles meeting since there is no curvature. The latter is determined via the Ricci scalar

$$\mathcal{R}_i = 2\pi\frac{6 - N_i}{N_i}, \tag{3.6}$$

and it is non-zero whenever $N_i \neq 6$. That this is the Ricci scalar can be verified by the following argumentation: each triangulation is characterised by a number of vertices V, a number of edges E, and a number of faces F. By construction it holds hat $V = \sum_i N_i$ and topologically each edge is shared by two vertices such that $2E = V$. Moreover, each face has three edges and each edge is shared by two faces, therefore $2E = 3F$. The area of triangulation is

$$\mathcal{A} = \int \mathrm{d}^2\sigma\sqrt{h} = \sum_i \frac{N_i}{3} = \frac{V}{3} = \frac{2E}{3} = F. \tag{3.7}$$

Indeed this is the total number of triangles. In addition the Einstein-Hilbert term is

$$\int \mathrm{d}^2\sigma\sqrt{h}\mathcal{R} = \sum_i \frac{N_i}{3}2\pi\frac{6 - N_i}{N_i} = 4\pi\left(V - \frac{F}{2}\right) = 4\pi(V - E + F) = 4\pi\chi, \tag{3.8}$$

as it should be. As a result, the partition function becomes discretised and given by

$$\mathcal{Z}_d = \sum_n g_s^{2n-2}\sum_{T_n} e^{-\Lambda F}, \tag{3.9}$$

with the sum running over the dynamical triangulations T_n of the surfaces $\mathcal{M}_n$. Importantly the number of triangles F should not be predetermined such that it remains a dynamical variable, and hence in a sense, summation over T_n translates to summation over F.

The exponential dependence on F is the reason for the convergence of the sum over triangulations, at least for (sufficiently) large values of Λ. However, as Λ starts decreasing the partition function could diverge at the critical value $\Lambda = \Lambda_c$. Of crucial importance for dynamical triangulations is the fact that the total number of graphs of genus n formed by F triangles increases exponentially with F as $\exp(\Lambda_c F)/F^{-b_n}$ [91], with the exponent b_n depending on n. The continuum limit is defined as

$$\Lambda \longrightarrow \Lambda_c, \tag{3.10}$$

and it is independent of n. In this limit, the discretised statistical sum $\mathcal{Z}_d$ reproduces continuous Z_{2D}. The contribution of entropy (the number of different graphs for a given F) dominates over the exponentially suppressed energy contribution of the Boltzmann weight and, as a result, the partition function diverges in a second-order phase transition. This behaviour is reflected in the string susceptibility given by

$$f = \frac{\partial^2 \mathcal{Z}_d}{\partial \Lambda^2} = \sum_n g_s^{2n-2} \left(\Lambda - \Lambda_c\right)^{-\gamma_n} \quad , \quad \gamma_n = -b_n + 3, \tag{3.11}$$

with γ_n being the string susceptibility index. This index characterises the scaling of the entropy since as we saw it appears in the area of the triangulation F^{b_n}. For further details see the original reference [95].

3.1.1 Zero dimensional matrix model

Let us consider the cubic model with partition function

$$\mathcal{Z}_\alpha = \int [\mathrm{d}\Phi] e^{-N \operatorname{Tr} V(\Phi)} \quad , \quad V(\Phi) = \frac{1}{2}\Phi^2 - \frac{1}{3}\alpha\Phi^3, \tag{3.12}$$

where Φ are $N \times N$ Hermitian matrices, α is a constant and $[d\Phi]$ is the measure over these matrices explicitly given as

$$[\mathrm{d}\Phi] = \prod_{i>j}^{N} \mathrm{d}\mathbf{Re}\Phi_{ij}\, \mathrm{d}\mathbf{Im}\Phi_{ij} \prod_{i=1}^{N} \mathrm{d}\Phi_{ii}. \tag{3.13}$$

The propagator of this theory is arising as the simplest Gaussian matrix integral [86]

$$(2\pi)^{-N^2/2} \int \mathrm{d}\Phi e^{-\frac{N}{2} \operatorname{Tr} \Phi^2} \langle \Phi_{ij} \Phi_{kl} \rangle = \frac{1}{N} \delta_{ij} \delta_{kl}, \tag{3.14}$$

and is represented as a double line (double indices). These two lines are oriented due to Hermiticity and are opposite oriented. A typical Feynman diagram consists of an oriented two-dimensional surface formed by polygons that are bounded by index loops. Three propagators construct a three-point matrix vertex. Then one can imagine this three-point vertex to be dual to a triangle and hence the so-called dual diagram will be a dynamical triangulation of a Riemann surface.

Now by using 'tHooft [96] counting we can organise the diagrammatic expansion in powers of $\frac{1}{N}$ where each order corresponds to a different topology. We can furthermore translate the

number of vertices V, edges E and faces F to vertices, propagators and loops respectively. The vertex carries one factor of N as well as the loop while the propagator carries N^{-1} factor. Combining all leads to $N^{V-E+F} = N^{\chi} = N^{2-2n}$. From this follows that the partition function can be expanded in powers of N

$$\mathcal{Z}_\alpha = N^2 \mathcal{Z}_\alpha^{(0)} + \mathcal{Z}_\alpha^{(1)} + N^{-2}\mathcal{Z}_\alpha^{(2)} + \cdots = \sum_n N^{2-2n}\mathcal{Z}_n. \tag{3.15}$$

Therefore, also the free energy admits a $1/N$ expansion via

$$\mathcal{F}_\alpha = \log \mathcal{Z}_\alpha = \sum_n N^{2-2n}\mathcal{F}_n, \tag{3.16}$$

where $\mathcal{F}_n$ is given by the sum of the connected Feynman diagrams that can be drawn on a sphere with n handles. On the other hand, $\mathcal{Z}_\alpha$ generates both connected and disconnected diagrams.

Let us consider an arbitrary (connected) diagram Γ. Since each three-point vertex is dual to a triangle the number of three-point vertices v_Γ equals the number of triangles F. By normalising the area of each triangle to one the total area is $A = F = v_\Gamma$. This corresponds to a Feynman diagram which is proportional to α^{v_Γ} and to avoid over-counting we shall also normalise it by the order of the relevant discrete symmetry group $\mathcal{S}_\Gamma$. This discrete symmetry group of the Feynman diagram is the analog of the isometry group manifold of continuum manifolds [87].

The free energy for connected diagrams is then

$$\mathcal{F}_n = \sum_\Gamma \frac{\alpha^{v_\Gamma}}{\mathcal{S}_\Gamma}, \tag{3.17}$$

while for arbitrary diagrams

$$\mathcal{F}_\alpha = \log \mathcal{Z}_\alpha = \sum_n N^{2-2n} \sum_\Gamma \frac{\alpha^{v_\Gamma}}{\mathcal{S}_\Gamma}. \tag{3.18}$$

Using, (3.9) and assigning

$$N = e^{-\langle\phi\rangle} = \frac{1}{g_s} \quad , \quad e^{-\Lambda} = \alpha, \tag{3.19}$$

the free energy of this model equals the partition function of the dynamical triangulated model

$$\mathcal{F}_\alpha = \mathcal{Z}_d. \tag{3.20}$$

As it is expected in lattice theories, there should exist a critical value of $\alpha \to \alpha_c$ such that there is a phase transition. Moreover, since the number of degrees of freedom is setted by N, one has to consider $N \to \infty$ limit to make this transition feasible. Therefore, the continuum limit at fixed string coupling constant is a double scaling limit with $N \to \infty, \alpha \to \alpha_c$ with

$$\phi := \frac{1}{N\,(\alpha_c - \alpha)^{5/4}} = \text{fixed}, \tag{3.21}$$

where ϕ is dimensionless by the requirement that $\frac{1}{N} = \alpha^{\frac{5}{2}}$ and $[\alpha] = 2$ in length units. At this limit the partition function diverges, signalling a second order phase transition. That is because the first term of (3.15) (planar partition function) behaves as

$$\begin{aligned} \mathcal{Z}_\alpha \approx & N^2 \mathcal{Z}_\alpha^{(0)} + \cdots \\ \approx & N^2\,(\alpha_c - \alpha)^{2-\gamma} \approx -N^2 \mathcal{A}^{\gamma-2}, \end{aligned} \tag{3.22}$$

where $\mathcal{A}$ is the expectation value of the area $\mathcal{A} = \langle F \rangle = \langle v_\Gamma \rangle$ and γ is the string susceptibility.

We have used a zero-dimensional cubic matrix model to describe discretization of Riemannian surfaces resulting in a dynamical triangulation because the dual graph of the three-point vertices are triangles. It is straightforward to claim that instead of a cubic matrix model, we could have used an arbitrary polynomial potential yielding in this way to a dynamical polygonization of Riemannian surfaces.

3.1.2 One-dimensional matrix models

In the previous subsection we saw a single matrix, zero-dimensional model. This can be generalised first of all to multi matrix models and accordingly the strings described by this model are embedded in a space of greater dimensionality. In fact we can consider a (open) chain of q matrices given by the partition function

$$\mathcal{Z}_\beta = \int \prod_{i=1}^{q} [\mathrm{d}\Phi_i] \exp\left(-\sum_{i=1}^{q} N \operatorname{Tr} V(\Phi_i) + N \sum_{i=1}^{q-1} \operatorname{Tr} \Phi_i \Phi_{i+1} \right). \tag{3.23}$$

Such matrix models describe the discretization of bosonic strings in the regime $0 < D \leq 1$ since the diagrammatic expansion generates discretized surfaces where q different Φ_i states exist at the vertices [87]. In addition, it describes two-dimensional quantum gravity coupled to conformal matter in D dimensions, which recalling the unitary discrete series of conformal field theories they are labeled by an integer $m \geq 2$ which specifies the central charge c

$$c = D = 1 - \frac{6}{m(m+1)}. \tag{3.24}$$

The central charges are normalised such that the $c = 1$ case corresponds to one boson. In addition, if we couple conformal field theories with these fractional dimensions to two-dimensional gravity the approach from Liouville theory predicts a relationship between the susceptibility and the central charge of the conformal field theory given by (see for example [87])

$$\gamma_{\mathrm{str}} = \frac{1}{12}\left[D - 1 - \sqrt{(D-1)(D-25)} \right] = -\frac{1}{m}. \tag{3.25}$$

Previously we discussed the case $m = 2$ where $c = D = 0$ and $\gamma_{\mathrm{str}} = -\frac{1}{2}$ corresponding to pure gravity. From $m \geq 3$ the fractional dimensions start with the case $m = 3$ belonging to Ising model where $c = D = \frac{1}{2}$ and $\gamma_{\mathrm{str}} = -\frac{1}{3}$. The case under consideration is the limit $m \to \infty$ giving $c = D = 1$ and $\gamma_{\mathrm{str}} \to 0$.

In this limit we only have one boson, and moreover when we consider the limit $q \to \infty$ we get the description of a one-dimensional lattice where the coupling term is a nearest neighbour interaction. More precisely, the i index above may be substituted by a continuous variable t and the matrix chain with $q \to \infty$ can be regarded as a lattice regularization of the statistical sum of one-dimensional matrix model. The partition function becomes

$$\mathcal{Z}_\beta \int [\mathrm{d}\Phi(t)] \exp\left[-N \int \mathrm{d}t \left(\frac{1}{2}\dot{\Phi}^2 + \frac{m^2}{2}\Phi^2 + V_{\mathrm{int}}(\Phi) \right) \right]. \tag{3.26}$$

Each perturbation theory diagram is accompanied by its Feynman integral given as [86]

$$F_\Gamma = \int \prod_i \frac{\mathrm{d}X_i}{2m} \exp\left(-m \sum_{\langle ij \rangle} |X_i - X_j| \right) \tag{3.27}$$

in coordinate space. The variables X_i are regarded as the values of string coordinate X in diagram vertices and the summation is over links $i \to j$. In this case, the one-dimensional propagator reproduces the kinetic term for the bosonic field Φ.

Based on this demonstration a matrix model of string theory can be built up equivalent to string theory in any dimension where the matrix model lives (D) [97]. However, there are several problems arising with the obvious one being that for $D > 1$ the critical exponent γ_{str} admits an imaginary part. In addition, for greater D where one should consider the matrix field theory and not zero-dimensional integrals and quantum mechanics neither the exact solution in the limit $N \to \infty$ nor the construction of $1/N$ expansion is possible. Furthermore, the squared mass of the lowest string excitation scales like $(1 - D)$ and for $D > 1$ the ground state becomes a tachyon. Due to this infrared instability, the string worldsheet degenerates to a quasi-one-dimensional object, known in the literature as a branching polymer. Hence the bosonic string fails to describe a system with an infinite number of degrees of freedom because it cannot accommodate them.

$D = 1$ is the upper barrier for writing a consistent matrix model for string theory.

3.2 Matrix String Theory

3.2.1 A unification of matrices, membranes and D0-branes

We shall start by presenting the correspondence between matrix theory, membranes, and contents of type IIA string theory. This idea starts with the work of Hoppe, de Witt and Nikolai back in 1988 [98], where a quantization of the supermembrane was performed in terms of matrices. We shall explain this idea in detail but before doing so, let us remark that in 1988 there was no such thing as M-theory! After Witten's proposal [99], the eleven-dimensional super membrane was thought of as being part of the content of the so-called M-theory, yet in 1997 it was realised by Banks-Fischler-Shenker-Susskind [53] that there should be a connection between matrices and supermembranes. This was established even further by the work of [100] where D0-brane dynamics in the low energy limit, give the same Hamiltonian as the BFSS. We present all these connections with a graphic representation given in Fig. 3.1. As we proceed, we shall explain these ideas at a level that depends on the effort one needs to understand the connection between them.

Quantization of the membrane

Let us then start with a historically ordered presentation and let us write an action for an arbitrary p-brane in D-dimensional spacetime with metric given by $G_{MN} = (-1, 1, \cdots, 1)$ and $p < D$. As we saw and it can be easily understood a p-brane is a p-dimensional object and as such, moving in a D-dimensional spacetime will produce a (p+1)-dimensional worldvolume. Let us denote the p-brane coordinates as $\sigma^\mu, \mu = 0, \cdots, p-1, \sigma^0 = \tau$, and a local (auxiliary on word-volume) metric denoted as $h_{\mu\nu}$. The embedding maps X^M thought of as coordinates of the spacetime that hosts the p-brane can be written in terms of the latter as

$$X^M = X^M(\sigma^0, \cdots, \sigma^{p-1}), \tag{3.28}$$

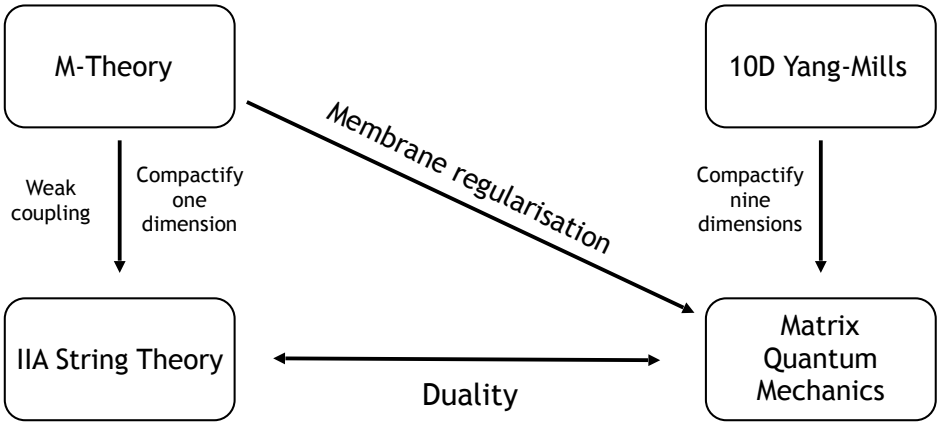

Figure 3.1: The correspondence between supersymmetric matrix quantum mechanics M-theory and type IIA string theory.

and therefore the induced metric on the p-brane will be given as the pullback

$$g_{\mu\nu} = G_{MN}\partial_\mu X^M \partial_\nu X^N. \tag{3.29}$$

The Lorentz invariant infinitesimal world-volume element is given as

$$\mathrm{d}s_p = \sqrt{-\det g_{\mu\nu}}\,\mathrm{d}^{p+1}\sigma. \tag{3.30}$$

To construct the action, we shall need one more piece of information, that is the tension of the p-brane denoted by T_p. Therefore, we end up with the quite general action

$$S_p = -T_p \int \mathrm{d}s_p = -T_p \int \sqrt{-\det g_{\mu\nu}}\,\mathrm{d}^{p+1}\sigma, \tag{3.31}$$

which describes *any* free, subject to no interactions, p-brane. The relevant case for us, is when $p = 2$ yielding a membrane with action

$$S_2 = -T_2 \int \sqrt{-\det g_{\mu\nu}}\,\mathrm{d}^3\sigma. \tag{3.32}$$

This goes along the lines of string theory analysis we did in Sec. 2.2.1, and indeed the above action is the Nambu-Goto action for a p-brane. Similarly, we can write a Polyakov action also by adding a cosmological term Λ

$$S_2 = -T_2' \int \mathrm{d}^3\sigma\sqrt{-h}\left(h^{\mu\nu}g_{\mu\nu} - \Lambda\right). \tag{3.33}$$

The difference with the Polyakov action of a string given by (2.40), is the cosmological term Λ. The latter has been introduced to make the world-volume theory scale invariant since one can check that for $p \neq 1$ there is not such invariance. In the same sense that string theory lives in $D = 10$, the supermembrane does in $D = 11$ [73, 98, 101]. Using the well-known variation

$$\delta(\sqrt{-h}) = -\frac{\sqrt{-h}h_{\mu\nu}\delta h^{\mu\nu}}{2}, \tag{3.34}$$

one can find the equation of motion for the metric $h_{\mu\nu}$

$$g_{\mu\nu} = \frac{1}{2}h_{\mu\nu}\left(h^{\mu\nu}g_{\mu\nu} - \Lambda\right). \tag{3.35}$$

By tracing with $h^{\mu\nu}$ we get

$$h^{\mu\nu}g_{\mu\nu} = 3\Lambda \Rightarrow g_{\mu\nu} = \Lambda h_{\mu\nu}, \tag{3.36}$$

and substituting this into the Nambu-Goto action above we get a relation between the tension T_2 and the new tension T_2'

$$2T_2' = \sqrt{\Lambda}T_2. \tag{3.37}$$

In fact, we see that the equations of motion for h yield the fact that the auxiliary metric h that was introduced is the physical metric $g_{\mu\nu}$ up to rescaling by Λ. The metric $h_{\mu\nu}$ being three-dimensional, contains six independent components and the membrane action is invariant under three diffeomorphisms $\sigma^\mu \to \sigma'^\mu = f^\mu(\sigma)$. This means that three components of this metric can be fixed by using three suitable gauge choices. We can restrict ourselves to positive curvature geometries where the membrane will be given as $\mathbb{R} \times \mathbf{\Sigma}$, where $\mathbf{\Sigma}$ is a Riemannian surface of fixed topology. For the case in which $\mathbf{\Sigma}$ has the topology of a sphere, one can fix the $h_{0\nu}$ components of the metric as follows

$$h_{0a} = 0, \tag{3.38}$$

$$h_{00} = -\frac{4}{v^2}\det g_{ab}. \tag{3.39}$$

In this gauge, the constraints in terms of the embeddings language become

$$G_{MN}\partial_0 X^M \partial_a X^N = 0, \tag{3.40}$$

$$G_{MN}\partial_0 X^M \partial_0 X^N = -\frac{4}{v^2}\det g_{ab}. \tag{3.41}$$

We may note that v here is a normalisation constant that will be chosen later for convenience. We then wish to write the Polyakov action in terms of the above terminology. The square root yields

$$\sqrt{-\det g_{\mu\nu}} = -\frac{v}{2}G_{MN}\partial_0 X^M \partial_0 X^N = \frac{2}{v}\det g_{ab}, \tag{3.42}$$

therefore the membrane action becomes

$$S_2 = \frac{vT_2}{4}\int \mathrm{d}^2\sigma\,\mathrm{d}\tau\left(G_{MN}\partial_0 X^M \partial_0 X^N - \frac{4}{v^2}\det g_{ab}\right). \tag{3.43}$$

It is also natural to rewrite this theory in terms of a canonical Poisson bracket on the membrane at constant τ where $\{f, g\} := \epsilon^{ab}\partial_a f \partial_b g$ with $\epsilon^{12} = 1$. The idea behind expressing this action in terms of Poisson brackets will reveal its power when we will discuss the quantization of the membrane. We also assume that the coordinates σ are such, that with

respect to the symplectic form associated to this canonical Poisson bracket the volume of the Riemann surface $\mathbf{\Sigma}$ is $\int \mathrm{d}^2\sigma = 4\pi$. In addition, when we write the pulled-back metric in a matrix notation we can easily prove that

$$\begin{aligned}\det g_{ab} =&\partial_1 X^M \partial_1 X^M \partial_2 X^N \partial_2 X^N - \partial_1 X^M \partial_2 X^M \partial_1 X^N \partial_2 X^N \\ =&\frac{1}{2}\{X^M, X^N\}\{X_M, X_N\},\end{aligned} \tag{3.44}$$

and adopting the notation $\partial_0 X^M := \dot{X}^M$ we may rewrite the action as

$$S_2 = \frac{vT_2}{4}\int \mathrm{d}^2\sigma\,\mathrm{d}\tau \left(\dot{X}^M \dot{X}_M - \frac{2}{v^2}\{X^M, X^N\}\{X_M, X_N\}\right). \tag{3.45}$$

The equations of motion for the embeddings X^M are computed to be

$$\ddot{X}^M = \frac{4}{v^2}\{\{X^M, X^N\}, X_N\}, \tag{3.46}$$

while the constraints due to the gauge freedom we used on h_{0i}, h_{00} become

$$\dot{X}^M \partial_i X^N = 0, \tag{3.47}$$

$$\dot{X}^M \dot{X}_M = -\frac{2}{v^2}\{X^M, X^N\}\{X_M, X_N\}. \tag{3.48}$$

The first constraint can be expanded to write

$$G_{MN}\{\dot{X}^M, X^N\} = \{\dot{X}^M, X_M\} = 0, \tag{3.49}$$

which later on we will be calling as the Gauß constraint.

Let us furthermore, rewrite the the above action in light-front coordinates. To this end, we introduce

$$X^{\pm} = \frac{X^0 \pm X^{D-1}}{\sqrt{2}}, \tag{3.50}$$

and choose the light-cone gauge

$$X^+(\tau, \sigma_1, \sigma_2) = \tau. \tag{3.51}$$

Note that after doing this, we reduce the number of degrees of freedom from D to $D-2$ since the X^+ embedding is constrained by X^0 and X^{D-1}. On the other hand, X^- can be computed by solving the constraints in the same way it is done for the bosonic string theory. The latter are

$$\dot{X}^- = \frac{1}{2}\dot{X}^i \dot{X}_i + \frac{1}{v^2}\{X^i, X^i\}\{X_i, X_i\}, \tag{3.52}$$

$$\partial_a X^- = \dot{X}^i \partial_a X^i. \tag{3.53}$$

We want to bring our system to a Hamiltonian formalism. To this end we may write the Lagrangian

$$\mathcal{L}_2 = \frac{vT_2}{4}\left(\dot{X}^- + \frac{1}{2}\dot{X}_a^2 - \frac{1}{v^2}\{X^a, X^b\}^2\right), \tag{3.54}$$

from which we can compute the conjugate momenta and Legendre transform to obtain the Hamiltonian. This results in

$$P^+ = \frac{\delta \mathcal{L}_2}{\delta \dot{X}^-} = \frac{vT_2}{4}, \tag{3.55}$$

$$P^a = \frac{\delta \mathcal{L}_2}{\delta \dot{X}^+} = \frac{vT_2}{4}\dot{X}^a \tag{3.56}$$

with Hamiltonian

$$\begin{aligned} H_2 =& \int \mathrm{d}^2\sigma \left(P^+ \dot{X}^- + P^a \dot{X}_a - \mathcal{L}_2 \right) \\ =& \frac{vT_2}{4} \int \mathrm{d}^2\sigma \left(\frac{1}{2}\dot{X}_a^2 + \frac{1}{v^2}\{X_a, X_b\}^2 \right). \end{aligned} \tag{3.57}$$

The remaining constraint affects the transverse degrees of freedom which furthermore satisfy the Gauß constraint

$$\{\dot{X}^i, X^i\} = 0. \tag{3.58}$$

Before we move further on, we remark on some important issues. Recalling the constraints from eq. (3.47) we see that the Hamiltonian (3.57) is written as a sum of constraints. In addition, the Gauß constraint is a first-class constraint and as such, according to Dirac's conjecture [102], it creates gauge redundancy on the theory. In particular, there is a residual invariance under time-independent area-preserving diffeomorphisms. These diffeomorphisms do not change the symplectic form and thus leave the hamiltonian of the system invariant.

This system in the light-cone reminds the case of bosonic string theory, and one would expect that the quantization will be straightforward as is usually done in string theory. However, the fact that the equations of motion are non-linear in matrices X raises some obvious obstacles to this procedure, and hence following the well-established technique as in the case of string theory is not preferred. On the other hand, a particular regularization in light-front membrane theory was found in [103] for the case where the Riemannian surface $\mathbf{\Sigma}$ has the topology of a sphere $\mathbf{S}^2$. According to this regularisation, functions on the membrane surface are mapped to $N \times N$ matrices, the Poisson bracket is replaced by the commutator, the integral gives its form to a normalised trace, differentiation is performed by adjoint commutators, and coordinates on the surface are mapped to $SU(2)$ generators J_i. The representation of the latter is the irreducible one with maximal spin $s = (N-1)/2$, while the total number of degrees of freedom N^2 equals the number of linearly independent polarization tensors T_{lm} with $l \leq N-1$, where the latter and in the large N limit they map to the usual spherical harmonics.

We can rephrase everything we mentioned above passing to the quantum theory as

Regularization map for the membrane

$$\xi_a \mapsto \frac{2}{N} J_a \quad , \quad a = 1, 2, 3, \tag{3.59}$$

$$\{\cdot, \cdot\} \mapsto -\frac{iN}{2}[\cdot, \cdot], \tag{3.60}$$

$$\mathcal{L}_i = -i\epsilon_{ijk} x^j \partial^k \mapsto [L_i, \cdot], \tag{3.61}$$

$$\int \mathrm{d}^2\sigma \{\cdot\} \mapsto \frac{4\pi}{N} \operatorname{Tr} \{\cdot\}. \tag{3.62}$$

The analysis above and the regularization map can be generalised to membranes of arbitrary topology [104]. With this new regularization procedure, the Hamiltonian of the membrane system reads

$$H_2 = \frac{1}{2\pi l_p^3} \operatorname{Tr} \left(\frac{1}{2}\dot{X}_a^2 - \frac{1}{4}[X_a, X_b]^2 \right), \tag{3.63}$$

where we have used the normalization $v = N$ and the conventions $\pi T_2 = 1/2\pi l_p^3$. The equations of motion are given as before

$$\ddot{X}^i + [[X^i, X^j], X^j] = 0, \tag{3.64}$$

which must be supplemented with the Gauß constraint

$$[\dot{X}^i, X^i] = 0. \tag{3.65}$$

The quantization procedure of such a system with finite degrees of freedom is straightforward, yet solving the system is still non-trivial due to the non-linearity of the equations of motions as we mentioned. The Gauß constraint forces the observables of the theory to be invariant under the gauge group $U(N)$, while the non-commutativity gives rise to fuzzy physics and in particular the fuzzy sphere in the context of geometric quantization [105]. In the large N limit, the fuzzy sphere approximates the continuous sphere while the group $U(N \to \infty)$ gives the area-preserving diffeomorphisms on the sphere [106]. At finite N on the other hand the matrix membrane is like a "fuzzy" membrane which is discrete and preserves the $SU(2) \cong SO(3)$ rotational symmetry of the original smooth sphere.

The supermembrane

To make contact with M-theory, and in addition, to make our membrane well-behaved it is necessary to use supersymmetry. Supersymmetric membrane theories can be constructed in 4, 5, 7, and 11 dimensions. These theories have different degrees of supersymmetry, with 2, 4, 8, 16 independent supersymmetric generators respectively. Among these, only the latter is free from anomalies in the Lorentz algebra. In the same sense that supersymmetric string theory selects $D = 10$, for the case of the supersymmetric membrane theory this becomes $D = 11$. Details about the whole construction can be found in the original work of [73], while a review is given in [107]. The so-called, local, fermionic κ-symmetry implies that the background of the theory satisfies the equations of motion of $11D$ supergravity. The construction of the supermembrane theory, follows the rules of the bosonic membrane theory upon taking care of the various extra symmetries. Using the light-cone formalism and gauge fixing one arrives in the supersymmetric Hamiltonian of the system

$$H = \frac{1}{2\pi l_p^3} \text{Tr} \left(\frac{1}{2}\dot{X}_a^2 - \frac{1}{4}[X_a, X_b]^2 + \frac{1}{2}\psi^T \gamma^a [X^a, \psi] \right), \tag{3.66}$$

where $a, b = 1, \cdots, D-2$ with $D = 11$. The γ^a are 16×16 Euclidean $SO(9)$ matrices and ψ is a 16-component Mayorana spinor of $SO(9)$. This Hamiltonian will play a major role in what follows.

One more piece of information at this level that we will encounter later is the flat direction problem or the membrane instability. A supermembrane which consists of N^2 degrees of freedom constructing its surface will result in a continuous spectrum of its energy [2] since one can think that these degrees of freedom combine collectively to describe the dynamics of membrane. A more detailed explanation about this was given in [109]. This continuous spectrum is in contrast with the string theory spectrum where the states in the Hilbert

[2] Note that this result holds only in the supersymmetric membrane since the bosonic membrane can have a discrete energy spectrum [108].

space of the string can be put into one-to-one correspondence with elementary particle-like states in the target space. That the massless particle spectrum contains a graviton and that there is a mass gap separating massless states from massive excitations are crucial for this interpretation.

An instability can be realised even for the bosonic membrane with the following reasoning: we consider two matrices

$$X_1 = \begin{pmatrix} x & 0 \\ 0 & 0 \end{pmatrix} \quad , \quad X_2 = \begin{pmatrix} 0 & y \\ y & 0 \end{pmatrix}, \tag{3.67}$$

which gives a potential term of the form $[X_1, X_2]^2 \sim x^2 y^2$. Then it is straightforward that if either $x = 0$ or $y = 0$, the other coordinate is unconstrained, giving flat directions in the moduli space of solutions to the classical equations of motion. In the quantum bosonic membrane theory, the apparent instability from the flat directions is cured because of the 0-modes of off-diagonal elements. This manifests, in the above example for instance, because if x takes a large value then y could be treated as a harmonic oscillator with a large mass. The zero-point energy of the oscillator becomes larger as x increases, giving an effective confining potential that removes the flat directions of the classical theory. This is actually the reason why in bosonic membranes we have a discrete spectrum of energies. The zero-point energies of the fermionic oscillators associated with the extra Grassmann degrees of freedom in the supersymmetric theory conspire to precisely cancel the zero-point energies of the bosonic oscillators. This cancellation gives rise to a continuous spectrum in the supersymmetric matrix theory where the instability re-emerges.

Matrix theory as a second quantization

That the membrane has a continuous spectrum can be explained if we consider a second quantised theory from the point of view of the target space. Let us consider a block diagonal matrix of the form

$$X^i = \begin{pmatrix} \bar{X}^i & 0 \\ 0 & \tilde{X}^i, \end{pmatrix} \tag{3.68}$$

where $\bar{X}$ and $\tilde{X}$ describe matrix objects. The equations of motion for these two in the case where the block diagonal derivatives also decouple from each other result in

$$\ddot{\bar{X}}^i = -\,[[\bar{X}^i, \bar{X}^j], \bar{X}^j], \tag{3.69}$$

$$\ddot{\tilde{X}}^i = -\,[[\tilde{X}^i, \tilde{X}^j], \tilde{X}^j]. \tag{3.70}$$

We can imagine now that we have two matrix objects in the diagonal with a center of mass

$$\bar{x}^i = \frac{1}{N} \operatorname{Tr} \hat{X}^i, \tag{3.71}$$

$$\tilde{x}^i = \frac{1}{N} \operatorname{Tr} \tilde{X}^i, \tag{3.72}$$

which furthermore have classically independent equations of motion. The construction where we have M of these objects is straightforward and this gives a nice, simple indication of how matrix theory can encode, even at finite N, a configuration of multiple objects. This idea constructs a second quantization theory with a continuous spectrum. We can use these two

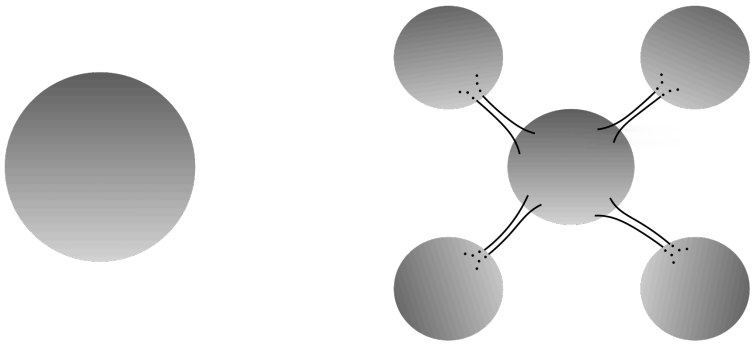

Figure 3.2: [Left]: The original membrane picture. [Right]: This can map to a multimembrane configuration connected by thin tubes. Each membrane corresponds to a diagonal block (M) of the mother matrix $X^i_{N\times N}$ and represents a different matrix object of the system.

matrix objects, which are separated but connected via a small tube, in a scenario when their relative velocity is small. Then, we can arbitrarily pull them apart from each other creating in this way arbitrarily small energy in a volume invariant way. Even if the two matrix objects have themselves discrete energy spectrum, we can expect their combined energy to have a continuous spectrum even when the size of the matrix is $N = 2$ as in the above example. This resolves the continuous energy spectrum puzzle by considering the matrix theory as a second quantised theory in the target space, a feature that is absent for string theory.

Matrix theory as a second quantised theory

It is possible to consider the block diagonal form of a mother matrix $X^i_{N\times N}$ whose diagonal entries $x^i_a, a = 1, \cdots, N$ describe different matrix objects. Then the equations of motion for these objects decouple classically, and upon quantisation this constructs a second quantised theory from the target space point of view. In the same spirit, the membrane can be mapped topologically to a multimembrane configuration connected by long and thin tubes (see Fig. 3.2).

3.2.2 The BFSS model: Dimensional reduction

We shall demonstrate how one arrives at the BFSS Lagrangian by dimensional reducing $D = 10, \mathcal{N} = 1$ super Yang-Mills theory down to one dimension [110]. It will turn out that this procedure generates a one-dimensional matrix quantum mechanics model which describes the low energy dynamics of a system of N D0-branes [111].

We therefore start in $D = 10$ dimensions with a flat metric $\eta^{MN} = (-1, +1 \cdots, +1), M, N = 0, \ldots, 9$. The Clifford algebra is 32-dimensional and given by $\{G^M, G^N\} = 2\eta^{MN}\mathbf{1}_{32}$. Having one supersymmetry, the basic object in 10 dimensions is a 32-component complex spinor $\mathcal{S}$

which satisfies the following conditions

$$\begin{cases} \tilde{\mathcal{S}} = \mathcal{S}^+ G^0 := \mathcal{S}^T C_{10} \quad , \quad \text{Majorana condition,} \\ C_{10} G^M C_{10}^{-1} = (G^M)^T \quad , \quad \text{Weyl condition,} \end{cases} \tag{3.73}$$

and also $G_{11}\mathcal{S} = \mathcal{S}$, $G_{11} = G^0 \cdots G^9$. In ten dimensions, the supersymmetric Yang-Mills action with $\mathcal{N} = 1$ is given as

$$S_{10} = \frac{1}{g^2} \int \mathrm{d}^{10}x \ \mathrm{Tr} \left[\left(-\frac{1}{4} F_{MN} F^{MN} \right) + \frac{i}{2} \left(\tilde{\mathcal{S}} G^M D_M \mathcal{S} \right) \right]. \tag{3.74}$$

We can now use the form of the covariant derivative $D_M = \partial_M - i[A_M, \cdot]$, with $A_i = X_i$ and $\partial_i = 0$ to rewrite the fermionic part of the action in the lower dimensional space. In particular it becomes

$$-\frac{1}{2} \left(\tilde{\mathcal{S}} G^M D_M \mathcal{S} \right) \Big|_{d=10} = -\frac{1}{2} \left(\tilde{\mathcal{S}} G^\mu D_\mu \mathcal{S} \right) \Big|_{p+1} + \frac{i}{2} \tilde{\mathcal{S}} G^a [X_a, \mathcal{S}]. \tag{3.75}$$

Furthermore, the reduction of the bosonic part of the action becomes

$$\left(-\frac{1}{4} F_{MN} F^{MN} \right) \Big|_{d=10} = \left(-\frac{1}{4} F_{\mu\nu} F^{\mu\nu} \right) \Big|_{p+1} + \frac{1}{4} [X_a, X_b]^2 - \frac{1}{2} (D_\mu X_a)(D^\mu X_a), \tag{3.76}$$

$$F_{\mu\nu} = \partial_\mu A_\nu - \partial_\nu A_\mu - i[A_\mu, A_\nu]. \tag{3.77}$$

The indices take the values $\mu = 0, 1, \cdots, p$ and $a = p{+}1, p{+}2, \cdots, 9$. In other words, the index μ runs on the redacted dimensions while the index a runs in the transverse dimensions. This construction is quite generic, and indeed it is a dimensional reduction of a super Yang-Mills theory on the worldvolume of N coincident Dp-branes. We will be particularly interested in the case of D0-branes, i,e $p = 0$, resulting in a super Yang-Mills theory on the worldline of N coincident D0-branes. The action on the D0-branes, is given as

$$S_1 = \frac{1}{g^2} \int \mathrm{d}t \ \mathrm{Tr} \left(\frac{1}{4} [X_I, X_j]^2 - \frac{1}{2} \left(D_0 X_I \right) \left(D^0 X_I \right) + \frac{1}{2} \tilde{\mathcal{S}} G^I [X_I, \mathcal{S}] - \frac{i}{2} \mathcal{S}^+ D_0 \mathcal{S} \right). \tag{3.78}$$

Choosing a particular representation, we can write this action in a more specific form. In particular, we will choose the representation of G in terms of Pauli (σ_i), and 10-dimensional gamma matrices (Γ) as

$$G^0 = i\sigma_2 \otimes \mathbf{1}_{16} \quad , \quad G^I = \sigma_1 \otimes \Gamma^I \quad , \quad I = 1, \cdots, 9. \tag{3.79}$$

In addition the charge conjugation decomposes as

$$C_{10} = \sigma_1 \otimes C_9, \tag{3.80}$$

and in nine dimensions it satisfies $C_9 \Gamma^I C_9^{-1} = (\Gamma^I)^T$. Using the Weyl and Majorana conditions above, the 32-component spinor $\mathcal{S}$ can be rewritten as a 16-component spinor Ψ as follows

$$\mathcal{S} = \sqrt{2} \begin{pmatrix} \Psi \\ 0 \end{pmatrix} \ , \ \Psi^+ = \Psi^T C_9. \tag{3.81}$$

Thus, the action becomes

$$S = \frac{1}{g^2} \int \mathrm{d}t \ \mathrm{Tr} \left(\frac{1}{4} [X_I, X_j]^2 - \frac{1}{2} \left(D_0 X_I \right) \left(D^0 X_I \right) + \Psi^T C_9 \Gamma^I [X_I, \Psi] - i \Psi^T C_9 D_0 \Psi \right). \tag{3.82}$$

In $D = 9$ dimensions, we can do a splitting [3] [112]

$$\Gamma^a = \begin{pmatrix} -\sigma_a \otimes \mathbf{1}_4 & 0 \\ 0 & \sigma_a \otimes \mathbf{1}_4 \end{pmatrix}, \ \Gamma^i = \begin{pmatrix} 0 & \mathbf{1}_2 \otimes \rho_i \\ \mathbf{1}_2 \otimes (\rho_i)^+ & 0 \end{pmatrix}, \ a = 1, 2, 3, \ i = 4, \cdots, 9. \tag{3.83}$$

The 4×4 matrices ρ^i satisfy

$$\rho^i \rho^{j\dagger} + \rho^j \rho^{i\dagger} = \rho^{i\dagger} \rho^j + \rho^{j\dagger} \rho^i = 2\delta^{ij} \mathbf{1}_4, \tag{3.84}$$

while the charge conjugation matrix in this representation is

$$C_9 = \begin{pmatrix} 0 & -i\sigma_2 \otimes \mathbf{1}_4 \\ i\sigma_2 \otimes \mathbf{1}_4 & 0, \end{pmatrix} \tag{3.85}$$

We can effectively work with a charge conjugation matrix C_9 which equals $\mathbf{1}_8$ resulting in $\Psi^+ = \Psi^T$, where an integration over Ψ leads to a Pfaffian $Pf(C_9\mathcal{O})$ where $\mathcal{O} = -iD_0 + \Gamma^I[X_I, \cdot]$. Therefore, the operator C_9 will drop from calculations, leading to the action

$$S = \frac{1}{g^2} \int \mathrm{d}t \ \mathrm{Tr} \left(\frac{1}{4}[X_I, X_J]^2 + \frac{1}{2}(D_0 X_I)^2 + \Psi^T \Gamma^I [X_I, \Psi] - i\Psi^T D_0 \Psi \right). \tag{3.86}$$

Now using the gauge $A_0 = 0$ such that $D_0 = \partial_0$ and the canonical momentum $P_I = \partial_0 X_I, \Pi_\alpha = -i\Psi_\alpha$ we can Legendre transform to write the Hamiltonian

$$\begin{aligned} H =& \frac{1}{g^2} \ \mathrm{Tr} \ \left(P_i \partial_o X_i + \Pi^T \partial_0 \Psi - \mathcal{L} \right) \\ =& \frac{1}{g^2} \ \mathrm{Tr} \ \left(\frac{1}{2} \dot{X}_I^2 - \frac{1}{4}[X_I, X_J]^2 - \Psi^T \Gamma^I [X_I, \Psi] \right). \end{aligned} \tag{3.87}$$

With some identifications, and reminding that we are in Lorentzian signature, this Hamiltonian is equivalent to the supermembrane regularised Hamiltonian (3.66). That two different treatments correspond to the same Hamiltonian, means that we are describing the same system with different terminology. Indeed, this discussion, includes two routes of Fig. 3.1, the supermembrane regularization and the dimensional reduction of super Yang-Mills theory, while to understand the third route, we need to add gravity in the discussion.

3.2.3 An unconventional holography

Before we discuss the gravitational side, let us also comment that the Hamiltonian (3.87), and therefore the action has a rotational $SO(9)$ global symmetry that rotates the nine matrices X_I among them. Indeed, we have nine $N \times N$ matrices X each of which corresponds to a transverse direction. The idea is the following: each $X^I_{N\times N}$, $I = 1, \cdots, 9$ matrix contains information about the behaviour of D0-branes along this specific transverse direction and taking the large N limit equivalents to taking a big matrix X which in addition means to gain more and more access to D0-brane dynamical behaviour. This is also considered to be the thermodynamic limit of the system. When we want to describe on the other hand a state corresponding to the full system containing all nine matrices we should consider a wavefunction $\mathbf{\Psi} \in \mathbb{R}^{9N^2}$ and the previously believed argument that the BFSS model can not

[3] This particular splitting will be usefull when we will be studying the BMN model, a parameter (mass) deformation of the BFSS because the indices a, i run in $SO(3)$ and $SO(6)$ part of the spacetime respectively.

be put into the traditional gauge/gravity duality gets lifted [113]. On the other hand, dealing with this kind of wavefunctions makes the problem analytically intractable. As we will see later, this unfortunate fact is avoided using simulations in (super)computers.

Let us comment a bit more here on the contents of the matrix X. The latter is obtained from the dimensional reduction of super Yang-Mills theory, which by default contains a $U(N)$ gauge symmetry. This is even more manifest when we recall that this dimensionally reduced theory describes/lives on the worldline of N coincident D0-branes, and on a world (p+1)-volume of N coincident Dp-branes we can always write a $U(N)$ gauge theory. Being a $N \times N$ matrix, X^I contains diagonal and non-diagonal elements. The interpretation is the following [99]: diagonal elements correspond to locations of D0-branes along this particular direction I while non-diagonal elements to open strings connecting them. This is a bit more manifest for D0-branes, since being 0-dimensional objects they are point-like and an open string beginning and ending on the same D0-brane becomes effectively a closed string since it attaches to the same spacetime point. Then it is understood that positions of D0-branes give a meaning of locality in this theory, while non-diagonal elements are non-local. Indeed, the $U(N)$ group indices, say i, j, are the Chan-Paton indices which can be understood as the x_{ij} entries of the matrix, whose interpretation is an open string connecting the $i-$th D0-brane with the $j-$th D0-brane. A pictorial representation is shown in Fig. 3.3 Therefore, having

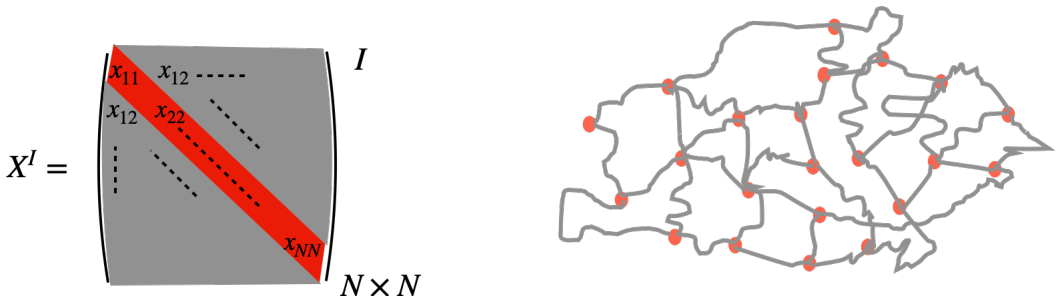

Figure 3.3: A pictorial representation of the matrix degrees of freedom discussed in the main text. The diagonal entries of the matrix correspond to positions of D0-branes while non-diagonal entries correspond to open strings between them. Having in mind that there are nine matrices since $I = 1, \cdots, 9$ these correspond to spatial positions of D0-branes along the $\mathbb{R}^{1,9}$ spacetime.

access to the values of the matrix entries, we gain information for the dynamical behaviour of the D0-branes in this I direction. It is manifest that when we consider all nine matrices we are essentially building a ten-dimensional spacetime that contains pointlike degrees of freedom, the D0-branes which are filling and moving in $\mathbb{R}^{1,9}$ spacetime. This is the intuitive idea behind the BFSS model and we shall make it more precise as the reading time progresses.

An unconventional holography for matrix models

In the usual gauge/gravity duality a d-dimensional gauge theory (for example a CFT) is dual to $(d+1)-$dimensional gravity (for example in AdS), in a sense that one can build the degrees of freedom of the gravity, known as the bulk reconstruction procedure, via the gauge field theory. This is the justification of the name holography that one finds in the holograms of the real world where a three-dimensional structure is built from two-dimensional surfaces. For matrix models we have a surprising situation. A one-dimensional matrix quantum mechanical theory constructs a theory that contains gravity in a ten-dimensional spacetime. It is indeed unconventional holography and the construction can be summarised in Fig. 3.3.

3.2.4 The IKKT model

Let us now discuss another, yet very similar, model that is closely related to BFSS, and it is known as the IKKT model (from the initials of the authors: Ishibashi-Kawai-Kitazawa-Tsuchiya) [114]. Even though the main purpose of this thesis has nothing to do with this particular model, its simple connection with BFSS makes it hard to not mention a few words. In a precise sense, the IKKT model is the T-dual of BFSS, and while it is known that compactifying type IIA superstring theory on a circle and performing T-duality one gets type IIB superstring theory, it might not be so difficult to expect that a T-dual model of BFSS should exist. On the other hand, when we perform a T-duality along the compact circle of radius R the Dp-branes moving along the compact circle become D(p-1)-branes with $\tilde{R} = \frac{\alpha'}{R}$ in the T-dual theory[4]. Therefore, the type IIB, IKKT model is a model describing D(-1)-branes, i.e D-instantons. The interpretation of this model is that there is not even a free, dynamical parameter that we can integrate over to write an action and all the dynamical parameters are encoded into the fields. The fields themselves, accompanied with the Laplace (or Dirac) operator $\mathfrak{d}$ and equipped with an algebra $\mathcal{A}$, act on a Hilbert space $\mathcal{H}$ and this spectral triplet $(\mathcal{A}, \mathfrak{d}, \mathcal{H})$ represents a commutative/non-commutative geometry according to Conne's approach [115].

Rephrasing the above statements, the geometry/spacetime in the IKKT model is believed to be precisely and entirely emergent. Now, the algebra $\mathcal{A}$ in the large N limit, is given by hermitian operators, with smooth eigenvalue distributions and bounded square traces [116]. The Dirac operator gives information about the geometry of the spacetime since it is given via background solutions while the Hilbert space is given by the adjoint representation of the gauge group $U(N)$.

The action itself has a very similar form as the one of the BFSS (3.86) upon omitting the integral

$$S_{\text{IKKT}} = \frac{1}{g^2}\,\text{Tr}\left(\frac{1}{4}[X_I, X_J][X^I, X^J] + \frac{1}{2}\Psi^T_\alpha \Gamma^I_{\alpha\beta}[X_I, \Psi^\beta]\right). \tag{3.88}$$

This model was firstly presented by IKKT [114] in 1996. This has $\mathcal{N} = 2$ supersymmetry between the Hermitian $X^I_{N\times N}$ bosonic matrices and the Hermitian $\Psi^\alpha_{N\times N}$ fermionic matrices. The relevant indices now run as $I = 1, \cdots, 10$ and $\alpha, \beta = 1, \cdots, 16$. The fermionic field/matrix

[4]This can be generalised for k compact circles with the modification that we get D(p-k)-branes. For the case of Dp-branes which are non-compact, i.e they move on the transverse directions of the compact circle we have that Dp-branes $\to$ D(p+1)-branes.

provides a Majorana-Weyl representation of $Spin(10)$ while the bosonic degrees of freedom provide a vector representation of $SO(10)$. The latter equips the action with this rotational symmetry that rotates the ten matrices among each other.

As in the case of the BFSS model, the IKKT could be also obtained as a dimensional reduction of $\mathcal{N}=1$ super Yang-Mills theory in $D=10$ dimensions. The indices I,α,β could be, in principle, generalised to describe a matrix model in arbitrary dimensionality, replacing 10 with D above.

In addition, the IIB superstring (precisely the supergravity) action can be obtained from the IKKT model in the double scaling limit $N\to\infty, g^2\to 0$ while keeping $\tilde{g}=Ng^2$ fixed.

In Euclidean signature, however, there is an important technical problem as discussed in [117–119]. In particular, the fermion Ψ is a complex Weyl spinor that satisfies the Majorana reality condition and thus it contains only in $2^{10/2-2}$ independent degrees of freedom. On the other hand, Majorana-Weyl fermions do not exist in the Euclidean signature. The absence of Majorana-Weyl fermions means that there is no $SO(D)$ invariant real cycle (reality condition) in the space of Weyl spinors, which is required to perform the integral over the complex supermanifold. The latter is spanned by the bosonic and fermionic fields and is the space on which the partition function is performed

$$Z_{\rm IKKT}=\int [\mathrm{d}X][\mathrm{d}\Psi]e^{-S_{\rm IKKT}}. \tag{3.89}$$

This integral exists in $D=10,6,4$ dimension, but the result of integration does not depend on the choice of cycle for odd variables (spinors) [117–119].

One last, yet important point for the IKKT model is that it can be put in a computer but in a different logic than that of BFSS, and important and fruitful paths are-and remain to be-discovered [120–124].

Seinberg's argument for matrix models

We return to the BFSS case. We shall demonstrate Seinberg's argument about the BFSS matrix model [125]. In a nutshell, the argument consists of the idea of lightlike and spacelike compactifications. The original proposal of BFSS [53] is that the particular matrix model with Hamiltonian (3.87) is related with M-theory in the lightcone gauge in the large N limit, while on the other hand, the finite N version demands the discrete light cone quantization (DLCQ) [126]. We shall show that a lightlike compactification of M-theory, corresponds to a spacelike compactification under certain limits. This plays a particular role to understand the finite N correspondence considered in [126]. The spatial compactification is type IIA superstring theory as we saw and therefore one can directly obtain the BFSS model as we demonstrated above.

A compactification on a lightlike circle corresponds to the identification

$$\begin{pmatrix} x^{10} \\ t \end{pmatrix} \simeq \begin{pmatrix} x^{10} \\ t \end{pmatrix} + \begin{pmatrix} \frac{R}{\sqrt{2}} \\ -\frac{R}{\sqrt{2}} \end{pmatrix}, \tag{3.90}$$

with x^{10} being a spatial compact coordinate with radius R. Now the idea is that we can consider this as the limit of a compactification on a spacelike circle with radius $R_s \ll R$

which is almost lightlike

$$\begin{pmatrix} x^{10} \\ t \end{pmatrix} \simeq \begin{pmatrix} x^{10} \\ t \end{pmatrix} + \begin{pmatrix} \sqrt{\frac{R^2}{2} + R_s^2} \\ -\frac{R}{\sqrt{2}} \end{pmatrix} \simeq \begin{pmatrix} x^{10} \\ t \end{pmatrix} + \begin{pmatrix} \frac{R}{\sqrt{2}} + \frac{R_s^2}{R\sqrt{2}} \\ -\frac{R}{\sqrt{2}} \end{pmatrix}. \tag{3.91}$$

In the limit $R_s \to 0$, the lightlike circle (3.90) is obtained from (3.91) with a boosting parameter

$$\gamma = \frac{R}{\sqrt{R^2 + 2R_s^2}} \approx 1 - \frac{R_s^2}{R^2}, \tag{3.92}$$

while the latter is related to a spatial compactification on a circle

$$\begin{pmatrix} x^{10} \\ t \end{pmatrix} \simeq \begin{pmatrix} x^{10} \\ t \end{pmatrix} + \begin{pmatrix} R_s \\ 0 \end{pmatrix}. \tag{3.93}$$

From this point one can actually relate the physical quantities of the two theories, the one compactified on the lightlike circle and the one compactified on the spatial circle upon taking into account the rescalings of the quantities and thus relate the two theories. Now, the former theory is M-theory on the lightcone gauge, while the latter is M-theory compactified on a spatial circle. From the second theory, being type IIA, we can indeed obtain the BFSS model as we saw, and therefore we can relate it with the theory compactified on the lightlike circle [125].

In addition, the lightlike momenta are given as

$$P^+ = \frac{N}{R}, \tag{3.94}$$

reminding the example of the Kaluza and Klein momentum on the compactification procedure. Being a light-like circle, the value of the radius R can be changed by a boost. Hence, to discuss physical quantities in the uncompactified theory of the lightlike compactification one cannot simply take the $R \to \infty$ limit but these are obtained by the ordered limit [5]

$$P^+ = \frac{N}{R} = \text{fixed} \quad , \quad N \to \infty \ , \ R \to \infty. \tag{3.95}$$

The compactified M-theory along the circle with R_s radius, where $R_s = \sqrt{\alpha'} g_s$ becomes ten-dimensional in the $R_s \to 0$ limit. In fact, many times this is used as the definition of the type IIA string theory. Moreover, in this limit, the low energy sector consists of D0-branes which decouple. One way to realize this is that M-theory contains also membranes and these, in general, can wrap the compactification circle, and in the boosted frame these membranes become non-local while the longitudinal modes remain local. From the type IIA point of view, the only local elements are the D0-branes. Thus, this sector decouples from the rest of the system. The $N-$th Kaluza-Klein mode corresponds to N units of momentum $\frac{1}{R_s}$ in the compact dimension, and in this case, the $U(1)$ sector is the R-R one form of type IIA. Hence, we interpret D0-charge as eleven-dimensional momentum. In this way, the arbitrary Kaluza-Klein modes on the compactified circle we described above are massless modes and are materialized as supegravitons. Being themselves massless in the eleven-dimensional spacetime, they appear in the ten-dimensional spacetime as pointlike D0-branes.

[5] We may remind that the relevant limit for the spacelike compactification is $\{N, R_s, P\} \to \infty$.

Having sketched the connection of D0-branes with supergravitons (of eleven-dimensional M-theory), one might ask what about the rest of the objects like membrane or fivebrane? As it is nicely explained in [65], there is no need to add extra degrees of freedom in the action to describe also these objects, but rather they can be described via D0-branes and T-dualities.

The procedure of boosting relates the non-relativistic ten-dimensional theory of many D0-branes (large N) with a particular frame of the M-theory, the so-called infinite momentum frame (IMF). Then the conjecture is that the dynamics of the D0-branes are in one-to-one correspondence with the Hermitian matrices of the $(0+1)-$dimensional Yang-Mills theory and they describe all the contents of M-theory in this particular IMF frame[6]. The previous statement holds when N is large. Further investigations have proposed that the relation between matrix models and M-theory should hold even at finite N [126], however since the equivalence principle breaks down for the finite N version of the theory [104], [127] it is quite unlikely that it can be related to a smooth theory of Einstein-Hilbert gravity. On the other hand, this might not be a real problem since, in the spirit of holography, finite N corrections seem to correspond to quantum corrections, and from many different approaches quantum spacetime is believed to be discrete. Thus, it is more likely that the finite N version of the model would correspond to a (quantum corrected) gravity theory on a non-commutative space. This is the famous statement that the analog of $\hbar$ in a quantum theory with N constituents is $\frac{1}{N}$, in a sense that in the large N limit, this quantum theory becomes classical.

3.3 The BMN model

A few years after the initial proposal of BFSS, it was soon realised that one can explore this duality more. The work of Berestein Maldacena and Nastase [89] was along these lines. We shall explain qualitatively the model and then proceed with details. The deformed model, which we will be calling the BMN model from now and onwards is constructed by adding terms in the action (3.86). In particular, the bosons and fermions now acquire mass terms with mass parameter μ, while the latter from the point of view of string/M-theory can be understood as compactification flux. In addition to mass terms, there is also a new term known as the Myers term which will be of particular importance for this model. Let us, therefore, write the action in a common notation in the literature

$$\begin{aligned} S =& \frac{1}{g^2}\int \mathrm{d}t\ \mathrm{Tr}\left\{\frac{1}{2}(D_t X^I)^2 + \frac{1}{2}\psi_\alpha D_t\psi^\alpha + \frac{1}{4}[X^I,X^J]^2 + \frac{1}{2}i\psi_\alpha\gamma^I_{\alpha\beta}[\psi_\beta,X^I]\right. \\ &\left. - \left[\frac{1}{2}\left(\frac{\mu}{3}\right)^2\sum_{i=1}^{3}(X^i)^2 + \frac{1}{2}\left(\frac{\mu}{6}\right)^2\sum_{a=4}^{9}(X^a)^2 + \frac{\mu}{8}\psi\gamma_{123}\psi + i\frac{\mu}{3}\sum_{i,j,k=1}^{3}X^iX^jX^k\epsilon_{ijk}\right]\right\}. \end{aligned} \tag{3.96}$$

We certainly recognise the mass terms while the Myers term is the last term in the above action. In addition, the 't Hooft coupling $\lambda = g^2N$ is dimensionful, following from dimensional analysis, and has dimension $[\lambda] = (\text{energy})^3$, which makes the theory non-conformal. For the BFSS model, one can create an effective dimensionless coupling

$$g_{\text{eff}}^{BFSS} := \frac{\lambda}{E^3}, \tag{3.97}$$

[6]Note however that the five-brane of M-theory can not be easily realized from the Matrix model [89].

and study different regimes of the model. At strong coupling, we are in the supergravity description while at weak coupling one can perform a perturbative analysis. The BMN model has already a parameter that serves as energy, and this is the mass term μ. Indeed, for this case, the effective coupling is constructed as

$$g_{\text{eff}}^{BMN} := \frac{\lambda}{\mu^3}. \tag{3.98}$$

Since μ is an independent, adjustable parameter of the system, it can be tuned to study different regimes of the theory as in the BFSS case. In addition, and together with the temperature T (serving as energy), they parametrize a two-dimensional phase space to be discussed later.

Being a dimensional reduction of super Yang-Mills theory in higher dimensions, the models (both BMN and BFSS) have an inbuilt $U(N)$ gauge symmetry. This is known in the literature as the Gauß constraint (which is essentially a first-class constraint of the system) and it is given as

$$\mathcal{G} = \frac{i}{2g^2}\left(2[D_t X^i, X_i] + 2[D_t X^a, X_a] + [\psi_\alpha, \psi_\alpha]\right) = 0. \tag{3.99}$$

The only purpose of this constraint is to force all states of the theory to be singlets under the $U(N)$ symmetry. From the point of view of string theory, this constraint makes gauge invariant states to be formed by closed strings.

The indices appearing in the action are as follows, $I, J = 1, \cdots, 9$, $\alpha, \beta = 1, \cdots, 16$ while the $\gamma^M, M = 1, \cdots, 10$ are ten-dimensional 16×16 gamma matrices which are real, symmetric, traceless and they are subpart of the 32×32 ten-dimensional gamma matrices Γ^M (see Sec. 3.2.2) . The matrix γ_{123} is given in the ten-dimensional representation by

$$\gamma_{123} = \begin{pmatrix} -i\mathbf{1}_2 \otimes \mathbf{1}_4 & 0 \\ 0 & i\mathbf{1}_2 \otimes \mathbf{1}_4 \end{pmatrix}. \tag{3.100}$$

On the other hand, ψ_a are hermitian $N \times N$ matrices, which can be expanded as $\psi_\alpha = \psi_\alpha^r T^r$, where T^r are a complete set of hermitian $N \times N$ matrices and r is a real index of the adjoint representation of $U(N)$. Therefore, ψ_a^r are $16 \times N$ Majorana fermions and the model is invariant under 16 supersymmetries. Even though the first line of (3.96) (BFSS) is invariant under a $SO(9)$ symmetry the second line obviously breaks this symmetry to $SO(9) \to SO(3) \times SO(6)$. In a sense, the degrees of freedom, or in other words the matrix constituents are living exclusively in subparts of the whole space, with the first three matrices constructing a three-dimensional space which together with the six-dimensional space created by the rest six matrices construct the desired nine-dimensional space. The dynamical behaviour of the models is analysed upon integrating over the time variable constructing the ten-dimensional spacetime of string theory.

Let us discuss the vacua of this model. Being a deformation of BFSS we expect to share some of the vacua, and indeed this is the case as we shall see. Writing the bosonic potential terms appropriately

$$\begin{aligned} V =& \frac{1}{4}[X^i, X^j] + \frac{1}{4}[X^a, X^b] - \frac{1}{2}\left(\frac{\mu}{3}\right)^2 X_i X^i - \frac{1}{2}\left(\frac{\mu}{6}\right)^2 X_a X^a - i\frac{\mu}{3} X^i X^j X^k \epsilon_{ijk} \\ =& \frac{1}{4}\left([X^i, X^j] + \frac{i\mu}{3}\epsilon_{ijk} X^k\right)^2 + \frac{1}{4}[X^a, X^b] - \frac{1}{2}\left(\frac{\mu}{6}\right)^2 X_a X^a, \end{aligned} \tag{3.101}$$

one can easily see that there are two classes of vacua:

BMN classical vacua

There is a vacuum for which

$$X^i = X^a = 0 \quad , \quad \psi_\alpha = 0, \tag{3.102}$$

and vacua for which

$$X^i = \frac{\mu}{3} J^i, J^i \in SU(2) \qquad \underline{\text{and}} \qquad X^a = 0 \quad , \quad \psi_\alpha = 0. \tag{3.103}$$

Of course, these are all classical vacua and their quantum versions are expected to add fluctuations to the classical solutions.

For completeness, we also included the fermionic matrices but they will not affect our arguments.

Let us discuss now how to understand these solutions. The first vacuum (3.102) physically means that all nine matrices are around the origin of the spacetime which classically takes zero values and it is the only vacuum appearing also in the BFSS model. We shall call them the trivial vacua (or trivial background). The second class of vacua (3.103), appears only in the BMN model and means that the matrices which construct the three-dimensional spacetime form structures which are furthermore placed at the center of the transverse six-dimensional space. The structures we are talking about are of course the fuzzy spheres [105], and we shall call them the fuzzy sphere vacua (or fuzzy sphere background). The idea behind it was explained earlier when we were talking about the spherical membrane in 3.2.1, and indeed the same structure appeared there since coordinates that describe the surface of the membrane were matrix-valued and non-commuting. This made the spherical membrane appear as a fuzzy sphere, and the same mechanism constructs fuzzy spheres in the BMN model, where the three matrices are related with the $SU(2)$ generators. Recalling our discussion in 2.7 and 3.2.1, it is not so difficult to imagine that the fuzzy spheres appearing in the BMN model as vacua are related to the membrane of M-theory since an unwrapped membrane in M-theory is interpreted as a D2-brane in type IIA string theory. If we add non-commutativity on top of the above characteristics, then a spherical, non-commutative membrane is interpreted as a spherical, non-commutative D2-brane, while the latter in addition can be constructed by polarised D0-branes via the Myers effect [128, 129].

The BMN model has a richer set of different vacua. Having fixed the size of the matrix to be N, there could be many different vacua whose number is given by partitions of N [89], i.e by a Young tableau of N rows and N columns. We can construct a big matrix which is $N \times N$, which can have block diagonal submatrices given by $N_i \times N_i$ with the index i running over the number of different blocks. Put it differently, we could have a solution which is given as

$$X^i = \frac{\mu}{3} \bigoplus_i J^i_{d_a} \quad , \quad d_a = 2j_a + 1 \quad , \quad a = 1, \cdots, N \quad , \tag{3.104}$$

with d_a being the dimensionality of the $a-$th $SU(2)$ representation. Generically, we have the following constraint

$$N = \sum_{a=1}^{N} n_a d_a, \tag{3.105}$$

with n_a being the degeneracy of the d_a-dimensional $SU(2)$ representation and for $n_a > 1$ we have n_a coincident fuzzy spheres. We shall return to this feature occasionally in what follows, but for now let us give another piece of information related with this.

The introduction of the mass term has (mainly) a two-fold role, on one hand, it gives mass to bosons and fermions and on the other hand, the flat direction problem of BFSS is lifted. The latter is the apparent fact that one of the eigenvalues of one matrix X^I could escape to infinity, and indeed this is energetically free as we discussed for the case of membrane developing spikes in 3.2.1. A more detailed discussion about this is given in [104]. Now, this problem is absent in the BMN model because the introduction of mass terms is like putting the BFSS model in a box. In particular, the first three dimensions which form the fuzzy sphere background, serve as a box due to the potential terms appearing. We refer the reader to appendix A for more details.

Note that the limit $\mu \to 0$ and assuming that there is no apparent, or non-trivial transition of the model, gives immediately the BFSS model. The deformation terms become zero and one obtains the BFSS action directly.

Motivated by the initial idea of holography and specifically AdS/CFT [130], we are instructed to ask whether the two models above have in some sense gravity duals. However, this holography or duality is in a precise sense not in anti-de Sitter space and not a conformal field theory ($\text{non}-AdS/\text{non}-CFT$) as we shall also demonstrate. In an also precise sense, as we showed in the dimensional reduction of the BFSS model, it is a one-to-ten correspondence where supersymmetric quantum mechanical models are dual to specific supergravities in ten dimensions.

3.4 The gravity duals

We expect that in the large N limit the previous models (BFSS and BMN) should have gravity duals. Even though, a priori we do not really have any reason to believe that this is the case, let us justify this statement now. As we described in Sec. 3.2.2 the dimensional reduction of super Yang-Mills where we obtained the BFSS model we claimed that each matrix contains information about D0-branes in the respective dimension. Being, dynamical and having non-zero mass they backreact into a geometry and the question is what is the metric that describes this geometry. The answer depends on the details of the theory and the generic case has been introduced in [49] for generic Dp-branes. Here we will concentrate in the case for which $p = 0$ but let us give more general details to understand the picture later.

To describe the gravitation dual it is usual to consider the quantum mechanical system of N D0-branes in the limit

$$U := \frac{r}{\alpha'} = \text{fixed} \quad , \quad g_{YM}^2 = \frac{1}{4\pi^2}\frac{g_s}{\alpha'^{3/2}} = \text{fixed} \ , \ \alpha' \to 0. \tag{3.106}$$

U plays the role of a specific scale of the theory and can be regarded as e.g an energy scale. We will imagine that when we refer to U effectively we are referring to the energy. The t' Hooft coupling $\lambda = g_{YM}^2 N$ controls the regimes of the duality. Large λ means that we are in the gravity region while for small λ we are in the quantum mechanical region. In the limit

(3.106) the gravity description becomes near extremal [7]

$$\begin{aligned}\frac{\mathrm{d}s^2}{\alpha'} =& H(U)_p^{\frac{1}{2}}\,\mathrm{d}x_{||_p}^2 + H(U)_p^{-\frac{1}{2}}\,\mathrm{d}U^2 + \sqrt{d_p\lambda}U^{\frac{p-3}{2}}\,\mathrm{d}\Omega_{8-p}^2,\\ d_p =& 2^{7-2p}\pi^{\frac{9-3p}{2}}\Gamma\left(\frac{7-p}{2}\right),\\ e^{\phi} =& (2\pi)^{2-p}g_{YM}^2\left(\frac{\lambda d_p}{U^{7-p}}\right)^{\frac{3-p}{4}} \sim \frac{g_{\text{eff}}^{\frac{7-p}{2}}}{N}.\end{aligned} \tag{3.107}$$

As g_{eff} here it is the dimensionless effective coupling

$$g_{\text{eff}} \simeq \frac{\lambda}{U^{3-p}}. \tag{3.108}$$

The limit in which ten-dimensional, supergravity description is valid is given by

$$1 \ll g_{\text{eff}}^2 \ll N^{\frac{4}{7-p}}, \tag{3.109}$$

which emanates from the restriction that the dilaton should be small and the curvature of the metric (3.107) should also be small, the latter given by

$$\text{and} \quad \frac{\mathcal{R}_{\text{eff}}^2}{\alpha'} \simeq \frac{1}{g_{\text{eff}}} \sim \sqrt{\frac{U^{3-p}}{\lambda}} \ll 1. \tag{3.110}$$

This g_{eff} above is actually the same as (3.97) or (3.98) if we set $p = 0$. Therefore, we can use equally well g_{eff} without ambiguity to describe the three different regions that characterise the system with parameter the energy (or temperature). These are:

- For high energies we are in the perturbative regime of the quantum mechanical system with perturbation parameter(s) (3.97) or (3.98).
- For small energies we are in the supergravity regime where we expect a black-zero geometry of type IIA supergravity to be valid
- For even lower energies we are entering the M-theory region and the matrix black holes.

Let us elaborate more on these three different regimes giving more attention to the low energy limit. The perturbative regime is more or less better understood and more familiar to all readers since the constituents of the matrices, i.e the D0-branes can be regarded as harmonic oscillators. We shall see explicit examples later on but for now let us change to the more interesting regimes, namely the low energy regimes.

At low energies the system is characterised by the zero-brane geometry as we explain in the next subsection and this geometry is well understood. It is the ideal test example to compare the duality between the matrix quantum mechanics side with the gravity side, since some analytic results are possible from both sides. Going to even lower energies we are entering the M-theory region and the matrix black holes as we see pictorially in Fig. 3.4. This region is less understood but let us now explain the physical meaning of the straight line separating the type IIA description and the M-theory description.

[7] We report the full construction here leaving p generic, which denotes the dimensions of the Dp-brane, but later we will be interested mainly in $p = 0$.

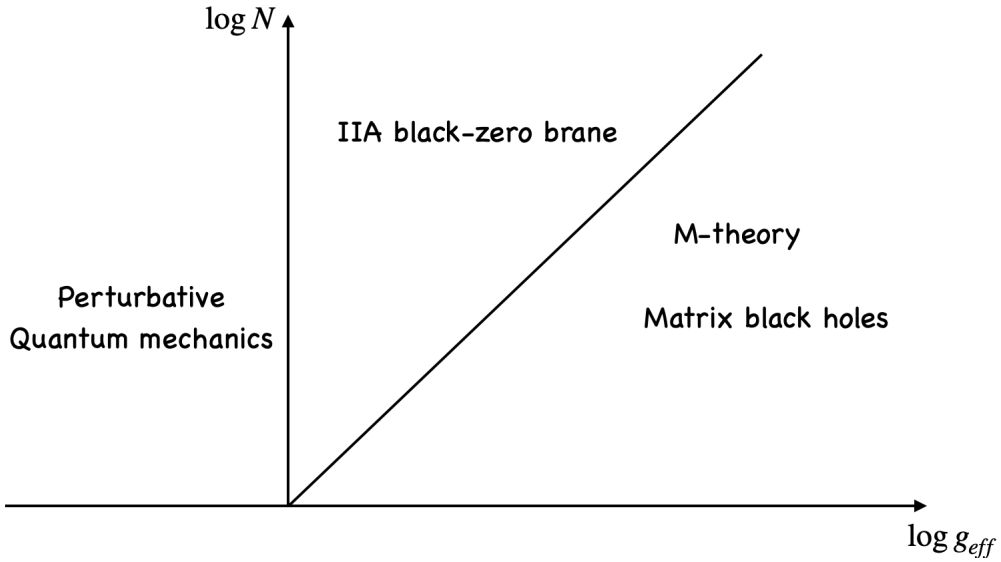

Figure 3.4: A cartoon of the coupling and N controlling the different regimes of the matrix quantum mechanics based on [49]. To better understand the idea we remind the effective couplings given in equations (3.97) and (3.98). For very high energies we are in the perturbative quantum mechanics region. Lowering the energy we are entering the type IIA supergravity description which is a black-zero brane. Lowering even more the energy we are entering the M-theory and matrix black holes region.

To this end, let as recall that the eleventh dimension distinguishing M-theory from type IIA is related with the string coupling (see e.g (2.221)). The latter is also related with the dilaton, such that via the dilaton we have an effective string coupling related with the radius of the compact dimension via (2.221). When the dilaton is large, then keeping N and λ fixed, via (3.108) we have

$$\frac{R_{11}}{\sqrt{\alpha'}} = g_s \simeq e^{\phi} \simeq \frac{g_{\text{eff}}^{7/2}}{N} \overset{E\to 0}{\gg} 1. \tag{3.111}$$

Effectively the eleventh dimension starts opening up. As we explained below (2.221) this procedure results in eleven dimensions, hence as one goes to very low energies one has to lift the description up to eleven dimensions.

Therefore, we can imagine a scenario such that we keep N fixed and tune the energy E. Then from Fig. 3.4 this corresponds to movements along the horizontal axis $\log g_{\text{eff}}$ and taking the limit $E \to 0$ we are moving towards the $+$ direction entering the M-theory region. For every fixed N there is a point along the straight line which transfers us from the type IIA description to M-theory description. This transition though is not the only fate of the system, because it could be the case that a Gregory-Laflamme type [131] of transition happens along the eleventh compact dimension. Let us not forger after all that, if this duality is correct, the matrix model describes a geometry boosted along the compact x_{11} direction. When the latter is small, we usually neglect it and from the ten-dimensional point of view it appears as the system of N D0-branes (see next section). Having a black hole-like construction along a compact dimension and changing the radius of this black hole-like geometry or the size of the compact circle can lead to a Gregory-Laflamme instability when a black string along the compact dimension collapses to a localised black hole along the same dimension or the other

way around [131]. We leave a more detailed discussion about this for section 4.2.

We will present now an argument, based on [37] where a black hole collapses to a black string and vice versa. We will need this to understand the results of section 4.3. Let us imagine that we have a black hole (BH) and a black string (BS) in the same spacetime dimensions $D = d + 1$ and we want to write their entropies [37]

$$S_{\rm BH} \sim \left(\frac{\ell_P^9}{L^d}\right)^{\frac{1}{D-3}} M^{\frac{D-2}{D-3}}, \tag{3.112}$$

$$S_{\rm BS} \sim N^{-\frac{1}{D-4}} \left(\frac{\ell_P^9}{L^d}\right)^{\frac{1}{D-4}} M^{\frac{D-2}{D-4}}, \tag{3.113}$$

where L^d is the volume of the compact space (here a $\mathbf{S}^1$). Now if we assume that $S_{\rm BH} = S_{\rm BS}$ for some choice of the mass M and the boost[8] N, then by changing N one system is entropically favoured from the other because it has greater entropy. Increasing N and keeping M fixed, causes the black hole to have greater entropy, while decreasing N causes the black string to be entropically favoured.

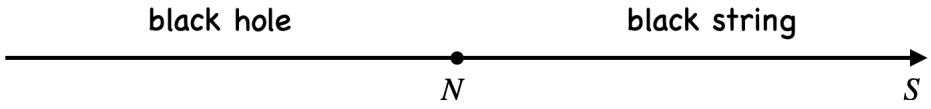

Figure 3.5: A cartoon of the matrix model describing the gravitational system. For larger N the gravitational system behaves as a black string while for smaller N it behaves as a black hole-like geometry.

3.4.1 Weak and strong notions of holography for matrix models

As we saw earlier and we start to understand the matrix model holography is slightly different that the usual one [2]. The first hint was when we discussed the interpretation of matrices in terms of D0-branes around Fig. 3.3. The difference is due to the fact that N not only does serve as the number of degrees of freedom of the system (e.g the number of D0-branes) but also is the parameter that controls the boost given, e.g via (3.94). The holographic bound due to Bekenstein [7] states that at most one information bit per Planck area is allowed. This was in fact one of the main motivations for matrix models. Let us now define the weak and strong forms of holographic principles for matrix models.

Weak holographic principle for matrix models

The dynamics of the theory is encoded in lower-dimensional surfaces. For the conventional holography, it is usually the case that the dynamics is encoded in a co-dimension two surface $(D-2)$ and one of the primary examples is that of a black hole. Indeed, this notion of holography seems possible for matrix models due to the matrix nature of these models where the degrees of freedom (dynamics) are encoded into the matrices themselves. We discussed this interesting unconventional holography around Fig. 3.3.

[8] We remind that the relation between the momentum P^+ and N, $P^+ = \frac{N}{R_{11}}$.

Strong holographic principle for matrix models

Upon boost, the physical size of objects increases. This is the case because as we increase the boost, we increase N and hence necessarily the physical size of any object should expand to accommodate the degrees of freedom respecting Bekenstein's bound. This strong holography is not a necessary consequence of the weak holography nor it is needed to account for the black hole entropy.

3.4.2 The gravity dual of BFSS

The BFSS model has only one kind of classical solution, namely when all matrices are zero $X^I = 0$. Such a configuration means that all D0-branes are at position zero in the respective dimension, and having an orthogonal coordinate system that is spanned by $x^i, i = 1, \cdots, 9$ we get the intuition that we have N D0-branes sitting on the origin of this coordinate system. In other words, we have N coincident D0-branes sitting on top of each other at the center of a 10-dimensional spacetime. On the other hand, D-branes are solutions extended in p dimensions of the supergravity action and N-coincident D-branes backreact in a geometry described by a specific metric. For the case of D0-branes, we have a point-like source that resembles a black hole. Indeed there exists a metric that belongs to the type IIA supergravity family of solutions and describes the geometry of N-coincident D0-branes, which is known by the name of type IIA black zero brane, and its near extremal limit has the following form

$$\begin{aligned}
\frac{\mathrm{d}s^2}{\alpha'} =& -\frac{f(r)r^{7/2}}{\sqrt{\lambda d_0}}\,\mathrm{d}t^2 + \sqrt{\frac{\lambda d_0}{r^3}}\left(\frac{1}{f(r)r^2}\,\mathrm{d}r^2 + \mathrm{d}\Omega_8^2\right)\\
e^{\phi} =& \frac{4\pi^2}{d_0}\frac{1}{N}\left(\frac{\lambda d_0}{r^3}\right)^{7/4}\\
A_t =& \frac{N}{4\pi^2}\frac{r^7}{\lambda^2 d_0}\\
f(r) =& 1 - \frac{r_0^7}{r^7} \quad , \quad d_0 := 240\pi^5 \quad , \quad \lambda := g_{YM}^2 N.
\end{aligned} \tag{3.114}$$

The limit at which we are studying this metric is given by keeping λ fixed while taking the limit $N \to \infty$ and $\alpha' \to 0$. This is the standard limit that allows for a supergravity description of the field theory (or in our case the quantum mechanics theory) [130]. The position r_0 dictates the location of the horizon, which is related with the temperature $T := 1/\beta$ via

$$T = \frac{7}{4\pi\sqrt{\lambda d_0}} r_0^{\frac{5}{2}}. \tag{3.115}$$

In addition to this, the geometry has an effective curvature radius given by the radius of S^8

$$\frac{\mathcal{R}_{eff}^2}{\alpha'} = \sqrt{\frac{\lambda d_0}{r^3}}. \tag{3.116}$$

The above metric (3.114) is valid whenever the following apply. First of all, we are restricting ourselves to the low temperature (low energy) limit of the theory, secondly, we should have small curvature given by the inverse of (3.116) and thirdly the string coupling (the dilaton) should be small, such that the supergravity description is valid. The second restriction results

in $r \lesssim \lambda^{1/3}$ where the dimensions of the radius are the same as the energy's $[r] = [E]$. Using this we can construct an effective dimensionless coupling in terms of r (see equation (3.108))

$$g_{\text{eff}}^{(r)} = \frac{\lambda}{r^3}. \tag{3.117}$$

This r behaves like an energy scale of the theory and demands the curvature to be very small resulting in $T^3 \ll \lambda$. The third restriction results in $\frac{\lambda}{T^3} \ll N^{10/7}$, such that the validity parameter is transferred to the temperature (keeping λ fixed)

$$1 \ll \frac{\lambda}{T^3} \ll N^{10/7}, \tag{3.118}$$

and hence, when we take the large N limit, we solely control the system with the temperature T [9].

The energy density is given by [49]

$$E = \frac{r_0^7}{a_0 g_{YM}^4}, \quad a_p = \frac{\Gamma\left(\frac{9-p}{2}\right) 2^{11-2p} \pi^{\frac{13-3p}{2}}}{(9-p)} \quad \overset{p\to 0}{\longrightarrow} \quad a_0 = 11.63 \frac{2^{11}\pi^{\frac{13}{2}}}{9}, \tag{3.119}$$

which is the same as the energy in Yang-Mills theory. Substituting everything in the initial equation we get

$$E \simeq 7.41 N^2 \lambda^{-\frac{3}{5}} T^{\frac{14}{5}}. \tag{3.120}$$

The entropy of the black zero-brane is given as

$$S = \frac{8\pi\sqrt{d_0 N}}{9 a_0^{\frac{5}{14}}} g_{YM}^{-\frac{3}{7}} E^{9/14} \simeq 11.53 \lambda^{-\frac{3}{5}} T^{\frac{9}{5}}. \tag{3.121}$$

These quantities are a good estimate at very low temperatures, while when we turn the temperature on we expect higher order corrections coming from stringy (α') effects to be important. These have been studied in [132] and are of the form

$$\frac{E}{N^2} = \frac{\left(a_0 T^{\frac{14}{5}} + a_1 T^{\frac{23}{5}} + a_2 T^{\frac{29}{5}} + a_3 T^{\frac{32}{5}} + \cdots\right)}{N^0} + \frac{\left(b_0 T^{\frac{2}{5}} + b_1 T^{\frac{11}{5}} + \cdots\right)}{N^2} + \mathcal{O}\left(\frac{1}{N^4}\right). \tag{3.122}$$

The second term includes finite N corrections. We shall return to discuss about this in more depth in section 4.5.

When we consider the geometry without a horizon and we zoom in near the singularity, we can rewrite the metric as

$$\begin{aligned} \frac{\mathrm{d}s^2}{\alpha'} =& - H(r)^{-\frac{1}{2}} \,\mathrm{d}t^2 + H(r)^{\frac{1}{2}} \left(\mathrm{d}r^2 + r^2 \,\mathrm{d}\Omega_8^2\right), \\ H(r) :=& \frac{r_0^7}{r^7} \quad , \quad r_0^7 := \lambda d_0. \end{aligned} \tag{3.123}$$

Then, a change of variables

$$r \mapsto z = \frac{2}{5}\left(\frac{r_0}{r}\right)^{\frac{5}{2}}, \tag{3.124}$$

$$t \mapsto \tilde{t} = \frac{t}{r_0}, \tag{3.125}$$

[9] We assume that the parameter N, usually taken to infinity, is much larger than any other parameter of the system.

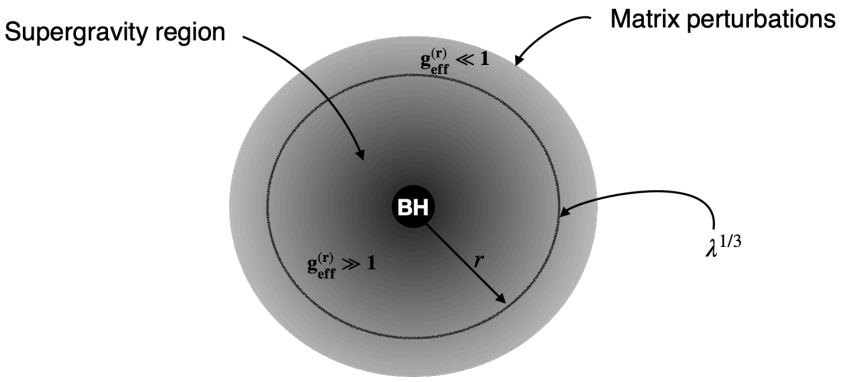

Figure 3.6: The duality between the type IIA metric (3.114) and the BFSS matrix model. This figure is based on [133] and summarises the situation between the validity of the gravity sector and the regimes of the model. The g_{eff} that controls the regimes is given via (3.97), while when $r \to \lambda^{\frac{1}{3}}$ the gravity description ends to be trustable. Of course the boundary and the bulk do not live in the same spacetime.

results in the metric

$$\frac{\mathrm{d}s^2}{\alpha'} = \left(\frac{2}{5}z\right)^{\frac{3}{5}} \left[r_0^2 \left(\frac{2}{5}\right)^{-2} \left(\frac{-dt^2 + \mathrm{d}z^2}{z^2}\right) + r_0^2 \, \mathrm{d}\Omega_8^2\right], \tag{3.126}$$

which is conformally equivalent to $AdS_2 \times S^8$ spacetime. We shall not discuss more about this feature but we shall concentrate more on (3.114), the reason being that we are outside the conventional AdS/CFT regime.

One of the most striking results of testing the gauge/gravity duality was obtained in [134] where the equation (3.122) was put in test and the coefficients a_i, b_i compared with analytic calculations. It was shown, to good precision, that the matrix model can reproduce the equation (3.120) as we go to low temperatures, while for larger temperatures α' corrections start contributing. After that, a more clever manipulation of the BMN model to specific parameter regimes allowed us to go even to lower temperatures and make the test even better. We shall discuss this more in 4.5.

In addition, quantum (finite N) and α' corrections were computed analytically for the thermodynamic gravitational quantities in [132] and were tested against simulations in [135] verifying the analytic results. A series of simulations have been performed [134–150] to test various analytic results [53, 132, 133, 151, 152].

3.4.3 The gravity dual of BMN

The gravity dual of BMN should be a deformed version of (3.114). However, since it is technically more sophisticated we shall choose a different route for this discussion. Based on the original claim of BMN [89], the matrix model is equivalent to M-theory on a Penrose limit. An excellent introduction for these metric limits can be found in [153], while this feature seems to hold for general spacetimes [154]. These metrics are also known as pp-waves from plane-fronted waves with parallel rays and are abbreviations that we will adopt in what follows.

Supergravity in eleven dimensions admits four types of maximally supersymmetric solutions [155]

1. The 11d Minkowski space and its toroidal compactification
2. The $AdS_7 \times S^4$ metric (the fivebrane)
3. The $AdS_4 \times S^7$ metric (the membrane)
4. The Kowalski-Glickman solution [155] which is a pp-wave metric.

In fact, all maximally supersymmetric pp-wave geometries can arise as Penrose limits of $AdS_p \times S^q$ spaces [156]. Indeed a powerful theorem of Penrose states that near null geodesics (along which the light rays travel) any spacetime becomes a pp-wave spacetime such that any metric near a null geodesic becomes a pp-wave metric [154]. We shall show this explicitly for the plane wave limit of a specific maximally supersymmetric spacetime in eleven dimensions.

The starting point of the BMN bulk dual is a metric in M-theory, which is either $AdS_4 \times S^7$ or $AdS_7 \times S^4$. Since the Penrose limits of these metrics are identical, a priori there is no distinction at this level. Let us therefore *construct* a metric, by choosing e.g to write down $AdS_4 \times S^7$ explicitly and then take the Penrose limit of this. We shall split the metric as follows

$$AdS_4: \quad \mathrm{d}s_1^2 = R^2\left(-\cosh^2\rho\,\mathrm{d}t^2 + \mathrm{d}\rho^2 + \sinh^2\rho\,\mathrm{d}\Omega_2^2\right), \tag{3.127}$$

$$S^7: \quad \mathrm{d}s_2^2 = R^2\left(\cos^2\theta\,\mathrm{d}\phi^2 + \mathrm{d}\theta^2 + \sin^2\theta\,\mathrm{d}\Omega_5^2\right). \tag{3.128}$$

In order to take the Penrose limit, we shall introduce new coordinates as follows

$$r = R\sinh\rho \quad , \quad y = R\sin\theta \tag{3.129}$$

$$x^+ = \frac{t}{\mu} \quad , \quad x^- = \mu R^2(t-\phi). \tag{3.130}$$

Here, μ is an arbitrary mass scale introduced so that $x^\pm$ have dimensions of length. The Penrose limit intuitively means that we are blowing up the neighbourhood of a light-like trajectory in the spacetime in such a way as to obtain a non-trivial limit. At this case specifically, we want to focus on a neighbourhood of a point moving around a circumference of the sphere with the speed of light. Blowing up, means that we are considering the infinite-radius limit $R \to \infty$, holding $r, y, x^\pm$ fixed. Substituting into $\mathrm{d}s_1^2$ and $\mathrm{d}s_2^2$ and taking the Penrose limit we obtain

$$\begin{aligned}\mathrm{d}s^2 &= \mathrm{d}s_1^2 + \mathrm{d}s_2^2, \\ &= -2\,\mathrm{d}x^+\,\mathrm{d}x^- - \mu^2\left(r^2+y^2\right)\left(\mathrm{d}x^+\right)^2 + dr^2 + r^2\,\mathrm{d}\Omega_2^2 + \mathrm{d}y^2 + y^2\,\mathrm{d}\Omega_5^2.\end{aligned} \tag{3.131}$$

This can be rewritten as

$$\mathrm{d}s^2 = -2\,\mathrm{d}x^+\,\mathrm{d}x^- + g_{++}(x^i, x^a)\left(\mathrm{d}x^+\right)^2 + \sum_{i=1}^{3}\left(\mathrm{d}x^i\right)^2 + \sum_{a=4}^{9}\left(\mathrm{d}x^a\right)^2, \tag{3.132}$$

with $g_{++}(x^i, x^a)$ given as

$$g_{++}(x^i, x^a) = -\mu^2\left[\left(\frac{r_3}{3}\right)^2 + \left(\frac{r_6}{6}\right)^2\right] \tag{3.133}$$

The coordinate r_3 is the radial coordinate for the first three coordinates while r_6 is the radial coordinate for the rest six. The transverse symmetry is then $SO(3) \times SO(6)$. In addition, the M-theory four-form field strength is related with the parameter μ as

$$Q_4 \sim \mu \, \mathrm{d}x^+ \wedge \mathrm{d}x^1 \wedge \mathrm{d}x^2 \wedge \mathrm{d}x^3. \tag{3.134}$$

This is the gravity dual of the BMN model from the M-theory perspective. It is known in the literature as the plane wave limit of M-theory, or pp-wave.

Let us now see how this metric is connected with type IIA supergravity. In the usual arguments, discrete-light-cone-quantum (DLCQ) M-theory with N units of momentum is obtained by taking a compactification of M-theory on a spacelike circle of radius R_s and then performing a boost with parameter

$$\gamma = \sqrt{\frac{R^2}{R_s} + 1}, \tag{3.135}$$

while taking the limit $R_s \to 0$ we obtain a theory on a lightlike circle of finite radius R. This is Seiberg's argument that relates lightlike and spacelike compactifications since the boosting parameter above matches (3.92). As we discussed earlier, the unboosted frame with a spacelike circle of radius R_s, is equivalent to type IIA string theory with N D0-branes in a limit $g_s \to 0, \alpha' \to 0$ in which only the low energy D0-brane degrees of freedom remain. In order to find exact agreement between the lightcone energies in the DLCQ and the D0-brane descriptions, we must rescale the dimensionful quantities of the system (κ) as $\kappa \to (R/R_s)\kappa$.

We can yet use another change of coordinates, the so-called lightcone gauge defined via

$$x^{\pm} = \frac{t \pm x^{10}}{\sqrt{2}}, \tag{3.136}$$

and rewrite the metric in this gauge. Noting that we can absorb the $1/2$ factor appearing into the four form field, we can write the metric as

$$\mathrm{d}s^2 = -(1 + \frac{Q^2}{4}) \, \mathrm{d}t^2 + (1 - \frac{Q^2}{4})(\mathrm{d}x^{10})^2 - \frac{Q^2}{2} \, \mathrm{d}t \, \mathrm{d}x^{10} + \sum_{i=1}^{3} \left(\mathrm{d}x^i\right)^2 + \sum_{a=4}^{9} (\mathrm{d}x^a)^2 \,, \tag{3.137}$$

where Q is defined as [10]

$$Q^2 := \frac{\mu^2}{9} \sum_{i=1}^{3} (X^i)^2 + \frac{\mu^2}{36} \sum_{a=4}^{9} (X^a)^2, \tag{3.138}$$

and the 4-form field is given as

$$Q_{123(10)} = -Q_{0123} = \frac{\mu}{2}. \tag{3.139}$$

We note again that this metric is written in the unboosted frame. Since any pp-wave metric is boost covariant [153], the effect of boosting is simply to rescale the deformation parameter μ. Furthermore, we note that this background is a general background that should capture general (but symmetry reduced) features of the BMN matrix model and in fact, one can derive the action of the BMN from this metric [157], [100].

[10] This μ is the deformation parameter, and it is the same that appears in the matrix model.

To transfer these data in ten dimensions, we recall that the most general metric which is invariant under translations in the 10-th direction (X^{10}) is of the form [56]

$$\mathrm{d}s_{11}^2 = G^{10}_{\mu\nu}(x^\mu)\,\mathrm{d}x^\mu\,\mathrm{d}x^\nu + e^{2\rho(x^\mu)}\left(\mathrm{d}x + A_\nu(x^\mu)\,\mathrm{d}x^\nu\right)^2, \quad \mu,\nu = 0,\cdots,9. \tag{3.140}$$

A_μ is the R-R form and comparing with (3.137) we immediately see that

$$\begin{aligned} e^{2\rho} =& 1 - \frac{Q^2}{4}, \\ A_0 =& \frac{-\frac{Q^2}{4}}{1-\frac{Q^2}{4}},\ A_i = 0 \\ G^{10}_{00} =& -e^{-2\rho}\ ,\ G^{10}_{0i} = 0\ ,\ G^{10}_{ij} = \delta_{ij}. \end{aligned} \tag{3.141}$$

The dilaton field Φ is defined through

$$\rho = \frac{2\Phi}{3}, \tag{3.142}$$

and solving for the ten dimensional metric we get

$$\mathrm{d}s_{10}^2 = -\left(1-\frac{Q^2}{4}\right)^{-\frac{1}{2}} dt^2 + \left(1-\frac{Q^2}{4}\right)^{\frac{1}{2}}\left[\sum_{i=1}^{3}\left(\mathrm{d}x^i\right)^2 + \sum_{a=4}^{9}\left(\mathrm{d}x^a\right)^2\right], \tag{3.143}$$

with

$$Q_{0123} = -\frac{\mu}{2}, \quad H_{123} = \frac{\mu}{2}. \tag{3.144}$$

H_{123} is the NS-NS three-form potential and Q_{0123} is the RR three-form field strength. These form fields arise from the distribution of the eleven-dimensional three form into the R-R and NS-NS sector. Geometrically, this corresponds to distributing the eleven-dimensional momentum into different geometric configurations of D-branes. When having in mind a single D0-brane we will consider only the one-form since it is the one that the D0-brane is naturally coupled with.

Even thought the eleven-dimensional metric is flat, the ten dimensional metric is not. This can be easily seen by a direct calculation of the Ricci scalar of (3.143) resulting in

$$\begin{aligned} \mathcal{R} =& \frac{\mu^2}{5184}\left(1-\frac{Q^2}{4}\right)^{-\frac{5}{2}}\sum_{i=1}^{3}\sum_{a=4}^{9}\Big\{\mu^2(7-Q^2)\Big[(X^a)^4 + 48(X^a)^2(X^i+3) + 96X^a(X^i)^2 \\ &+ 16(X^i)^2\left((X^i)^2+36\right)\Big] + 252\left[(X^a)^2 + 4\left((X^i)^2+9\right)\right]Q \\ &- 63\left[(X^a)^2 + 4\left((X^i)^2+9\right)\right]Q^3\Big\}. \end{aligned} \tag{3.145}$$

The supergravity geometry can be trusted only when $\mathcal{R} \ll 1 \Rightarrow \frac{Q^2}{4} \ll 1$. We see μ appearing in the Ricci scalar, hinting that a deformation parameter in eleven dimensions could appear as curvature in ten-dimensional geometries. This is not so difficult to understand because the effect of boosting the system deforms also the metric since μ appears also in the latter. Trivially when $\mu \to 0$ we have $\mathcal{R} \to 0$.

The above discussion sketches the connection of the BMN model with supergravity theories, however, the story complicates considerably when we try to think precise details

from the type IIA and M-theory point of view [158–161]. In fact, we want to give a geometric interpretation of the vacua of BMN discussed earlier in Sec. 3.3. In the original paper [89], it was claimed that the trivial vacuum of BMN model (3.102) corresponds to a fivebrane from the point of view of M-theory. This idea was explored in [160] and in what follows we shall give the ten-dimensional interpretation of the problem.

In general we should look for a ten-dimensional supergravity solution that preserves half of the supersymmetries[11] and respects the $SO(3) \times SO(6)$ symmetry. This can be motivated from the specific form of the action of the matrix model (3.96) since the gravity solution should respect the symmetries therein. The most general solution in type IIA string theory that meets these conditions is [160]

$$\mathrm{d}s_{10}^2 = \left(\frac{\ddot{V}-2\dot{V}}{-V''}\right)^{\frac{1}{2}} \left[-\frac{4\ddot{V}}{\ddot{V}-2\dot{V}}\,\mathrm{d}t^2 - \frac{2V''}{\dot{V}}\left(\mathrm{d}\rho^2+\mathrm{d}z^2\right) + 4\,\mathrm{d}\Omega_5^2 + 2\frac{V''\dot{V}}{\Delta}\,\mathrm{d}\Omega_2^2\right], \tag{3.146}$$

with

$$\begin{aligned} &\dot{V} = \rho\partial_\rho V\ ,\ \ddot{V} = \rho\partial_\rho(\dot{V}),\quad V' = \partial_z V\ ,\ V'' = \partial_z^2 V,\\ &\Delta = \left(\ddot{V}-2\dot{V}\right)V'' - \left(\dot{V}'\right)^2, \end{aligned}$$

and the dilaton and NS-NS and R-R forms are given as

$$\begin{aligned} e^{4\phi} &= \tfrac{4(2\dot{V}-\ddot{V})^3}{V''\dot{V}^2\Delta^2}, \qquad B_2 = 2\left(\frac{\dot{V}\dot{V}'}{\Delta}+\rho\right)\mathrm{d}\Omega_2\\ A_1 &= \tfrac{2\dot{V}\dot{V}'}{2\dot{V}-\ddot{V}}\,\mathrm{d}t, \qquad A_3 = -\frac{4\dot{V}^2V''}{\Delta}\,\mathrm{d}t\wedge\mathrm{d}\Omega_2. \end{aligned} \tag{3.147}$$

The function $V(z,\rho)$ appearing in (3.146) can be interpreted as a potential that sources different brane (NS5, D2, D0) configurations, and depending on the specific form of this function one realizes different gravity solutions, which correspond to different vacua in the matrix model side. We are interested in the bosonic sector of BMN because in that case, we can write a metric ansatz that respects the symmetries. In the BMN case, we see from (3.96) that these symmetries are $\mathbb{R}\times SO(3)\times SO(6)$. The first of these implies that there is a Killing vector associated with translations of the time coordinate. The second implies that we can imagine a sector of the spacetime to consist of a S^2 sphere[12] while the third is the existence of a S^5 sphere, on which the bosonic generators act. Thus one can analyse solutions in eleven dimensions by using only three variables, x_1, x_2, y which satisfy the Toda equation in three dimensions [158, 160]

$$\left(\partial_{x_1}^2+\partial_{x_2}^2\right)V + \partial_y^2 V = 0. \tag{3.148}$$

Here y is used as a combination of the radii of S^2 and S^5 respectively, $y = r_2 r_5^2$. Exploiting the translational invariance under one coordinate (x_1), and after changing variables $(x_2, y)\mapsto(\rho, z)$ one can recast this equation to the Laplace equation in a three dimensional space [158]

$$\frac{1}{\rho}\partial_\rho\left(\rho\partial_\rho V\right) + \partial_z^2 V = 0. \tag{3.149}$$

[11] This is because the BMN model has various BPS states, but here in particular we are interested for 1/2-BPS states.

[12] Actually it is more appropriate to say that we have a non-commutative sphere since the coordinates that are assigned to $SU(2)$ generators do not commute.

We note that this three-dimensional space is *not* a sub-part of the ten-dimensional one but rather casts this problem to an electrostatic problem in a three-dimensional space, where all gravity solutions are classified by ρ, z. Here, both ρ and z are radial coordinates, and hence one can actually think of them as two different scales of the theory. The former captures the size of fivebranes and the latter the positions of the conducting disks, which are actually being set by the five-branes. If one, naively tries to find a gravity solution by just plugging in a solution of (3.149) into the metric (3.146) will end up with singular gravity solutions [158, 160, 162]. To avoid this, one has to impose boundary conditions at $y = 0$ such that $V(y = 0) = 0$. This condition corresponds to regimes with vanishing radii of S^2 or S^5. Indeed S^2 shrinks for constant z in the z, ρ space (see figure 3.7), and S^5 shrinks between two nearby disks in the $\rho = 0$ line.

In the case of the BMN model, the asymptotic expansion is decomposed into two parts the first of which represents the electrostatic potential and the second one the specific electrostatic configuration imposed by the boundary conditions. In other words, this means that one can specify the solution but not necessarily to which vacuum corresponds since in principle there will be vacua with the same boundary conditions. The first non-trivial potential is [162]

$$V \approx \rho^2 z - \frac{2}{3} z^3 + \mathcal{P} \frac{z}{(\rho^2 + z^2)^{\frac{3}{2}}}, \tag{3.150}$$

where $\mathcal{P}$ is a short of dipole sub-leading correction, produced by the conducting disks and their images with respect to the infinite conducting plane at $z = 0$. Its value is given by

$$\mathcal{P} = 2 \sum_i z_i \mathcal{Q}_i \sim N, \tag{3.151}$$

where i runs over the various disks, $\mathcal{Q}_i$ is the charge of the i-th disk and N is the total number of D0-branes.[13] The number of D0-branes can be extracted from the particular configurations of the disks. Suppose for example that there is a finite set of conducting disks at positions $z_i = \frac{\pi}{2} N_5^i$, with radii R_i and charge $\mathcal{Q}_i = \frac{\pi^2}{8} N_2^i$. Then the disks are sourced by the NS5-branes in the background, with the charge $\mathcal{Q}_i$ being associated with the D2-brane charges. In this sense, one can write the number of D0-branes as

$$N = \sum_k \left(\sum_{k<l} N_5^l \right) N_2^k. \tag{3.152}$$

Comparing this equation with the constraint (3.105), we see that N_2^k is related to the copies (degeneracy) of dimension $N_5^l = (2j+1)$ irreducible $SU(2)$ representations, giving a geometric realization of the situation of the matrix model. The case $N_2^k > 1$ corresponds to concentric spheres and due to non-commutativity, they are actually concentric fuzzy spheres. From this relation, one can construct all possible vacua of BMN. Indeed, let us consider the case where we have one fivebrane ($N_5^1 = 1$), then from the constraint (3.152) we see that $N = 1 \cdot N_2^1$, meaning that we have a single fivebrane with charge $Q_1 = \frac{\pi^2}{8} N$.

Let us clarify a bit more the situation here. In order to do this let us decode what we wrote above. We claimed that the trivial vacuum (the no-fuzzy sphere vacuum) is given when $N_5^1 = 1$, and since the latter is related with the dimensionality of the respective $SU(2)$

[13] Here we make contact with the introductory remarks, where we stated that all the contents can be reconstructed from D0-branes.

representation $N_5^1 = 2j+1$, it simply means that $j=0$. Indeed, for $j=0$ we can think that we have "fuzzy spheres" of radius $r \simeq \frac{j}{3} = 0$, which can be interpreted as D0-branes. Then we have a one-dimensional representation and $Q_1 = N_2^1 = N$ D0-branes. In other words we have N copies of the trivial $j=0$ representation. In a sense, the spherical D2-branes here are interpreted as zero-radius spherical branes which indeed are the D0-branes.

To get the trivial vacuum metric one has to perform a two-step procedure. The first step is to plug (3.150) into the metric (3.146) and expand at large ρ and z. Then change coordinates as

$$r^2 = 16\left(\rho^2 + z^2\right), \tag{3.153}$$

and in the large r limit the metric approximates the near horizon geometry of N coincident D0-branes [160]

$$\mathrm{d}s^2 \approx -H(r)^{-\frac{1}{2}}\,\mathrm{d}t^2 + H(r)^{\frac{1}{2}}\left(\mathrm{d}r^2 + r^2\,\mathrm{d}\Omega_8^2\right) + \cdots, \quad H(r) \approx \frac{d_0 \cdot 15\mathcal{P}}{r^7}. \tag{3.154}$$

However, the large r region is a bit subtle. Let us try to clarify some possible issues. The supergravity description is valid when $g_{\text{eff}} = \frac{\lambda}{\mu^3} \gg 1$ while for $g_{\text{eff}} \ll 1$ we can trust perturbative calculations in matrix model. The first case corresponds to a region between the black hole (i.e near the core of the geometry in Fig. 3.6) and $r \sim \lambda^{1/3}$, while the second case is near the boundary. However, near the boundary, the supergravity solution is not valid since the curvature is high. Hence, we are in a region when r is large but nevertheless not near the boundary. It is large with respect to the core of the geometry and a good estimate would be $r \lesssim \lambda^{1/3}$. Here we can imagine the following situation, we suppose that we want to study the system in a specific energy scale (i.e fixed λ), where we can trust the supergravity solution for the trivial vacuum. This amounts to

$$r \gg 1 \quad \underline{\text{and}} \quad g_{\text{eff}} = \frac{\lambda}{\mu^3} \gg 1, \quad \lambda = \text{fixed}, \ \Rightarrow \mu \to 0. \tag{3.155}$$

Thus, to leading order, we recover the case of the BFSS model and this is what the metric (3.154) indicates.

Let us try now to calculate the potential and the force for a D0-brane in this trivial vacuum geometry. Specifically, we have in mind the following scenario, we are in the small μ range such that g_{eff} is large and hence the deformation does not change the geometry by much. We can also imagine that we can take one of the D0-branes and move it away from the core of the geometry, namely the bunch of D0-branes that form this geometry. Then the question we want to answer is if we would measure the gravitational force that this D0-brane feels from the geometry what would be its behaviour?

To achieve this, we need to write down a metric and then use the Dirac-Born-Infeld action for the D0-brane. In addition, to find an acceptable metric, we start by substituting (3.150) into (3.146) and then take the trivial vacuum limit (3.155) after performing the variable change as in (3.153). The idea is that we fix $z \sim \mathcal{O}(1)$ while $\rho \gg 1$ which is dictated from the

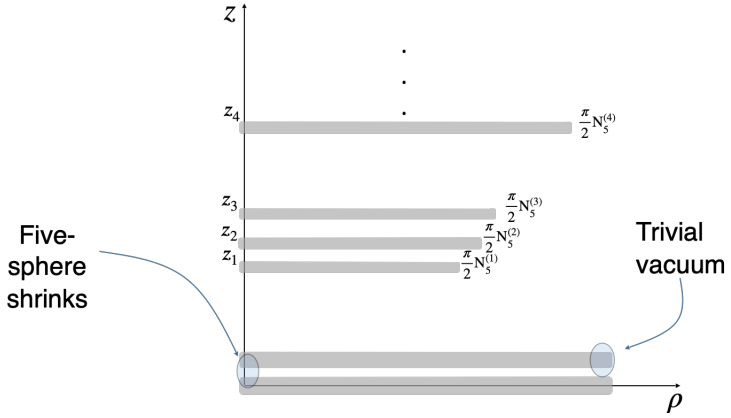

Figure 3.7: A cartoon of the $z-\rho$ plane. Constant z lines indicate that the two-sphere shrinks while the five-sphere shrinks in the region between nearby disks near $\rho = 0$. We have a conducting disk at $z = 0$ which extends to infinity in the ρ direction.

electrostatic analysis we did above. Carrying out carefully this procedure, results in a metric

$$\mathrm{d}s^2 = -H(r)^{-\frac{1}{2}}\,\mathrm{d}t^2 + 16H(r)^{\frac{1}{2}}\left(\mathrm{d}z^2 + z^2\,\mathrm{d}\Omega_2^2\right) + H(r)^{\frac{1}{2}}\left(\mathrm{d}r^2 + r^2\,\mathrm{d}\Omega_5^2\right), \tag{3.156}$$

$$H(r) := \frac{256\cdot 15\mathcal{P}}{r^7}, \tag{3.157}$$

$$e^{\phi} = \left(\frac{2^{12}15\mathcal{P}}{r^7}\right)^{\frac{3}{4}}, \tag{3.158}$$

$$A_1(r) = -\frac{r^7}{2^{11}15\mathcal{P}} - \frac{7z^2r^5}{2^8 15\mathcal{P}} - \frac{7z^4r^3}{192\mathcal{P}} + \frac{r^2}{10} - \frac{7z^6r}{24\mathcal{P}} - \frac{12z^2}{5}. \tag{3.159}$$

We kept only leading terms both in the expression of dilaton and the one-form. We kept explicitly the z dependence but one should remember that is of order one. The next correction to the dilaton is of order $\mathcal{O}(r^{-29/4})$ and in the large r limit we neglect it. In the same limit, the contribution of the R-R one form is significant. Furthermore, we see that in this limit and for the same energy scale (or the same radius r), the effective curvature of the five-sphere, which in string units is the inverse of $\frac{\mathcal{R}_5^2}{\alpha'} = H(r)^{\frac{1}{2}}r^2$, is much smaller than the one of the two-sphere, which is the inverse of $\frac{\mathcal{R}_2^2}{\alpha'} = H(r)^{\frac{1}{2}}z^2$. This means that curvature corrections coming from the two-sphere part of the metric may become important when compared with the ones of the five-sphere [160] [14]. We also note that the validity of the supergravity solution is when the dilaton is not too large and when the effective curvature of the five-sphere is not too big. Recalling that $\mathcal{P} \sim N$ this translates to the range

$$N^{\frac{1}{7}} \ll r \ll N^{\frac{1}{3}}. \tag{3.160}$$

[14] Both r and z here are energy scales, and this condition reflects the fact that we push the regime of validity of the metric to its boundary. In [133], and based on [163] was argued that the breaking of Einstein supergravity starts at scales $\lambda^{1/3}$.

The Ricci scalar of (3.156), can be computed and it is given by

$$\mathcal{R} = -\frac{49\sqrt{\frac{3}{5}}}{64}\left(\frac{r^3}{\mathcal{P}}\right)^{\frac{1}{2}}. \tag{3.161}$$

We see that in the regime where the supergravity description for the trivial vacuum is a good approximation, the spacetime is almost flat provided that N is large.
Lastly, before moving to finite temperature, it worths mentioning that after a coordinate rescalling and transformation, namely

$$z \to \frac{\zeta}{4} \quad , \quad R \to \frac{2}{5}\frac{r_0^{5/2}}{r^{5/2}}, \quad r_0^7 := 256 \cdot 15\mathcal{P}, \quad t \to r_0 t \tag{3.162}$$

the metric (3.156) becomes

$$\mathrm{d}s^2 = \left(\frac{2/5}{R}\right)^{7/5} r_0^2 \left[-\mathrm{d}t^2 + \mathrm{d}R^2 + \left(\frac{5}{2}\right)^2 R^2\,\mathrm{d}\Omega_5^2\right] + \left(\frac{R}{2/5}\right)^{7/5}\left(\mathrm{d}\zeta^2 + \zeta^2\,\mathrm{d}\Omega_2^2\right). \tag{3.163}$$

Therefore, the near horizon limit of the vacuum solution is conformally equivalent to $AdS_2 \times S^5 \times S^3$. It is possible that in the limit $N \sim \mathcal{P} \gg 1, r \gg 1$ such that taking the limit $R \to 0$ and keeping ζ small and fixed, the geometries decouple. We may also note that taking $R \gg 1$ amounts $r \ll 1$ but then the construction limit of the metric would be spoiled and the metric will not be consistent any more, hence it is not possible to arbitrary grow the size of $\mathbf{S}^5$ and describe it with this metric.

This comment however will not really affect our arguments nor will enter any calculation, hence we included it for the sake of completeness.

Let us move to finite temperature now. All we have to do is to write down a metric with a horizon. At finite temperature the BMN model has 1/2- BPS states [89], [157] and we should expect the force to be present even if we consider fermions. Eventually, we would also like to make some contact with the quantum mechanics side. Quantum mechanics however is a subsector of the SYM theory. So let us be a bit more illustrative here. The parameters that control the vacua of the BMN are the number[15] of D2-branes N_2, the number of D5-branes N_5, and the number of D0-branes N_0, whose relation is given as [160]

$$N_2 = \frac{N_0}{N_5}. \tag{3.164}$$

As we showed, the trivial vacuum is dictated by $N_5 = 1, N_2 = N_0 = N$, with N being the copies of the trivial ($j = 0$) representation. This particular configuration is given in figure 3.7. Then to understand the situation in the gauge theory side, we need to convert the gravity data to gauge data. By direct comparison with [49], we find the following [160][16]

$$\rho_0^4 = \frac{\pi^4}{2} g_{YM}^2 N \quad , \quad d = \frac{\pi}{2} N_5 = \frac{\pi}{2} \quad , \quad \mathcal{Q} = \frac{\rho_0^4}{8} \quad , \quad \mathcal{P} = 2d\ \mathcal{Q} = \frac{\pi^5 g_{YM}^2\ N}{16}. \tag{3.165}$$

Here, ρ_0 is the value of the coordinate ρ on which the tip of the conducting disk lies (see figure 3.7), d is the charge of N_5 which is also the distance between the two conducting disks.

[15] To be more precise it is the charge of the various D-branes.

[16] We suppress μ dependence here by setting $\mu = 1$ but we can restore it by using $g_{\text{eff}} = \frac{\lambda}{\mu^3}$ and by dimensional analysis, e.g $[\mu] = 1,\ [\lambda] = 3$ in units of energy.

Before we continue, let us mention that the size of the fivesphere is much larger than the one of S^2, which can be seen from the radius of the fivesphere [160]

$$\frac{R^2_{S^5}}{\alpha'} = 4\pi\rho_0 = 4\pi\left(\frac{\lambda}{2\mu^3}\right)^{\frac{1}{4}} \ , \ g_{\text{eff}} = \frac{\lambda}{\mu^3} \gg 1, \tag{3.166}$$

where in the second equality we putted back μ to have the correct dimensions.

We investigate the gravity solution at finite temperature T in this vacuum. We can write an ansatz for the finite T black brane solution as

$$\begin{aligned}
\frac{ds^2_T}{\alpha'} &= -H(r)^{-\frac{1}{2}} f(r) dt^2 + 16 H(r)^{\frac{1}{2}} \left(dz^2 + z^2 d\Omega_2^2\right) + H(r)^{\frac{1}{2}} \left(\frac{dr^2}{f(r)} + r^2 d\Omega_5^2\right), \\
H(r) &= \frac{\lambda d_0}{r^7} \ , \ e^{\phi} = 2^6 \left(\frac{\lambda 15\pi^5}{r^7}\right)^{\frac{3}{4}} \ , \ f(r) = 1 - \frac{r_0^7}{r^7}, \\
A_1(r) &= -\frac{r^7}{1920\pi^5\lambda} - \frac{7r^5}{960\pi^3\lambda} - \frac{7r^3}{192\pi\lambda} + \frac{r^2}{10} - \frac{7\pi r}{96\lambda} - \frac{3\pi^2}{5}, \\
d_0 &\equiv 240\pi^5 \ , \ \lambda \equiv g^2_{YM} N \ , \ g_s = 4\pi^2 l_s^3 \frac{\lambda}{N} \ , \ G_{10} = g_s^2 l_s^8,
\end{aligned} \tag{3.167}$$

and the horizon is located at $r = r_0$, with r_0 representing the thermal energy scale. The horizon is dictated only from the radius r, but we have implicitly assigned $r^7 := r_5^5 \cdot z^2$, where r_5, z are the radii of the 5-sphere and 2-sphere respectively. In other words, we have merged the two scales into one. We can proceed even more and pick a scale for the S^2 part such that we measure everything at this fixed scale. We will choose this to be $z = \frac{\pi}{2} r_2$ and this was already implemented in the expressions of (3.167) by setting $r_2 = 1$, but not in the metric itself. This choice reflects the trivial vacuum limit discussed above and will be used when we calculate the force.

Demanding the curvature of the spheres to be not too large we get the condition

$$r \lesssim \lambda^{1/3} \qquad \text{both from } S^5 \text{ and } S^2. \tag{3.168}$$

There is also one more constraint coming by demanding that the dilaton is not too large on the horizon which results in

$$\lambda\beta^3 \lesssim N^{10/7}, \tag{3.169}$$

and for sufficiently large N compared to the combination $\lambda\beta^3$ the last condition is automatically satisfied.

From this metric one can extract the temperature via the surface gravity

$$T = \frac{7 r_0^{5/2}}{4\pi\sqrt{\lambda d_0}} \tag{3.170}$$

Now we can proceed calculating the force based on the discussion in appendix B. By writing the DBI action we can read off the potential

$$V_{D_0}(r) = T_0 \left[e^{-\phi} H(r)^{-\frac{1}{4}} f(r)^{\frac{1}{2}} - A_1(r)\right]. \tag{3.171}$$

Now we have everything we need to calculate the potential and the force. Let us state that without loss of generality, we can consider the dilaton from (3.114) since we expect the two

metrics to be close to each other.[17] The advantage of considering the dilaton from (3.114) will show up as the ability to obtain finite N effects as we shall see.

Now, using the data of the finite temperature gravity solution (3.167) we get the behaviour in figure 3.8. We see a repulsive force for finite N, while there is a clear trend that this repulsive behaviour becomes less dominant when we consider the large N limit. Reminding that finite N effects are analogous to quantum effects we make immediate contact with previous works [132, 164] where the repulsive force was an effect of quantum corrections. The whole discussion takes always place in the limit $g_{\text{eff}} \gg 1 \Rightarrow \mu \ll 1$, while r serves as the temperature here via equation (3.170). This repulsive behaviour and the profile of the potential strongly remind the Coleman-Weinberg mechanism which was studied for D3-branes in [165]. Here, we could imagine that we have similarities for a different system consisting of D0-branes.

One important caveat of the above construction is that we did not check explicitly whether this metric solves the Einstein equation or not but we rather constructed it. It is a deformed version of the one of BFSS (3.114) and in very large r approaches the BFSS metric (3.154) as we observed. We constructed the deformation to be large in intermediate values of r such that the trivial vacuum solution makes sense, following the recipe in [158, 160, 161].

Before moving to the discussion of the thermodynamic quantities of the model let us comment what the above analysis might add to the description of the BMN model.

We were interested in understanding the force that a probe D0-brane feel whenever we place it in the BMN gravity background. The reason why this question is interesting is because it can be tested using Monte-Carlo simulations along the lines of [164], where the same idea was tested using a different calculation [132]. The punchline in these findings is that quantum (i.e finite N) corrections lead to a repulsive force acting on the D0-brane probe. Intuitively this is not so unexpected if we recall similar phenomena happeing in electromagnetism and charged particles. Our findings, using a different approach, show also a repulsive force acting on the D0-brane probe for finite N (see Fig. 3.8).
One interesting observation is that for a fuzzy sphere, the same force vanishes (see Appendix B) and this might come as a surprise at first sight. On the other hand the BMN model has BPS solutions, and a fuzzy sphere is a BPS solution of the BMN such that when the gravitational force acting on it vanishes.

[17] Note that one can consider the dilaton emanating from (3.147), but this choice results in a quite complicated expression for the dilaton without adding much to the discussion. Indeed we have checked that the arguments do not change and the results remain the same independent of the form of the dilaton we are using.

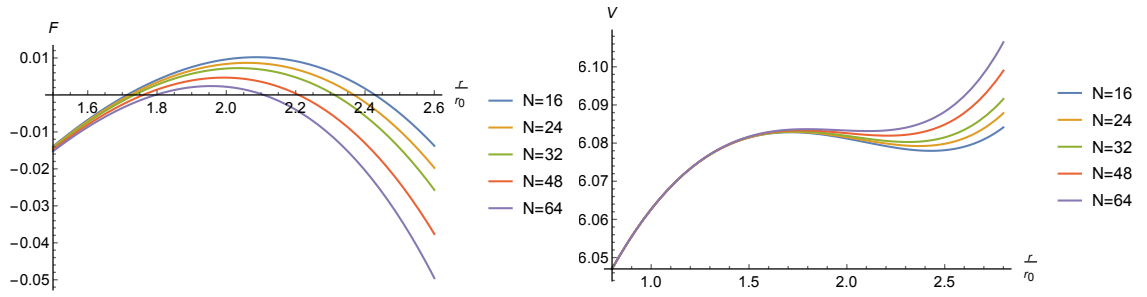

Figure 3.8: Force (left) and potential (right) at finite temperature T with respect to the radial coordinate r (or equivalently the temperature T). We have set for the horizon $r_0 = 1$, and $\lambda = 1 = T_0$. In the large N limit we expect the curves to be monotonous such that the force will be always attractive.

3.5 Thermodynamics of the BMN model

In this section, we shall discuss the thermodynamic quantities of the BMN model emanating from gravity analysis. To this end, we shall follow closely the construction done in [166]. The latter discuss also an important feature of the models, namely the transition from a confined configuration and vice-versa, a feature we discuss in Sec. 3.6. The strong coupling prediction of the transition temperature in terms of the mass parameter μ was obtained as

$$\lim_{g_{\text{eff}}\to\infty} T_c = 0.105905\mu. \tag{3.172}$$

The argument then is that this confinement/deconfinement transition occurring at this temperature corresponds to a Hawking-Page like phase transition in the dual gravity side. We shall discuss this issue later on, but for the moment let us focus on thermodynamic quantities. The latter, are all obtained in the strong coupling limit with expansion parameter

$$\hat{\mu} = \frac{7}{12\pi}\frac{\mu}{T}, \quad \hat{\mu} \ll 1, \tag{3.173}$$

and they are a deformed version of the BFSS gravity dual quantities. Writing the dimensionless free energy of the BFSS model in terms of dimensionless temperature $\tau := T/\lambda^{1/3}$ we get [18]

$$\frac{F(\tau,0)}{\lambda^{\frac{1}{3}}N^2} = \left(c_0\tau^{\frac{14}{5}} + c_1\tau^{\frac{23}{5}} + \cdots\right) + \frac{\left(d_0\tau^{\frac{2}{5}} + d_1\tau^{\frac{11}{5}} + \cdots\right)}{N^2} + \cdots, \tag{3.174}$$

where the coefficients c_i, d_i are known, e.g $c_0 = -\frac{1}{21}\left(\frac{120\pi^2}{49}\right)^{7/5} \approx -4.11$. The dimensionless entropy is given also as

$$\frac{S(\tau,0)}{N^2} \approx 11.53\tau^{\frac{9}{5}}, \tag{3.175}$$

and the BMN versions are given as deformations of those as

$$\frac{F(T,\mu)}{F(T,0)} := f(\hat{\mu}), \quad \frac{S(T,\mu)}{S(T,0)} := s(\hat{\mu}), \quad \hat{\mu} = \frac{7\mu}{12\pi T}, \tag{3.176}$$

[18] We shall use both τ and T interchangeably without risk of confusion, by recalling the definition. Note also that we will come back to this expression with more details in Sec. 4.5.

with $f(0) = 1 = s(0)$. The deformation functions can be expanded in series [166]

$$f(\hat{\mu}) = \sum_{n=0}^{\infty} \frac{14 s_n}{14 - 5n} \hat{\mu}^n, \tag{3.177}$$

$$s(\hat{\mu}) = \sum_{n=0}^{\infty} s_n \hat{\mu}^n, \tag{3.178}$$

with the coefficients of s_n being unknown at least analytically. Numerically instead one can find their behaviour for first few orders [19] and this is depicted in Fig. 3.9

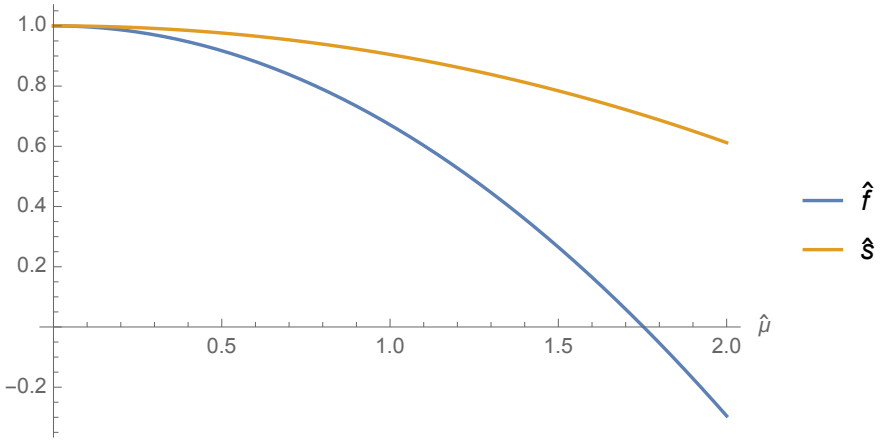

Figure 3.9: Behaviour of functions $f(\hat{\mu})$ and $s(\hat{\mu})$ to first few orders in $\hat{\mu}$.

The vanishing point is at $\hat{\mu}_c \approx 1.75336$. In addition, we see from (3.176) that also the free energy vanishes at $\hat{\mu}_c$. Above this value, the free energy is positive and of order N^2, while for $\hat{\mu}$ below this critical value the free energy is of order N^0 and will dominate the thermal ensemble.

Let us work at fixed μ and write down the equation of state

$$\frac{\partial F}{\partial T}\Big|_{\mu} = -S, \tag{3.179}$$

to get the relation

$$(1 - \frac{5}{14}\hat{\mu}\partial_{\hat{\mu}}) f(\hat{\mu}) = s(\hat{\mu}). \tag{3.180}$$

Now using the equation of state for fixed μ

$$E\Big|_{\mu} = F + TS\Big|_{\mu}, \tag{3.181}$$

and plugging in the leading orders of free energy and entropy results in

$$\frac{E(T)}{N^2} \approx -4.11 \lambda^{-3/5} T^{\frac{14}{5}} f(\hat{\mu}) + 11.52 \lambda^{-3/5} T^{\frac{14}{5}} s(\hat{\mu}). \tag{3.182}$$

Then by substituting $\hat{\mu} = \frac{7\mu}{12\pi T}$ and fixing μ we get the $E(T)$ dependence as shown in Fig. 3.10. In the limit $\hat{\mu} \to 0$ the energy of BFSS $E(T, 0) = 7.41 T^{\frac{14}{5}} \lambda^{1/3} N^2$ is recovered because the deformation parameters become $f(0) = 1 = s(0)$. This limit is a bit subtle as we shall

[19] I would like to thank Jorge Santos for sending me these data.

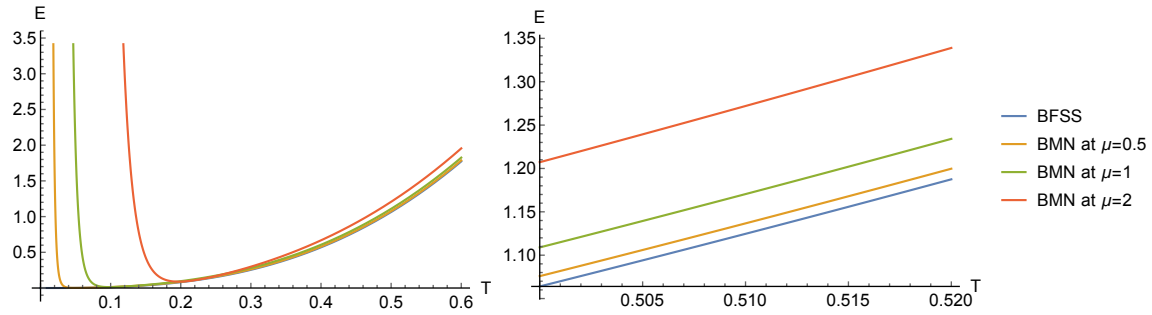

Figure 3.10: Energy with respect to temperature for a few values of μ. [Left] is full range [Right] is zoomed in $T \in [0.5, 0.51]$ to check the comparison between the BMN and BFSS energies. The blowing up behaviour in the left panel is due to the fact that we are truncating the expansions of $f(\hat{\mu}), s(\hat{\mu})$.

comment later on, because the way it is taken may result in different gravity descriptions. Here in particular we are fixing the temperature T and send $\mu \to 0$ to make contact with the type IIA black zero brane description. In addition, at the critical mass ($\hat{\mu}_c$) the functions $s(\hat{\mu})$ and $f(\hat{\mu})$ become

$$s(\hat{\mu}_c) \approx 0.7036628, \tag{3.183}$$

$$f(\hat{\mu}_c) = 0. \tag{3.184}$$

Using now the equation of state at the critical point $\hat{\mu}_c$,

$$E\Big|_{\hat{\mu}_c} = F + TS\Big|_{\hat{\mu}_c}, \tag{3.185}$$

we see that only $s(\hat{\mu}_c)$ is relevant. The energy is given as

$$\begin{aligned} E_c(T,\mu) =& \lambda^{-3/5} T_c(\mu) S_c(T,\mu) \qquad (3.186)\\ =& S(T,0) s(\hat{\mu}_c) \\ =& \lambda^{-3/5} 11.52 N^2 T^{\frac{14}{5}} s(\hat{\mu}_c) \\ \simeq& \lambda^{-3/5} 8.11 N^2 T^{\frac{14}{5}}. \qquad (3.187) \end{aligned}$$

It is straightforward to get the μ dependence of the energy *at the transition points* via (3.173). We may however emphasize that this relationship holds precisely and only at the confinement-to-deconfinement transition points for each T, or μ.

As long as we are in temperatures $T > T_c = 0.1059\mu$ we are always in the deconfined phase and indeed we can compare the matrix results with gravity. We shall see this interesting comparison in Sec. 4.5.

3.6 Confinement and deconfinement phases and their relations with gravity interpretations

3.6.1 The gauge theory side

Being a dimensional reduction of super Yang-Mills theory, matrix models should have a confining and a deconfining behaviour in different energy regimes. Before move to matrix

model details and their gravity interpretation let us comment more on these different phases, how to distinguish them and what do they mean physically. To this end, it will be instructive to understand where this idea originates from. This behaviour is expected to be universal whenever we have $SU(N)$ gauge theories [167] and an interesting overview of the topic is given in [168] and more generally in [50].

It is widely believed that pure $SU(N)$ gauge theories in $d = 4$ confine at zero temperature [169,170]. Let us try understand this intuitively using as a test example quantum chromodynamics (QCD) with coupling Λ_{QCD}. The low energy spectrum of such theories can be understood as a Fock space of interacting glueballs. Therefore, it is expected that for low temperatures such that $T \ll \Lambda_{QCD}$ dynamics can be understood in terms of a sparsely populated thermal bath of glueballs. At the same time, asymptotic freedom permits a reliable computation of the $T \gg \Lambda_{QCD}$ behaviour of such theories (for the case of finite volume) revealing that this high temperature phase may be understood in terms of a weakly coupled gas of gluons [171, 172]. Therefore, the high and low temperature phases appear qualitatively different, and it might be possible to find an order parameter (or two) that distinguish these phases by a possible phase transition.

Let us consider a confining theory with no fields in the fundamental $SU(N)$ representation and let us try to insert a single external particle in the fundamental representation (such as a quark) into this theory. This action can be done only with an infinite cost of energy. The reason, heuristically speaking, is because such a quark forms the end of a QCD string which has nowhere to end and thus it is infinitely long. In the low energy (confining) phase this long string has also infinite positive free energy. Analysing the form of the coupling of an external quark to the gauge fields, it follows that the free energy of this gauge theory of an external quark $\mathcal{F}_q(T)$ satisfies the relation [168]

$$e^{-\mathcal{F}_q(T)/T} = \langle P \rangle, \tag{3.188}$$

where P is the so-called Polyakov loop defined as the trace of a Wilson loop

$$P := \frac{1}{N} \operatorname{Tr} \mathcal{P} e^{-\oint A_\mu}, \tag{3.189}$$

where $\mathcal{P}$ stands for path ordering. It should be clear that in the low temperature confining phase where $\mathcal{F}_q(T) \to \infty$ we have $\langle P \rangle = 0$.

As we mentioned earlier, asymptotic freedom allows reliable calculations that establish $\langle P \rangle \neq 0$ in the high temperature limit. Hence, $\langle P \rangle$ serves as an order parameter that distinguishes the confinement and deconfinement phases. In addition, in the large N limit with fixed Λ_{QCD} (or fixed 't Hooft coupling) the deconfinement phase transition has another order parameter [173]. The low energy confined phase is dominated by gauge-invariant bound states such that its free energy $\mathcal{F}(T)$ scales as N^0 at large N. On the other hand, the deconfined high temperature phase is described by *free* gluons, and as a result its free energy scales like N^2 in the large N limit. Therefore, in the large N limit, $\lim_{N\to\infty} F(T)/N^2$ serves as another order parameter.

Let us discuss a bit more the Polyakov loop. The latter could be given via an effective action, by integrating all other fields out of the path integral which generates the Yang-Mills free energy. P is a complex scalar field on the manifold $\mathcal{M}$ of the theory[20]. In addition there

[20] In this thesis we will particularly interested in the case $\mathcal{M} \cong \mathbf{S}^1$.

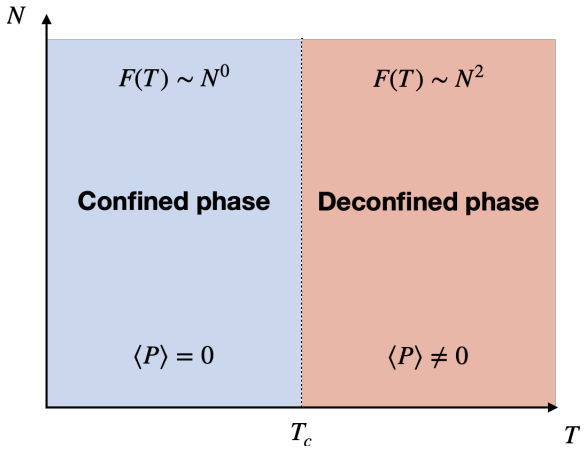

Figure 3.11: A graphical representation of the discussion around (3.189). In the confinement phase the Polyakov loop is zero and in the large N limit the free energy is of order N^0. In the deconfinement phase the Polyakov loop is non-vanishing and again in the large N limit the free energy scales as N^2. These are the two parameters that distinguish the two phases resulting in a critical temperature T_c.

is a symmetry such that the Polyakov loop is invariant under a phase shift

$$P \to e^{\frac{2\pi i}{N}} P, \tag{3.190}$$

originating from the invariance of the $SU(N)$ Yang-Mills path integral [174]. This is generated by gauge transformations that are single valued only up to an element of the center of the gauge group which is $\mathbb{Z}_N$ in this particular case. Such gauge transformations act trivially on the dynamical fields of the pure Yang-Mills theory, and its spontaneous breaking is related with the deconfinement phase transition. In other words, breaking/restoration of this symmetry results in a deconfinement/confinement transition.

Let us now try to use the Polyakov loop in a one dimensional manifold. This affects only the integration, now written as

$$P = \frac{1}{N} \operatorname{Tr} \left(\mathcal{P} \exp \left(i \int_0^\beta A_t \, \mathrm{d}t \right) \right), \tag{3.191}$$

and when we consider the one-dimensional model under consideration to be thermal with temperature T, the manifold is $\mathcal{M} \cong \mathbf{S}^1$ where the radius is $\beta = \frac{1}{T}$. When $\mathcal{M} \cong \mathbf{S}^1$ we can consider a one-dimensional lattice on which our model is defined. The $N \times N$ unitary matrix inside the trace is called the Polyakov line and being unitary, its eigenvalues can be written as $e^{i\theta_1}, \cdots, e^{i\theta_N}$ where the phases $\theta_1, \cdots, \theta_N \in [-\pi, \pi)$. This allows for a discrete interpretation and we may rewrite the Polyakov loop in terms of its eigenvalues as

$$P = \frac{1}{N} \sum_{j=1}^{N} e^{i\theta_j}. \tag{3.192}$$

Let us also introduce a distribution function $\rho(\theta)$ nornalised as

$$\int_{-\pi}^{\pi} \rho(\theta) \, \mathrm{d}\theta = 1. \tag{3.193}$$

Then the Polyakov loop becomes

$$P = \int_{-\pi}^{\pi} \rho(\theta) e^{i\theta} \, \mathrm{d}\theta. \tag{3.194}$$

This way we are placing the eigenvalues of the Polyakov loop at the perimeter of the $\mathbf{S}^1$ and the way they distribute along the perimeter will play a major role to understand the order of the phase transition.

This eigenvalue distribution description serves as a parameter for the order of a phase transition used in [175] and latter on was established as the so-called Gross-Witten-Wadia (GWW) transition which further can be 2nd or even a 3rd order phase transition. It essentially means that from a non-uniform and non-gapped eigenvalue distribution the configuration transitions to a non-uniform and gapped distribution. The term gap refers to the possibility that the distribution function becomes negative in the range $-\pi \leq \theta \leq \pi$.

But how is this connected with the matrix models, and what is in fact confined and deconfined?

Confinement-to-deconfinement parameters

There are at least two parameters that can help us to detect if the system we are studying is in the confined or deconfined configuration. These are

1. The Polyakov loop P which is zero in the low temperature confined phase of the gauge theory and non-zero in the high energy deconfined phase
2. The free energy $\mathcal{F}$ which is of order N^0 in the confined phase and of order N^2 in the deconfined phase.

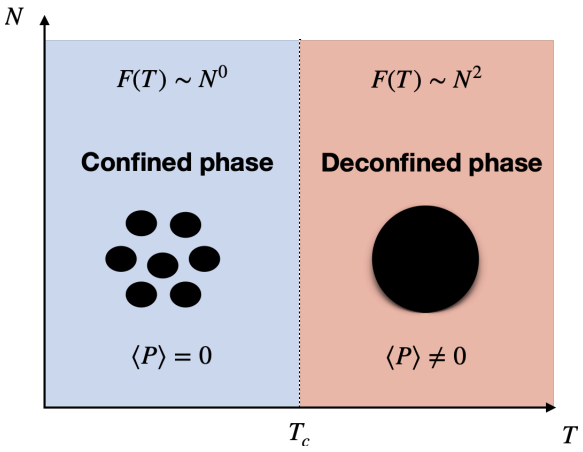

Figure 3.12: A graphical representation of the discussion of this whole section. Vanishing Polyakov loop corresponds to a gas-like interpretation of constituents of a geometry (left), while non-vanishing Polyakov loop corresponds to the existence of a black hole constructed as a result of the condensation of the constituents of the geometry.

3.6.2 The gravity side

To understand the answer of the above question let us briefly try to understand the same question in the conventional holography, i.e in the AdS/CFT description. We will use as a test example the original proposal for a stack of N coincident D3-branes which backreact into a $AdS_5 \times S^5$ geometric description. The latter is the holographic dual of a super Yang-Mills in a four-dimensional spacetime ($\mathcal{M} \cong \mathbf{S}^3 \times \mathbb{R}$) which is furthermore a CFT_4 [130][21]. The above geometry can be understood via the metric

$$\mathrm{d}s^2 = R_0^2 \left(-\cosh^2 \rho d\tau^2 + \mathrm{d}\rho^2 + \sinh^2 \rho \, \mathrm{d}\Omega_3^2 + \mathrm{d}\Omega_5^2 \right). \tag{3.195}$$

Under the conventional duality, the Hamiltonian of the Yang-Mills theory is identified with the generator of global time translations ∂_τ in the above geometry. The radius of the geometry R_0 is related with the 't Hooft coupling $\lambda = g_{YM}^2 N$ and the string scale as $R_0 \simeq \lambda^{1/4}\sqrt{\alpha'}$. Therefore, the parameter that controls the regimes of the system is λ which is compared with the energy of the gauge theory E on a sphere of unit radius. The relation with the proper energy in string theory is $E_{\text{prop}} = E/R_0$.

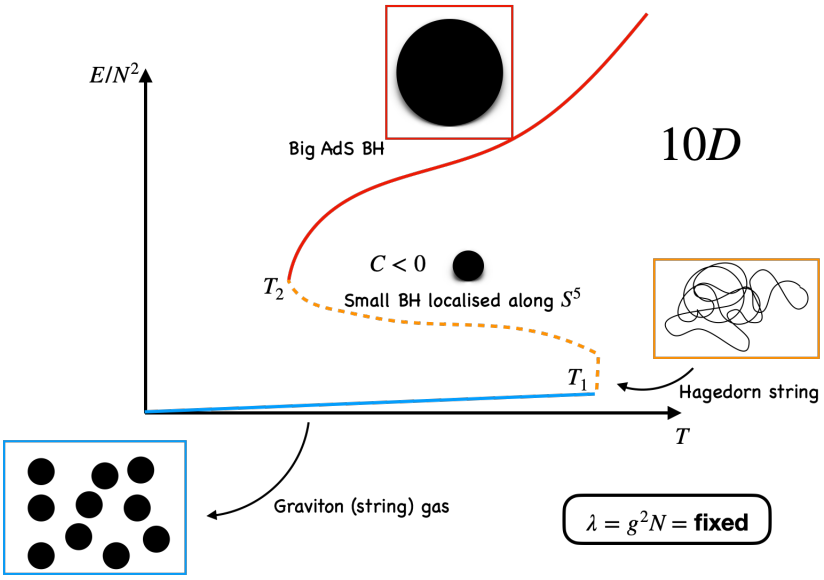

Figure 3.13: A graphical representation of the situation discussed in the text also. For small energies, the system behaves like a graviton gas in a box, for intermediate energies there is a transition at $T_1 = T_H$ where the system develops the behaviour of a long Hagedorn string. For higher energies we have a small black hole localised along the $\mathbf{S}^5$ sphere with negative specific heat C. For even higher energies there is a transition to a big black hole in AdS with positive specific heat.

AdS_5 effectively behaves like a four-dimensional box of physical radius R_0, and this can be deduced from the fact that the spectrum of ∂_τ is discrete with unity steps. Therefore, all

[21] It is important enough to mention that this holographic duality does not necessarily mean that the gauge theory lives on the boundary of the gravity spacetime. This is a confusion arising usually outside of the field of holography. The two theories have different spacetimes and there is a mapping between them such that the d-dimensional gauge field theory data can construct a $(d+1)$-dimensional spacetime where a gravitational theory lives, and not a gauge field theory.

the states of finite energy are localised about $\rho = 0$. The spectrum of energies defining the density of states $\rho(E)$ depends on the regimes we are in terms of the energy E and it contains four main parts. The situation is reported in Fig. 3.13 and can be understood in terms of the temperature and energy. Let us start with the temperature. For $T < T_2$ the only available saddle point is the thermal gas of gravitons. In the range $T_2 < T < T_1$ there exist three different saddle points, however the small black hole is unstable due to negative specific heat and therefore it cannot appear in the canonical ensemble. The other two saddles, namely the free graviton gas and the big AdS black hole are stable and they compete with each other. Finally, for temperatures $T > T_2$ the only available phase is the big black hole in AdS. The deconfined phase is always related with a black hole phase in the gravity side [168]. This can be understood using the Polyakov loop we discussed above and gravitational black hole horizons. As we explained the Polyakov loop is realised as the partition function in Euclidean space for a string whose boundary wraps around the time-like loop. This partition function is zero when the Euclidean time circle is non-contractible, but on the other hand it is non-zero if it is contractible. This situation is clear for black hole where we have a geometric interpretation of the background in which case the Euclidean time circle around the core of the black hole, assigned to the horizon, gives the temperature of the black hole. Inverting the reasoning for difficult geometric backgrounds, whenever we do not have a clear geometric interpretation, the existence of contractible time-like circles can be explored by using the Polyakov loop [168]. This summarises this section and can be understood via Fig. 3.12. In what follows we will distinguish the gravitational description using the Polyakov loop.

Part III

Simulating matrix models in a supercomputer

4 Simulations

Τα πάντα ρει

Heraclitus

Solving gauge theories is not easy. Usually, theorists focus on a specific parameter region of the theory where they impose strong constraints on the system and solve some related problem. Yet, the full sector of the theory is unknown and one may fall in the trap to apply the results obtained in this highly constrained region on the full theory and make interesting claims. This is an unfortunate event that should be avoided because analytically we do not have the theory under control.

What helps us on the other hand to access the full theory in a non-perturbative fashion is putting it in a (super)computer. The advantage of this can be easily illustrated for the case of matrix models, say the BFSS model, where we have an action containing nine bosonic $N \times N$ matrices, sixteen fermionic $N \times N$ matrices, evaluated on S lattice points parametrising a circumference of $\beta = 1/T$. The interested reader can consult [176] and especially [177] for more technical details. In what follows, we will entirely focus on physics and summarise the important points.

4.1 Introduction to simulations

The idea of simulating matrix models is heavily based on the approach of lattice QCD. However, the same problems appearing there appear also for the case of matrix models. Let us discuss a bit about their occurrence and their resolution in the context of matrix models.

In order to study maximally supersymmetric Yang-Mills theories with dynamical fermions, one has to integrate out the fermions in the same way that it is done in lattice QCD. Then because of the Mayorana-Weyl fermions that are contained in the model, the Pfaffian that occurs is the square root of the determinant up to a sign. This is the famous sign problem in lattice approaches to supersymmetric theories. For example when we write a theory which

contains bosons (X), a gauge field (A) and fermions (ψ) we can write a fermionic term as $\bar{\psi}L\psi$ which we can integrate out as follows

$$\int [\mathrm{d}A][\mathrm{d}X][\mathrm{d}\psi] e^{-S_{\text{bosonic}}-\bar{\psi}L\psi} = \int [\mathrm{d}A][\mathrm{d}X] \mathrm{Pf}L(A,X) e^{-S_{\text{bosonic}}}. \tag{4.1}$$

At the same time $\mathrm{Pf}L(A,X)$ is usually complex, and therefore the standard method of importance sampling is not valid any more. The latter method assumes the fact that the biased estimate $g(Y)$ and the actual estimate $f(Y)$ are given by the ratio

$$\frac{f(Y)}{g(Y)}, \tag{4.2}$$

with $Y : \mathbb{R} \to \mathbb{R}$ being the real sample. Then the problem rephrases to choosing a specific $g = g^*$ which minimizes the above ratio, i.e

$$g^* = \min_g \mathrm{var}_g \left(Y \frac{f(Y)}{g(Y)} \right). \tag{4.3}$$

This technique though does not work for $Y \in \mathbb{C}$. One way out of this, is to consider a phase-quenched ensemble with the weight $|\mathrm{Pf}L(A,X)|e^{-S_{\text{bosonic}}}$ and take into account a phase factor with the help of the phase re-weighting method, in other words for the expectation value of an observable $\mathcal{O}$ we consider

$$\langle \mathcal{O}(A,X) \rangle_{\text{full}} = \frac{\langle \mathcal{O}(A,X) e^{i\theta} \rangle_{\text{phase quench}}}{\langle e^{i\theta} \rangle_{\text{phase quench}}}. \tag{4.4}$$

The phase here is formulated via

$$e^{i\theta} = \frac{\mathrm{Pf}L(A,X)}{|\mathrm{Pf}L((A,X))|}. \tag{4.5}$$

Usually this phase re-weighting method is quite costly because one has to always calculate the Pfaffian, but the point is that θ approximates zero in a wide parameter region and practically one has

$$\langle \mathcal{O}(A,X) \rangle_{\text{full}} \simeq \langle \mathcal{O}(A,X) \rangle_{\text{phase quench}} \tag{4.6}$$

within statistical error. For the cases that the Pfaffian is computable it has been observed that the last relation holds within statistical error and this is true because of the absence of correlations between the phase and the observables [134].

4.1.1 Real time dynamics

Real time physics are usually more interesting. For the case of a field theory, real time dynamics makes the system a thermal field theory having a specific temperature T. Then, for a thermal field theory one can do a thermodynamic analysis that might be available and depending on the nature of the fields one can also perform a statistical analysis studying in this way the microcanonical degrees of freedom that shape the theory.

For the sake of the clarification let us consider a QFT on a four-dimensional Minkowski spacetime, which is indeed the most commonly found example in the literature. In the Lorentzian picture, we are putting the theory in a Lorentzian signature of the manifold which has the form $\mathbb{R}^{1,3}$. Treating the same theory as thermal, i.e having a universal temperature

that governs the field theory and making it a thermal field theory amounts to the so-called Wick rotation trick where one replaces the time coordinate according to $\tilde{t} \to it$ giving an Euclidean signature $\mathbb{R}^4$.

The thermodynamic behaviour of the system, is studied by using the Euclidean time picture, where the dimension that corresponds to "time" is compactified, having usually the topology of a circle $\mathbf{S}^1$. The temperature in this case, is related with the periodicity of the circle such that a point on the circle becomes periodic $x_0' \to x_0 + 2\pi\beta$, with β defined as

$$\beta := \frac{1}{T}. \tag{4.7}$$

It seems in fact that the radius of the time circle $\mathbf{S}^1$ controls the temperature of this field theory and vice versa.

At the other face of the gauge/gravity duality we ask what this temperature corresponds to. Going back to the work of Hawking [4] (for a nice review see e.g [178]) we learned that black holes evaporate via radiation, so if there is a radiation, this should correspond to a specific temperature. One interesting possibility would be to check whether or not the temperature of a thermal field theory is related with temperatures of a specific black hole in a gravitational theory.

Indeed, in the gauge/gravity community Euclidean time dynamics are related with the study of Hawking radiation of a gravitational system, such as a black hole or black p-brane [179] in AdS spacetime. To put it simply, the temperature of the field theory corresponds to the Hawking temperature of this black object. We might recall that for the case of a Schwarzschild black hole in four dimensions the temperature is related with the mass as

$$T_H = \frac{1}{8\pi M}, \tag{4.8}$$

in units of $G = 1 = c$ while the mass is related with the Schwarzschild radius as

$$r_s = 2M, \tag{4.9}$$

resulting in

$$T_H \sim \frac{1}{r_s}. \tag{4.10}$$

In string theory, and depending on the Dp-branes that construct the geometry, the radii have different exponents with the temperatures of the respective field theories. For our case the black-zero brane has the relation (3.115), with T being also the temperature of the matrix quantum mechanics. The latter is actually connected with the size of the Euclidean one-dimensional time dimension and specifically with the radius of the circle as we saw above. The gravitational analogue of this temperature is again the temperature of a black object while if the system undergoes a phase transition at a critical temperature (T_c) , the type of the transition depends on the details of the underlying theory we are describing [179–187].

Therefore, the punchline is that simulating in a specific temperature means that we are enforcing a canonical ensemble in the system (as we will comment also later on) and this temperature corresponds to the Hawking temperature of the black-zero brane.

4.1.2 Preserving supersymmetry on the lattice

Preserving supersymmetry on the lattice is an important feature for all lattice approaches on supersymmetric theories. One of the most important and pioneering paradigms is the

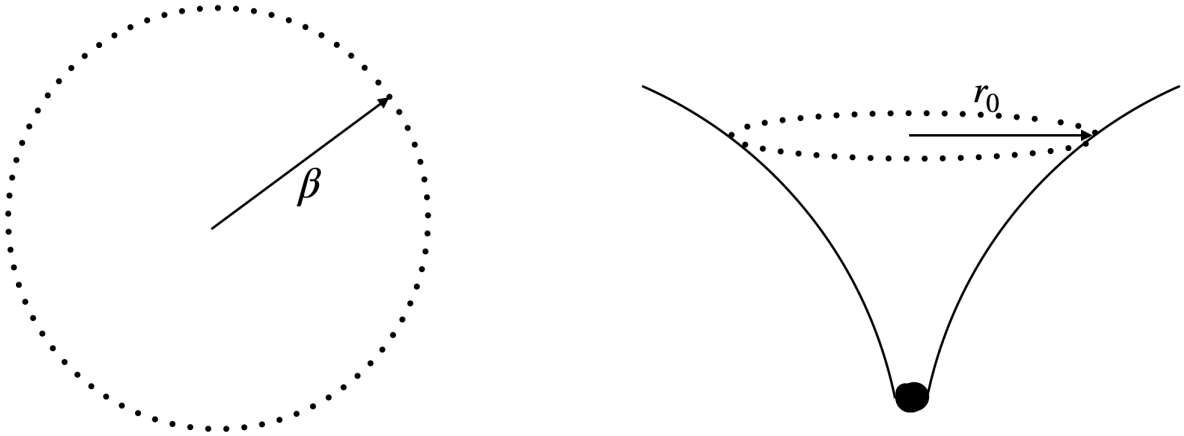

Figure 4.1: The temperature interpretation of the gauge theory side [Left] and the gravity side [Right]. The temperature in the gauge theory corresponds to the inverse size of the time circle which in simulations will be discretized. The discretization points correspond to the dots and are denoted as S in simulations. In the gravity picture consisting of N coincident D0-branes, this corresponds to the Euclidean time circle which is also discrete and shapes the horizon. This is a specific picture where we use a lattice discretization, while taking the continuous limit, the discrete circle is replaced by a continuous one.

approach of lattice quantum chromodynamics (QCD), while here we are interested in one-dimensional matrix quantum mechanics. These approaches share the same problem but for the case of matrix quantum mechanics we have just one dimension and thus it might be easier to explain the main arguments. The idea of formulating these physical models on a lattice is due to the possibility of performing simulations by using a finite number of spacings and gradually take the continuum limit. In lattice QCD one has always $N = 3$, which denotes the number of colours and the interesting parameter is S, the lattice spacing. On the other hand one has also a three-dimensional spacetime and simulating this problem starts manifest some difficulties. With the exchange of keeping N free the one-dimensional matrix integral can be done more easy, such that simulating one-dimensional matrix models becomes easier.

The supersymmetry algebra between the supersymmetry generators is of the form

$$\{Q_\alpha, Q_\beta\} \propto \gamma^\mu_{\alpha\beta}\partial_\mu, \tag{4.11}$$

such that in a sense the algebra contains an infinitesimal translation. The moment we are introducing a lattice, the derivative operator is not formally defined any more because of continuity since the lattice breaks explicitly supersymmetry. The problem then manifests at the very beginning and the question is what can possibly be done to circumvent this unfortunate problem.

There are two approaches attacking and curing this problem. For a review see [188, 189] and references therein.

- **The fine tuning approach**: The idea behind this, is based on the renormalization procedure of the gauge theories. Simple actions break supersymmetry on the lattice yielding in addition a proliferation of such terms breaking the supersymmetry. This requires to add equal number of counter terms in the effective action describing the model, and carefully tune their coefficients as the lattice spacing decreases. This

eventually will lead to supersymmetry restoration in the continuum limit, and this procedure is known as the fine tuning problem of lattice supersymmetry.

This approach is simple for super-renormalizable theories, where the coefficients can be calculated perturbatively, as in the case of Wess-Zumino model [190] and the in $\mathcal{N} = 1$ super Yang-Mills theory where the counter term needed to restore chiral symmetry in the continuum appears as the gluino mass term [191]. On the other hand, the same procedure starts becoming particularly challenging in theories with scalar fields. The latter appear as part of the matter multiplet in supersymmetric QCD or appear in the vector multiplet alongside the gauge field in theories with extended supersymmetry. To put it simply, supersymmetry forbids the appearance of scalar mass!

- **The preservation of a supersymmetric sublagebra on the lattice**: In theories which preserve part of the supersymmetry algebra it is sometimes possible to reduce the number of fine tunings dramatically. While discretisation of supersymmetric theories generically breaks supersymmetry completely there are indeed situations that a subpart of the algebra can be preserved. It is also possible that the constraints implemented in this way, could (at some cases) eliminate the fine tuning procedure.

  These cases involve theories with extended supersymmetry and in fact it has been realised that in $(0+1)-D$ and $(1+1)-D$ models this strategy can be materialised to all orders in perturbation theory. Likely our model(s) discussed, and to be discussed fall into this category.

4.1.3 Lattice discretization

Below, we explain the details of the lattice regularization done in such a way to put the model in a (super)computer. The action is that of the BMN model, while for the case of the BFSS model we simple set $\mu = 0$.

Gauge fixing

The action of the matrix models are invariant under the SU(N) gauge transformation. For numerical efficiency, we take the static diagonal gauge,

$$A_t = \frac{1}{\beta} \cdot \mathrm{diag}(\alpha_1, \cdots, \alpha_N), \qquad -\pi < \alpha_i \leq \pi. \tag{4.12}$$

Associated with this gauge fixing, we add the Faddeev-Popov term

$$S_{F.P.} = -\sum_{i<j} 2 \log \left| \sin\left(\frac{\alpha_i - \alpha_j}{2}\right) \right| \tag{4.13}$$

to the action.

Lattice action

We regularize the gauge-fixed continuum theory by introducing a lattice with S sites and spacing A. We write the action for the BMN model which is the most general one. The relevant BFSS lattice action is obtained by setting $\mu = 0$ while the bosonic actions are

taken by ignoring the fermionic terms. We may also discretise the time variable as follows $t = a, 2a, \cdots, aS$. Therefore we write [1]

$$S_{BMN_{\text{lattice}}} = S_b + S_f + \Delta S_b + \Delta S_f, \tag{4.14}$$

where

$$S_b = \frac{N}{2a}\sum_t \sum_{I=1}^{9} \mathrm{Tr}\left(D_+ X_I(t)\right)^2 - \frac{Na}{4}\sum_t \sum_{I,J=1}^{9} \mathrm{Tr}[X_I(t), X_J(t)]^2, \tag{4.15}$$

$$S_f = iN\sum_t \mathrm{Tr}\bar{\psi}(t)\begin{pmatrix} 0 & D_+ \\ D_- & 0 \end{pmatrix}\psi(t) - aN\sum_t\sum_{I=1}^{9}\bar{\psi}(t)\Gamma^I[X_I(t),\psi(t)], \tag{4.16}$$

$$\Delta S_b = aN\sum_t \mathrm{Tr}\left\{\frac{\mu^2}{2}\sum_{i=1}^{3}X_i(t)^2 + \frac{\mu^2}{8}\sum_{a=4}^{9}X_a(t)^2 + i\sum_{i,j,k=1}^{3}\mu\epsilon^{ijk}X_i(t)X_j(t)X_k(t)\right\}$$

and

$$\Delta S_f = \frac{3i\mu}{4}\cdot aN\sum_t \mathrm{Tr}\left(\bar{\psi}(t)\gamma^{123}\psi(t)\right). \tag{4.17}$$

In addition we have the conventions

$$D_\pm\psi(t) \equiv \mp\frac{1}{2}U^2\psi(t\pm 2a)\left(U^\dagger\right)^2 \pm 2U\psi(t\pm a)U^\dagger \mp \frac{3}{2}\psi(t) = aD_t\psi(t) + O(a^3).$$

Here, $U = \mathrm{diag}(e^{i\alpha_1/S}, e^{i\alpha_2/S}\cdots, e^{i\alpha_N/S})$, $-\pi \le \alpha_i < \pi$. The Faddeev-Popov term $S_{F.P.}$ is simply the same as the original form, (4.13)

4.1.4 The parameters that control the system

Before starting to present more detailed situations and simulation results let us recap. We will be using the matrix models (3.86) and (3.96), part of them or just their bosonic analogue on a one-dimensional lattice. In a sense, what the simulation does, is to evaluate terms of the actions on lattice points giving as output numbers. The input is the size of the matrix, the size of the lattice, namely lattice points, the temperature, the number of the matrices and the flux (for BMN). We collect all this information in the following

Simulation parameters

The parameters that control the system are given in the following table

parameters	matrix model interpretation
N	size of the matrices $X_{N\times N}$
S	number of lattice points
T	temperature
d	number of matrices
μ	mass parameter of BMN model

The parameter N plays a special role here. Let us remind that the degrees of freedom are encoded in the entries of the matrices with diagonal elements corresponding to positions

[1] We assume that it will be obvious for the reader by now the distinction between the action and the lattice size which both are represented by S.

of D0-branes and non-diagonal elements to open strings connecting them. Let us also recall the relation of string coupling with N

$$2\pi g_{YM}^2 = g_s \alpha'^{-3/2} \Rightarrow g_s = 2\pi \frac{\lambda}{N} \alpha'^{3/2}. \tag{4.18}$$

In simulations we are always fixing $\lambda = 1$, such that the large N limit corresponds to $g_s \to 0$ limit. In other words the large N limit is classical string theory (since λ is also fixed) while keeping finite N means that we are introducing quantum corrections in the system. It seems that in a sense the large N limit is the analogue of $1/\hbar$. Then it is understood that for the system of $N \times N$ matrices which describe N D0-branes, keeping N finite amounts to introduce quantum corrections on the system.

Then the question is what is the role of α'. The latter is related to the string length $\ell_s = \sqrt{\alpha'}$ such that large ℓ_s means large non-diagonal entries. From (4.18) it is also clear that from the gauge theory side, when we fix g_{YM}^2 we put our gauge theory in a specific scale. On the contrary, fixing $\lambda = g_{YM}^2 N$ and taking the large N limit, we might have classical results but we still do have large α' corrections since $g_{YM}^2 \to 0$ and via (4.18) α' is arbitrary. Eventually, classical, quantum, supergravity, string theory are all facets of the same system taking different limits.

The punchline is that there are two kinds of stringy corrections. One is the finite N which amounts to quantum corrections and the other one is α'. Despite the fact that we can control quantum corrections by extrapolating to large N we cannot easily control α' corrections.

The parameters and their physical meaning

$N \to \infty$, $\lambda \to \infty$	$\leftrightarrow$	classical supergravity
$\frac{1}{N}$ corrections	$\leftrightarrow$	quantum (g_s) corrections
$\frac{1}{\lambda}$ corrections	$\leftrightarrow$	stringy (α') corrections

In what follows we will always set $\lambda = 1$.

4.2 Some interesting examples at large d

4.2.1 Theoretical analysis

Let us then start our investigations with some easy, yet interesting examples. The model under consideration is a bosonic analogue of the BFSS [53] which has been extended to $d = D - 1$ spatial dimensions and has a simple (Euclidean) action

$$S = \frac{N}{2\lambda} \int_0^\beta \mathrm{d}t \ \mathrm{Tr} \left\{ (D_t X_i)^2 - \frac{1}{2} [X_i, X_j]^2 \right\}, \quad i, j = 1, \cdots, d. \tag{4.19}$$

It is an one dimensional model, which can be understood as a d dimensional reduction of pure Yang-Mills theory living in D spacetime dimensions. The covariant derivative acts as $D_t X_i = \partial_t X_i - i[A_t, X_i]$ with A_t being the gauge field. The variables of the action are matrices X_i which enjoy a global $SO(d)$ symmetry that rotates them and in addition there is a $U(N)$ gauge symmetry associated with A_t. The center symmetry is $U(1)$ under which the Polyakov loop is invariant. The latter is defined as we saw via

$$P := \frac{1}{N} \mathrm{Tr}\, e^{i \int_0^\beta \mathrm{d}t A_t}, \tag{4.20}$$

and is considered to be an order parameter that is associated with this center symmetry. If we denote as θ the eigenvalues of the Polyakov loop, then it is invariant under $P \to e^{i\theta}P$. When this symmetry is broken (or restored) signals a phase transition. This phase change is also related with the confinement-to-deconfinement transition. In fact, this breaking of the $U(1)$ symmetry could happen *simultaneously* with the transition of P getting a non-zero expectation value. In addition to the Polyakov loop there is also another parameter that controls the phase transition, that is the free energy. As previously discussed, in a confined phase the free energy of the system scales as $F \sim N^0$ while in a deconfined phase as $F \sim N^2$. It is instructive in these type of works the usage of the Polyakov loop to study phase transitions. In this model, the parameter that controls the regimes of the model is the temperature T.

When $d = 9$ we have superstring theory, where the gauge/gravity duality holds for specific Dp-brane constructions. In the spirit of gauge/gravity duality, the confinement/deconfinement transition in the gauge theory traditionally is believed to correspond to a Hawking-Page transition in a theory of gravity [179]. The question now is what the analogue of the confinement/deconfinement transition is for non-AdS spacetimes and non-CFT gauge theories.

In addition there is another phase transition which a non-uniform, ungapped distribution of the eigenvalues of the Polyakov loop (see Fig. 4.2) becomes non-uniform and gapped distribution and the latter is believed to correspond to Gregory-Laflamme instability [131] in the gravity side (for a review see [185]). This transition is a topology change of the spacetime, which, as we will also discuss below for the case of a Schwarzschild black hole collapses to-and-from a black string, consisting of n such black holes forming a compact array and repeating after 2π. In the case of the BFSS model it is realized in terms of D0-branes on the compactification circle depending on how their eigenvalues spread along this circle [192]. This can be studied by analysing the Polyakov eigenvalue distribution, which furthermore connects the ungapped-to-gapped transition with a Gross-Witten-Wadia (GWW) transition [175]. However, the picture of eigenvalues does not refer necessary only to Dp-branes but rather to whatever they describe, hence nothing forbids us to generalise this picture to dynamical objects like partons in $(d+1)-$dimensional spacetimes.

Indeed this will be our motivation. We are considering bosonic partons living in a $(d+1)$-dimensional spacetime being part of a gauge theory and subject to the action (4.19). The latter is actually a one-dimensional model consisting of d matrices, which each matrix as we explained before gives information for a parton regarding the respective dimension. We will be as agnostic as ambitious here but the point is that higher order transitions and especially in higher dimensions are not well understood and such kind of questions have already started to be asked (and sometimes answered) in matrix models. The fact that these questions can be easily answered by using matrix Monte-Carlo simulations makes them attractive [183, 193]

When we consider $d + 1 > 11$ we cannot make any claims about gauge/gravity duality or string theories, because not only is unknown for both whether they apply to more than $D = 10$ spacetime dimensions but also there is no known bulk dual. On the other hand, Yang-Mills theories can be consistently written to arbitrary dimensions and nothing forbids us to consider N bosonic partons moving in an arbitrary $\mathbb{R}^{1,d-1} \times \mathbf{S}^1$ spacetime. In other words, we wish to extend the results of [193] to more than $D > 26$ spacetime dimensions. Our ambition is to compare with the three-loop result obtained in [183] which predicts that in gauge theories, higher order phase transitions should be happening after $D > 36$.

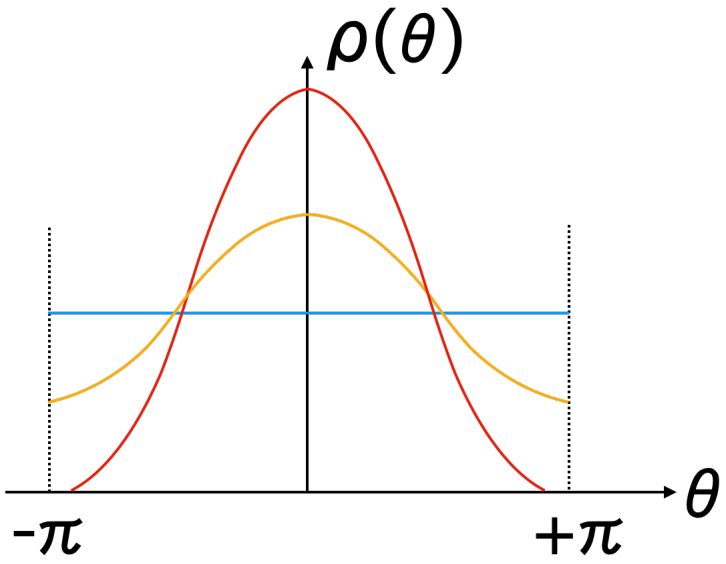

Figure 4.2: Distribution of the Polyakov loop eigenvalues θ. Uniform distribution corresponds to horizontal line (blue). Non-uniform and un-gapped distribution (orange) indicates partial deconfinement while non-uniform and gapped distribution (red) corresponds to GWW transition.

Along the way, we may also compare the results with the large d analysis of a Gregory-Laflamme instability that occurs for a Schwarzschild black hole collapsing to-and-from a black string.
The work of [182] performed in a large N and large d spirit predicts the critical temperature from gauge theories that signals transition in arbitrary dimensions with perturbation parameter $1/d$. The relevant relations are

$$T_1 = \frac{d^{1/3}}{\log d}\left[1+\frac{1}{d}\left(\frac{203}{160}-\frac{\sqrt{5}}{3}\right)\right]^{-1}, \tag{4.21}$$

and

$$T_2 = \frac{1}{A+\frac{1}{T_1}}, \tag{4.22}$$

$$A := \frac{\log d}{d^{\frac{4}{3}}}\left[-\frac{1}{6}+\frac{1}{d}\left(\left(-\frac{499073}{460800}+\frac{203\sqrt{5}}{480}\right)\log d-\frac{1127\sqrt{5}}{1800}+\frac{85051}{76800}\right)\right], \tag{4.23}$$

$$\Delta T := T_2 - T_1. \tag{4.24}$$

The first temperature (T_1) signals a phase transition which is accompanied by an onset of non-uniformity of the eigenvalue distribution. The latter is given via the eigenvalue θ density of the Polyakov loop as

$$\rho(\theta) = \frac{1}{N}\sum_{i=1}^{N}\delta(\theta-\theta_i). \tag{4.25}$$

The second temperature (T_2) signals the formation of a gap in the above eigenvalue distribution and hence it is related with a GWW transition (this actually means that $\rho(\theta)$ can become

negative in the region $-\pi$ to π, see again figure 4.2). The order parameter we are using to find the transition temperatures is the Polyakov loop P, and as we explained previously when getting an expectation value around $\langle P\rangle \simeq \frac{1}{2}$ from $\langle P\rangle \simeq 0$ we have a confinement-to-deconfinement transition as we discussed in Sec. 3.6. Therefore we can determine the transition temperature for every d.

To determine the order of the transition we have to take N to be sufficiently large because at this case the tunnelling between $\langle P\rangle = 0$ and $\langle P\rangle = \frac{1}{2}$ is exponentially suppressed by $e^{-\frac{N^2}{\lambda}}$. We expect that the Polyakov loop has a two peak signal in a scenario with first order transition, because the latter is characterized by a phase where $\langle P\rangle = 0$, an intermediate (perhaps stable) phase and a final phase where $\langle P\rangle = \frac{1}{2}$. We see this in Fig. 4.3, where the corresponding phases are denoted with red, orange and blue lines respectively. In a first order case, the unstable phase is also accompanied with negative specific heat (see Appendix C). In the BFSS model, this unstable phase is connected to eleven-dimensional Schwarzschild black hole [194], but in our case there is no bulk dual interpretation known. On the contrary, a higher order phase transition has an intermediate stable phase between $\langle P\rangle = 0$ and $\langle P\rangle = \frac{1}{2}$, denoted by a solid line in figure 4.3. Therefore, for a higher order scenario, in the simulations we expect to see a three peak signal of the Polyakov loop in the range $[0, 1/2]$ with the interpretation that the theory stabilizes momentarily in this intermediate phase. In other words, whenever the simulation spends a reasonable time in a specific phase this creates points, namely signals in Monte-Carlo history. We are able to see this from the value of the Polyakov loop and one should have in mind that since the simulation is "quantum" there are fluctuations such that we consider the expectation value $\langle P\rangle$. Hence, we expect signals around $\langle P\rangle \approx 0$ and $\langle P\rangle \approx 0.5$ in a first order scenario. In a higher order scenario, when a suitable stable phase is present we shall have also a phase $\langle P\rangle \approx B$ with $0 \lesssim B \lesssim 0.5$.

4.2.2 Black strings in higher dimensions

Higher order phase transitions have been predicted also from gravity calculations [195], and the critical dimension was found to be[2] $D_c \approx 13.5$. The latter claim is accompanied with a Gregory-Laflamme instability which indicates a topology change of the black hole horizon. For example, for the case of a Schwarzschild black hole the topology of the horizon changes according to $\mathbf{S}^{D-2} \to \mathbf{S}^{D-3} \times \mathbf{S}^1$. The horizon topology $\mathbf{S}^{D-3} \times \mathbf{S}^1$ is interpreted as a black string, namely an arrow which contains localised black holes every $2n\pi R$ with n integer, and R being the radius of the compact dimension of $\mathbf{S}^1$.

Even though we are agnostic if we can apply the technognosy of gauge/gravity duality, we may explore the following idea. Along the lines of the motivation to generalize the spacetime dimensions of the gauge theory, one may ask if there is a similar analogue in gravity side. Of course, this goes along the lines of generalizing the Einstein-Hilbert gravity to arbitrary dimensions. Since, it is not clear how to generalize string theory in higher dimensions, we deploy some minimalistic ingredients to complete the picture. Based on the discussion of Sec. 3.6, the main motivation is to use the Polyakov loop as a detecting parameter to check whether or not there exists a black hole in the dual gravity theory in higher dimensions. When $d + 1 = 10$ the situation is more under control since the gravity dual is that of a black-zero brane in type IIA superstring theory where the eigenvalues of the Polyakov loop

[2]The difference between the the prediction of [183] and [195] indicates that the gauge/gravity duality might not apply anymore, at least in the usual way.

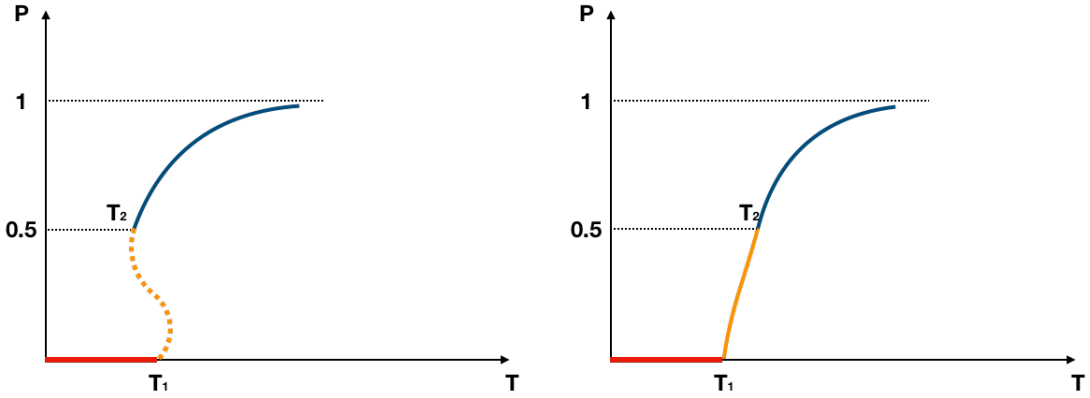

Figure 4.3: [Left]: the first order transition with $T_2 < T_1$ and the intermediate unstable phase denoted with dotted line. [Right]: higher order transition with a stable intermediate phase denoted with a solid line and $T_2 > T_1$.

represent D0-branes along the $\mathbf{S}^1$. In our general D dimensional case they represent partons spreading along the $\mathbf{S}^1$ part of $\mathbb{R}^{1,d-1} \times \mathbf{S}^1$. The interpretation is determined via $\rho(\theta)$, since a uniform (non-uniform) gapless distribution corresponds to uniform (non-uniform) black string [3] winding the $\mathbf{S}^1$ part of the spacetime. On the other hand a non-uniform and gapped distribution corresponds to a black hole localized on $\mathbf{S}^1$. There is a natural candidate for this local black hole which is a Schwarzschild black hole generalised in arbitrary dimensions. From this we can also construct a $(d+1)$-dimensional black string accompanied with the topology of $\mathbb{R}^{1,d-1} \times \mathbf{S}^1$ with line element

$$\mathrm{d}s^2 = \mathrm{d}s^2_{ST} + \mathrm{d}z^2. \tag{4.26}$$

The horizon topology of this geometry is $\mathbf{S}^{d-3} \times \mathbf{S}^1$. The coordinate dz^2 parametrizes the $\mathbf{S}^1$ part of the topology and sets the periodicity $\int_0^{2\pi} \mathrm{d}z = L$. When we take L to be large, we have a long array of black holes, and is more likely that an instability appears in the $\mathrm{d}z^2$ part of the metric. In fact this instability is related to tachyonic modes [131] and it reminds the Jeans instability. In the latter, inhomogeneities on a gas of particles (or partons) cause clusters in regions which are denser due to gravitational pull, leading in this way in an non-uniform string. This is due to the negative specific heat of the individual Schwarzschild black holes that form the string and their tendency to de-stabilize the black hole array because the entropy of this string can increase by re-distributing its mass in a non-homogeneous way. In

[3] With the terminology black string we are not referring to the string of string theory but rather a string consisting of n small black holes repeated after $2\pi R$.

a similar manner this instability is strikingly analogous to the Rayleight-Plateau instability for liquids [180].

The metric decomposes according to (4.26) and $\mathrm{d}s^2_{ST}$ is the d-dimensional Schwarzschild black hole (which is also known as Schwarzschild-Tangherlini [196]) whose metric is given by

$$\mathrm{d}s^2_{ST} = -f(r)\,\mathrm{d}t^2 + f(r)^{-1}\,\mathrm{d}r^2 + r^2\,\mathrm{d}\Omega^2_{d-2}. \tag{4.27}$$

Let us examine more this d-dimensional black hole. The metric is characterized by

$$f(r) = 1 - \frac{r_0^{d-3}}{r^{d-3}}, \tag{4.28}$$

$$\mathrm{d}\Omega^2_{d-2} = \mathrm{d}\phi^2 + sin^2\phi\,\mathrm{d}\theta_1 + \cdots + (\sin^2\phi\sin^2\theta_1\cdots\sin^2\theta_{d-4})\,\mathrm{d}\theta^2_{d-3}. \tag{4.29}$$

The mass of this d-dimensional black hole is related with the value of r for which there exists a killing horizon at

$$r_0^{d-3} = \frac{16\pi G_N M}{(d-2)\Omega_{d-2}}, \tag{4.30}$$

with G_N being the d-dimensional Newton constant, and $\Omega_{d-1} = d\frac{\pi^{\frac{d}{2}}}{(\frac{d}{2})!} = \frac{2\pi^{\frac{d}{2}}}{\Gamma(\frac{d}{2})}$ is the area of the unit sphere $\mathbf{S}^{d-1}$. In the Euclidean description, the black hole is thermal with temperature

$$T = \frac{1}{\beta} = \frac{\kappa}{2\pi} = \frac{f'(r_0)}{4\pi} = \frac{d-3}{4\pi}\left(\frac{16\pi G_N M}{(d-2)\Omega_{d-2}}\right)^{\frac{1}{3-d}} = \frac{d-3}{4\pi r_0}. \tag{4.31}$$

We have used the 0-th law of thermodynamics for the surface gravity defined as $\kappa := \frac{f'(r_0)}{2\pi}$ with prime denoting derivative w.r.t r. By using the first law, it is easy to obtain the entropy

$$S = \frac{4\pi}{d-2}\left(\frac{16\pi G_N}{(d-2)\Omega_{d-2}}\right)^{\frac{1}{d-3}} M^{\frac{d-2}{d-3}}. \tag{4.32}$$

Moreover, the specific heat follows from

$$\frac{1}{C} = \frac{dT}{dM} \Rightarrow C = -4\pi\left(\frac{16\pi G_N}{(d-2)\Omega_{d-2}}\right)^{\frac{1}{d-3}} M^{\frac{2-d}{3-d}}. \tag{4.33}$$

4.2.3 Large d analysis

We start by showing that there are two regions of the black hole parameterised by a different scale [197]. The Newtonian potential in d dimensions is normalised with a scale set by the horizon radius and it is given as

$$\Phi \sim \left(\frac{r_0}{r}\right)^{d-3}. \tag{4.34}$$

When d is a fixed number the only scale of the system, to describe all the relative phenomena in this geometry, is setted by r_0. On the other hand when we regard d as a parameter of the system that we take it also to be large, one finds that there is a different scale that characterises the gravitational force near the horizon

$$\nabla\Phi|_{r_0} \sim \frac{d}{r_0}. \tag{4.35}$$

Hence the large d limit introduces a new, parametrically separated length scale in the system

$$\frac{r_0}{d} \ll r_0. \tag{4.36}$$

This scale not only determines the slope of the gravitational potential, but also sets the distance at which gravitational effects are noticeably zero. In other words the two regions of the system are:

- The far way region, where the metric is asymptotically flat and characterised by

$$r > r_0 \quad \Rightarrow \Phi(r) \to 0. \tag{4.37}$$

- The near horizon limit setted by

$$r - r_0 \lessapprox \frac{r_0}{D} \quad \Rightarrow \quad \Phi(r) = \mathcal{O}(1). \tag{4.38}$$

It will turn out convenient in what follows if we set

$$n = d - 3, \tag{4.39}$$

and use this as a perturbation parameter instead of d, and furthermore introduce

$$q = \left(\frac{r}{r_0}\right)^n, \tag{4.40}$$

which is regarded as the finite radial variable near the horizon. By the introduction of a near horizon time also

$$\bar{t} = \frac{n}{2r_0} t, \tag{4.41}$$

one can find that the metric (4.27) takes the following form in the near horizon limit [197]

$$\mathrm{d}s^2_{\mathrm{nh}} = \left(\frac{r_0}{n}\right)^2 \left[-4\left(1 - \frac{1}{q}\right)\mathrm{d}\bar{t}^2 + \frac{\mathrm{d}q^2}{q(q-1)}\right] + r_0^2 q^{\frac{2}{n}}\,\mathrm{d}\Omega_{n+1}. \tag{4.42}$$

The prefactor of the $(\bar{t}, q)$ part of the metric reflects that the short scale r_0/n is a measure of the small proper radial extend of this near horizon zone, and of the short proper time required to cross it, measured with respect to units and times of an observer in the far away zone. One more coordinate transformation

$$\cosh^2\rho = q, \tag{4.43}$$

leads to

$$\mathrm{d}s^2 = 4\left(\frac{r_0}{n}\right)^2 \left(-\tanh^2\rho\,\mathrm{d}\bar{t}^2 + \mathrm{d}\rho^2\right). \tag{4.44}$$

Interestingly, this metric is the two-dimensional string black hole which is the coset manifold $SL(2,\mathbb{R})/U(1)$ [198–200]

This follows from ref's [201, 202] about the spherical reduction of Einstein gravity in the limit $d \to \infty$. Indeed, for a metric of the form

$$\mathrm{d}s^2 = g_{\mu\nu}\,\mathrm{d}x^\mu\,\mathrm{d}x^\nu + r_0^2 e^{-4\phi/(n+1)}\,\mathrm{d}\Omega^2_{n+1}, \tag{4.45}$$

where $g_{\mu\nu}$ is a two-dimensional metric and $\phi(x^\lambda)$ a two-dimensional scalar field, the Einstein-Hilbert action reduces to

$$I = \frac{\Omega_{n+1} r_0^{n+1}}{16\pi G} \int \mathrm{d}^2x\sqrt{-g}e^{-2\phi}\left(R + \frac{4n}{n+1}(\nabla\phi)^2 + \frac{n(n+1)}{r_0^2}e^{4\phi/(n+1)}\right), \tag{4.46}$$

and in the limit $n \to \infty$ becomes the two-dimensional string effective action

$$I = \frac{1}{16\pi G_2} \int \mathrm{d}^2x \sqrt{-g} e^{-2\phi} \left(R + 4\left(\nabla\phi\right)^2 + 4\Lambda_2^2 \right), \tag{4.47}$$

with

$$G_2 = \lim_{n\to\infty} \frac{G}{\Omega_{n+1} r_0^{n+1}} \quad , \quad \Lambda_2 = \frac{n}{2r_0}. \tag{4.48}$$

Indeed the metric (4.44) is a solution of this action with dilaton profile

$$\phi = -\ln\cosh\rho. \tag{4.49}$$

We notice that keeping n/r_0 finite amounts to keeping finite the Hawking temperature

$$T_H = \frac{\Lambda_2}{2\pi}, \tag{4.50}$$

for the large d Schwarzschild-Tangherlini black hole, while for the two-dimensional string black hole, the temperature conjugate to the time t is $1/2\pi$, in other words $1/n$ times smaller.

An interesting and, somehow, surprising fact is that one can motivate the appearance of effective strings living near the horizon. This argument uses the Hagedorn behaviour of the system via thermodynamics. Indeed for a Schwarzschild black hole in arbitrary dimensions we saw that the entropy (4.32) scales as $S(M) \sim M^{1+\frac{1}{d-3}}$. Taking the large d limit the entropy becomes that of a gas of strings with a Hagedorn spectrum

$$S(M) \sim M \tag{4.51}$$

whose thermodynamic stability depends on the details of logarithmic correction of this entropy formula.

Analogously, the entropy of a conformal gas with energy E in d dimensions is given as $S(E) \sim E^{1-\frac{1}{d}}$ where in the large d limit again gives

$$S(E) \sim E, \tag{4.52}$$

but now from the side of positive specific heat. In a sense, two-dimensional effective string theory instructs us to relate the string length as

$$\sqrt{\alpha'} \sim \frac{r_0}{d}, \tag{4.53}$$

such that the large d expansion is related to the α' expansion of the two-dimensional effective string. This leads to a Hagedorn temperature

$$T_H \sim \frac{d}{r_0} \tag{4.54}$$

For each dimension d there is a critical value of compactification length (L_{GL}) for which the black string becomes unstable [185]. In [203] it was proved analytically and in the large d limit the relation of the black hole horizon with the wavelength is

$$k_{\mathrm{GL}} \approx \sqrt{d}\frac{1}{r_0}, \tag{4.55}$$

d	5	6	7	8	9	10	11	19	29	49	99
$k_{\rm GL}$	1.27	1.58	1.85	2.09	2.30	2.50	2.69	3.89	5.06	6.72	9.75
$k_{\rm GL}^{\rm phys}$	1.33	1.63	1.9	2.13	2.34	2.54	2.72	3.90	5.02	6.72	9.75

Table 4.1: Critical wavelengths of (4.55) (up) and (4.58) (down) for various dimensions. Here $k_{\rm GL}$ is in units of r_0 from the original work of [203] and the agreement between them in large values of d is evidence of the validity of the large d analysis.

the latter being the tachyonic mode which signals the Gregory-Laflame instability. The wavelength is also given as

$$L_{\rm GL} = \frac{2\pi}{k_{\rm GL}} \approx \frac{2\pi r_0}{\sqrt{d}}. \tag{4.56}$$

At exactly this length the black string becomes unstable and we expect the Gregory-Laflame transition to be happening [185]. Note however that in order for this to be feasible we have to ensure that it is *not* the case $r_0 \gg L_{\rm GL}$ because then the black hole would not "fit" into the compact dimension. This argument was initially appeared in [185, 204]. After the appearance of the first negative Schwarzschild mode from Gregory and Laflamme, many other works appeared improving these results [185, 197, 205–208]. The wavelength has been improved to [207]

$$\tilde{k}_{\rm GL} = 1 - \frac{1}{2n} + \frac{7}{8n^2} + \frac{-\frac{25}{16} + 2\zeta(3)}{n^3} + \mathcal{O}(n^4), \tag{4.57}$$

where $n = d - 3$ as in (4.39) and $\zeta(x)$ is the Riemann zeta function. In the same work it is reported that the physical wavelength number is rescaled as

$$k_{\rm GL}^{\rm phys} \to \sqrt{n}\tilde{k}_{\rm GL} \tag{4.58}$$

due to the large D metric of black strings.
When we use these data to give a rough estimate of the Hagedorn temperature (4.54) we get that the physical Hagedorn temperature is

$$T_H^{phys} \sim \frac{\sqrt{d-3}}{\sqrt{d}}\tilde{k}_{\rm GL}. \tag{4.59}$$

Note that the treatment at this level is qualitative and precise coefficients are not known.

The physical wavelength (4.58) indeed reproduces the previous known values up to accuracy 2%. In table 4.1 we give a comparison between $k_{\rm GL}$ and $k_{\rm GL}^{\rm phys}$. In addition we give a comparison of the various temperatures (4.21), (4.22) and (4.59) in Fig. 4.4. It is important to note that we are just pointing out a striking similarity of large d expansion between a quantum mechanical large d theory and a gravitational higher dimensional theory.

Validity of the comparison

The comparison between the gravitational theory and the gauge theory should not be taken as established. In fact we are missing many precise factors in the gravitational side and therefore any quantitative analysis is at most preliminary. This is most obvious to see if one is willing to continue the comparison in Fig. 4.4 to larger d values where the gravitational curve crosses the gauge curves for the temperature.

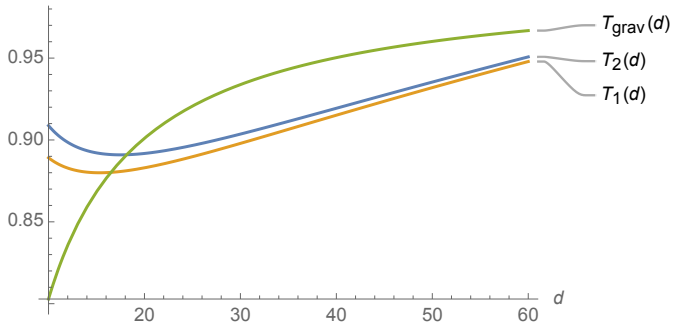

Figure 4.4: Behaviour of temperatures with respect to spatial dimensions d. T_1 and T_2 are taken from large d expansions of field theory while T_{grav} is from the gravitational analysis of black strings.

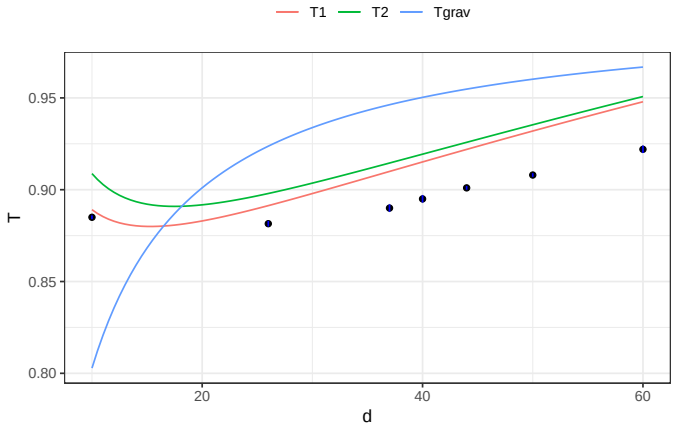

Figure 4.5: Comparison of the concluded simulation transition temperatures T_c with respect to T_1 and T_2 from (4.21) and (4.22) respectively. The two left-most points are from [193]. We note that we simulate $N = 64, S = 24$ so that we do not take into account the large N limit and continuous values in simulations due to time efficiency and hence the mild discrepancy. However the points follow the pattern of the analytic curves in the large N, continuous and large d limit modulo a shift on the y-axis.

On the other hand, and based on the gauge/gravity duality, it is not unreasonable to ask the question whether the growth of the temperature predicted by a gauge theory could be qualitative reproduced by a gravitational theory. This is a well-defined question and the comparison between the two could be done at least qualitatively because not all ingredients are known (at least for the gravitational side). Such a scenario has not been discussed in the past and indeed it is an interesting question to ask. In fact, the main motivation was to check whether or not we can confirm the predictions for $T_{1,2}(d)$ quantitatively from simulations, while the comparison with gravity will be at best qualitatively.

In any case, the former motivation, e.g to capture the characteristic behaviour of the gauge theory prediction was of legitimate interest, but the comparison with any gravitational theory in a precise sense will be a mystery until these kind of projects will get more scientific momentum and putted into more solid grounds.

	d=37	d=40	d=44	d=49	d=59
T_1	0.909947	0.915124	0.921955	0.931965	0.946347
T_2	0.914528	0.919358	0.925803	0.933779	0.949235
ΔT	0.004581	0.004234	0.003849	0.003460	0.002888
T_c	0.890(2)	0.8950(2)	0.901(1)	0.908(1)	0.922(2)

Table 4.2: Critical temperatures predicted for $T_{1,2}$ using equations (4.21) and (4.22). T_c is the observed temperature in the simulations.

4.2.4 Numerical results

For the numerical analysis we have simulated the model (4.19) for different dimensionality of the spacetime. Note that in the matrix model this simply translates to different number of matrices. We shall write $D = d + 1$ as usual.

We have performed a broad scan of temperatures for $D = 38$, $D = 41$, $D = 45$, $D = 50$ and $D = 60$ starting from $T = 0.1$ and up to $T = 1.5$ with $N = 32$ and $S = 24$. Having located approximately the transition to be happening around T_c we switched to $N = 64, S = 24$ and performed high statistics to see any possible signal structure of the Polyakov loop. The relevant critical temperatures are reported in table 4.2. Near these transition temperatures we observe a non-uniform and gapped distribution in the Polyakov eigenvalues as can be seen in Fig. 4.6.

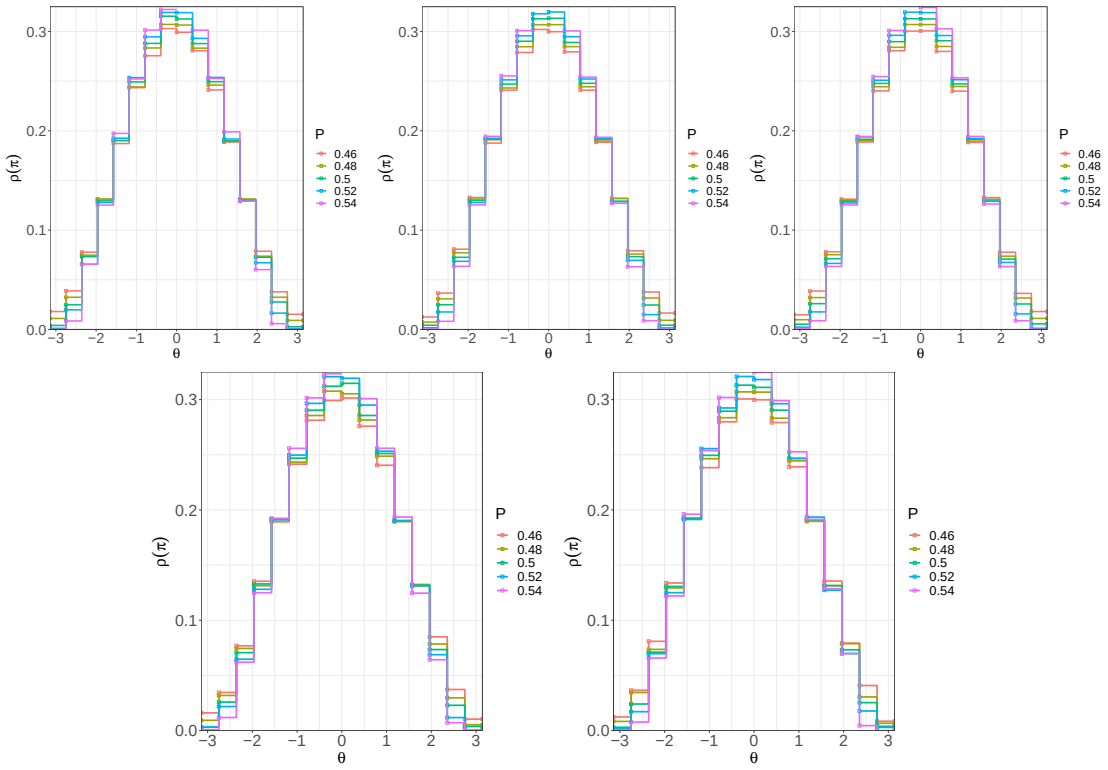

Figure 4.6: Distribution of the eigenvalues of Polyakov loop around the transition temperature T_c for $N = 64, S = 24$. [Up]: From left to right $d = 37, 40, 44$ and $T_c = 0.89, 0.8946, 0.901$ respectively. [Down]: From left to right $d = 49, 59$ and $T_c = 0.908, 0.922$ respectively. According to Fig. 4.2 we observe a non-uniform gapped distribution for all temperatures.

Both in Figs. 4.7 and 4.8 we observe an obvious transition. This transition, indeed qualifies to be related to a confinement/deconfinement transition. First of all, as we explained, the Polyakov loop gets an obvious amplification from $\langle P \rangle \simeq 0$ to $\langle P \rangle \simeq 1/2$. Secondly, the (free) energy gets shifted by $\mathcal{O}(N^2)$. When these parameters behave in this way, we recall from the discussion in Sec. 3.6 that in the dual gravity theory (if there exists) upon the transition to the deconfined phase the system behaves as a black hole, in a sense that the geometry it forms has the topology of a black hole with a horizon setted by the temperature T. The Fig. 4.7 has significant more statistics than Fig. 4.8. Note that while it is obvious to find the transition temperature for each d, it is not so easy to draw meaningful conclusions for the order of the transition at this level. We have approximately located the confinement/deconfinement

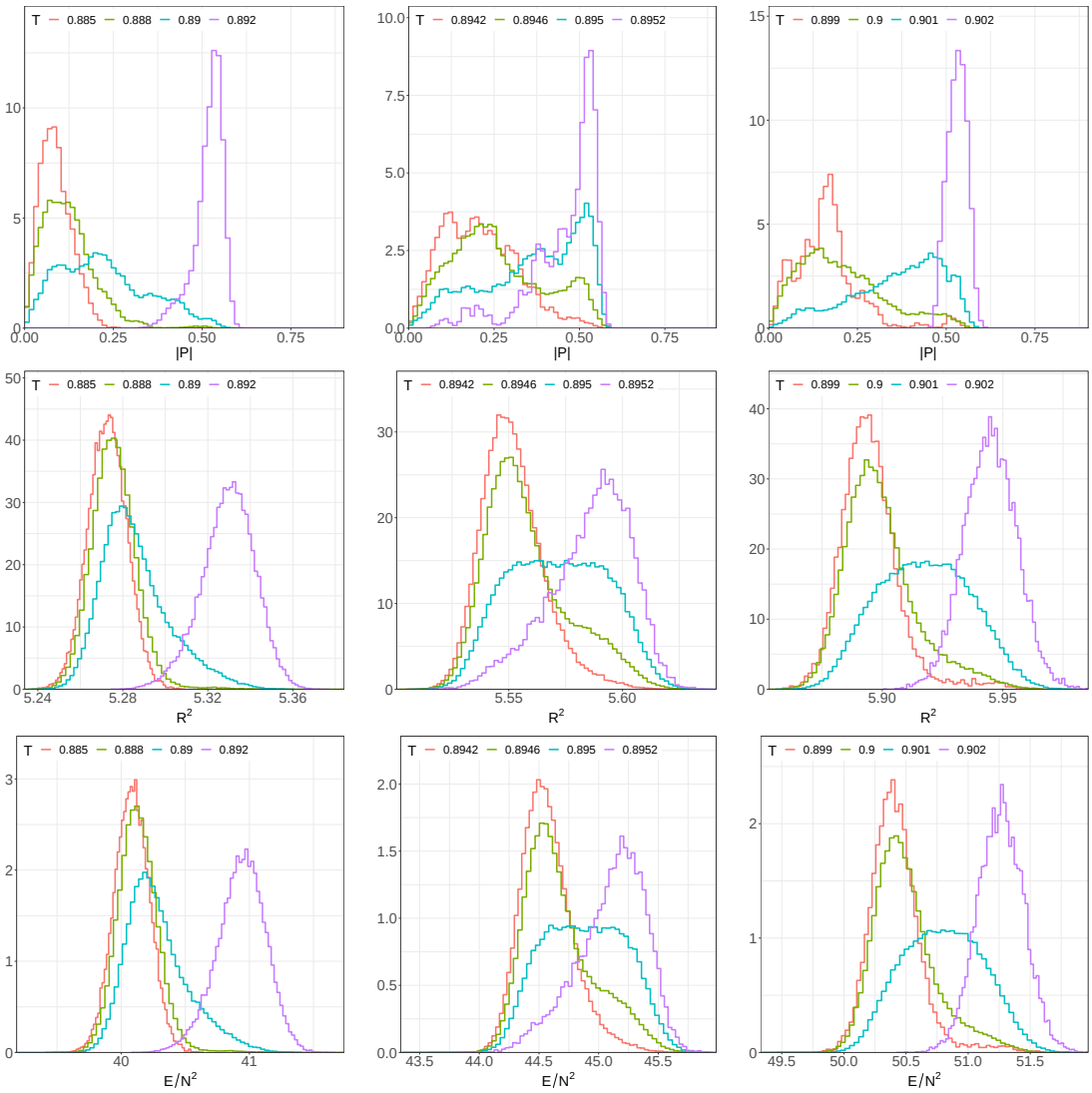

Figure 4.7: [First row] The Polyakov loop around the transition temperature T_c for $N = 64, S = 24$ at $d = 37, 40, 44$ respectively. [Second row] the same parameters for $\sum \mathrm{Tr}\, X_i^2$. [Third row] Again the same parameters for the energy. We see that for the energy there is a jump of order N^2 which confirms a confinement-to-deconfinement transition as it can also be shown from the Polyakov loop in the first row.

temperatures by looking in the Polyakov histograms and observing peaks near zero and one

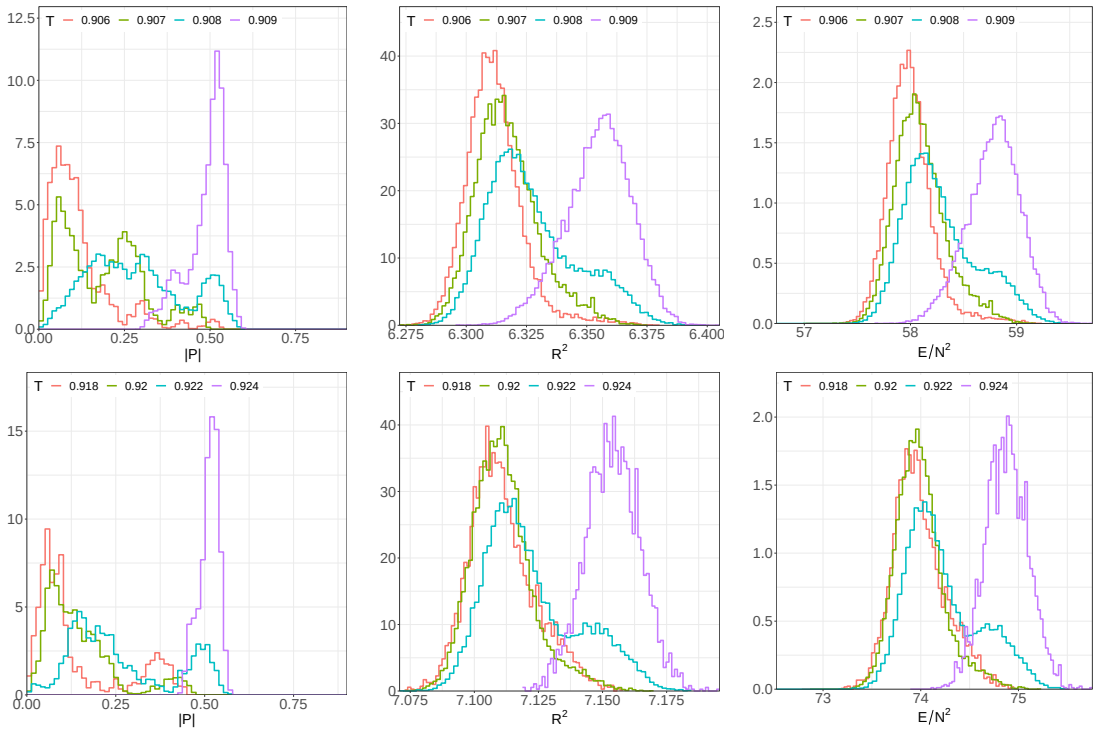

Figure 4.8: [First row] The Polyakov loop, the energy and $\sum \mathrm{Tr}\, X_i^2$ around the transition temperature T_c for $N = 64, S = 24$ at $d = 49$. [Second row] the same parameters for $d = 59$. We see again that the energy jump is of order N^2 which is accompanied by a transition in the Polyakov loop signalling a confinement/deconfinement transition.

half. A two peak signal indicates a first order transition while a three state peak a higher order. The main point, as can be seen from Figs. 4.7, 4.8 is that there is not a clear distinction between a first and a higher order transition because we do not clearly see neither a two-state nor a three state signal. There could be mainly two reasons for this. Either larger statistics is needed or larger N and d values or just both. Even though the order of the transition is not clear, what is more clear is the temperature for which this transition happens. We clearly see a jump in the Polyakov loop from around $\langle P \rangle \simeq 0 - 0.2$ to $\langle P \rangle \simeq 0.4 - 0.6$ accompanied with an energy jump of order N^2. Indeed this is a formation of a black hole-like geometry as we discussed previously.

Even more interestingly, the transition temperatures follow the patterns of the continuous lines predicted from the gauge theory using large d analysis given by equations (4.21) and (4.22) as it can be observed in Fig. 4.5. The discrepancy with the continuous lines is shows an almost constant shift towards the y axis and it could be a number of factors contributing on this. At the same time, the pattern of the continuous lines is reproduced by the observed temperatures up to a(n almost) constant shift along the y-axis.

We may also note that the comparison with the gravity analysis is not precise since the precise coefficients used are not known and not included in the gravitational temperature investigation. Yet the connection of large d black holes with two-dimensional string theory with a specific dilaton profile might shed some light on this in the future. Since our interest is not a high d analysis we do not investigate more on this direction but rather report an interesting observation. We leave the continuation of this work for a future observer.

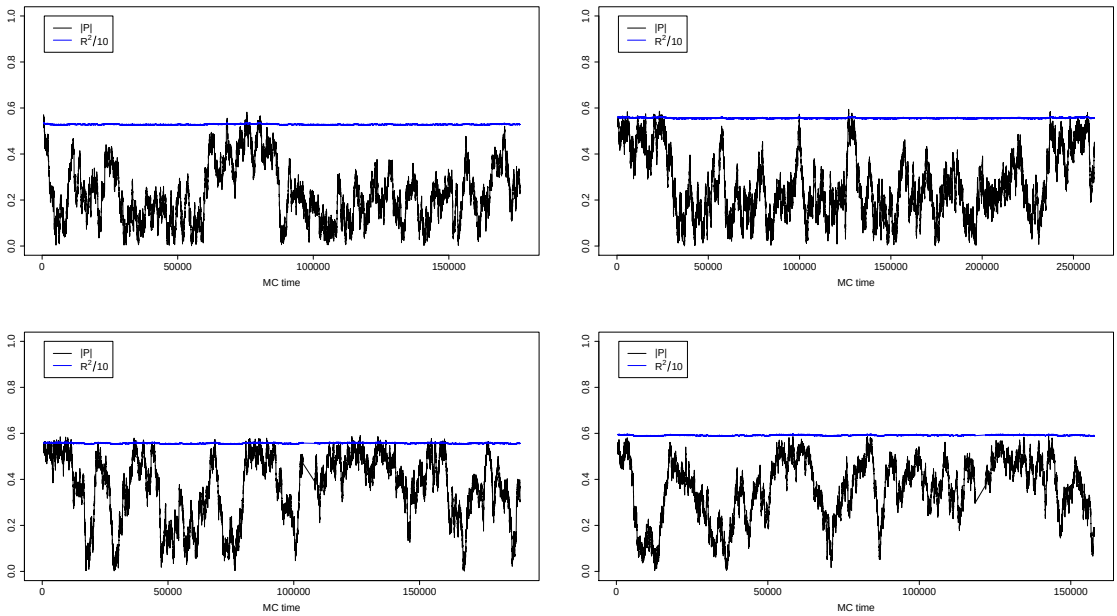

Figure 4.9: Monte Carlo histories near the transition temperatures at $N = 64, S = 24$ configurations. [Up-left]: Monte Carlo history for $d = 37$ at $T = 0.89$. [Up-right]: similarly for $d = 40$ at $T = 0.8946$. [Bottom-left]: $d = 40$ and $T = 0.895$. [Bottom-right]: $d = 44$ and $T = 0.901$.

Gauge gravity duality for large d?

It seems like an interesting possibility to relate high d gauge theories written in terms of matrices with high d gravitational theories. A relation between the two, if exists does not necessarily mean duality. We just saw above that the confinement-to-deconfinement transition temperature in the gravity side, could be related to the topology transition temperature of a higher dimensional black hole known as the Gregory-Laflamme instability. We may also note that the details of both theories at this level do not necessarily lead to any obvious claims, since only bosonic data are used from the gauge side and not precise coefficients are used for the gravity side. At this level we can claim that simulations seem to capture the right behaviour for the transition temperature motivated by large d gauge theories. Whether or not this is related with a gravitational theory containing a Gregory-Laflamme or some other transition we do not yet know.

4.3 Confinement-deconfinement in BMN model and appearance of M-theory

In this section we are changing a bit gears and explore more deeply the confinement-to-deconfinement transition and its relation with a known gravitational dual. More precisely, we will see that the type IIA black zero-brane is not always a good gravity candidate for the description of matrix models especially in the very low energy/temperature regime (recall also Fig. 3.4). The black zero-brane geometry is always deconfined, while as we will argue in

this section we could also observe the confined phase at very low temperatures. This amounts to crossing the diagonal line of Fig. 3.4 and entering the M-theory region. The question that arises in this case is what is confined then? Building intuition from the analysis we did in Sec. 3.6 we will argue that this amounts to a confined gas of supergravitons in eleven dimensions as we pictorially demonstrate in Fig. 4.15.

4.3.1 Introduction

The thermodynamic features of the D0-brane matrix model [53,209,210] and its one-parameter deformation BMN matrix model [211] are of great theoretical interest and, therefore, have been the subject of many investigations. Here we extend the insights gained by numerical simulations of these theories and provide a different viewpoint on their properties. Our main motivation is to give evidence that M-theory [212] and Schwarzschild black holes can be described by these matrix models.

M-theory plays an important role in the web of string dualities. It is the eleven-dimensional theory which has membranes as fundamental degrees of freedom. It appears as the strong-coupling limit of type IIA superstring theory, and its low-energy limit should be eleven-dimensional supergravity [213]. There exist a few proposals for nonperturbative formulation of M-theory based on the holographic principle. Among them, we consider the one based on the matrix-model approach [53, 209, 210]. [4] The history of this approach dates back to the 1980s when the M-theory proposal had not been made yet. At that time, the quantization of a supermembrane in eleven-dimensional spacetime was discussed, and a matrix model, which is called the BFSS matrix model today, was introduced as a natural regularization of the supermembrane in the light-cone gauge [209]. Later, this model was re-discovered as a candidate for the nonperturbative regularization of M-theory [53].

Further analysis using gauge/gravity duality [130] suggested that the BFSS matrix model can describe M-theory, type IIA superstring theory, and the phase transition between them [210], based on the calculations on the string/M-theory side of the gauge/gravity duality. The BMN matrix model [211] is a one-parameter deformation of the BFSS matrix model discussed in Refs. [53,209,210]. It has a rich phase structure and is often easier to analyze both analytically and numerically. Thermodynamic features of the BFSS matrix model have been studied intensively, starting from Ref. [214]. Agreement with type IIA superstring has been obtained with good precision using lattice simulations; for example, see Ref. [134] for numerical results at large-N and in the continuum limit. However, the parameter region in which the BFSS matrix model is expected to be dual to M-theory has not been studied in the past. Doing so was believed to be a very hard task because the stringy correction to the effective string coupling constant becomes large at temperature $T \sim N^{-10/21}$, which is a parametrically low temperature in the large-N limit. In this project, we propose a much easier way to identify the M-theory parameter region.

Black hole thermodynamics [215, 216] led to various deep insights into quantum gravity and quantum field theory, and gauge/gravity duality provides us with an ideal setup for the

[4] Another promising direction, to which numerical method similar to the one used in this project can be useful, is to study gauge theories dual to D2-branes or M2-branes. Maximally supersymmetric Yang-Mills theory in $2+1$ dimensions is dual to D2 or M2, depending on the parameter region [210], and hence, physics similar to the one considered in this project would be seen. See Ref. [142] for a lattice simulation of this theory.

study of the quantum aspects of black holes and emergent geometry in holographic duality. It has been successful for describing 'large' black holes which have positive specific heat. Detailed nonperturbative and quantitative tests based on Monte Carlo simulations for the BFSS matrix model were performed in Ref. [214] and following projects, and good agreement was also observed for D1-brane and D2-brane theories [139, 140, 142, 217]. Here, however, we are especially interested in small black holes with negative specific heat. Holographic duality should also be applicable to small black holes, including usual Schwarzschild black holes. For example, 4d SYM on S^3 should describe the 10d Schwarzschild black hole [218]. The BFSS matrix model at very low energy should describe an 11d Schwarzschild black hole in M-theory [210]. One of the goals of this project is to give evidence that the BFSS matrix model and BMN matrix model do describe small black holes.

In principle, the real-time dynamics of the matrix model can be efficiently simulated on quantum computers [141]. Hence, in the future, it might even become possible to study the entire life of a small black hole — from the formation via gravitational collapse to eventual evaporation — in a controlled manner in a fully quantum setup, in the context of superstring/M-theory.

Another, but very closely related, motivation is that we want to understand the microscopic mechanism of the confinement/deconfinement transition. Under the prism of gauge/gravity duality, deconfinement and the formation of a black hole are equivalent as we explained in Sec. 3.6 [219]. Strong-coupling results based on dual gravity analyses and weak-coupling results [167, 220] show striking similarity, while the latter show universal features regardless of the details of the theories [220]. Such generic features can naturally be understood in the framework of partial deconfinement [136, 152, 221, 222]: Between the confined phase ($\sim$ thermal AdS) and the deconfined phase ($\sim$ large black hole) of SU(N) gauge theory, there exists a partially-deconfined phase ($\sim$ small black hole) in which an SU(M) subgroup ($0 < M < N$) is deconfined. For several theories, partial deconfinement has been demonstrated analytically at weak coupling [221, 223], and numerically at strong coupling [224]. In this project, we provide evidence that the D0-brane matrix model provides us with an ideal setup to which a dual gravity analysis is tractable. As a byproduct, we will see that the confined phase, which has not been considered before, should exist, and can be (meta-)stable up to rather high temperature (see Fig. 4.10 for our conjecture). Once knowing it to exist, it is not hard to find such a confined phase numerically. Note that the existence of the confined phase is a consequence of the dual M-theory description and *not* the type IIA string theory description.

4.3.2 Short summary of the main claim

In this section, we summarize the main claims of the paper. The numerical evidence will be explained in later sections, together with various potential subtleties.

We study the thermodynamic features of the BFSS matrix model and BMN matrix model. These models can have various nontrivial backgrounds. In this paper, we are interested in the 'trivial' background. We carefully study the properties of the configurations obtained in our simulations and extract the configurations corresponding to the trivial background. The relevant parameters are the temperature T and the flux parameter μ. The BFSS matrix model is obtained by setting $\mu = 0$.

Based on lattice Monte Carlo simulations and dual gravity analyses, we propose the

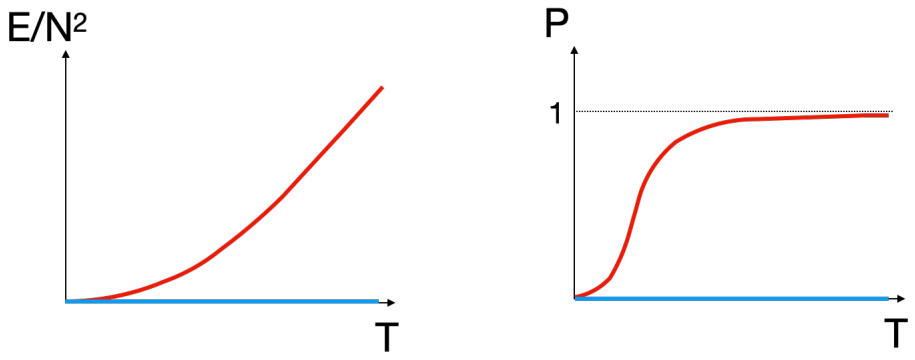

Figure 4.10: A cartoon picture of the (meta-)stable phases in the BFSS matrix model at finite temperature in the 't Hooft large-N limit ($\lambda = g^2N$ fixed). Red and blue lines characterize the deconfined and confined phases, respectively. In the past, the existence of the confined phase was not pointed out. Both are minima of the free energy, and the deconfined phase is the global minimum at any temperature. The existence of the confined phase is a natural consequence of the dual M-theory description, hence, the numerical confirmation of the confined phase on the matrix model side would be an interesting clue towards demonstrating the validity of the M-theory description.

following phase structure in the μ-T plane. If we vary T at fixed μ, there is a first-order phase transition with a strong hysteresis (see the left panel of Fig. 4.11, and also Fig. 4.16). The high-temperature, high-energy phase is deconfined (the Polyakov loop P is nonzero)q, low-energy phase is confined (the Polyakov loop is zero). These phases are the minima of free energy. There is a local maximum of free energy separating these two phases, whose corresponding states are partially-deconfined.[5] There are three kinds of critical temperatures, T_c, T_1, and T_2 (see Fig. 4.11, and also Fig. 4.16). T_c is the temperature where the free energies of the confined and deconfined phases coincide. At $T > T_c$ (resp., $T < T_c$), the deconfined phase (resp., confined phase) is the global minimum. Temperature T_1 is the highest temperature for the confined phase, i.e, the confined phase is a local minimum of the free energy for $T_c < T < T_1$, and this minimum disappears for $T > T_1$. Temperature T_2 is the lowest temperature of the deconfined phase which is a local minimum of the free energy at $T_2 < T < T_c$. As a function of μ, T_c is monotonically decreasing, as shown in Fig. 4.22.

Let us briefly summarize how this phase diagram is obtained and how it is related to M-theory.

BFSS matrix model ($\mu = 0$)

Let us start with the BFSS matrix model ($\mu = 0$). Ref. [210] studied the BFSS matrix model based on the dual gravity picture. The authors found the phases corresponding to a type IIA black zero-brane and the M-theory black string or black hole. It is natural to identify the type IIA and M-theory phases with the completely- and partially-deconfined phases,

[5] The partially-deconfined phase is stable in the microcanonical ensemble.

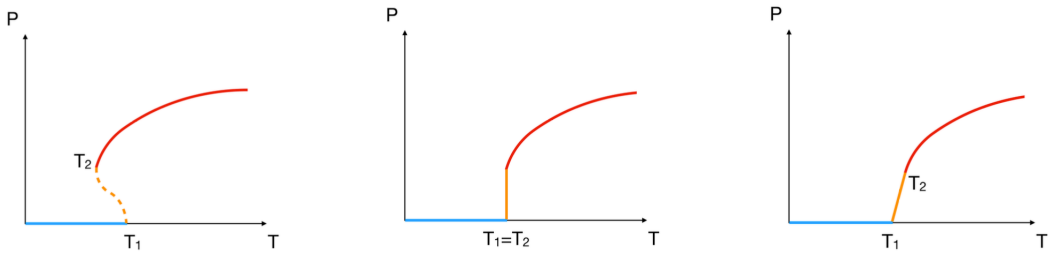

Figure 4.11: Typical shapes of confinement/deconfinement phase transition line in large-N gauge theories. The solid and dashed lines are minimum and maximum of the free energy at each fixed temperature. Similar plots can be drawn by taking the vertical axis to be the energy E instead of the Polyakov loop P. (This figure appeared originally in Ref. [136].)

respectively.[6,7]

Because of the existence of the partially-deconfined phase, we expect yet another, namely a completely-confined phase, which is likely to be dual to a graviton gas in eleven-dimensional spacetime; see Fig. 4.12. (Such a phase was not discussed in Ref. [210].) On the gravity side, T_1 is the highest possible temperature of the eleven-dimensional black hole. A very rough estimate for T_1 is $T_1 \gtrsim N^{2/9}$, as explained in Sec. 4.3.5, and hence, the confined phase should survive up to a rather high temperature. T_2 is interpreted as the temperature where the M-theory circle becomes large, and the transition from black string to black hole (Gregory-Laflamme transition [229]) takes place [210] and is estimated to be $T_2 \sim N^{-5/9}$ [230]. In fact this is easily estimated if we set the entropy of the black zero-brane (3.121) to be $\sim N$ recalling the discussion we did around Fig. 3.5. (See, e.g., Refs. [231–234] for detailed calculations for Gregory-Laflamme transition, and Ref. [235] for those with a boost.) Our numerical simulations confirm the existence of the confined phase. Such a confined phase is tantalizing evidence for the M-theory phase in the matrix model.[8]

T_c should be close to T_2, because otherwise the black zero-brane in type IIA supergravity (or boosted uniform black string in M-theory, which is essentially the same as a black zero-brane) is a good approximation, and we find sufficiently small free energy. Specifically, both T_2 and T_c are expected to be zero in the strict large-N limit. For $T_2 < T < T_1$, we expect a two-state signal in the Monte Carlo simulations if N is sufficiently large. In the histograms of the energy or the Polyakov loop observables, there should be two peaks corresponding to two minima of free energy. The local maximum of the free energy should be seen as a dip separating the two peaks. However, in our simulation, we did not observe the two-state signal; the deconfined phase is too unstable for the small values of N we could study with available computer resources ($N \leq 16$). As a consequence, we could not determine T_2 and T_c.

[6] Here, we are assuming that the latter has negative specific heat and hence corresponds to the local maximum of free energy; see Sec. 4.3.5 and Appendix C. On the large-energy, low-temperature side of the M-theory phase the dual picture is a black string, while on the low-energy, high-temperature side it is a black hole.

[7] From a different angle, Refs. [225–228] proposed that the BFSS matrix model describes an 11d black string or black hole boosted along the M-theory circle.

[8] As far as we notice, the existence of the confined phase in the BFSS matrix model has not been appreciated in the past.

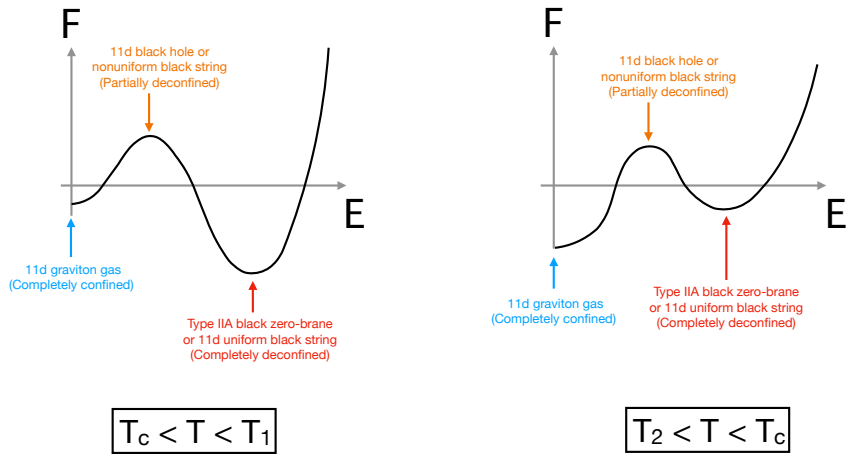

Figure 4.12: A conjecture for the relationship between free energy F versus energy E at fixed temperature T in the BFSS matrix model. An 11d Schwarzschild black hole gives the local maximum which separates the two minima. (See Appendix C for why negative specific heat implies a free energy maximum.)

BMN matrix model

We studied the BMN matrix model in order to confirm the two-state signal and give stronger support for the validity of the M-theory description in the BFSS limit. The large-μ region is weakly-coupled, and hence perturbative methods are applicable. The small-μ region (more precisely, small but order N^0) can be studied via dual type IIA supergravity. By combining the large-μ and small-μ analyses, Ref. [236] conjectured that the transition is of first order at any μ, and the critical temperature T_c decreases monotonically as a function of μ and becomes zero at $\mu = 0$ (the left of Fig. 4.13).

We performed Monte Carlo simulations at various values of μ and observed quantitative agreement with the phase diagram conjectured in Ref. [236]. We observed clear two-state signals at $\mu \geq 0.5$, and even at $\mu = 0.3$ our results support the existence of a first-order transition. As shown in Fig. 4.22, the critical temperature T_c agrees well with the conjecture in Ref. [236] at $\mu \geq 0.8$. Apparent deviation at $\mu < 0.8$ can naturally be explained by taking into account finite-N corrections on the gravity side.

The BFSS and BMN matrix models are defined via the actions (3.86), (3.96). In this project, we will consider the thermodynamic features of the BFSS and BMN matrix models. There are three parameters: the 't Hooft coupling $\lambda = g_{YM}^2 N$, the temperature T and the flux μ. As explained earlier the 't Hooft coupling has a dimension of $(\text{mass})^3$, and can be set to 1 by proper rescaling of time t and matrices. In other words, all dimensionful quantities are considered in units of λ. For example T, μ, and the energy E are actually $\lambda^{-1/3}T, \lambda^{-1/3}\mu$ and $\lambda^{-1/3}E$. We mainly focus on the 't Hooft large-N limit,[9] in which T and μ are fixed and the energy is proportional to N^2.

[9]The only exception is when we discuss a relation to the M-theory region, which requires a different kind of large-N limit.

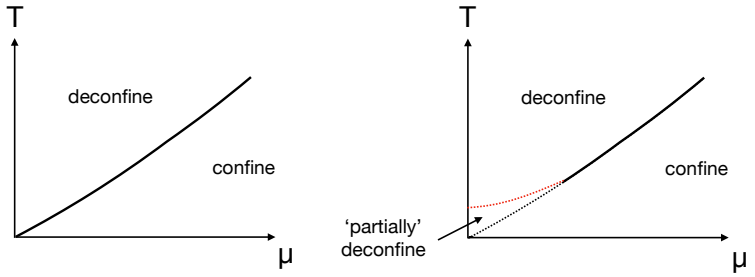

Figure 4.13: Two kinds of conjectured phase diagrams of the BMN matrix model. The large-μ region permits perturbative calculations [151, 237], and the transition is found to be of first order. The small-μ region has been studied by using the dual gravity description [236] but the order of the transition has not been established. We will argue that the left panel (first-order scenario) is likely to be true.

As we saw, in the BFSS matrix model, the potential term $-\frac{1}{4}[X_I, X_J]^2$ vanishes if the matrices commute with each other. Therefore, at the classical level, there are flat directions. Due to supersymmetry, a remnant of these flat directions survives at the quantum level. Namely, the energy of almost-diagonal configurations $X_I \simeq \mathrm{diag}(x_I^1, x_I^2, \cdots, x_I^N)$ can be asymptotically small when the distance between diagonal entries $\sqrt{\sum_I |x_I^i - x_I^j|^2}$ is large. These diagonal entries are regarded as the locations of D0-branes.

Despite the existence of flat directions, D0-branes can form a bound state.[10] In this project, we will consider the 'trivial vacuum', in which all D0-branes are bound together. The trivial vacuum becomes more and more stable as N becomes large.

4.3.3 Trivial and fuzzy-sphere vacuum in the BMN matrix model

In the BMN matrix model, the flat direction is lifted due to the deformation term. Instead, it has multiple supersymmetric vacua characterized by the fuzzy-sphere classical solution[11]

$$X_i = \mu J_i \ (i = 1, 2, 3) \ , \qquad X_a = 0 \ (a = 4, \cdots, 9) \ , \qquad \psi = 0 \ , \tag{4.60}$$

where J_i are the generators of an SU(2) algebra. As long as they satisfy the standard commutation relation $[J_i, J_j] = \sqrt{-1}\epsilon_{ijk}J_k$, any representation is allowed. In addition, a generic representation is characterized by the spin $s = 0, \frac{1}{2}, 1, \frac{3}{2}, \cdots$ and the number of spin-s

[10] For the precise meaning of this bound state, see Ref. [238].

[11] Strictly speaking, the configuration (4.60) should be interpreted as the center of a wave packet. See [238] for details.

representations n_s. The matrix size N is $N = (2s+1)n_s$ and the classification of vacua is characterized by partitions of N [211]. One more interesting point of view is that the classification of these vacua on the gravity side can be interpreted as an electrostatic problem [239, 240].

The mathematical reason why these vacua are interpreted as fuzzy-sphere vacua is that the matrices X_i can be interpreted as the embeddings $X_i : \mathbf{S}^2 \hookrightarrow \mathbb{R}^3$. Being assigned to generators of $SU(2)$ they generate non-commutativity on the surface of $\mathbf{S}^2$ justifying the fuzzy-sphere interpretation [241]. On equal footing is the interpretation from string theory, where the diagonal elements of the matrices $X_{i,a}$ are interpreted as positions of D0-branes and non-diagonal elements as open strings between them. In the case of fuzzy sphere configurations, D0-branes are in a non-commutative sense localized on the surface of $\mathbf{S}^2$ which furthermore lives in $\mathbb{R}^3 \subset \mathbb{R}^9$. The interpretation of D2-branes as consisting of D0-branes is well known in string theory where under the presence of fluxes (μ in our case) D0-branes polarize and form non-commutative structures [242].

Hence, fuzzy-sphere vacua can be interpreted from the gravity perspective as concentric fuzzy spheres consisting of D0-branes, placed at the center of $\mathbb{R}^6$ and living only in the three dimensional subpart of spacetime whose radii scale as

$$r_s \simeq \mu s \ . \tag{4.61}$$

When $n_0 = N$ and $n_{s\geq 1} = 0$, the ground state is given by

$$X_1 = X_2 = \cdots = X_9 = 0 \ , \qquad \psi = 0 \ . \tag{4.62}$$

This state is called the "trivial" vacuum. Despite its simple appearance, the trivial vacuum has rich, nontrivial features. In this project, we focus on this vacuum.[12]

At the classical level, the radius of the spin-s fuzzy sphere is $\mu\sqrt{s(s+1)}$. As μ becomes smaller, the radii of the fuzzy spheres approach zero, and hence, tunneling from the trivial vacuum to nontrivial fuzzy-sphere vacua can happen more easily. Hence, it is crucial to ensure that the combination μN (see appendix A) is large enough to avoid ending up in an undesirable vacuum. At zero temperature, the quantum fluctuation of each matrix entry is roughly $0.6N^{-1/2}$ [238].[13] The radius of the smallest nontrivial fuzzy sphere ($s = \frac{1}{2}$) is $\frac{\mu}{2}\sqrt{3}$. The radius of the largest fuzzy sphere ($s = \frac{N-1}{2}$) is $\frac{\mu}{2}\sqrt{N^2-1}$. Therefore, when N is not so large, say $N = 16$, all possible fuzzy spheres are buried in quantum fluctuations if $\mu \lesssim 0.018$. On the other hand, if μ is fixed and N is sent to infinity, all fuzzy-sphere vacua are distinguishable [238].

The Myers term is a convenient order parameter for the formation of fuzzy spheres. It is defined by

$$M = \frac{i}{3N\beta}\int_0^\beta \mathrm{d}t \sum_{i,j,k=1}^{3} \epsilon_{ijk}\,\mathrm{Tr}\,X^i X^j X^k \ . \tag{4.63}$$

We monitor it during the simulations. In addition, the different $\mathrm{Tr}\,(X^i)^2$ for each i are measured to identify nontrivial vacua. The classical value of M is $\frac{\mu^3}{3N}\sum_s n_s s(s+1)(2s+1)$,

[12] Unlike here, Ref. [243] focused on the transition between various vacua.

[13] The value $0.6N^{-1/2}$ is the standard deviation. The order-one factor can be determined numerically, from the expectation value of $\sum_{I=1}^{9}\mathrm{Tr}X_I^2$, which is approximately $3.5N$ [134]. There are $9N^2$ matrix entries and hence $\sqrt{\frac{3.5N}{9N^2}} \approx 0.6N^{-\frac{1}{2}}$.

which is 0 for the trivial vacuum, $\frac{\mu^3(N^2-1)}{12}$ for the largest fuzzy sphere (single fuzzy sphere of $s=\frac{N-1}{2}$), and $\frac{\mu^3}{4}$ for $\frac{N}{2}$ fuzzy spheres of $s=\frac{1}{2}$. We can detect a formation of a large fuzzy sphere or many small fuzzy spheres, unless μ is too small, by monitoring M or R^2 defined by

$$R^2 = \frac{1}{N\beta}\int_0^\beta \mathrm{d}t \sum_{I=1}^{9} \mathrm{Tr} X_I^2. \tag{4.64}$$

However, it is difficult to detect the formation of a small number of small fuzzy spheres by monitoring M. Still, when such ambiguity arises, it is unlikely that the properties of those vacua such as the deconfinement temperature are significantly different. Therefore, we neglect this subtlety in the present project. To summarize all the above, we show the normalized R_i^2 and R_a^2 as well as the Myers term (4.63) in Fig. 4.14.

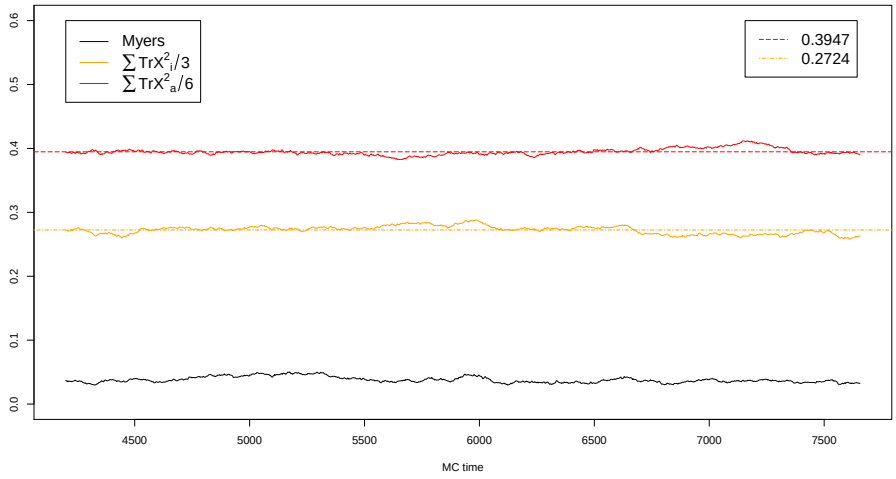

Figure 4.14: Fluctuations of the first three matrices $\mathrm{Tr}\, X_i^2/3$ and $\mathrm{Tr}\, X_a^2/6$ grouped together show an obvious breaking of the symmetries. The parameters shown are $N=16, S=24, T=0.23$ and $\mu=0.6$. We see that the Myers term is very small, indicating not a formation of a big fuzzy sphere. On the other hand, a priori there could be many small fuzzy spheres and in such a scenario the Myers term cannot distinguish these configurations.

4.3.4 Conjectured phase structure at finite temperature

In this section we present our conjecture regarding the phase diagram of the BMN and BFSS models. Numerical evidence will be shown in Sec. 4.3.7.

First, let us discuss some generic features of the confinement/deconfinement transition at large N.

As we saw earlier, the distribution of the phases of the Polyakov line, which we denote as $\theta_1, \theta_2, \cdots, \theta_N$, provides us with a convenient way to understand the confinement/deconfinement transition. In the large-N limit, we can use a continuous function $\rho(\theta)$ defined at $-\pi \le \theta < \pi$ and normalized as $\int_{-\pi}^{\pi} d\theta \rho(\theta) = 1$ to describe the distribution of θ. Roughly speaking, there are three kinds of phases visualized in Fig. 4.2 [167, 220]:[14] the uniform (blue), non-uniform and non-gapped (orange) and non-uniform and gapped (red) phases. They can

[14]Note that we are considering the thermal transition here. When the different boundary conditions such

be understood as the confined, partially-deconfined (equivalently, partially-confined) and completely-deconfined phases, respectively [136, 221, 222].

For historical reasons, let us call the transition between the uniform phase and the non-uniform, non-gapped phase (resp., the non-uniform, non-gapped phase and the non-uniform, gapped phase) the Hagedorn-like transition (resp., the Gross-Witten-Wadia (GWW) transition).[15] Let T_1 (resp., T_2) be the transition temperature for the Hagedorn-like transition and the GWW transition, respectively. In Fig. 4.11, a sketch of the temperature dependence of the Polyakov loop P is shown. From left to right, the panels correspond to $T_1 > T_2$, $T_1 = T_2$, and $T_1 < T_2$ respectively. The case with $T_1 = T_2$ can be found, e.g., for the weak-coupling limit of 4d Yang-Mills theory on $\mathbf{S}^3$. In this case, at the critical temperature $T = T_1 = T_2$, states with different values of P have the same free energy, and hence, all of them are equally important in the canonical ensemble. Such degeneracy in the free energy comes from the cancellation of the entropy factor and the Boltzmann weight, which is the same as the mechanism of the Hagedorn growth in string theory [246]. As we argued before, this gives a nice intuitive connection between deconfinement and the formation of a black hole [167, 220]. When the interaction is introduced, depending on the details of the theory, the vertical orange line can be tilted toward the left ($T_1 > T_2$) or right ($T_1 < T_2$). In the former case, the non-uniform, non-gapped phase has negative specific heat (i.e. $\frac{dE}{dT} < 0$; note that the energy E increases with P), and in the canonical ensemble, this is a maximum, rather than a minimum, of the free energy at each fixed T. Such phase resembles the so-called small black hole [220]. Partial deconfinement gives a natural way to understand the negative specific heat [136]. Note that, in the canonical ensemble, a first-order transition analogous to the Hawking-Page transition [219, 249] with hysteresis is expected when $T_1 > T_2$.

4.3.5 BFSS matrix model ($\mu = 0$)

In this subsection, we argue that the BFSS matrix model should have a confined phase corresponding to a metastable vacuum. The dual M-theory description plays a crucial role, and hence, the confirmation of confinement is tantalizing evidence for the dual M-theory description.

't Hooft large-N limit via dual IIA superstring theory

Let us consider the 't Hooft limit of the BMN matrix model at $\mu = 0$, corresponding to the BFSS model. The deconfined phase is dual to a black zero-brane in type IIA string theory [210]. According to this, the dual gravity analysis predicts that the energy at sufficiently low temperature is $E \simeq 7.41 N^2 \lambda^{-3/5} T^{14/5}$ up to stringy corrections. No phase transition

as the periodic boundary condition are used, other types such as the multi-peak distribution can appear as well. Recently, an analogue of deconfinement in the index of 4d $\mathcal{N} = 4$ SYM was found [244], and multi-peak distributions were reported in, e.g., Ref. [245]. Sometimes, such phases are called 'partially-deconfined phase' as well. Note also that, at strong coupling, the phase structure may be richer, and we may need to use other order parameters as well; in the dual gravity description, various black hole solutions can exist.

[15] When the free-string picture is available, the transition between the uniform phase and the non-uniform, non-gapped phase is actually the formation of the Hagedorn string [246], as long as the 't Hooft coupling is not too large. Such an interpretation may not be valid when the gravity dual is M-theory. The word "GWW transition" is used to mean the formation of the gap in the eigenvalue distribution. In the weakly-coupled theory studied in Refs. [167, 220], this transition is of third order, resembling the original Gross-Witten-Wadia model [247, 248].

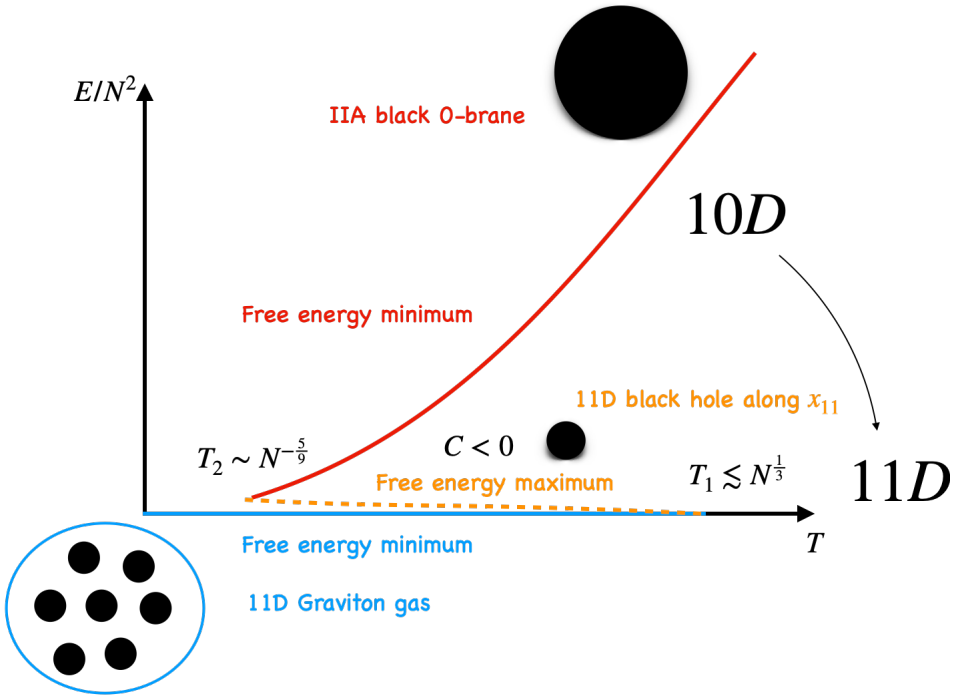

Figure 4.15: This figure summarises the discussion in the main text. The colours are selected such that they much with Fig's. 4.12, 4.2 and 4.16. In particular, going downwards in the diagram we are going to strong coupling regime since $g_{\text{eff}} = \frac{\lambda}{E^3}$, and according to the discussion in the main text we expect a Gregory-Laflamme type of transition to be happening. The intermediate phase with negative specific heat ($C < 0$) corresponds to a Schwarzschild black hole localised along the compact dimension x_{11}. The reason how this black hole appears small and how it fits in x_{11} is explained in Appendix D. In addition, it serves as phase separator between the phase of confinement which corresponds to a graviton gas in $11D$ and the phase of deconfinement which represents a black string in $10D$. These phases themselves correspond to maximum, and two minima respectively in the free energy.

is expected; at any nonzero temperature, the energy is of order N^2, and hence, the system is in the deconfined phase. This conjecture has been tested via Monte Carlo simulation by several groups, e.g., Refs. [134, 143–146, 150, 214, 250]. In Ref. [134], the large-N, continuum limit has been taken in a wide temperature region $\lambda^{-1/3}T \geq 0.4$. Even at $\lambda^{-1/3}T = 0.4$, the distribution of the Polyakov line phases $\rho(\theta)$ is clearly gapped, and the energy can be fit by the ansatz based on the weakly-coupled string theory. As long as the dual type IIA description is valid, we expect only the deconfined phase.

As we will discuss below, a confined phase ($\frac{E}{N^2} \to 0$, $P \to 0$ as $N \to \infty$ at fixed T and fixed λ) can also exist.[16] Except for the parametrically low temperature, the confined phase has larger free energy than the deconfined phase, and hence, it does not dominate the canonical ensemble. Still, such a metastable phase can be identified in Monte Carlo simulations if we choose the initial configuration for the simulation carefully. We will argue that the existence

[16]This is not the 't Hooft large-N limit, and standard 't Hooft counting does not hold.

of this confined phase constitutes strong evidence for M-theory on the gravity side.

M-theory and confinement

Let us continue the study of $\mu = 0$, but depart from the 't Hooft limit and go to parametrically small energy in the microcanonical ensemble. As we will see, dual gravity picture suggests a first-order transition in the canonical ensemble.

Based on the gauge/gravity duality, it was conjectured [210] that there are two phases dual to the type IIA black zero-brane and M-theory black hole (11d Schwarzschild black hole), based on the analysis of the gravity side. Separately, Refs. [225, 226, 228] studied the matrix-model description of the 11d Schwarzschild black hole and discussed how thermodynamic relations might be explained. More precisely [210, 228]:

- At $E \gtrsim N^{2/3}\lambda^{1/3}$ and $T \gtrsim N^{-10/21}\lambda^{1/3}$, a type IIA black zero-brane is a good dual description. The energy and entropy scales as $E \sim N^2\lambda^{-3/5}T^{14/5}$, $S \sim N^2\lambda^{-3/5}T^{9/5}$. The specific heat is positive.

- Below $E \sim N^{2/3}\lambda^{1/3}$, the M-theory circle is relevant in the thermodynamic analysis. When the energy is not too small, the appropriate object in the dual picture becomes the uniform black string wrapped around and boosted along, the M-theory circle. This object is a trivial M-theory uplift of black zero-brane, and hence thermodynamic properties are similar to those of a black zero-brane.

- When the energy is lowered further, the Gregory-Laflamme transition [229] to a localized boosted 11d black hole takes place at $S \sim N$ and $T \sim N^{-5/9}$ [230].

Therefore it is natural to expect $T_2 \sim \lambda^{1/3}N^{-5/9}$. Note that this is outside of the 't Hooft scaling regime $T \sim \lambda^{1/3}N^0$ and we expect that T_c is close to T_2.

The detailed properties of the M-theory black hole are not known. However, a few generic features can be inferred. Firstly, we expect that the dual geometry is a black hole and graviton gas in a finite-size box, analogous to AdS times sphere. In Refs. [225–227], it is assumed only a part of D0-branes (or more precisely, matrix degrees of freedom) participate in the Shwarzschild black hole. Other D0-branes can describe gravitons emitted from the black hole. This can naturally be understood in terms of partial deconfinement [238], i.e., the deconfined sector describes the degrees of freedom in the black hole. By assumption all eigenvalues are bounded (i.e., we imposed such constraint in the numerical simulation), hence the degrees of freedom in the confined sector contribute to the bulk geometry as well and the geometry would not be too different from black zero-brane seen from an observer at sufficiently far from the black hole. Specifically, we expect a large M-theory circle near the center of the bulk geometry. Secondly, the KK-momentum of the black hole along the M-theory circle can decrease as the energy is lowered, because the KK momentum corresponds to the number of D0-branes. Therefore, we expect that the thermodynamic properties is not drastically different from a small black hole without boost. Specifically, we conjecture that the M-theory black hole has negative heat capacity, namely the temperature increases as the energy decreases.[17]

In the canonical ensemble, such a phase corresponds to the local maximum of free energy separating the zero-brane phase (deconfined phase) and vacuum or graviton gas (confined

[17] We emphasize that this statement is speculative and it is desirable to have a more elaborate analysis.

phase). To give a very rough estimate of T_1, we use the Schwarzschild solution in the non-compact space without boost, $S \sim \frac{T^{-9}}{G_{\mathrm{N},11}} \sim N^3 T^{-9}$, as an approximation. Then we obtain $T \sim N^{2/9}$ for the entropy at the Gregory-Laflamme transition, $S \sim N$. There is a jump of the temperature compared to the boosted uniform black string. It is likely that a non-uniform black string phase connects these two phases. For complete evaporation to graviton gas, the black hole would have to be much smaller than the Gregory-Laflamme point. Therefore, we expect $T_1 \gtrsim N^{2/9}$. A natural upper bound would be the 11d Planck scale $\sim N^{1/3}$. We emphasize again that this is a very rough estimate; the important point is that T_1 can become parametrically large at large N. In Appendix D we show how to obtain the scaling $T_1 \lesssim N^{1/3}$.

Schwarzschild black holes have negative specific heat in all dimensions (see e.g eq (4.33)). It is natural to conjecture that such phases with negative specific heat, for which the nontrivial geometry along the eleventh direction is important, are partially-deconfined. See Fig. 4.12 for a sketch of the relationship between the free energy and energy at a fixed temperature. The transition between the partially-deconfined phase and the completely-deconfined phase is the Gross-Witten-Wadia (GWW) transition where the gap is developed in the distribution of Polyakov line phases [136, 222]. In this sense, it would be natural to interpret the GWW transition as a 'phase transition between string theory and M-theory'.

Our study in the 't Hooft limit suggests the phase diagram shown on the left of Fig. 4.13. Assuming the dual gravity analysis for the $\mu \to 0$ limit [210] is valid, a cross-over from type IIA string theory to M-theory should be found as the energy is lowered if we zoom into the lower-left corner of this phase diagram. Although the heat capacity is positive in the type IIA region, it can turn negative in the M-theory region. Therefore, it is not unreasonable to expect that the phase transition we observe in this project is connected to the typeIIA/M-theory phase transition.[18] Therefore, we might be able to learn about the M-theory black hole by studying the partially-deconfined phase in the BMN matrix model.

The highest temperature of the trivial-confined phase T_1 is the highest temperature of the partially-deconfined phase. Because we expect that the partially-deconfined phase is dual to the eleven-dimensional Schwarzschild black hole, we should find the temperature of the smallest possible black hole. We can use the Gregory-Laflamme-transition temperature $T_1 \gtrsim N^{2/9}$ as a lower bound for T_1. A loose upper bound can be obtained by the Planck scale $T_1 \lesssim N^{1/3}$.

A parametrically large T_1 is probably a generic feature of string/M-theory [251]. As a well-known example, let us consider the case of the duality between 4d SYM and type IIB string theory on $\mathrm{AdS}_5 \times \mathrm{S}^5$ with large fixed 't Hooft coupling $\lambda_{4\mathrm{d}} = O(N^0)$ [218, 220]. In this case, we have two scales: The Planck scale and the string scale. Supergravity is a good approximation when the black hole is bigger than the string length because strings can behave like point particles. Below this scale, the description as Hagedorn string is more appropriate. Therefore, $T_1 \sim \ell_s^{-1} \sim \lambda_{4\mathrm{d}}^{1/4}$ is expected, where $\lambda_{4\mathrm{d}}$ is the 't Hooft coupling of 4d SYM. Note that this is the same as the Hagedorn temperature of the free string.[19] Note also that the mass of the 10d Schwarzschild black hole at T_1 is much larger than the Planck mass in this

[18] This expectation may not be valid if there is a phase transition separating the $\mu \to 0$ limit and $\mu \sim N^0$ region. A theoretically complicated feature of the limit of $\mu \to 0$ is that different fuzzy-sphere vacua become identical with the trivial vacuum of the BFSS matrix model unless the spin is increased as μ approaches zero.

[19] The length of the string is related to the energy E and entropy S as $E \sim \frac{L}{\ell_s^2}$ and $S \sim \frac{L}{\ell_s}$. The Hagedorn temperature T_H is the temperature at which the free energy of the free string $F = E - TS$ becomes zero, and hence, $T_H \sim \frac{1}{\ell_s}$.

case. Still, in the strong coupling limit ($\lambda_{4d} \to \infty$), T_1 becomes parametrically large. See also Fig. 3.13 and the discussion around it.

Strictly speaking, the 10d black hole phase considered above is the equilibrium state of a 10d black hole plus graviton gas filling the rest of $AdS_5 \times S^5$. In the 't Hooft large-N limit, the energy of the graviton gas is much smaller than that of the black hole. Hence it could be ignored in the thermodynamic analysis, and the 10d black hole is stable in the microcanonical ensemble. The situation can change away from the 't Hooft large-N limit [251]. A weakly-coupled string description is justified as long as $g_s \sim g_{4d}^2 \ll 1$ and $\frac{\ell_s}{R_{AdS}} \sim \lambda_{4d}^{-1/4} \ll 1$. If $\lambda_{4d} \gtrsim N^{8/17}$ (which is allowed while still satisfying $g_{4d}^2 \ll 1$), the graviton gas can have larger entropy than the 10d black hole, even when the latter is not as small as ℓ_s and hence supergravity is a good approximation. Therefore, at $\lambda_{4d} \gtrsim N^{8/17}$, a sufficiently small 10d black hole can evaporate completely to the gas of gravitons; it is unstable even in the microcanonical ensemble. This argument identifies the highest possible temperature of the 10d black hole, or more precisely, the system of graviton gas and the 10d black hole, which is equivalent to T_1. The scaling with N can be estimated by requiring the entropies of the black hole $\sim (\ell_{p,10d} E)^{8/7}$ and graviton gas $\sim (R_{AdS} E)^{9/10}$ to be of the same order at $T = T_1$. By using $\ell_{p,10d}^9 \sim N^{-2}$ for $R_{AdS} \sim 1$, we obtain $E \sim N^{20/17}$ and $T_1 \sim N^{2/17}$. This is smaller than the Hagedorn temperature $\sim \lambda_{4d}^{1/4}$ if $\lambda_{4d} \gtrsim N^{8/17}$, but still it becomes parametrically large in the large-N limit.

The same analysis [251] can be applied to the $AdS_4 \times S^7$ geometry dual to the ABJM theory [252]. A rough estimate of the highest possible temperature of the 11d black hole T_1 is obtained by requiring that the entropies of graviton gas $\sim (R_{AdS} E)^{10/11}$ and black hole $\sim (\ell_{P,11d} E)^{9/8}$ are of the same order at $T = T_1$. By using $\ell_{P,11d}^{-1} \sim \frac{N^{1/6}}{R_{AdS}}$, we obtain $T_1 \sim \frac{1}{R_{AdS}} \left(\frac{\ell_{P,11d}}{R_{AdS}}\right)^{-9/19} \sim \frac{N^{3/38}}{R_{AdS}}$. This T_1 is smaller than the Planck mass, and hence the approximation by eleven-dimensional gravity is self-consistent.

The same logic could be applied to the BFSS matrix model if the gravity side were understood more precisely. It would be nice if we could see the trivial-confined phase at a much larger N and a higher temperature. That it was not observed in past studies is not necessarily a contradiction because a careful choice of the initial condition for the simulation is needed to see such a phase which has small free energy.

4.3.6 BMN matrix model ($\mu > 0$)

Let us now consider the $\mu > 0$ case with trivial vacuum, and gradually raise the temperature (canonical ensemble). At sufficiently low temperature, the system is in the confined phase.[20] In the same manner, if we take a nontrivial fuzzy-sphere vacuum and raise the temperature, the system is confined at a low temperature. To distinguish them, we use the names "trivial-confined phase" and "fuzzy-sphere-confined phase".[21]

As the temperature goes up, at some point, a transition to a deconfined phase can take place. As long as the thermal excitation of each matrix entry is not too strong, we can still

[20] By 'confined phase', we mean a phase in which the energy and entropy are of lower order in N than N^2, while they become of order N^2 in the deconfined phase. Confinement is also indicated by a uniform distribution of the Polyakov line phases. Note that 'confined phase' is sometimes used to indicate the phase with order N^0 energy and entropy.

[21] We could also call them 'confined phase on the trivial background' and 'confined phase on the fuzzy-sphere background'.

distinguish different fuzzy-sphere backgrounds. Therefore, both a "trivial-deconfined phase" and "fuzzy-sphere-deconfined phase" can exist.[22]

As we will see shortly, all these phases — trivial-confined phase, fuzzy-sphere-confined phase, trivial-deconfined phase, and fuzzy-sphere-deconfined phase — can be minima of free energy in the canonical ensemble. Multiple minima can coexist in certain parameter regimes, and the phase structure can be rather complicated. We will take the trivial-confined phase and study the transition to deconfinement, but a priori, we do not know whether the trivial-deconfined or fuzzy-sphere-deconfined phase is obtained. To make the analysis tractable, we split the discussion into two steps.

- First, we ignore the possibility of a transition to the fuzzy-sphere-deconfined phase and consider the transition between the trivial-confined phase and the trivial-deconfined phase. We argue that there are three kinds of critical temperatures, T_1, T_2, and T_c, that satisfy $T_2 < T_c < T_1$. The trivial-confined phase (resp. trivial-deconfined phase) exists as a minimum of free energy only at $T \leq T_1$ (resp. $T \geq T_2$). The free energy of these two phases coincides at $T = T_c$. The trivial-confined phase (resp. trivial-deconfined phase) is favored at $T < T_c$ (resp. $T > T_c$). See Sec. 4.3.6.

- Next, we take into account the fuzzy-sphere-deconfined phase. We show that a lower bound for T_1 is obtained if we observe the trivial-confinement/fuzzy-sphere-deconfinement phase transition. See Sec. 4.3.6.

- When μ is very small and N is not very large, we see yet another "phase transition"; one or few of the eigenvalues escape and roll to very large values. This corresponds to a run-away behaviour toward the flat direction at $\mu = 0$ [214, 253]. We can obtain a lower bound for T_1 also from this run-away behavior. See Sec. 4.3.6.

Trivial-confinement/trivial-deconfinement transition

Let us think about what kind of phase diagram can appear in the BMN matrix model. At each fixed μ, we expect one of the types of phase distributions shown in Fig. 4.11. The large-μ region permits perturbative calculations [151, 237], and the transition is found to be of first order, i.e., the left scenario in Fig. 4.11 is realized. Therefore, we expect one of the two phase structures depicted in Fig. 4.13, depending on the order of the phase transition at $\mu = 0$. Let us call them the first-order scenario and not-first-order scenario, respectively.

We expect that the first-order scenario is more likely to be realized for the following reasons:

- We expect a first-order transition in the BFSS matrix model, and if the $\mu \to 0$ limit is smooth, this first-order character should persist for finite μ. (Note that the smoothness of the $\mu \to 0$ limit is nontrivial, and the order of $\mu \to 0$ and $N \to \infty$ can be important.)

- In the not-first-order scenario, the first-order transition at large μ splits into two transitions at small μ (T_1 becomes smaller than T_2, and T_c disappears). Then the GWW transition should exist at some finite temperature $T_2 > 0$ even at $\mu = 0$. It

[22] If we fix μ and N and go to a very high temperature, the thermal excitation of each matrix entry becomes larger than the size of any fuzzy sphere, and the distinction between "trivial-deconfined phase" and "fuzzy-sphere-deconfined phase" disappears.

has to lie below $\lambda^{-1/3}T = 0.4$, because $\rho(\theta)$ is gapped there [134]. But if this were the case a big puzzle would pop up: why did the numerical simulations in the past agree well with dual gravity predictions, although they have been performed at higher temperature which could be separated from the low-temperature region, where gravity is precise, by the GWW transition? Thus, a not-first-order scenario is disfavored.

- If the GWW transition lies in the type IIA string theory region, there is yet another problem: below the GWW transition, it is natural to expect that the system is in the partially-confined phase, which corresponds to the RR-charge less than N; it does not agree with the charge counting in the gravity side.

More on the first-order scenario

Suppose the transition is of first order, as shown in the left panel of Fig. 4.13. Then, as $\mu \to 0$, the jumps of the energy and entropy have to approach zero (more precisely, $\frac{E}{N^2}$ and $\frac{S}{N^2}$ have to approach zero), otherwise the $\mu = 0$ limit disagrees with the dual gravity picture [210] which has been tested throughly by numerical simulations. It is natural to expect that the jump of the Polyakov loop also vanishes at $\mu = 0$; see Fig. 4.16. Then, the distribution $\rho(\theta)$ has to become almost flat, while staying gapped; see Fig. 4.17.[23]

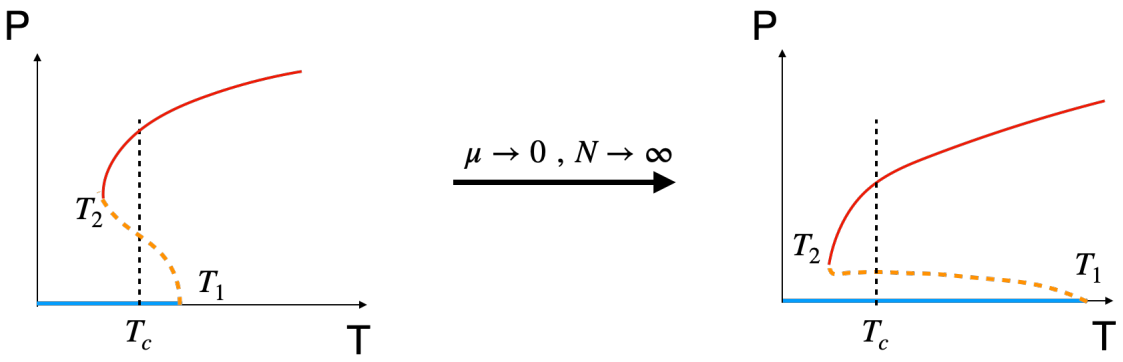

Figure 4.16: The first-order scenario. The left panel is for larger μ, and the right panel is for smaller μ. Both critical temperature and the size of the jump decrease as μ becomes smaller and N becomes larger, while T_1 can go up, as discussed in Sec. 4.3.5. Strictly speaking, the orange part further splits into two phases: the black string and black hole phases.

Let us summarize how the first-order scenario may work:

- The transition remains of first order at small μ. As μ becomes small, the transition temperature approaches zero (Fig. 4.13 left).
- The jump of the energy and Polyakov loop at critical temperature becomes smaller. (Fig. 4.16)
- The distribution of the Polyakov line phases at the GWW transition is distorted more and more at smaller μ and approaches the uniform distribution. (Fig. 4.17)

[23] This is consistent with the claim in Ref. [254] that the phase distribution becomes flat at zero temperature. It is also consistent with the unpublished observation made by using the simulation data for Ref. [250].

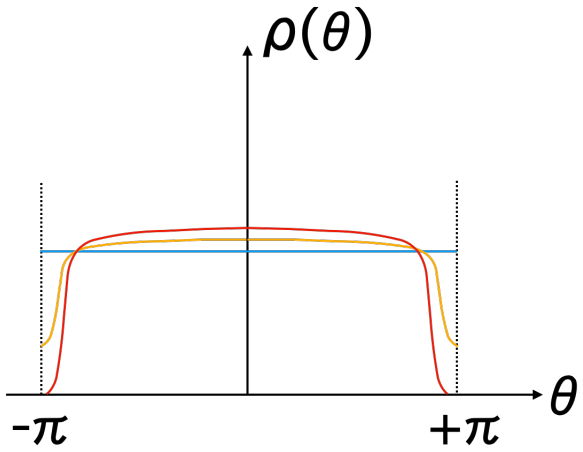

Figure 4.17: Possible form of the phase distribution around the phase transition at very small μ.

Trivial-confinement/fuzzy-sphere-deconfinement transition

Suppose the first-order trivial-confinement/fuzzy-sphere-deconfinement transition is observed at $\tilde{T}_c$ as T is increased before the trivial-confinement/trivial-deconfinement transition is observed. Here we consider the situation that initial configuration for the simulation is taken from the trivial-confined phase, and temperature is gradually raised. (We will encounter this situation later in Sec. 4.3.9.) Then, a natural expectation is that $\tilde{T}_c < T_c$.

More precisely: suppose that the two-state signal is observed between $\tilde{T}_2$ and $\tilde{T}_1$, where $\tilde{T}_2 < \tilde{T}_1$. Then, it is natural to expect $\tilde{T}_1 < T_2$. Otherwise, we should see the trivial deconfined phase as well.

Run-away behavior

The BFSS matrix model has flat directions. The BMN model shows remnants of these: When μ is small, scalars can be almost commutative, and eigenvalues can diverge as μ is sent to zero. All four phases under consideration can have an instability in this semi-flat direction. Let us denote such an instability as "run-away behavior". This effect is temperature-dependent: at sufficiently large temperatures, the flat directions are lifted.

In the trivial-confined phase, all D0-branes are placed at the origin without any energy excitation [238]. On the other hand, in the trivial-deconfined phase, each degree of freedom has an energy of order N^0. Because some amount of energy is needed for a D0-brane to move in the flat direction, it is natural to expect that the trivial-deconfined phase is more prone to the run-away behavior. We expect the same for the fuzzy-sphere background, i.e., the fuzzy-sphere-deconfined phase is more prone to the run-away behavior. It is also known that the problem with the flat direction is milder at high temperatures. Hence, in the small-μ and not-so-large-N region, it can be the case that the deconfined phase can be sufficiently stable only at higher temperatures. Consequently there can be a finite temperature range where we do not notice the metastable deconfined contribution in the simulations.[24]

[24]Note that it is hard to distinguish this possibility from a more standard scenario Fig. 4.16 with a very shallow meta-stable minimum; in Monte Carlo simulations, both would exhibit the run-away behavior.

All of these observations suggest the following scenario. Suppose we start with the trivial-confined phase, gradually raise the temperature, and observe run-away behavior at some temperature $T_{\text{run-away}}$. This temperature provides us with a lower bound for T_1, i.e., $T_{\text{run-away}} \leq T_1$. At sufficiently large N, $T_{\text{run-away}}$ and T_1 should not differ much.

4.3.7 Numerical determination of the phase transitions

After the discussion of the continuum physics and the conjectures about the phase transition, we now present our results from numerical simulations. The simulations have been done with the HMC algorithm. A careful analysis is needed to test the scenario described in Sec. 4.3.4. Prior to this description, we consider the simpler case of the bosonic analogue of the BMN matrix model, where the transition point can be precisely identified even in the small μ limit. After this exercise, we present the results of simulations for the full supersymmetric BMN model. The BFSS matrix model is the limit of $\mu \to 0$ in the BMN matrix model. Although our main interest lies in the limit of $\mu \to 0$ which has dual gravity descriptions, we will start from the large-μ region where the simulation is easier and gradually move toward smaller μ.

The lattice action used for the simulations is discussed in Sec. 4.1.3. We use S to denote the number of lattice points. The lattice spacing is $a = \frac{\beta}{S}$. The continuum limit is taken by sending S to infinity.

4.3.8 Phase transitions in the bosonic BMN model

In this section we study the bosonic analogue of the BMN matrix model (bosonic BMN), whose action is only the bosonic part of the original, supersymmetric BMN matrix model. That is, we use the action

$$S = S_b + \Delta S_b, \tag{4.65}$$

with

$$S_b = \frac{N}{\lambda} \int_0^\beta \mathrm{d}t \ \ \mathrm{Tr} \left\{ \frac{1}{2} \sum_{I=1}^{9} (D_t X_I)^2 - \frac{1}{4} \sum_{I,J=1}^{9} [X_I, X_J]^2, \right\} \tag{4.66}$$

and

$$\Delta S_b = \frac{N}{\lambda} \int_0^\beta \mathrm{d}t \ \ \mathrm{Tr} \left\{ \frac{\mu^2}{2} \sum_{i=1}^{3} X_i^2 + \frac{\mu^2}{8} \sum_{a=4}^{9} X_a^2 + i \sum_{i,j,k=1}^{3} \mu \epsilon^{ijk} X_i X_j X_k, \right\}. \tag{4.67}$$

This model is much easier to simulate than the full, supersymmetric BMN model. This exercise is performed to confirm convergence to the bosonic BFSS model [255] in the $\mu \to 0$ limit.

Historically, there was some confusion regarding the phase structure of the bosonic BMN model. At weak coupling (large μ), perturbative analysis shows that the phase transition is of first order. At $\mu = 0$, the first systematic study [137] used the data with $N \leq 32$ and suggested that the transition takes place at nonzero temperature and it is not of first order. However, a later study with $N > 32$ revealed that the transition is actually of first order after all [255]. From this fact, Ref. [255] concluded that the phase diagram of the bosonic BMN model looks like the left figure of Fig. 4.18.

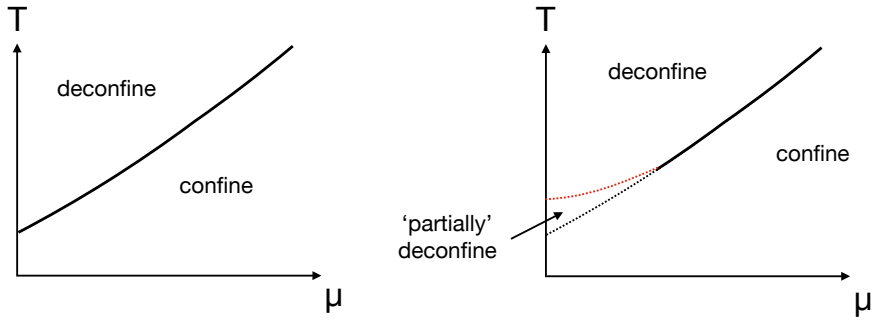

Figure 4.18: Possible phase diagrams of the bosonic BMN model for the canonical ensemble. Ref. [255] concluded that the left figure is the actual phase diagram.

Strictly speaking, to establish the phase structure unambiguously, it is necessary to confirm that the phase transition is of first order even in the intermediate-μ region. Below, we study a few intermediate values of μ, and confirm this. In addition, we study the features of the transition in detail.

That the transition is of first order can be confirmed by observing the two-state signal in the Polyakov loop. Indeed, this is shown in Fig. 4.19. We can see that the Polyakov loop jumps from $P \simeq \frac{1}{2}$ to $P \simeq 0$, at any μ. (In Fig. 4.19, the energy and Myers term are also shown. The two-state signal is not clearly visible for these quantities.) We can see that $P \simeq \frac{1}{2}$ corresponds to the GWW transition because the spectrum of the eigenvalues of the Polyakov line develops a gap as we can see at the phase distributions shown in Fig. 4.20.

The transition temperature, where the free energies of the confined and deconfined phases take the same value, can be determined from the two-peak signal; this is the temperature at which two peaks contain the same number of configurations. The separation of two peaks is obtained by considering approximately same areas enclosed under two peaks. The numbers of trajectories in our simulations are large enough to estimate the transition temperatures with errors of 0.02%. The critical temperatures determined for different μ in this manner are shown in Fig. 4.21. There is a symmetry $\mu \leftrightarrow -\mu$ and the μ-dependence in T_c is expected to be at least of quadratic order. T_c can actually be well described by a quadratic fit. The limit of $\mu \to 0$ is consistent with the results for bosonic BFFS [255], $T_c|_{\mu=0} = 0.885 \pm 0.001$ at $N = 64, L = 24$.

The dip in the histogram can be interpreted as the partially-deconfined phase, which sits at the maximum of the free energy in the canonical ensemble. At this point, $\rho(\theta)$ is expected to be nonzero everywhere between $-\pi$ and $+\pi$. This is consistent with the numerical

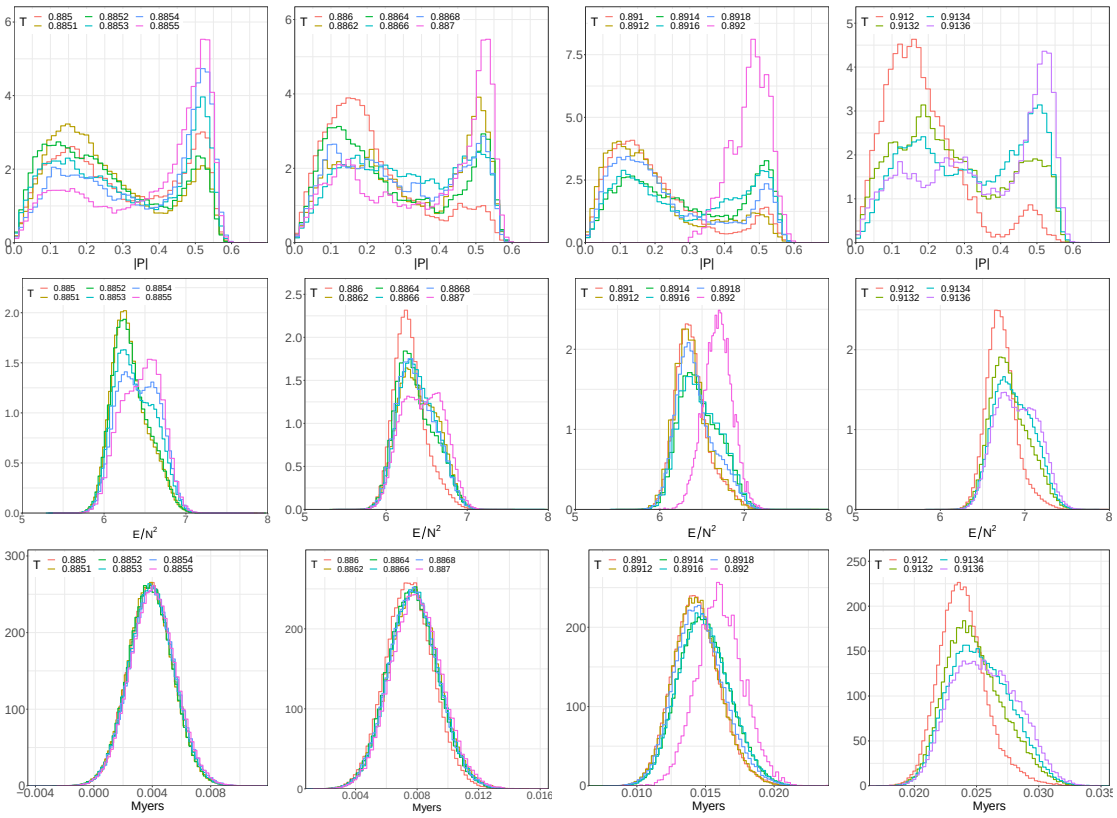

Figure 4.19: Histogram of the distribution of the Polyakov loop (first row), energy (second row), and Myers term (third row) during lattice Monte Carlo simulations for the bosonic BMN model at matrix size $N = 64$ and lattice size $S = 24$. The values of μ are 0.125, 0.25, 0.5 and 1.0, from left to right. A two-state signal near the transition temperature is observed at all values of μ, particularly for the Polyakov loop P. The jumps of energy and Myers terms are of order N^2, but we do not observe the formation of a fuzzy-sphere background.

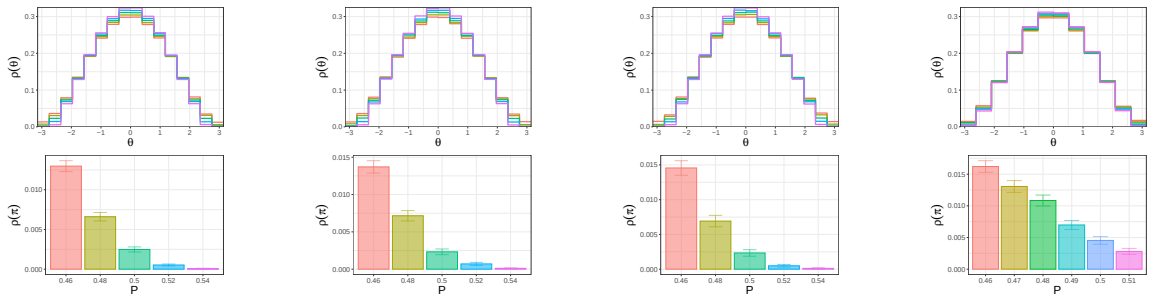

Figure 4.20: Distribution of the phases of the Polyakov line near the transition temperatures for the bosonic BMN model. From left to right, $\mu = 0.125, 0.25, 0.5, 1.0$ with $T_c = 0.8853, 0.8864, 0.8918, 0.9134$, respectively. The matrix size and the lattice size are $N = 64$ and $S = 24$, respectively. The gap opens at $P \simeq 0.5$.

observation: as mentioned above, if we look at configurations at each fixed P, then if $P < \frac{1}{2}$, $\rho(\theta)$ is nonzero everywhere between $-\pi$ and $+\pi$ as shown in Fig. 4.20.

The jumps of energy and entropy are of order N^2, at any μ (see Fig. 4.19). The jump of energy goes down with μ but does not vanish even at $\mu = 0$ [255]. In the supersymmetric theory, on the other hand, we expect the jump to vanish at $\mu = 0$, up to the $1/N$-suppressed corrections as we discuss in Sec. 4.3.4 and in Fig. 4.16.

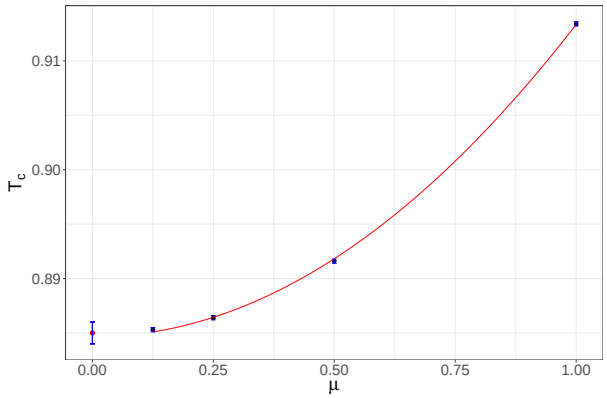

Figure 4.21: Transition temperatures for the bosonic BMN model against fluxes μ. The parenthesis indicates the errors of the fit, and the left-most point is the extrapolated BFSS transition temperature (matrix size $N = 64$, lattice size $S = 24$) from [255]. The fit is given by the equation $T_c = 0.8846(1) + 0.0297(2)\mu^2$.

4.3.9 Phase transitions in the full BMN model

Our main interest is the thermal transition from confinement to deconfinement, while the configuration of the X_i is kept in the trivial background with no relevant fuzzy sphere contributions.[25] This is due to the fact that this scenario is assumed in the dual gravity predictions. We want to verify a continuous transition line from perturbative predictions at weak coupling to the conjectures at strong couplings obtained with help from the dual gravity description.

A phase transition is a well-defined concept in the thermodynamic limit, which is the large-N limit in the case of the matrix models. In our numerical studies at finite N and finite simulation time, several ambiguities concerning the exact definition of the transition have to be taken into account.

The first one is related to the common difficulty in identifying a first order transition. In the ideal world, we would be able to study very large N efficiently. If N were sufficiently large such that the separation of two phases is clear, and at the same time, the number of configurations collected in the simulation would be very large such that the tunneling between two phases can be captured, then the two-state signal would be very clean. In this idealized case it would be possible to determine T_c, T_1, and T_2 precisely. For the bosonic BMN model, we can actually perform such an analysis. However, for the full BMN model, such a detailed study is not possible for all parameter sets because of large simulation cost. Compared to the

[25] Trivial (fuzzy-sphere) background means fluctuations around a configuration of the trivial (fuzzy-sphere) vacuum.

bosonic BMN model, we have fewer data points, and the $1/N$-corrections are larger. Still, the large-N behavior can be deduced by comparing the results for different values of N.

The second complication arises at finite N due to tunneling to fuzzy-sphere configurations. As we explained in Sec. 4.3.4, there can be confinement or deconfinement with either a fuzzy-sphere or a trivial background of the X_i fields. At small values of μ or N, tunneling between different backgrounds can take place with a non-negligible rate. At larger μ, the tunneling is well suppressed even at the values of N we study in this work, and we observe the trivial-confinement/trivial-deconfinement transition. However, at smaller μ, deconfinement is associated with the transition to a fuzzy-sphere background. Let $\tilde{T}_c$ be the critical temperature at which the transition between the trivial-confined phase and fuzzy-sphere-deconfined phase is observed. If we do not see the transition to the trivial-deconfined phase, then we expect $\tilde{T}_c \leq T_c$. T_c is the point where the free energies of the trivial-confined and trivial-deconfined phases coincide as explained in Sec. 4.3.6.

We have tested different strategies to disentangle the influence of the tunneling to a fuzzy-sphere background and to obtain more information about the deconfinement transition in the trivial background. One strategy corresponds to constraining the Myers term, which forces the system to stay in trivial background.[26] Alternatively we have also investigated indications of metastability related to hysteresis effects. These investigations will be detailed below.

Our investigation led us to some expected and some unexpected observations, depending on the parameter region. The results are summarized in Fig. 4.22. We split the parameter space into four regions:

- For $\mu \geq 2.0$, the transition between the trivial-confined and trivial-deconfined phases can be easily identified. We observe convergence to the perturbative limit as μ becomes large. At intermediate μ, the Padé resummation based on the large- and small-μ behaviors obtained via perturbative calculation and dual gravity analysis respectively gives a reasonable approximation to the simulation results. (See Refs. [243, 256] for similar observations.)

- For $0.8 \leq \mu < 2.0$, convergence to the dual gravity prediction is observed as μ becomes small. Below $\mu = 0.8$, the deviations from the predicted line start to increase again.

- For $\mu < 1.6$, transitions to fuzzy-sphere configurations are observed frequently (see Ref. [243] for a similar observation), which makes it in some regions impossible to observe the trivial-deconfined phase. In these cases, deconfinement and tunneling to a fuzzy-sphere background take place simultaneously, at least at the values of N and S we have studied.

- For $\mu < 0.8$, we observe pronounced metastable confined and deconfined phases. The system tends to remain in one of the phases for a longer simulation time, at least in the range of temperatures $T \in [0.26, 0.27]$. This effect is independent of any constraint of the Myers term and even appears for fuzzy-sphere background. We observe indications that the metastable confined state persists even in the BFSS limit. As we will see, this apparent deviation from the gravity prediction may be simply a finite-N effect.

[26] The full path integral contains multiple backgrounds, and we are interested in a particular background. Therefore, we have to restrict the path integral to the fluctuation around such a background, to obtain physically meaningful result [53, 214, 250]. In this project, we identify the background we are interested by specifying the value of the Myers term. See Sec. 4.3.9 for more details.

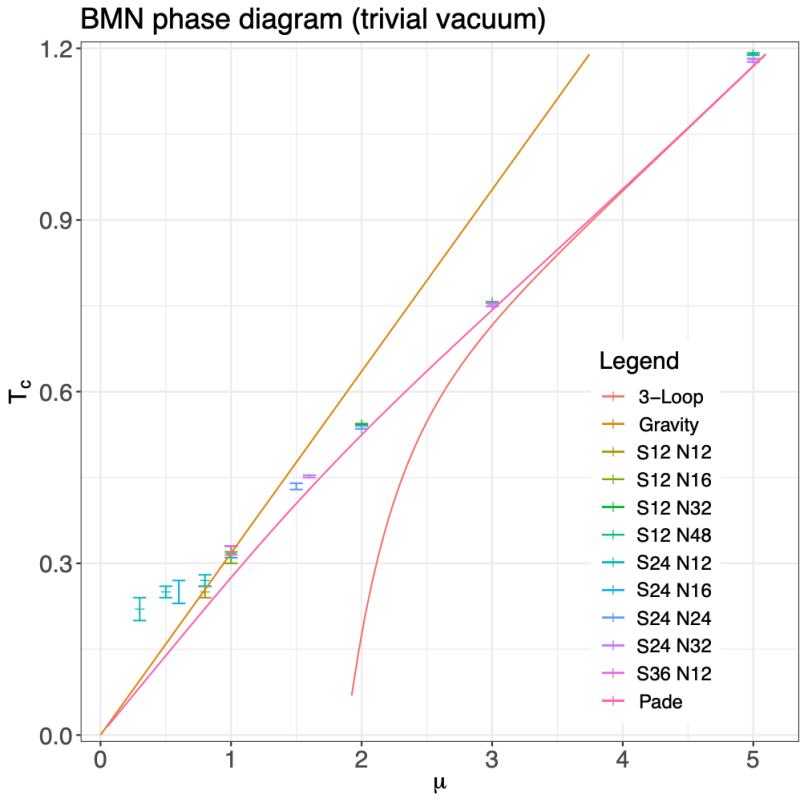

Figure 4.22: The critical temperature T_c vs. flux parameter μ for the full BMN model. The data points for the critical temperature correspond to a two-state signal with about equal probability for confined and deconfined phase, and their error bars are given by the neighboring simulated temperatures, for which these probabilities differ. The error bars without data points for $\mu = 0.6$ indicate observation of a hysteresis, see Fig. 4.34. For $\mu = 1.5$ and 1.6, we also observed hystereses in the region given by the error bars but did not investigate the full extent of the hysteresis region. For comparison, the prediction of the perturbative analysis [151], Padé resummation [243], and gravity calculation [236] are plotted. In the main text, the way the transition temperature at each parameter set is determined is detailed, and the apparent deviation from the gravity predictions at small μ is explained. (Note that the latter can simply be a finite-N artifact.) In the BFSS limit $\mu \to 0$, although we could not identify the two-state signal, we still conclude that we observe the confined phase; see Sec. 4.3.9.

Simulation setup

We use the same simulation program as done in earlier simulations of the BFSS model [134]. It is based on the RHMC algorithm [257], neglecting the phase of the Pfaffian based on the arguments presented already in the BFSS case [150, 214]. The program includes a possible constraint for $R^2 \equiv \frac{1}{N}\sum_{I=1}^{9} \mathrm{Tr}\, X_I^2$, which has been used in some simulations of the BFSS model to stabilize the trivial background in Ref. [134], but not in the current project. We have added in the same way constraints for the Myers term and the Polyakov loop. (See Ref. [224] as an example for a simulation with a constraint on P.) Each constraint forces an observable $\mathcal{O}$ to lie in the interval $[x_{\min}, x_{\max}]$ around a given value x depending on the coupling strength γ. Inside the chosen interval the constraint has no effect. Expressed in terms of the Heaviside function Θ, the additional contribution to the action is

$$S_{\text{constraint}}(x; x_{\max}, x_{\min}, \gamma) = \begin{cases} \gamma \cdot (\mathcal{O} - x_{\min})^2 & (\mathcal{O} < x_{\min}) \\ 0 & (x_{\min} \leq \mathcal{O} \leq x_{\max}) \\ \gamma \cdot (\mathcal{O} - x_{\max})^2 & (x_{\max} < \mathcal{O}) \end{cases} \tag{4.68}$$

where γ is a sufficiently large positive number. Consequently, the value of $\mathcal{O}$ is approximately constrained between $x_{\max}$ and $x_{\min}$. We have added this constraint contribution to the action in some of the simulations to stay as close as possible to the trivial background in certain parameter ranges. It prohibits tunneling to nontrivial backgrounds, which is expected to be suppressed in the large-N limit, even at small N. We will discuss in detail in which cases the constraints have been included.

In all our simulations, we have kept the trajectory length of the molecular dynamics constant and adjusted the stepsize to achieve a similar acceptance rate. Statements about tunneling time and probability are hence always in reference to this trajectory length.

In addition to a transition indicated by the Myers term, we observe a run-away behavior of the scalar fields in the BFSS limit, remnants of which show up already at small μ. We monitored $\mathrm{Tr}\, X_I^2$ for each $I = 1, 2, \cdots, 9$ to keep it under control. We observed that this effect appears preferably in the X^9-direction, presumably due to a lattice artifact specific to our regularization. The run-away behavior is generally enhanced by lattice artifacts and consequently reduced in the large S limit.

Convergence to perturbative limit at $\mu \geq 2.0$

In this region, the transition between the trivial-confined and trivial-deconfined phases can easily be identified. We observe convergence to the perturbative limit as μ becomes large, as shown in Fig. 4.22. The tunneling to a nontrivial background close to T_c is not relevant and we are able to determine T_c precisely from a two state signal in the Polyakov loop. This indicates a first order phase transition, as shown in Fig. 4.23. By monitoring $\mathrm{Tr}X_I^2$ and $\mathrm{Tr}X_1[X_2, X_3]$, we can confirm that the two peaks are both consistent with a trivial background. Due to the stability of the results, no constraint part has to be added to the action. The phase transition takes place at a rather high temperature, where the effect from the fermions is not so important. Therefore, the transition temperatures become similar to that of the bosonic theory.

We can also check more detailed features of the deconfinement transition and confirm the picture that we have already investigated in the bosonic BFSS model [255]: for each fixed T and μ in the first-order-transition region, the energy and $\langle \mathrm{Tr}X^2 \rangle$ depend on P as $a + bP^2$. For

large μ, the distribution of the phases of the Polyakov line is consistent with $\rho(\theta) = \frac{1+2P\cos\theta}{2\pi}$, and the GWW transition takes place at around $P = \frac{1}{2}$; see Fig. 4.24. However, already at $\mu = 2.0$, we can see a subtle but clear deviation from the large μ behavior: the GWW transition takes place slightly below $P = 1/2$, and the distribution of the phases of the Polyakov line becomes distorted, as we can see from Fig. 4.25.

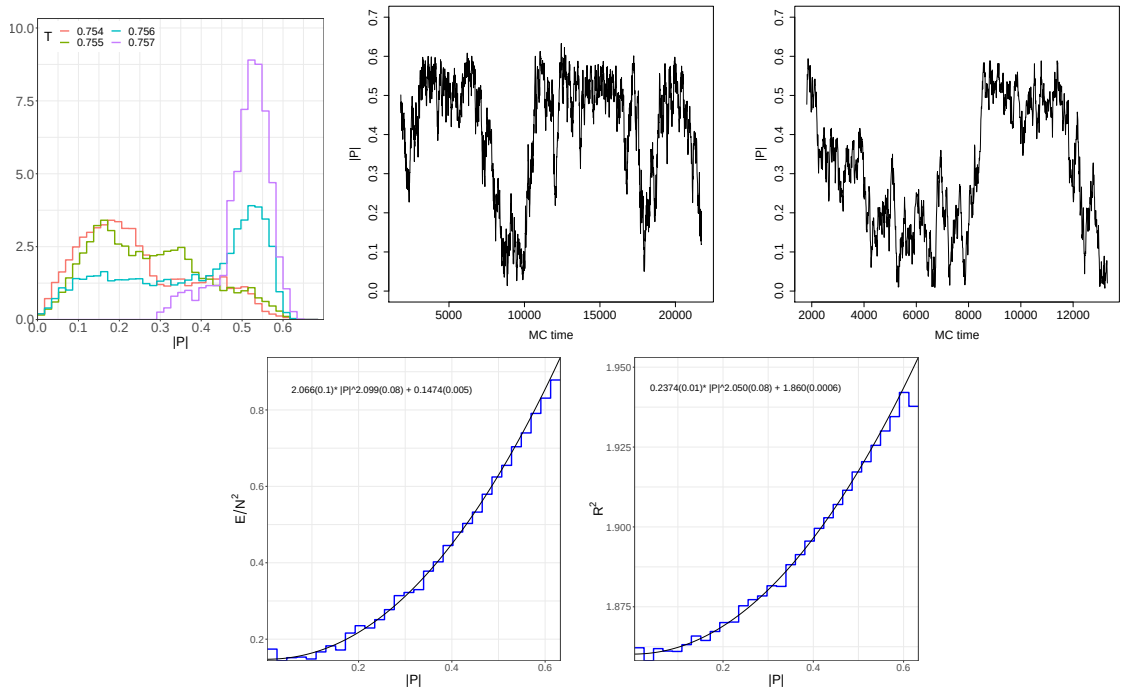

Figure 4.23: Full BMN model, flux $\mu = 3.0$, matrix size $N = 32$, lattice size $S = 12$ at temperature $T = 0.756$. [Top] From left to right, histogram of $|P|$ close to the critical temperature, and Monte Carlo history for the Polyakov loop at the same parameters for two typical runs with different sequences of random numbers. A two-state signal is observed. [Bottom] Binned E vs $|P|$ and binned R^2 vs $|P|$. Larger values of $|P|$ (more deconfined) corresponds to larger values of E and R^2, as expected.

Convergence to dual gravity prediction at $0.8 \leq \mu < 2.0$

As we can see in Fig. 4.22, the deconfinement transition line shifts from the perturbative to the dual gravity prediction as decreasing μ towards $\mu = 1.0$ and stays compatible with the latter down to $\mu = 0.8$. The probability of tunneling to fuzzy-sphere backgrounds increases at smaller μ. Fig. 4.26 shows an example of such a transition from trivial background to fuzzy-sphere background in the deconfined phase. Note that the Polyakov loop stays almost constant at this transition. Already below $\mu = 1.6$, we have to add a constraint for the Myers term to the action to stay in the trivial background. Without a constraint, the deconfinement transition also induces a transition in the Myers term. We expect this effect to be suppressed in the limit of large N. By using the constraint, we are able to confirm the trivial-confinement/trivial-deconfinement transition. As shown in Fig. 4.27, Fig. 4.28, Fig. 4.29, and Fig. 4.30, we observe two-state signals indicating the first-order transition.

In the considered region of μ we are able to investigate in more detail the nature of the

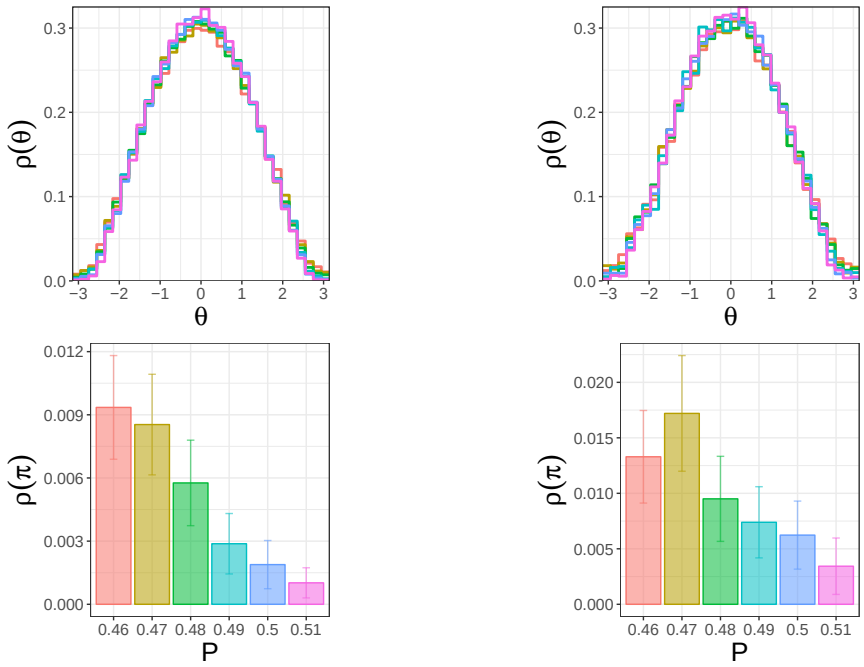

Figure 4.24: Full BMN model: [Top] The histogram of the Polyakov line phases for $[P - \Delta P, P + \Delta P]$, where $\Delta P = 0.005$ and $P = 0.46, 0.47, \cdots, 0.51$. [Bottom] $\rho(\pi)$ or more precisely, the height of the right-most bin in the histogram. Top and bottom rows use the same color for the same value of P. [Left] $T = 0.756$ (close to T_1) for $\mu = 3.0$, $N = 32$, $S = 12$. The Myers term was not constrained in this simulation. [Right] $T = 1.18$ (close to T_1) for $\mu = 5.0$, $N = 32$, $S = 24$.

phase transition. As μ becomes smaller, the shape of the distribution of Polyakov line phases changes. In Fig. 4.31, we plot the distribution of phases for different values of P, for $\mu = 1.5$ and $\mu = 1.6$ close to the critical temperature T_c. A clear deviation from the large μ behavior, now more pronounced compared to $\mu = 2.0$, is observed. We can see that the gap in the phase distribution of the Polyakov line closes around $P = 0.42$. In Fig. 4.32, we show an extrapolation of $\rho(\theta = \pm\pi)$ to the large-N limit for $\mu = 1.0$ and 1.5. The extrapolated value is consistent with zero for decreasing P as μ decreases. This is clearly different from the distribution at the large-μ region, that develops a gap at $P = \frac{1}{2}$, and continues the trend already observed at $\mu = 2.0$.

Small $\mu \leq 0.8$ regime and convergence to BFSS limit

The point $\mu = 0.8$ is the first point starting to depart from the gravity line and for even smaller μ our estimate for the critical temperatures shown in Fig. 4.22 is always larger than $T_c^{(\text{gravity})}$. However, this apparent deviation from the gravity prediction may be simply a finite-N effect: we used at most $N = 16$ to study the small-μ, small-T region. It is not unreasonable to compare to $\mu = 0$ as a first approximation. Then, a rough estimate of the critical temperature from the gravity side is $T_c \sim T_2 \sim N^{-5/9} \gtrsim 0.251$ for $N = 12$ and 0.214 for $N = 16$, up to an order one multiplicative factor. As we have seen in Sec. 4.3.6, T_1 should also be similar. Therefore, the critical temperatures observed in our simulations are in the

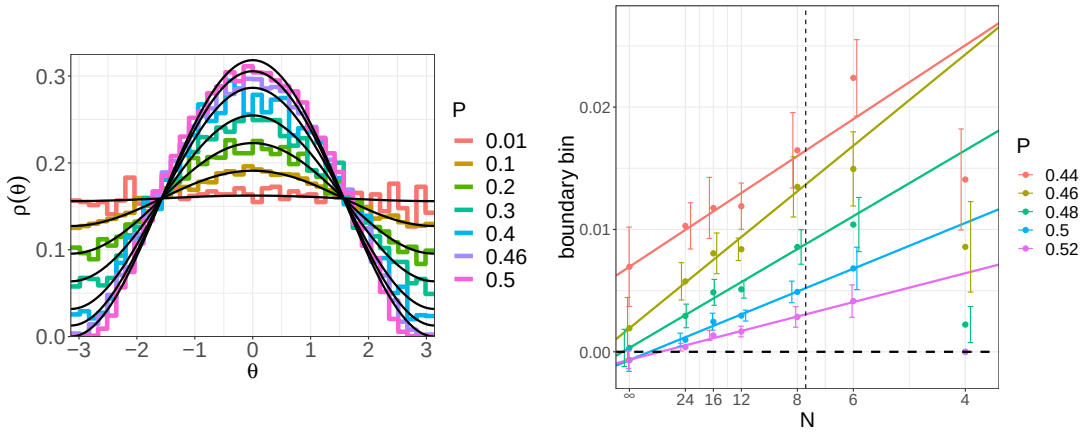

Figure 4.25: Full BMN model: [Left] Histogram of the Polyakov line phases in the interval $[P-\Delta P, P+\Delta P]$, for $\Delta P = 0.01$ and various values of P, for $\mu = 2.0$, $T = 0.543$ (close to T_1), matrix size $N = 32$, and lattice size $S = 12$. The large μ behavior $\rho(\theta) = \frac{1+2P\cos\theta}{2\pi}$ is shown in black. A clear deviation is observed close to $P = 0.5$. It appears that the GWW-point is between $P = 0.4$ and $P = 0.46$. The Myers term was not constrained in this simulation. [Right] Large N extrapolation of the size of the boundary bin for $S = 12$ and $\Delta P = 0.01$. The GWW transition is seen to take place around $P = 0.46$. Only data points left of the dashed vertical line were included in the linear fit.

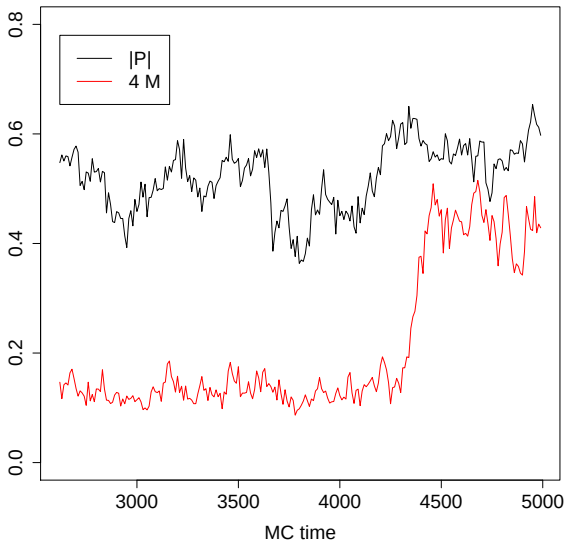

Figure 4.26: Full BMN model: Monte Carlo history of $|P|$ and M for $N = 24$, $S = 24$, $\mu = 1.5$, $T = 0.43$. The system is initially in the deconfined trivial background and tunnels to a fuzzy-sphere background around trajectory 4500.

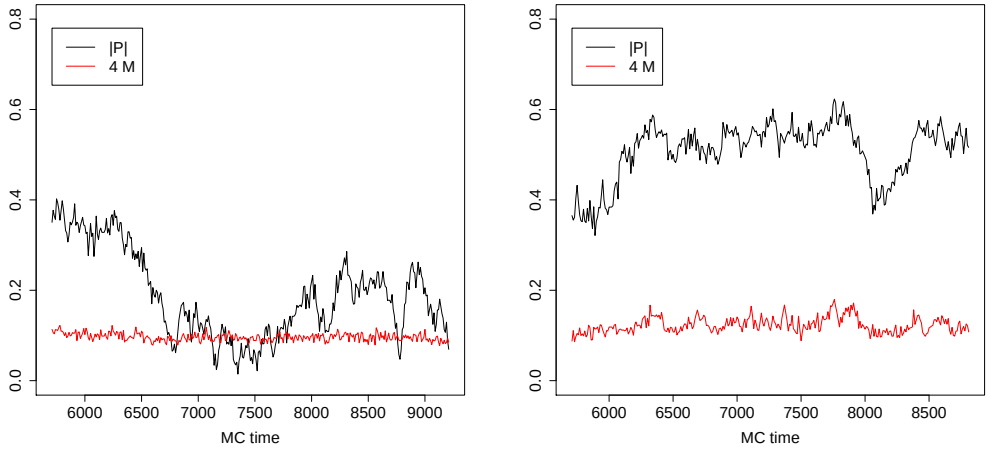

Figure 4.27: Full BMN model: $\mu = 1.6$, $N = 32$, $S = 24$, $T = 0.452$. Starting from the same initial configuration, a confined and deconfined stream is obtained from two different random number generator seeds. For these runs, no constraint on the Myers term is imposed and the simulation remained in the trivial background.

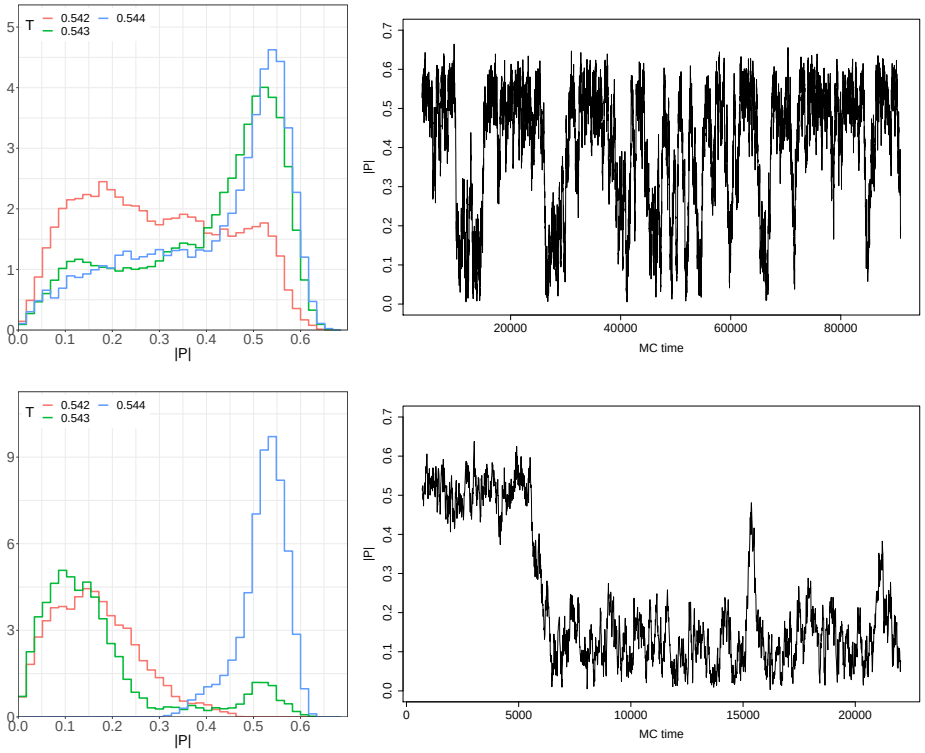

Figure 4.28: Full BMN model: the histogram (left) and typical Monte Carlo history (for $T = 0.543$) (right) of P close to the critical temperature for $\mu = 2.0$, for $N = 24$, $S = 12$ (top) and $N = 32$, $S = 12$ (bottom).

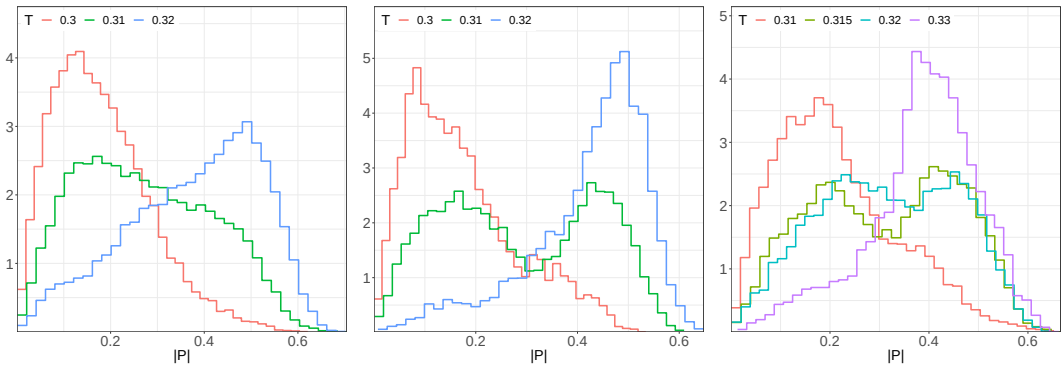

Figure 4.29: Full BMN model: Histogram of P close to the critical temperature for $\mu = 1.0$. From left to right, $N = 12$, $S = 12$; $N = 16$, $S = 12$; $N = 12$, $S = 24$. A two-state signal is observed. A consistent signal with lower statistics has also been observed for $N = 12$, $S = 36$, confirming the trend of the critical temperature to slightly increase in the continuum limit.

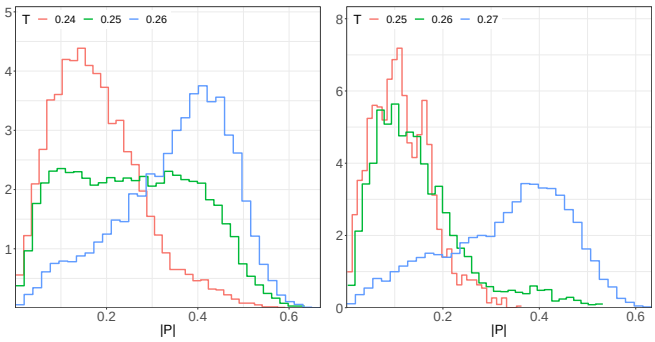

Figure 4.30: Full BMN model: Histogram of P close to the critical temperature for $\mu = 0.8$, $N = 12$, $S = 12$ (left); $N = 12$, $S = 24$ (right). A blurred two-state signal is observed. A consistent signal with lower statistics has been observed also for $N = 8$, $S = 36$; $N = 8$, $S = 48$, confirming the trend of the critical temperature to slightly increase in the continuum limit.

right ballpark. In fact, if we observed the values much closer to the gravity line shown in Fig. 4.22, this could even be seen as evidence against the duality conjecture. As N increases, T_2 and T_c should decrease while T_1 should increase, and the hysteresis should become more pronounced (Fig. 4.16). Thus, the numerical results should converge to the gravity line even at small μ.

Possible caveats of our analysis have been explained earlier. It is difficult to stabilize the trivial background, especially in the deconfined state.[27] In addition, the run-away of the scalar fields becomes more important towards the BFSS limit because the mass term $\sim \mu^2 \mathrm{Tr} X^2$ is turned off. On the other hand, in this low-temperature region, we observe an increased metastability which counteracts these effects. The trivial-confined phase gets stabilized, and simulations without the constraint are possible in some parameter regions.

The metastability in the small-μ, low-T region is indicated by a strong dependence on the

[27] It may not be an issue because the trivial background and fuzzy-sphere backgrounds are indistinguishable at $\mu \lesssim 0.018$ for $N = 16$, as explained in Sec. 4.3.3. However we never reached that small μ values.

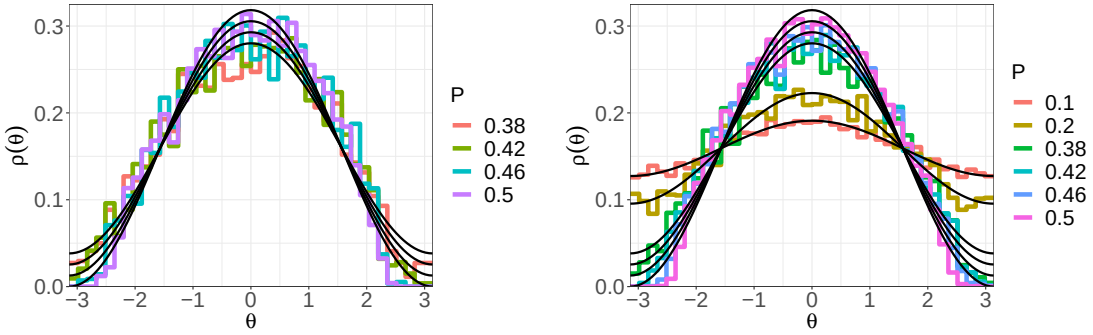

Figure 4.31: Full BMN, the histogram of the Polyakov line phases for $[P-\Delta P, P+\Delta P]$, where $\Delta P = 0.02$, [Left] $\mu = 1.5$, $N = 24$, $S = 24$, $T = 0.429$ (close to T_c) and [Right] $\mu = 1.6$, $N = 32$, $S = 24$, $T = 0.45$ (close to T_c) along with the large μ behavior $\rho(\theta) = \frac{1+2P\cos\theta}{2\pi}$ in black. A clear deviation is observed close to $P = 0.5$. The Myers term was constrained in the simulation for $\mu = 1.5$.

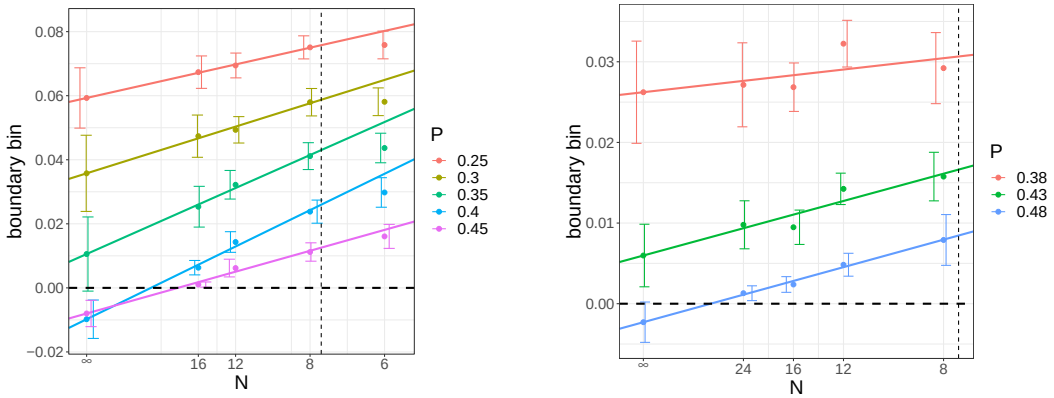

Figure 4.32: Full BMN, the large-N extrapolation of boundary bin, near T_1, for $T = 0.31$, $\mu = 1.0$, $S = 12$ (left) and $T = 0.429$, $\mu = 1.5$, $S = 24$ (right), as well as $\Delta P = 0.025$. The Myers term is constrained in these simulations.

initial conditions of the simulations which tend to stay in either a confined or deconfined state when started with the respective initial configuration. The observed metastability indicates a large separation of the temperatures T_1 and T_2 (see right panel of Fig. 4.16). As we will see in Sec. 4.3.9, the trivial-confined phase turns out to be rather stable at low temperatures even in the BFSS limit ($\mu = 0$), while we could not see the two-peak signal at $\mu < 0.3$ (i.e., at $\mu < 0.3$ and $T \lesssim 0.3$ we could not see the deconfined phase).

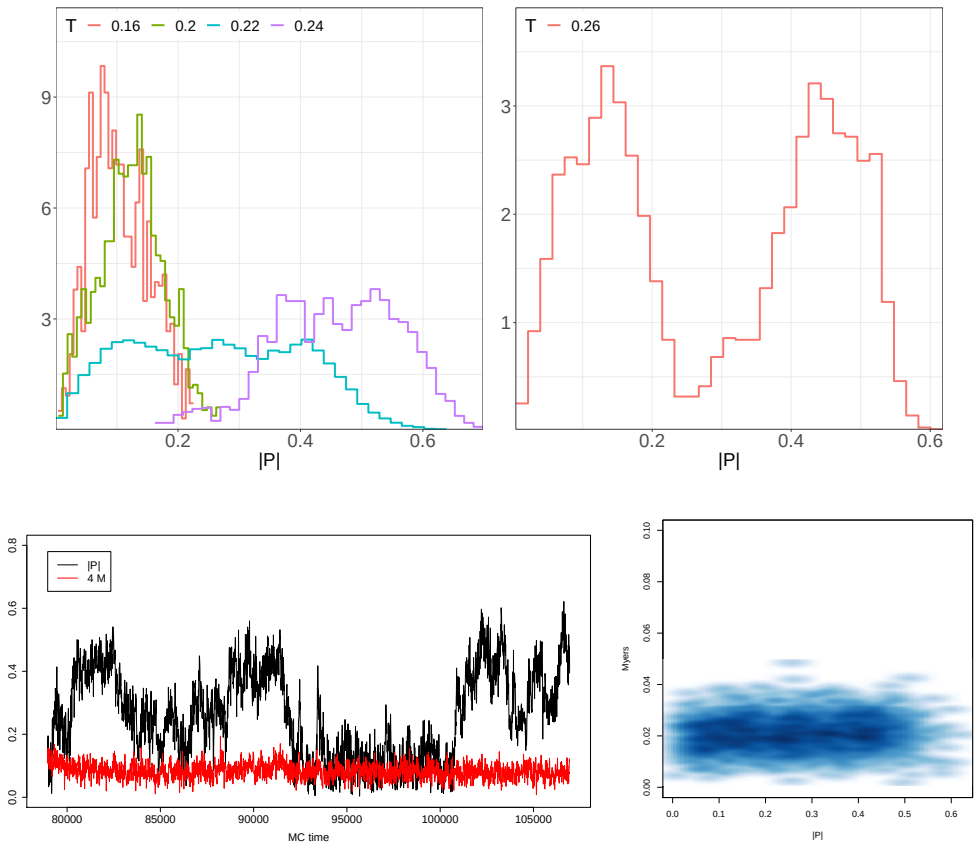

Figure 4.33: Full BMN, the histograms of the Polyakov distribution, and relative Monte Carlo histories for small μ. [Top-Left] $N = 12, S = 24$ at $\mu = 0.3$. A possible two-state signal is observed. At $T = 0.24$ we observe runaway behavior of R^2, as well as in the deconfined sector at $T = 0.22$. [Top-Right] $N = 16, S = 24$ at $\mu = 0.5$. For $\mu = 0.5$, the histogram was obtained by adding two independent streams which were initially prepared in a confined / deconfined state and remained there throughout a sufficiently long Monte Carlo evolution time due to the relatively large $N = 16$. [Bottom-Left] MC history of $N = 12, S = 24$ at $\mu = 0.3, T = 0.22$ from the up-left histogram. The signal suggests repeated tunneling between confined and deconfined states. Note that, at such a small value of μ, the distinction between trivial background and fuzzy-sphere background is not clear. [Bottom-Right] The relation between the Myers term and the Polyakov loop for the up-left histogram. No significant correlation is observed. Note that the Myers term was constrained to be below $M = 0.02$, but this cutoff was hit frequently, and often M became larger than the cutoff 0.02. (This is possible because the coefficient for the constraint term is large but finite.)

At very small μ, the difference in the Myers term for different fuzzy-sphere backgrounds is significantly reduced (see Sec. 4.3.3). Fuzzy-spheres can be buried in quantum fluctuations, and we expect that there is not a strong dependence of the deconfinement transition on the chosen background configuration. Therefore, the constraint on the Myers term should not affect the result in the small-μ region. Indeed we can, for example, observe very similar signals for metastable confined and deconfined state from the Polyakov loop distribution at $\mu = 0.3$, $N = 16$, $S = 36$, $T = 0.27$ independent of the constraint. The metastability extends over a large temperature range indicating the difference between T_1 and T_2. Fig. 4.33 presents

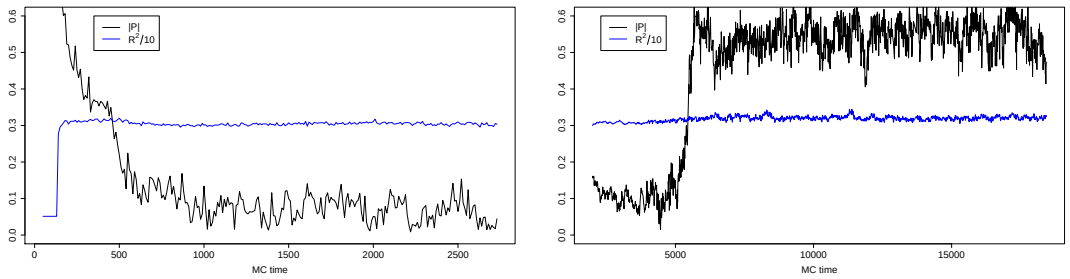

Figure 4.34: Full BMN model: [Left] Monte Carlo history for $N = 16, S = 24, \mu = 0.6, T = 0.22$. The confined phase ($|P| \simeq 0$) is observed. [Right] For $N = 16, S = 24, \mu = 0.6, T = 0.29$, starting with a confined configuration. A transition to the deconfined phase is observed. The temperature window is of order $\Delta T \approx 0.07$ at these parameters.

evidence for these assertions. For $\mu = 0.5$, a clear two-state signal is observed by joining a confined and deconfined stream with the same simulation parameters into a single histogram. Both streams remain in their respective state for a sufficiently long time to conclude that there is a strong hysteresis. For $\mu = 0.3$, repeated tunneling between a confined and deconfined state has been observed. In the deconfined parts of the Monte Carlo history, we observe runaway behavior in R^2. For our choices of N and S, $\mu = 0.4$ was the smallest mass parameter for which we could observe a stable deconfined phase at temperatures close to the transition temperature. Due to the choice $N = 12$, as opposed to $N = 16$ for $\mu = 0.5$, the two-state signal is not clear in the histogram, but we were able to see repeated tunneling due to the increased tunneling probability and simulation speedup at smaller N.

Let us give some more details on how we estimate T_1, T_c, and T_2 from results as those shown in Fig. 4.34 . In this example the parameters are $N = 16, S = 24$ at $\mu = 0.6$. It is challenging to observe a precise two state signal at these parameters and requires large statistics. Another way to give an estimate for T_c in a first-order scenario is by locating T_1 and T_2 since $T_2 < T_c < T_1$ (see Fig. 4.16). We then face the problem of locating T_2 which is indicated by the formation of a gap in the Polyakov eigenvalue distribution and T_1 which is the highest possible temperature with a metastable confined state. Both determinations require large statistics to be trustable, but one may be able to roughly estimate the difference $\Delta T = T_1 - T_2$ at the current level of statistics. Hence we do the following to locate T_2: we start by considering deconfined initial configurations and gradually lower the temperature until we see the simulation converge to a confined state. When this transition is accompanied by a gap in the eigenvalue distribution of the Polyakov loop, it provides an estimate of T_2. Following this procedure, see Fig. 4.34, we have located the temperature T_2 to be approximately $T_2 \approx 0.22$. Even though a precise determination would require larger N and much more statistics, we emphasize that this is nevertheless a valid estimate.

To locate T_1, we took the opposite direction. A confined initial configuration was used from smaller temperatures and the temperature was gradually raised to check whether the configuration remains confined or not. In the right panel of Fig. 4.34, we observe a transition to deconfined state for $T_1 \approx 0.29$ for the same parameters N, S, μ. This will be roughly the maximum confined temperature for this configuration. Then we see that the temperature window ΔT can be rather large even at these parameters. Towards lower μ, the situation starts becoming even more difficult to analyze, but the same pattern is observed.

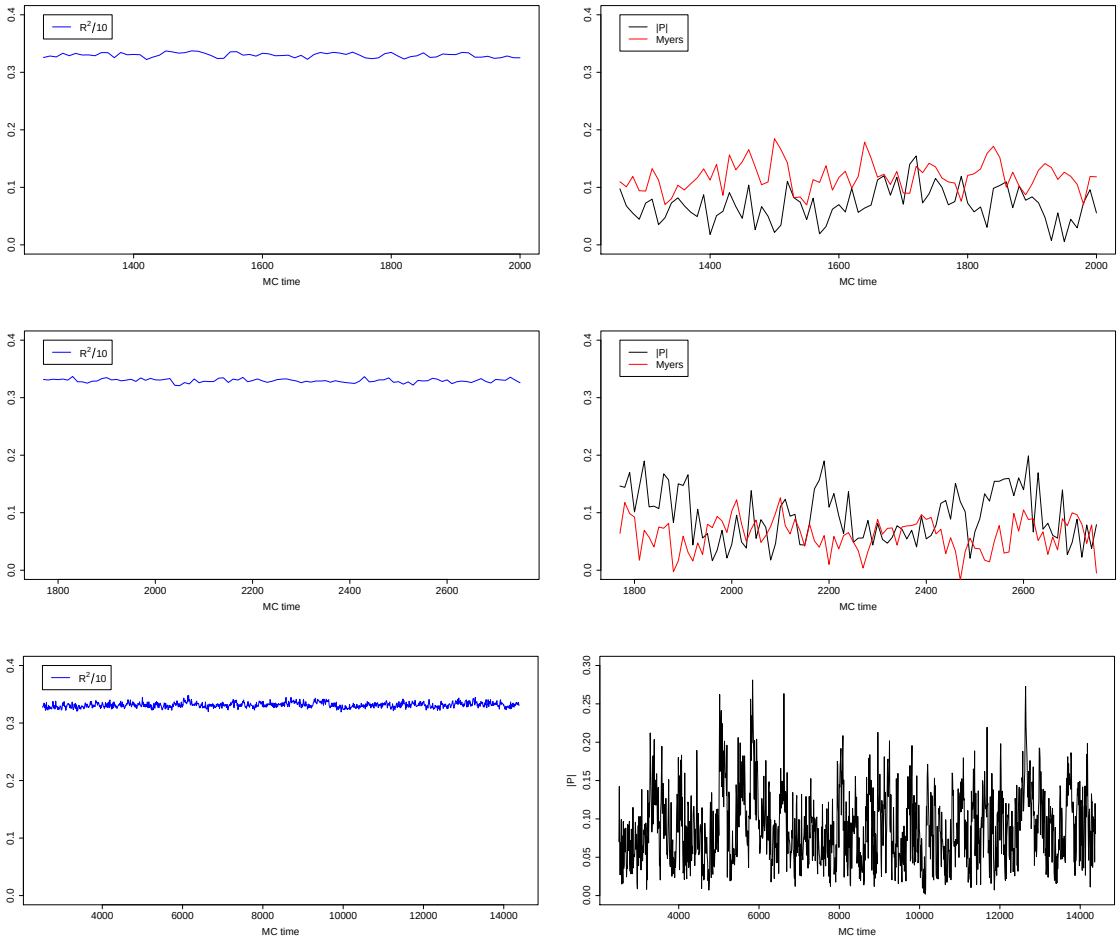

Figure 4.35: Monte Carlo histories showing confined, stable states for $N = 12, S = 48$ and temperature $T = 0.2$. From first row to third we have $\mu = 0.2, 0.1$, and $\mu = 0$ respectively. No constraint was imposed for the simulation.

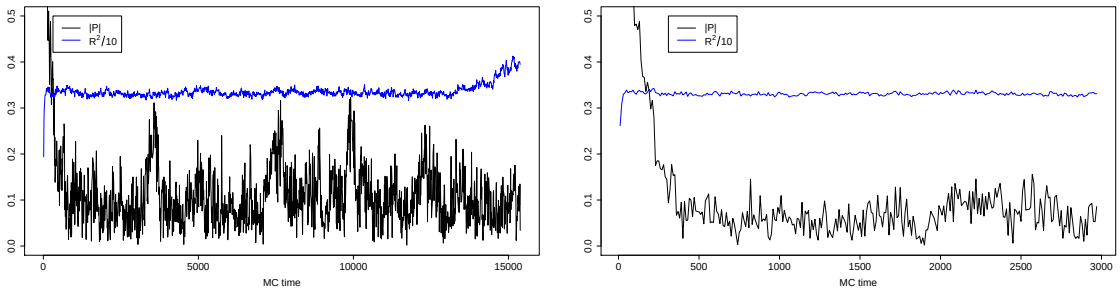

Figure 4.36: Monte Carlo histories from cold starts ($X_1 = X_2 = \cdots = X_9 = 0$) for $\mu = 0$, $T = 0.2$, $S = 48$, $N = 10$ (left) and $N = 16$ (right). For $N = 10$, the onset of the run-away behavior (i.e., the increase of R^2) can be seen at late time.

$\mu = 0$: BFSS limit

In this subsection, we review the information extracted from our simulations on the BFSS limit. As expected, the run-away of scalar fields becomes more relevant as we approach $\mu = 0$, especially at smaller N and S [134,150,214]. An interesting new observation is that the signal for metastability in a confined state even persists in the BFSS limit, see Fig. 4.35. Such a metastable state can exist because the tendency for the scalar field to diverge is reduced in the confined phase. On the other hand, we did not observe the deconfined phase in such a low-temperature region. As we have already seen in Sec. 4.3.9, this deviation from the gravity expectation can be due to finite N corrections. The expectation is that T_2 and T_c decrease with increasing N, as $T_c, T_2 \sim N^{-5/9}$, which is still sizable in our simulations (e.g., $12^{-5/9} \simeq 0.251$, $16^{-5/9} \simeq 0.214$). Therefore it is possible that the simulations at finite N and small T see only the confined phase, even though the deconfined phase exists all the way down to $T_2 = T_c = 0$ in the large N limit. T_1, on the other hand, increases with increasing N, which means larger N stabilizes the confined metastable state up to higher temperatures. Nevertheless, this is not in contradiction with $T_c = 0$ since the deconfined state has lower free energy.

We performed a detailed investigation at $T = 0.2$, where the confined phase is sufficiently stable. To obtain the confined phase, the initial configuration has to be tuned appropriately. We obtained confined configurations by taking the initial configuration to be a configuration from the BMN simulation at small μ, and $X_I = 0$ for all $I = 1, 2, \cdots, 9$ ('cold start'). Due to the flat directions, the latter often does not converge to a confined state, but we were able to observe such a convergence for $N = 16$, $S = 48$ and $N = 10$, $S = 48$; see Fig. 4.36. While the confined phase appears to stabilize the flat directions to a certain extent, instabilities may still appear after many Monte Carlo steps, as shown in the left part of Fig. 4.36. We generally observe that the confined state is more stable at larger N and/or larger S. We were not able to obtain a stable confined state for a sufficiently long time below $S = 30$. However, for larger S, by slowly increasing the temperature, we were able to see a confined phase up to about $T = 0.26$.

To build confidence that we are observing the confined phase, we performed continuum extrapolations (linear in $1/S$) for $N = 10, 12$ and 16, as well as large N extrapolations (linear in $1/N$) for $S = 30, 36, 48$, at $T = 0.2$; see Figs. 4.37, 4.38. (To obtain these data points, we only used the parts of the Monte Carlo histories before the instabilities due to the flat

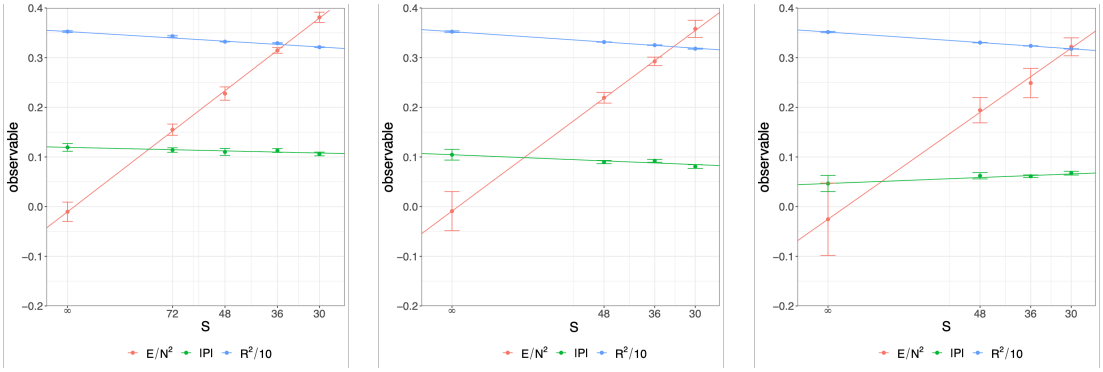

Figure 4.37: Full BFSS (i.e., full BMN with $\mu = 0$) at temperature $T = 0.2$. From left to right: continuum extrapolation (lattice size $S \to \infty$) for matrix size $N = 10, 12, 16$. The horizontal axis scales as $1/S$. We can see that the continuum extrapolation of $\frac{E}{N^2}$ is consistent with zero for all values of N. Therefore, $\frac{E}{N^2}$ is consistent with zero in the simultaneous continuum and large-N limits. We note that for the simulation with parameters $S = 30$, $N = 16$, we discarded configurations with a too-large value of R^2 due to the run-away behavior.

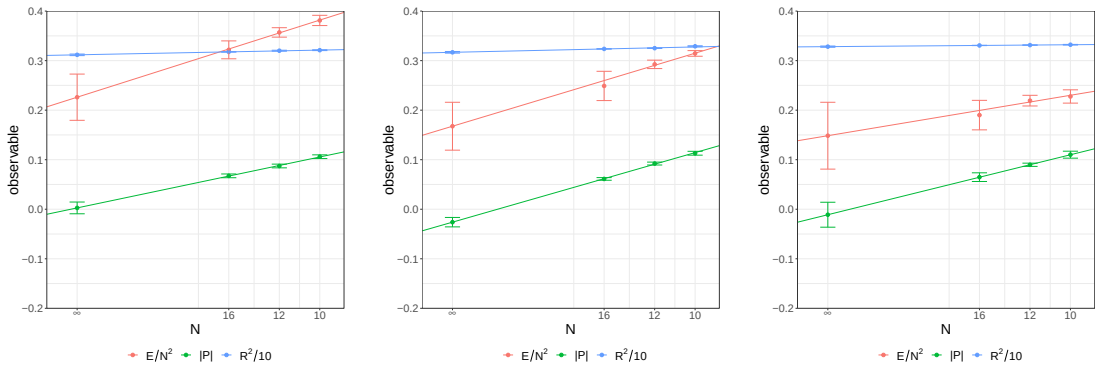

Figure 4.38: Full BFSS (i.e., full BMN with $\mu = 0$) at temperature $T = 0.2$. From left to right: large N extrapolation for lattice size $S = 30, 36$ and 48. The horizontal axis scales[29] as $1/N$. We can see that the large-N extrapolation of the Polyakov loop is very close to zero for all values of S. As a result, the Polyakov loop is consistent with zero in the simultaneous continuum and large-N limits.

directions set in.) We observe that the Polyakov loop P is consistent with zero in the large N limit, and thus consistent with a confined phase. Similarly, the energy is consistent with zero in the continuum limit independently of N.[28] Note that, in the deconfined phase, we expect larger values of the energy and the Polyakov loop that are clearly distinguishable from zero. The energy of the deconfined phase predicted by the gravity dual (the black zero-brane in type IIA superstring theory) is $\frac{E}{N^2} \simeq 7.41 T^{14/5} \simeq 0.0818$ at $T = 0.2$, up to string-theoretical corrections. As for the Polyakov loop in the deconfined phase, Ref. [214] observed $P \simeq \exp\left(-\frac{0.15}{T} + 0.072\right)$ at $0.475 \leq T \lesssim 1$. This fit agrees well with the values of P at $T \geq 0.4$ obtained in Ref. [134]. By assuming that this fit is valid at lower temperatures as well, we obtain $P \simeq 0.51$ at $T = 0.2$.

[28] Due to supersymmetry, the zero-point energy is zero.

4.3.10 Conclusion and discussion

In this project, we studied the thermodynamic features of the BFSS matrix model and BMN matrix model. Specifically, we studied the confinement/deconfinement transition in the trivial background. We conjectured the phase structure based on dual gravity description [210, 236] and previous numerical studies. According to our conjecture, there are two kinds of confined phases: the completely-confined phase, which is the (local) minimum of the free energy, and the partially-confined phase (eleven-dimensional Schwarzschild black hole), which is the local maximum of the free energy separating the completely-confined phase (M-theory vacuum up to a small thermal fluctuation) and completely-deconfined phase (black zero-brane in type IIA string theory). We provided the evidence supporting this conjecture by performing lattice Monte Carlo simulations, modulo a few subtleties associated with the finite-N effects. It is natural to expect that the confined phase of the BFSS matrix model can describe M-theory, and hence, we might have finally reached the M-theory region.

The relationship between the flux parameter μ and critical temperature T_c is shown in Fig. 4.22. Naively, it may appear that the matrix model and gravity disagree at small μ. However, this is not the case; the gravity line is from the strict large-N limit, while the matrix model results are obtained at finite N, and the apparent disagreement is consistent with the gravity analysis and finite-N correction. This apparent deviation is actually good news in a sense that are interpreted as quantum corrections!

Because such a confined phase was not observed in the past, the consistency has to be discussed carefully. All studies but Ref. [250] focused on the high-temperature region (for example, Ref. [134] studied $T \geq 0.4$, $N \leq 32$, $L \leq 32$), by gradually lowering the temperature, and hence, it could be a problem if the confined phase had been observed. It is straightforward to go to larger N, say $N = 64$ or 128, at $0.4 \lesssim T$, and we might be able to see the confined phase there if the sufficiently fine lattice is used and the initial configuration is carefully tuned. It would be a good consistency check. Ref. [250] studied lower temperature ($T \sim 0.1$) and much smaller N ($N = 3, 4, 5$). They introduced the cutoff for $\mathrm{Tr}X_I^2$ and studied the unstable phase, whose energy was consistent with the deconfined phase. This phase may be stabilized at sufficiently large N and become the stable deconfined phase.

One surprise, which we did not expect when we started this project, was that the confined phase exists up to a rather high temperature, even in the BFSS limit. Concerning Monte Carlo simulations, it is very good news: at higher temperatures, the temporal circle is smaller, and hence, the simulation cost is smaller. Therefore, the detailed study of M-theory via Monte Carlo simulation of the BFSS or BMN matrix models might be doable with much smaller computational resources than previously expected. Nontrivial fuzzy-sphere backgrounds corresponding to M2-branes or M5-branes may also be tractable targets. To deepen the understanding of the duality in the M-theory region, it is important to perform calculations in the gravity side that can be compared to the simulation results in the matrix model side. Of equal importance is a similar confinement-to-deconfinement analysis for the fuzzy sphere backgrounds, since in this case the precise dependence of the relevant temperature with N is not known. This is an interesting problem, not only from the matrix model side but also from the gravity analysis also, yet the difficulty to extract precise results is emanating from carefully manipulating multi-centered supergravity solutions [258]. A better understanding

[29] As opposed to the deconfined phase, it is not clear a priori whether $\frac{E}{N^2}$ and R^2 should have $1/N$ or $1/N^2$ corrections. Both options provide a reasonable fit to our data and we chose the $1/N$ option in figure 4.37.

of these solutions and their connection with analytic and Monte Carlo results, along the line of the trivial vacuum analysis, will lead to a better M-theory interpretation.

Note that our analysis on the M-theory regime of the gravity side was only qualitative. In order to understand the duality better, it is important to improve the analysis. It is natural to think that only a part of the matrix degrees of freedom is excited and form a black hole and graviton gas [225–227, 238], but the rest of the degrees of freedom can still contribute to the emergence of the background spacetime [238]. The number of degrees of freedom forming a black hole can be determined from the distribution of the Polyakov line phases [222]. As a rough estimate, it would be reasonable to identify it with the entropy [225–228].

For extremely low temperatures, we expect to enter the M-theory regime [210]. That is because the small temperature region is related to the small energy regime and the latter is expected to be connected with M-theory. Therefore, it might be possible that we can access the M-theory region by keeping μ fixed and taking the limit $T \ll 1$. This would correspond to a BMN M-theory description with a finite deformation, and indeed for low temperatures, this is assumed to be described by the M5-brane of M-theory [211]. We can see hints for this feature since the clustering of the six matrices that construct the five-sphere leads to an average mean value bigger than the rest of the three matrices that construct the $SO(3)$ part. Indeed, recalling Fig. 4.14 this phenomenon can be observed in simulations and we will report a more detailed analysis in a different project in section 4.4. We may also note that in the very low temperature regime we cannot compare with results from the gravity side, since at this level there is no such precise analysis for the M5-brane.

The completely-confined phase is rather stable, and hence, can be studied straightforwardly. The study of the partially-confined phase can be tricky because it is unstable in the canonical ensemble. Still, it may be doable by constraining the value of the Polyakov loop appropriately. This phase, which is expected to be the dual of the eleven-dimensional Schwarzschild black hole, would offer us an ideal framework to study the black hole evaporation. It might be possible to study the region near the border between string theory and M-theory ($T \sim T_2$) in a similar manner by introducing appropriate constraints.

Qualitatively, the BMN matrix model resembles four-dimensional maximal super Yang-Mills on three-sphere. For the latter, deconfinement is studied not just by using the thermal boundary partition function but also with the index [244]. The index is calculable analytically even at strong coupling, and impressive agreement with gravity has been observed [259]. Such an approach might be useful for the BMN matrix model as well, providing connections to the counting of the supersymmetric black hole in an analytically tractable manner.

Rich phase diagrams are expected for other gauge theories as well. Qualitative aspects of the phase diagrams of maximally supersymmetric Yang-Mills theories was discussed in Ref. [210] by utilizing dual gravity pictures and string dualities. These theories may exhibit confinement, as we observed for the matrix model. Two- and three-dimensional theories can be studied on lattice without having the parameter fine-tuning problem, and simulations on small lattices are already tried; see Refs. [139, 140, 217] for the two-dimensional theory and Ref. [142] for the three-dimensional theory. Lattice Monte Carlo simulation of these theories can be a powerful tool to reveal the nonperturbative aspects of string/M-theory and holography further.

Last but not least, it is important to understand how the information of eleven-dimensional spacetime is encoded in the BFSS matrix model in which only ten of eleven dimensions can

be seen manifestly; see e.g. Ref. [260]. We might be able to get some hints by studying the M-theory parameter region of the BFSS matrix model and identifying the gravity dual precisely.

The main message of this project

In this project we studied the phase diagram of BMN model [194]. It added the following new insights that can be summarised in the list:

- The phase transition of BMN matrix model has established to be of first order.
- The confined phase of BFSS model has been observed for the first time.
- The latter phase is argued to be connected with the Schwarzschild black hole of M-theory. If this is true, then we may revealed a possibility to study contents of M-theory by using the BMN model in low temperatures exploiting its stability at finite μ.
- The key point is that we can use the BMN model with small μ to probe the BFSS model in low temperatures. This was crucial in order to understand the behaviour of the two models in small temperatures and their connection.

4.4 Gauged and Ungauged matrix models

In this project we discuss an interesting conjecture made in [254]. Maldacena and Milekhin discussed whether the gauge-singlet constraint is necessary for the duality. Therefore, let us give some motivation why this project is interesting.

The holographic principle claims that quantum gravity can be described by a dual non-gravitational theory. AdS/CFT duality [130] provides us with concrete realizations of the holographic principle. But in fact, neither AdS nor CFT is crucial; actually, AdS/CFT duality is a special case of gauge/gravity duality that admits non-AdS/non-CFT duality. As yet other examples emerge, it became natural to ask if the gauge-singlet constraint is crucial on the QFT side. Indeed, this is something that gained more popularity since the appearance of the Sachdev-Ye-Kitaev (SYK) model [261, 262]. The SYK model is described by N one-dimensional quantum fermions with random interactions between them and it does not have a gauge symmetry. Despite the lack of gauge symmetry, fermion bilinears that look like "singlets" appear to have natural dual descriptions in an emergent two-dimensional spacetime [263]. The SYK model was believed to give a concrete realisation of a n(early)AdS/n(early)CFT correspondence because the bulk dual is related to near-extremal Reissner-Nordströ m black holes whose horizon topology back-reacts in $AdS_2 \times S^2$. The factor of AdS_2 in the previous topology can be described by the Jackiw-Teitelboim gravitational model [67, 264] . The same story holds for the Gurau-Witten tensor models [263, 265] in which the gauge-singlet constraint can be either imposed or not. In fact this is not surprising since both the tensor models and the SYK model are related with each other under the fact that their Feynman diagrams are dominated by the so-called melonic diagrams.

Maldacena and Milekhin [254] discussed whether the gauge-singlet constraint is necessary for more traditional types of gauge/gravity duality. They considered the D0-matrix model [53,

209] and its ungauged version and conjectured that the difference between the gauged model (with singlet constraint) and the ungauged model (without singlet constraint) is exponentially small at low temperature. In particular, they conjectured that the same gravity dual describes the low-energy dynamics of the gauged and ungauged models. Numerical simulation of the D0-matrix model [138] provided results consistent with the conjecture.

There is a natural generalization of the D0-brane matrix model keeping maximal supersymmetry, called the BMN matrix model [211]. Maldacena and Milekhin considered the ungauged version of the BMN matrix model as well. In this paper, we test their conjecture for the BMN matrix model by employing numerical methods. In addition to the original motivation coming from the Gurau-Witten tensor model, yet another motivation, in this case, comes from quantum simulations [141]. The gauge-invariant Hilbert space consisting only of singlet states is rather complicated, and merely writing down the orthonormal basis is already a difficult task. This problem can be avoided by introducing the extended Hilbert space that contains non-singlet states. A potential worry arises if the additional non-singlet degrees of freedom introduce other unexpected technical issues. Specifically, if many light modes emerge, they can easily be excited and lead to a large error. If the conjecture by Maldacena and Milekhin is correct, such light modes do not exist and hence the use of the extended Hilbert space can be rather straightforward.

The ungauged matrix model

If we turn-off the gauge field A_t in the BFSS or BMN matrix model, we obtain the *ungauged* matrix model. Specifically, we define the ungauged action S_{ungauged} as

$$S_{\text{ungauged}}[X,\psi] = S_{\text{gauged}}[X, A_t = 0, \psi]. \tag{4.69}$$

The thermal partition functions of gauged and ungauged models are defined by

$$Z_{\text{gauged}} = \int \mathcal{D}[A_t]\mathcal{D}[X_M]\mathcal{D}[\psi_\alpha] e^{-S_{\text{gauged}}[X,A_t,\psi]}, \tag{4.70}$$

$$Z_{\text{ungauged}} = \int \mathcal{D}[X_M]\mathcal{D}[\psi_\alpha] e^{-S_{\text{ungauged}}[X,\psi]}. \tag{4.71}$$

Here, the time direction is Wick-rotated to the Euclidean signature and compactified to circumference $\beta = T^{-1}$. We impose the periodic boundary condition for bosonic fields X and A_t, and antiperiodic boundary condition for fermionic fields ψ.

Gauge-singlet constraint

Let us discuss the meaning of the ungauging in terms of quantum states in the Hilbert space. By using the gauge-invariant Hilbert space $\mathcal{H}_{\text{inv}}$ and the extended Hilbert space $\mathcal{H}_{\text{ext}}$, thermal partition functions are written as (see for example Appendix A.2 in Ref. [266])

$$Z_{\text{gauged}}(\beta) = \frac{1}{V_{\text{SU}(N)}} \int_{\text{SU}(N)} \mathrm{d}g \mathrm{Tr}_{\mathcal{H}_{\text{ext}}} \left(\hat{g} e^{-\beta \hat{H}} \right) \tag{4.72}$$

$$= \mathrm{Tr}_{\mathcal{H}_{\text{inv}}} \left(e^{-\beta \hat{H}} \right) \tag{4.73}$$

and

$$Z_{\text{ungauged}}(\beta) = \mathrm{Tr}_{\mathcal{H}_{\text{ext}}} \left(e^{-\beta \hat{H}} \right). \tag{4.74}$$

In (4.72), $V_{\mathrm{SU}(N)}$ is the volume of the SU(N) gauge group, $\int_{\mathrm{SU}(N)} \mathrm{d}g$ is the integral with the Haar measure, and $\hat{g}$ is the operator acting on the Hilbert space as the SU(N) transformation corresponding to the group element $g \in \mathrm{SU}(N)$. By construction, $\frac{1}{V_{\mathrm{SU}(N)}} \int_{\mathrm{SU}(N)} \mathrm{d}g\hat{g}$ acts as the projector from $\mathcal{H}_{\mathrm{ext}}$ to $\mathcal{H}_{\mathrm{inv}}$. In fact, (4.72) is directly related to the path-integral formulation with gauge field A_t, (4.70). The projection operator tells us that we should count gauge-equivalent states only once, and hence, we obtain (4.73) from (4.72). The operator $\hat{g}$ is the counterpart of the Polyakov loop in the path-integral formalism. Integration over SU(N) is the remnant of the path integral with respect to A_t.

Gravity dual of ungauged matrix models

The idea behind gauging a symmetry or not in this particular example might become more intuitive if we present it in the language of string theory. The gauge invariant (physical) states are singlets. These states correspond to closed strings and are constructed by acting with combinations of matrix operators on the vacuum state upon taking the trace over the gauge group indices[30], i.e

$$|\text{physical}\rangle = \mathrm{Tr}\left(\hat{X}_{I_1}\hat{X}_{I_2}\cdots\hat{X}_{I_L}\right)|\text{vacuum}\rangle\,. \tag{4.75}$$

On the other hand, the ungauged model allows some room for non-singlets without a trace

$$|\text{physical}\rangle = \hat{X}_{I_1}\hat{X}_{I_2}\cdots\hat{X}_{I_L}\,|\text{vacuum}\rangle\,. \tag{4.76}$$

Even though the singlet sector of both theories is the same, in the ungauged model there is a new sector that hosts non-singlets. The latter can intuitively be realized as an arbitrary long open string made out of L bits whose end points can reach the boundary. Let us now discuss the continuum picture, e.g $L \to \infty$. In the bulk, this configuration of long strings is described by the gravity dual of non-supersymmetric Wilson loops and the difference with the usual supersymmetric Wilson loop is the fact that in the latter case the string obeys Neumann boundary conditions while in the former Dirichlet boundary conditions [254]. This means that the tip of the non-singlet string can freely move in the bulk and reach even to the boundary. In order to be able to compare with gravity, we should ask what would be a natural cut-off such that we could approximate the energy of this massive string/state with supergravity. This is dictated by the validity of (3.114) which reminding that $[r] = (\text{energy})^1$ we may demand that $E_{\mathrm{min}} \sim \lambda^{1/3}$. This indeed would be a natural cut-off because when we have a pair of a string and an anti-string, we can arbitrarily lower their energy (length) by placing both its endpoints on the boundary. On the other hand, we could not approximate its energy from the supergravity side in this case because the latter is not valid at the boundary. Hence, a natural non-zero, calculable from the gravity side, value of minimal energy would be

$$E_{\mathrm{min}} \propto C_{\mathrm{adj}}\lambda^{1/3}, \tag{4.77}$$

with C_{adj} being a number. The idea then is that the fate of non-singlet adjoint strings is to end on the boundary minimizing in this way its energy. Therefore, contributions from the energies of non-singlet states should be negligible in the large N and low-temperature limit

[30] Here the gauge group is $SU(N)$ and by taking the trace we mean summing over the $SU(N)$ indices $\mathrm{Tr}\,\hat{X}_I = \sum_{i=1}^{N}\left(\hat{X}_I\right)^i{}_i$, $\mathrm{Tr}\,\hat{X}_I\hat{X}_J = \sum_{i=1}^{N}\sum_{j=1}^{N}\left(\hat{X}_I\right)^i{}_j\left(\hat{X}_I\right)^j{}_i$, etc. This is different from the trace over the Hilbert space, $\mathrm{Tr}_{\mathcal{H}_{\mathrm{inv}}}$ or $\mathrm{Tr}_{\mathcal{H}_{\mathrm{ext}}}$.

and the gravitational dual of the non-singlet strings in this regime is the same as the one of the singlets in (3.114).

Hence, in addition to the geometry (3.114), there might be contributions in the partition function from the non-singlet sector, the latter being near the boundary. However as it has been previously verified in [138], we shall also see that when the ground state of the ungauged model is cyclic (in a sense that we allow cyclic permutations of the matrices $\hat{X}_1 \cdots \hat{X}_L$) and in particular in the low temperature regime of the theory the non-singlet sector is sub-leading and the two theories, gauged and ungauged are exponentially close to each other. This is the conjecture made in [254] which we focus on in what follows.

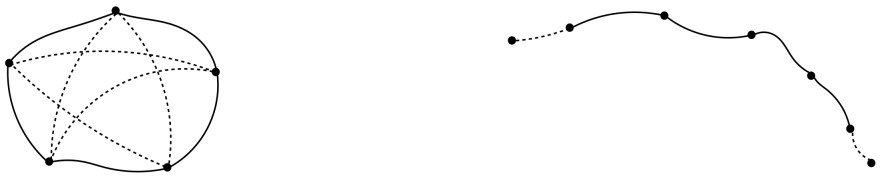

Figure 4.39: Five isolated D0-branes are connected with strings. [Left]: A gauge invariant state (solid line) is formed by a closed loop connecting the D0-branes. [Right]: A non-gauge invariant state represented by an open string that connects D0-branes and can be arbitrary long (depending on the number of D0-branes). The string bits are given by the spacing between the D0-branes and are represented by L.

4.4.1 Gauged vs ungauged: the conjecture

The temporal component of gauge field A_t is not dynamical. Its role is to impose the gauge-singlet constraint. Matrix models do not have spatial gauge field components $A_x, A_y, \cdots$, and hence, the only effect of gauge symmetry is to impose the gauge-singlet constraint. The ungauged version of the model does not obey the singlet constraint. The $SU(N)$ symmetry is treated as a global symmetry of the system.

In [254], Maldacena and Milekhin considered the BFSS matrix model ($\mu = 0$) and the BMN matrix model ($\mu > 0$), and claimed that gauged and ungauged versions are essentially the same at large N and strong coupling, in the sense that the contribution of the non-singlet sector in the partition function is negligible in the large N limit. The partition functions of the two models are given as (4.70), (4.72), (4.73) for the gauged model, and and (4.71), (4.74) for the ungauged model.

Let us denote the difference of the gauged and ungauged free energies in the large N limit as

$$\begin{aligned}\Delta\mathcal{F} &= -\log Z_{\text{gauged}}(\beta) + \log Z_{\text{ungauged}}(\beta) \\ &= \beta\mathcal{F}_{\text{ungauged}} - \beta\mathcal{F}_{\text{gauged}} \\ &= N^2 g(\beta) \end{aligned} \tag{4.78}$$

up to $\frac{1}{N}$-corrections, where $g(\beta)$ is a function that depends on the parameter regimes of the

model[31]. The factor N^2 comes from the 't Hooft counting.
Ref. [254] discussed the free energy difference in two different regimes and focused on the strong coupling regime. Actually the BMN model has two parameters that control the regimes of the system, that is μ and T. Let us remind the effective dimensionless coupling for the BMN model again here

$$g_{\text{eff}} = \frac{\lambda}{\mu^3}. \tag{4.79}$$

The high temperature and weak coupling regime

In this limit, the difference of the free energies is

$$\Delta\mathcal{F} \simeq N^2 \log(\mu\beta), \quad \frac{\lambda^{2/3}}{T^2} \ll 1, \quad \frac{\mu^3}{\lambda} \gg 1. \tag{4.80}$$

This is the weak coupling regime at high temperatures and large μ. At these temperatures we do not have a bulk dual so we will not be interested in this regime.

The low temperature and strong coupling regime

Under the presence of a gravitational dual the free energy difference is

$$\Delta\mathcal{F} \simeq N^2 n_{\text{adj}} e^{-C_{\text{adj}}/T}, \quad \frac{\lambda}{T^3} \gg 1, \quad \frac{\mu}{T} \ll 1. \tag{4.81}$$

This limit is a bit subtle. Note that for BMN it is not enough to consider just small temperatures, but one also has to consider the $\mu \to 0$ limit to compare with gravity. The reason is that even though for finite μ there is a gravitational dual description it is given by a deformed geometry [236].
From (4.81) we get the difference of energies $E = \frac{\partial(\beta\mathcal{F})}{\partial\beta}$ as

$$\Delta E = E_{\text{ungauged}} - E_{\text{gauged}} = N^2 n_{\text{adj}} C_{\text{adj}} e^{-C_{\text{adj}}/T} + \cdots, \tag{4.82}$$

to lowest order in temperature and $\mu = 0$. The consensus built in [254] and [138] is that n_{adj} is the degeneracy of the lightest mode and C_{adj} its energy. This result seems now to be understood for the $\mu = 0$ case. Indeed at $\mu = 0$, the factor n_{adj} is an $\mathcal{O}(1)$ integer, and C_{adj} is an $\mathcal{O}(1)$ positive number. Results of numerical simulation at $\mu = 0$ [138] are consistent with $n_{\text{adj}} = 2$ and $C_{\text{adj}} \simeq 1$.

The low temperature and weak coupling regime

The BMN model can be also weakly coupled in low temperatures, in contrast to the BFSS model. This is due to the effective coupling (4.79). In the large μ region the BMN model admits a perturbative analysis [157, 267, 268] with perturbation parameter (4.79). The spectrum is discussed in Sec. 4.4.6 and the lightest mode is the one created by $B_a^\dagger$ acting on $|0\rangle$. Whether we take the trace or not, corresponds the decision between the gauged or ungauged theory. The latter act without the trace and the lightest mode is created by $B_a^\dagger|0\rangle$ with energy (4.105). In fact this is what we called C_{adj} above and we have six of them because

[31] We remind that we are measuring everything in terms of t'Hooft coupling $\lambda = g_{YM}^2 N$ which we set to one from now onwards. In a general case it would also have a λ dependence as $g(\lambda^{1/3}\beta)$.

we have six harmonic oscillators (one for each direction in the $SO(6)$ part) which gives the degeneracy. In the low temperature region also, we can still use an exponential ansatz and we expect the perturbative result of the lightest mode to be given by

$$E_{\text{adj}} = N^2 \cdot 6 \cdot \frac{\mu}{2} e^{-\frac{\mu}{2}\frac{1}{T}}, \quad \frac{\lambda}{T^3} \gg 1, \quad \frac{\mu^3}{\lambda} \gg 1. \tag{4.83}$$

This is what we expect in the perturbative, low-temperature regime for the lightest mode of the theory. In fact, if we wish to study heavier modes and to be more precise we should consider the full $U(1)$ sector given by

$$\frac{E_{U(1)}}{N^2} = 6\frac{\mu}{2} e^{-\frac{\mu}{2}\frac{1}{T}} + 8\frac{3\mu}{4} e^{-\frac{3\mu}{4}\frac{1}{T}} + 3\mu e^{-\frac{\mu}{T}}, \quad \frac{\lambda}{T^3} \gg 1, \quad \frac{\mu^3}{\lambda} \gg 1, \tag{4.84}$$

(see Table 4.6) but as we discuss later on and we show in Fig. 4.45 at very low temperatures, the difference between the contribution of the lightest mode and that of the full $U(1)$ sector is negligible (at finite μ).

4.4.2 Numerical analysis

In this section we summarize the numerical analysis. We took large N and continuum limit systematically such that lattice artefacts and finite N corrections are eliminated.

4.4.3 Simulation strategy

The BMN matrix model has a few nice features that make the numerical simulation easier than the BFSS matrix model. A big problem for the latter is the existence of flat directions. To tame the them, we have to take N very large. In the BMN matrix model, the flat directions are lifted due to the mass term in the flux deformation. Therefore, we can study the BMN matrix model at relatively small values of N. Furthermore, the condition number of the Dirac operator decreases as μ becomes large. This makes simulations more tractable in this regime.

For small μ and T, e.g. if one wishes to study the trivial background of the model, choosing combinations of the mass parameter μ and the matrix size N is quite subtle. That is because a new class of BMN vacua allows for tunnellings between the trivial background ($X_i = 0 = X_a, \psi_\alpha = 0$) and fuzzy spheres ($X_a = 0 = \psi_\alpha, X_i = \mu J_i$). The potential barrier between them depends on μ and N. More precisely, Investigating the stability of a minimum of the potential $\frac{\partial V}{\partial X} = 0$ and relating $X \sim r$ one can find that the barrier between the two backgrounds scales as $\sim \mu^4 N^4$ (see Appendix A for a derivation). Therefore for very small μ and fixed N the trivial background configuration can tunnel to a fuzzy sphere background and the distinction between the two is not possible. Because the fluctuation of matrix entries is roughly given by $0.6N^{-1/2}$, demanding that the radius of the maximum fuzzy sphere is less than this value gives a constraint on μ. On the other hand at relatively large values of N, the simulation remains in the trivial background. To avoid lattice artefacts one should also have a large number of lattice points S.

Hence, the strategy we used is the following:

- For fixed μ we perform a series of simulations at different temperatures as well as varying N and S checking that we always stay in the trivial background of the confined phase.

- We extrapolate to the large N and continuum limit of the theory for our observables.
- Calculate the difference between gauged and ungauged observables such as the energy and those defined in (4.88) and (4.89), for different temperatures at fixed μ and then fit exponentials of the form (4.81), (4.90), (4.91) respectively.
- Finally, we take the limit $\mu \to 0$ to cross-check the results for $C_{\mathrm{E,R,F}}, D_{\mathrm{E,R,F}}$ and n_{adj}.

In the past, there were two possible kinds of conjectured phase diagrams of the gauged BMN matrix model at $N = \infty$ (Fig. 4.13). The large-μ region admits perturbative calculations [151,237] and the transition is found to be of first order. The small-μ region has been studied by using the dual gravity description [236] and recently via Monte-Carlo simulations [194] first order transition has been established both analytically and numerically, while in addition a surprising possibility to study aspects of M-theory, like the Schwarzschild black hole has been established. Numerical simulation is applicable to the intermediate-μ region as well, and the results are consistent with a first-order phase transition [194]. Therefore, the left diagram of Fig. 4.13 is most likely the correct one. In this paper we do not need to know the order of the phase transition as it does not affect our argument.

According to the Maldacena-Milekhin conjecture, the gauged and ungauged theories are exponentially close at low temperature. Therefore, we will focus on the confined phase. In it observables like e.g the energy, are independent of temperature up to $1/N$ corrections. We can determine these temperature-independent values by taking the large-N and continuum limit at some fixed value of T. In order to determine these values reliably, we will study different values of T at each μ.

To extrapolate to large N and continuum regime, we use the fit ansatz

$$\frac{E(S,N)}{N^2} = \varepsilon_{0,0} + \frac{\varepsilon_{1,0}}{N^2} + \frac{\varepsilon_{0,1}}{S} + \frac{\varepsilon_{1,1}}{N^2 S} + \cdots . \tag{4.85}$$

The continuum extrapolations are done with $\varepsilon_{0,1}$ corrections while the large N ones with $\varepsilon_{1,0}$ terms. The extrapolations of other observables are of the same form. For a discussion over different extrapolation fits of this form see Sec. 4.5.

The values of the flux that have been used are in the range $\mu = 2, 3, 4, 5$ while the range of temperatures is adjusted for each μ with $T \in [0.2, 1.1]$. In addition the size of the matrices and the lattice spacing runs over $N = 8, 12, 16$ and $S = 12, 24, 48, 96$, respectively. Then we extrapolate to large N and the continuum regime of the theory using the strategy we discussed in Sec. 4.4.3 and using fits of the form (4.85). We repeated this analysis both for the gauged and ungauged data.

In Fig. 4.40 we present some representative Monte Carlo histories from the data we used. Similar Monte Carlo histories appear in all range of μ and temperatures we have investigated.

4.4.4 Energy of the system

In the matrix model side, the energy of the system is given via $E = E(T)$ since we are in the canonical ensemble. In other words, we are fixing the temperature and obtain the energy of the system. On the other hand, in the gravity side the energy of the system is given by (3.122) for the BFSS gravity dual and from the deformed version (3.182) for the BMN gravity

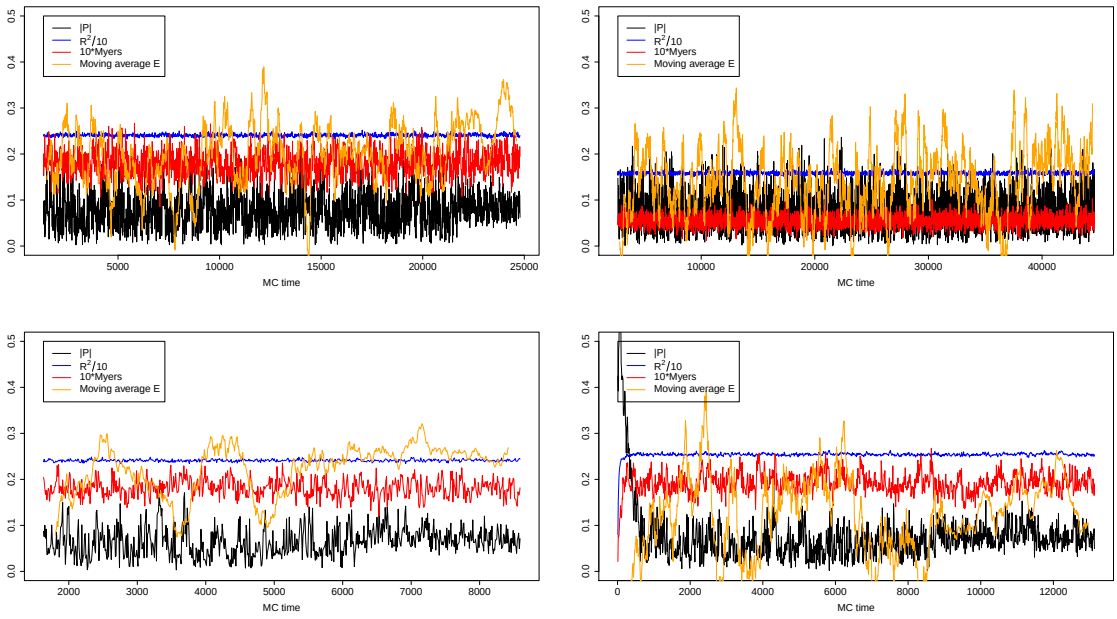

Figure 4.40: Typical Monte Carlo histories for gauged data. [Up]: from left to right $\mu = 2, T = 0.2, N = 12, S = 48$ and $\mu = 4, T = 0.4$ for same N, S. [Bottom]: from left to right $\mu = 2, T = 0.2, N = 16, S = 48$ and same μ, T for $N = 16, S = 96$.

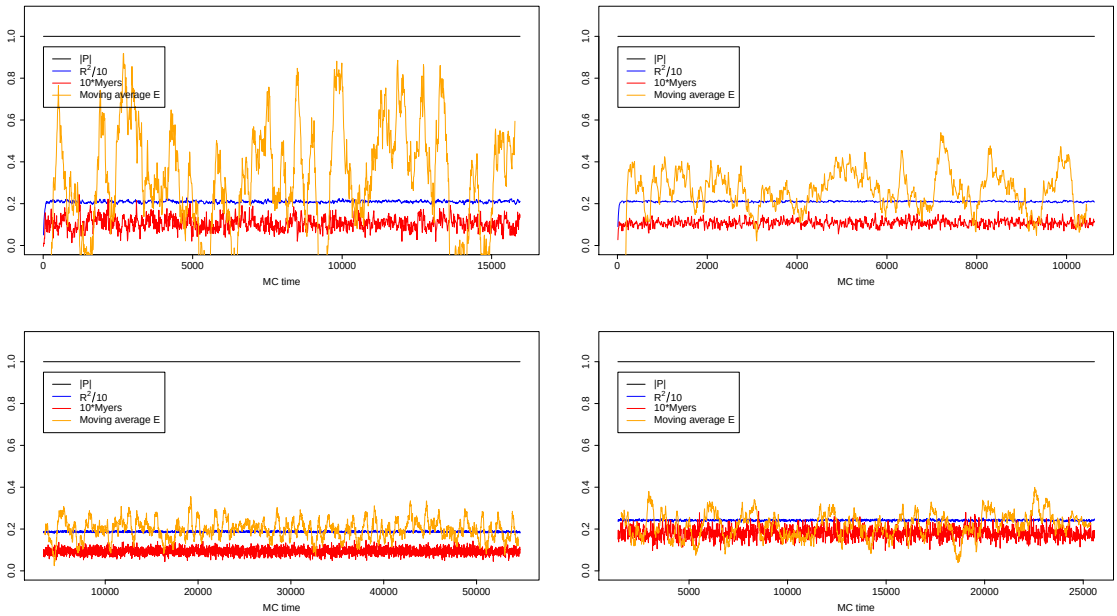

Figure 4.41: Typical Monte Carlo histories for ungauged data. [Up]: from left to right $\mu = 3, T = 0.4, N = 8, S = 96$ and same μ, T, S for $N = 16$. [Bottom]: from left to right $\mu = 3, T = 0.2, N = 12, S = 48$ and same T, N, S for $\mu = 2$. The Polyakov loop is $P = 1$ by definition in the ungauged model.

dual. In any case, the low-energy regimes of the models correspond to the low-temperature regimes.

In the BFSS limit $\mu = 0$, Maldacena and Milekhin conjectured (4.82), which we repeat here:

$$\Delta E = E_{\text{ungauged}} - E_{\text{gauged}} = N^2 n_{\text{adj}} C_{\text{adj}} e^{-C_{\text{adj}}/T} + \cdots .$$

Numerical simulation in Ref. [138] suggests $n_{\text{adj}} = 2$ and $C_{\text{adj}} \simeq 1$. We studied the behavior of ΔE at finite μ and low temperature. The results are given in Fig. 4.42 with perturbative results valid at large μ and two kinds of numerical fit. The punchline at this stage is that there is an exponential decay with $1/T$ verifying the ansatz (4.81). The nature of the fits depends on how many parameters we keep. The red curves in Fig. 4.42 are two-parameter fits with the following ansatz:

$$\Delta E(\mu, T) = N^2 D_E(\mu) e^{-C_E(\mu)/T}. \tag{4.86}$$

The fit results are shown in Table 4.3. We can extrapolate $C_E(\mu)$ to $\mu = 0$, by assuming a quadratic dependence on μ $C_E(\mu) = C_E(0) + A\mu^2$. As long as we are in the low values of μ we can assume that the Taylor expansion of this form is valid. We may also note that the sign of μ does not play an important role since whether we are considering μ or $-\mu$ is physically equivalent for the BMN model since we are just changing the sign of the mass. This symmetry is broken by lattice artefacts but gets restored when we are considering the continuum limit. Therefore, we can neglect the linear term in μ. The result we get is $C_E(0) = 0.860(68)$, which is consistent with the value 0.83(21) obtained in Ref. [138] and the other parameter is estimated as $A = 0.087(04)$. On the other hand, it is difficult to extrapolate $D_E(\mu)$ to $\mu = 0$; the quadratic ansatz gives 2.755 ± 2.153, which has a very large error (see Fig. 4.43).

The ratio $n := D_E/C_E$ is regarded as the degeneracy of the eigenstate of the system. At $\mu = 0$, simulations in Ref. [138] suggested that it is $n\big|_{\mu=0} = 2$. In particular, the numerical value was estimated as $n\big|_{\mu=0} = 1.91(78)$. At finite μ we do not know what to expect precisely, but it is possible that, in addition to the energy eigenstate, also the degeneracy can change. In fact this is what we observe numerically as shown in Fig. 4.44 and we shall call the degeneracy as effective degeneracy. We call it effective because it can take rational values as μ changes and it is possible that is not valid in all range of μ . Our numerical results suggest that indeed there is a change of degeneracy with μ as we observe in Fig. 4.44. This is the change we observe in the effective degeneracy from numerical data as we turn on μ. We stress again that there is no theoretical results on how the degeneracies of the gauged and ungauged sectors change as we turn on μ, but our data suggest a dependence on μ of the effective degeneracy of the energy, accompanied also by a change on the energy itself $C_E \to C_E(\mu)$. It might be possible that it appears as a systematic error, but on the other hand it could be of physical significance since at intermediate μ there could be some modes even in the gauged sector that are not light and they contaminate the simulation results such that the effective degeneracies have this peculiar shift which can be non-integer for non-zero μ. We do not know the nature of this peculiar shift but our findings are pointing towards a physical understanding.

We recall from (4.81) that the limit in which we are interested is $\frac{\mu}{T} \ll 1$ and $T^3 \ll 1$ which is indeed very difficult for simulating. What we do instead is to fix μ, perform a series of simulations for different decreasing temperatures, check the behaviour of the system as we change the coupling and then compare with the $\mu \to 0$ limit. Indeed, in the latter case we find good agreement with the numerical results obtained in [138] and expectations reported in [254]. Note that from theoretical expectations for the finite μ regime of the model we do not have a clear idea how the energy difference for the gauged and ungauged models

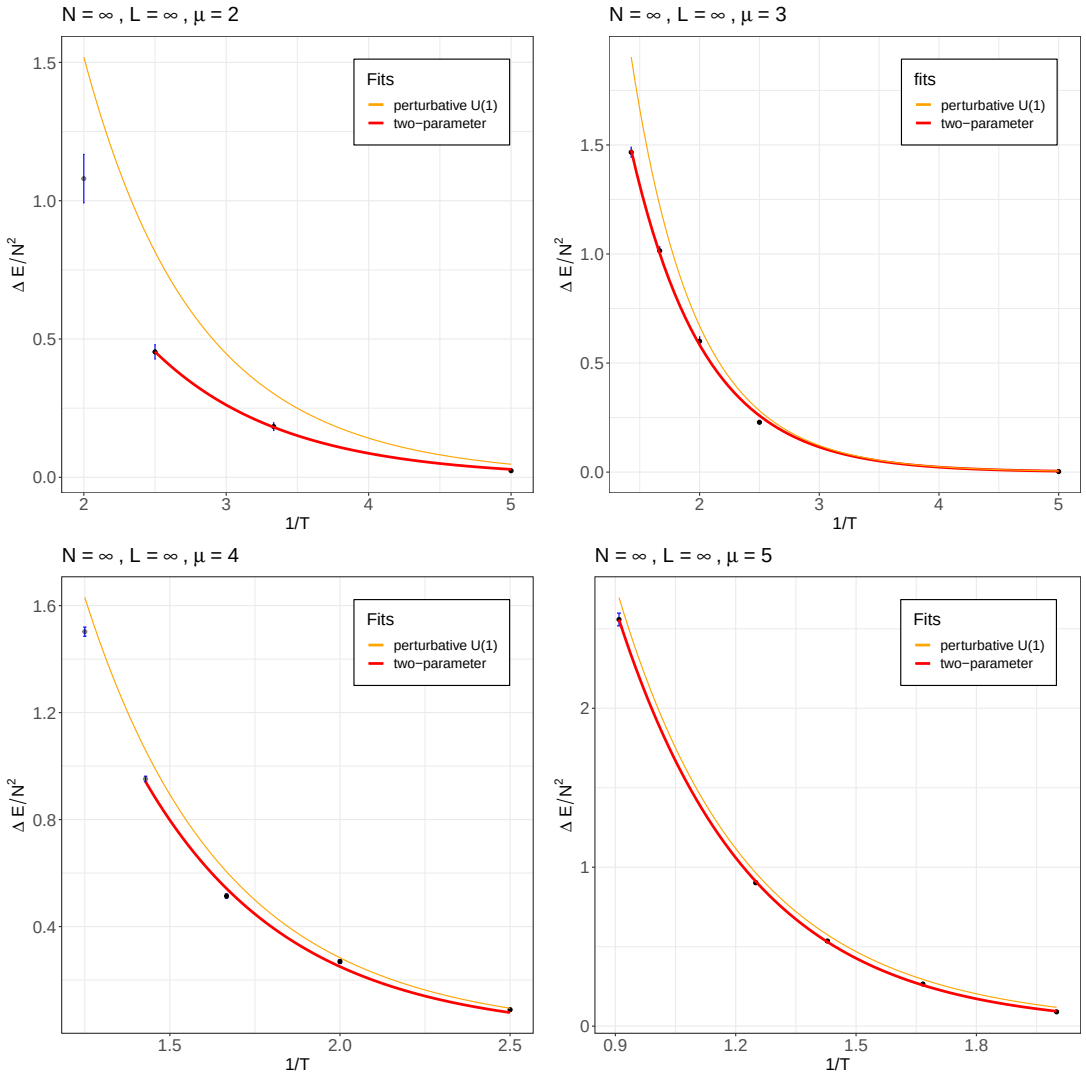

Figure 4.42: The large N and continuum fits of the difference of energies (4.82) for different μ and the relevant fits. The two-parameter fit is given in (4.86) with results reported also in Table 4.3. The perturbative fit is given by equation (4.84).

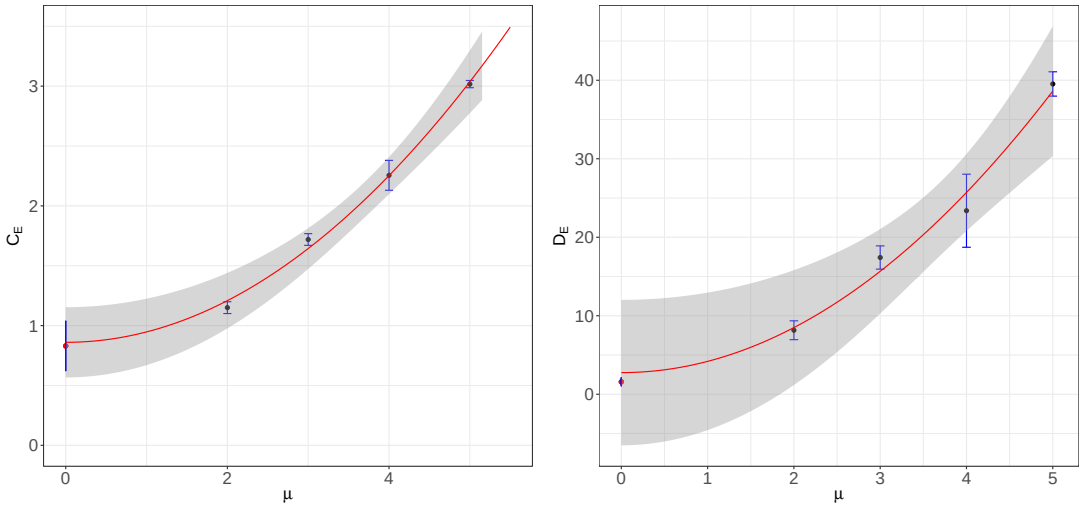

Figure 4.43: The dependence of the energy parameters on μ . [Left]: The fit is done by $C_E = 0.860(68) + 0.087(4)\mu^2$. [Right]: The fit curve is again given by $D_E = 2.8(2.2) + 1.44(14)\mu^2$. Points at $\mu = 0$ are from [138]. The extrapolated values agree within error bars with the points at $\mu = 0$.

is related. It is possible that finite μ effects even at low temperature can introduce some non-trivial corrections to the energy of the system. The reason is that when we turn on μ we also turn on some massive modes that can contribute in the partition function resulting in[32] $C_{\text{adj}} \to C_{\text{adj}}(\mu)$. Theoretically, this possibility of finite μ contributions to the interacting sector of the gauged model exists, but their precise form is unknown [268]. Let us clarify a bit this point. In perturbative investigations [157, 267–269] there is the claim that the free sector of the model does not receive any finite μ contributions to all orders in perturbation theory. In fact, this is the reason why we can use the perturbative result of the $U(1)$ sector (4.84) even at finite μ. The same claim has been tested for some states of the $SU(N)$ interaction sector to a few orders in perturbation theory [267, 269]. On the other hand in [268] is argued that there could be some terms in the interacting sector of the model that receive finite μ corrections, as well as it could be the case that we have mixing states at finite μ which could result in a non-trivial change of the energy of the system. We stress, that indeed, since such an analysis has not been done in the past, by turning on μ even at the level of the gauged sector we introduce some corrections to the energy. This possibility exists and is highlighted in the literature but a precise investigation has not been done yet.

However, at low temperatures and finite μ we can assume the partition functions to be close to each other such that we can still use the exponential ansatz. Indeed, the data suggest an exponential decay at small temperatures and all simulations have been done in small temperatures with respect to the relevant μ such that we remain in the confined phase [194, 236]. Therefore, using this information we can assume an ansatz such as (4.86) that works for our data.

To control the $\mu \ll 1$ limit in simulations is currently not possible. Hence, it makes more sense to study higher values of μ at the same (low) temperature and then extrapolate the results to $\mu \to 0$. On the other hand, when we study larger values of μ, contributions

[32] Without confusion we denote C_E also as C_{adj} since they are both referring to the energy.

coming from the massive modes might become significant as we explained above. For small temperatures and larger values of μ, we expect our data to converge to the perturbative prediction (4.83) and indeed we demonstrate this in Fig. 4.42. We also expect that in the BFSS limit ($\mu \to 0$, low temperature) to get $n_{\rm adj} \simeq 2$ and $C_{\rm adj}(0) \simeq 1$. This is compatible with the current results.

	two-parameter fit	
μ	C_E	D_E
0	0.860 ± 0.068	2.755 ± 2.153
2	1.150 ± 0.049	8.154 ± 1.200
3	1.719 ± 0.049	17.42 ± 1.48
4	2.255 ± 0.124	23.38 ± 4.65
5	3.017 ± 0.030	39.53 ± 1.55

Table 4.3: We fit ΔE by using the two-parameter ansatz (4.86). The $\mu = 0$ value is the extrapolation of the fits to the $\mu \to 0$ limit.

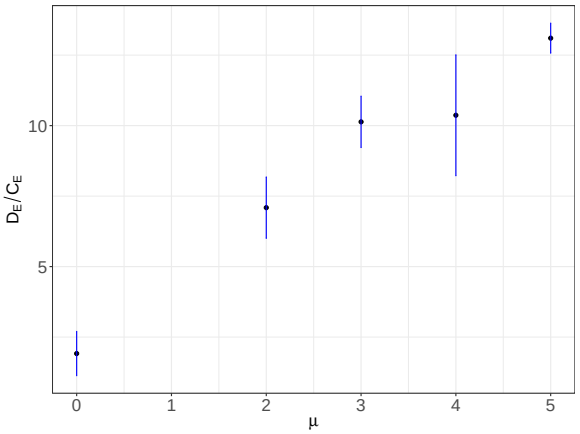

Figure 4.44: Extrapolated to $\mu \to 0$ value of the degeneracy of energy states from a two-parameter fit. At $\mu = 0$ we show the point measured with a two parameter fit in [138].

Validity of perturbative results

The perturbative prediction is expected to hold in the limit $\mu \to \infty$. Our non-perturbative methods allow us to check how much their range of validity extends towards lower μ. The perturbative estimates are shown in Fig. 4.42 in comparison to the numerical data. As expected, one observes a convergence of perturbative and non-perturbative data in the low temperature limit. For large μ this range of convergence should extend up to higher temperatures.

It is instructive to discuss in more detail the perturbative predictions. We will focus in this discussion on the largest μ ($\mu = 5$), which should provide the best convergence to the numerical data. In the large μ limit, the Hamiltonian of BMN decouples in two parts (see Appendix 4.4.6). In the energy plots in Fig. 4.42 the full $U(1)$ sector (4.84) is taken into account, but we can also investigate the relevance of the different contributions and compare the full $U(1)$ sector with the lightest mode (4.83).

At very low temperatures and finite μ the contribution of the full $U(1)$ sector almost coincides with the lightest mode (4.83) and we cannot distinguish them practically.

We observe that at finite μ the perturbative result of the lightest mode and the exponential fits from the numerical data cross at finite values of temperature as shown in Fig. 4.42. There is, consequently, no asymptotic convergence in the small temperature limit. When we include the one-loop correction given by [254, 269]

$$E_{\mathrm{SO}(6)} = \frac{\mu}{2} + \frac{\lambda}{2\mu^2} + \cdots , \tag{4.87}$$

we do not expect things to change by much because the one-loop corrections in the gauge and ungauged models cancel each other [254]. Indeed, we checked that this is the case and at small temperatures, the difference between the two is suppressed. Fig. 4.45 is an additional illustration of these findings.

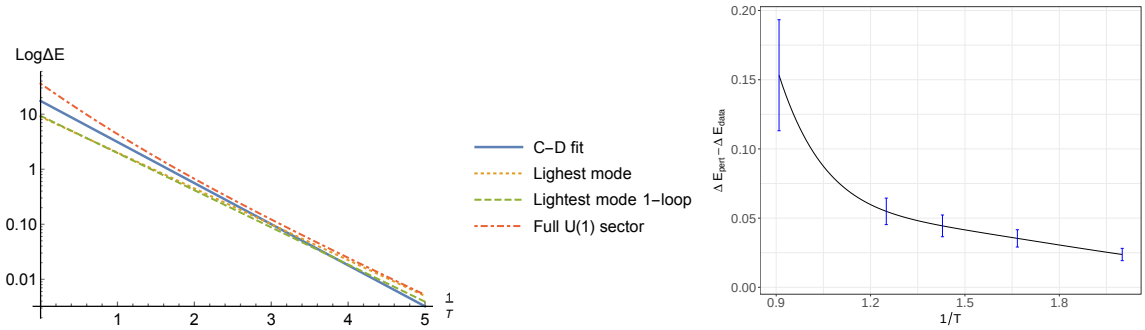

Figure 4.45: [Left]: Various perturbative results for the $U(1)$ sector of the model compared with the two-parameter fit data for $\mu = 5$ with logarithmic scaling on the y-axis. There is a crossing of the two-parameter data with the lightest mode (4.83) and its one-loop correction (4.87) but no crossing for the full $U(1)$ perturbative sector (4.84). [Right]: The difference of the perturbative result (4.84) and the two-parameter fit with respect to temperature including the error bars of the data points for $\mu = 5$. We observe an indistinguishability between the actual data and the perturbative result using the full $U(1)$ sector within the error bars of the data. At smaller temperatures the difference approaches to zero.

However, in view of the overall behaviour we still conclude that the full $U(1)$ sector (4.84) provides a cleaner description of the data since there is an asymptotic convergence instead of a crossing with the fitted non-perturbative result. Only a small shift smaller than our statistical uncertainty remains in this case. In the parameter region we studied, considering only the lightest mode shows a large deviation from the numerical data at lager temperatures. Except for the region where the fit and the lightest mode contribution cross, the full $U(1)$ contribution is closer to the data and it seems to capture the asymptotic behaviour better. Therefore we decided to show the contribution of the full $U(1)$ sector in Fig. 4.42. If we insist that the $U(1)$ sector is protected from finite μ corrections [157, 267, 268, 270] we could carry these results to finite μ and the slight shift from the actual data could be related with the $SU(N)$ sector where we do not precisely know what to expect at finite μ. This would require, however, a further detailed analysis. Such investigation can reveal more about the fine print of the perturbative calculations. Overall we can, however, conclude that our results reproduce correctly the perturbative predictions.

4.4.5 Other observables

The same analysis can be done for other gauge invariant quantities such as the sum of traces of the squared matrices defined via

$$R^2 \equiv \frac{1}{N\beta}\int \mathrm{d}t \left(\sum_{I=1}^{9} \mathrm{Tr}\,(X_I)^2\right), \tag{4.88}$$

and the commutator

$$F^2 \equiv -\frac{1}{N\beta}\int \mathrm{d}t \left(\sum_{I,J=1}^{9} \mathrm{Tr}\,[X_I, X_J]^2\right). \tag{4.89}$$

Similarly with energy, we may take the difference between the gauged and ungauged results which we expect to be exponentially close to each other in the limit of (4.81). The justification for this comes from the partition functions, which are close to each other. Therefore we expect the relevant observables to scale as

$$\Delta R^2 = R^2_{\text{ungauged}} - R^2_{\text{gauged}} = N^2 D_R e^{-C_R/T}, \tag{4.90}$$

$$\Delta F^2 = F^2_{\text{ungauged}} - F^2_{\text{gauged}} = N^2 D_F e^{-C_F/T} \tag{4.91}$$

with a priori unknown parameters D_R, D_F, C_R and C_F. We report the results in Table 4.4 while the respective diagrammatic fits are shown in Figs. 4.42 and 4.47. It is important to note that there is no prediction whatsoever for the parameters $C_{R,F}$ and $D_{R,F}$. In addition there are no constraints between C_R, D_R and C_F, D_F.

Due to finite μ deformations, we expect the situation to be different than for the BFSS model. However, in the $\mu \to 0$ limit one should recover the BFSS values. For the R^2 observable both for C_R (see left panel of Fig. 4.48) and D_R there are no precise values available at $\mu = 0$ but a rough estimate made in [138] seems to agree. On the other hand, for the commutator works only for C_F (right panel of Fig. 4.48) while for D_F we observe a discrepancy with respect to the BFSS value. We do not know precisely how these observables are behaving when we turn on μ, as well as we do not know if they are smoothly connected with the ones at $\mu = 0$. The results from analysing the energy suggest that this should be the case. The small discrepancy at intermediate μ for $C_{R,F}$ and $D_{R,F}$ could probably be an effect caused by finite μ contributions or part of the simulations has transitioned to a fuzzy sphere background. The important result is that $C_{E,R,F}$ agree nicely when $\mu = 0$ as we can see from the left panel of Fig. 4.49. Since, no correlation is assumed between $D_{R,F}$ and $C_{R,F}$ we can not claim the same for $D_{R,F}$.

In Fig. 4.46 we show that our results are consistent with theoretical expectations. Finite μ effects could be observed even though we are putting the system in the trivial background $X^I = 0, I = 1, \cdots, 9$. This can be already observed in Monte Carlo histories (see for example Figs. 4.40, 4.41) and by studying the $SO(3)$ potential of the action. We remind that on top of the classical trivial background there are quantum fluctuations that give actually some non-zero expectation values for the matrices. The classical potential of the bosonic $SO(3)$ part of the action is found to be (see Appendix A and specifically eq. (A.3))

$$V(r) \sim r^2\,(r-\mu)^2\,. \tag{4.92}$$

On top of that, we have quantum fluctuations on the r value resulting in fluctuations on $V(r)$. For the case of $\mu = 0$, we immediately get the BFSS result $V(r) \sim r^4$ which, in the

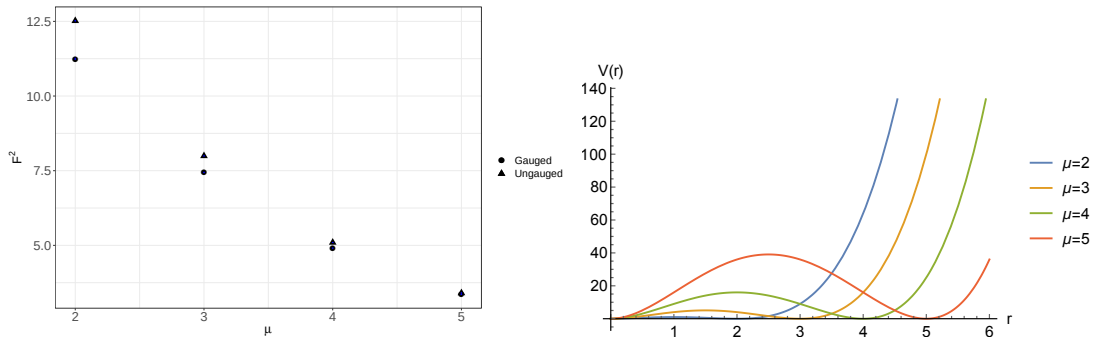

Figure 4.46: [Left]: The observable F^2 (errors included but are very small) with respect to μ for the gauged and ungauged data at temperature $T = 0.5$ in the large N and continuum limit. [Right]: The $SO(3)$ potential corresponding to extrema of the $SO(3)$ action with respect to μ in the positive-r axis. This potential is symmetric with respect to the $y-$axis. As we increase μ we see that when we are in the trivial background $r = 0$ the simulation becomes more and more stable, such that we observe a decrease of F^2 as we increase μ. The same scaling behaviour holds for all observables (see also Fig. 4.51).

matrix model language is given by the observable F^2 since considering quantum fluctuations the matrices do not strictly commute. We may now ask how this observable behaves for $\mu \neq 0$ and the answer is clear from (4.92). Bigger values of μ result in smaller values of $V(r)$ because the effect of finite μ is to confine the simulation more into the classical vacuum $r = 0$. For finite μ, the matrices (to be more precise their eigenvalues) are grouped around $r = 0$ while for $\mu = 0$ they can spread in the whole range of the potential barrier and this makes (some of) the eigenvalues escape to infinity resulting in the flat direction problem. Indeed, this is the behaviour we observe in the left panel of Fig. 4.46 both for gauged and ungauged models, and the theoretical explanation is because for bigger values of μ the fluctuations of the potential become smaller due to a bigger potential wall created by finite μ. This is shown in the right panel of Fig. 4.46 and it affects all observables $\{E, R^2, F^2\}$ such that they decrease as we increase μ (see also Fig. 4.51). At the same time, the observable F^2 for the gauged and ungauged models studied at $\mu = 0$ in [138] is of order $\mathcal{O}(15)$ always while here we see clearly a decreasing trend as we increase μ.

Another point of view that arrives at the same conclusion is to consider the large μ limit. In this case, all the bosonic matrices can be written in terms of harmonic oscillators, and they all scale as $1/\mu$ (for the $SO(3)$ part) and $2/\mu$ (for the $SO(6)$ part) as it can be seen from eq.'s (4.96) and (4.97).

An interesting puzzle to understand is the role of the unstable solution of the $SO(3)$ potential given by $r = \mu/2$ in our conventions (see again Appendix A). It is not known in the literature how this term appears in the simulations and how it affects them. Thus, we do not exclude the possibility that the simulation reaches frequently this solution altering the results non-trivially at finite μ.

Nevertheless, finite μ effects change the observables non-trivially as we saw, and indeed a better understanding of the smaller μ region will be important in the future since currently, it is out of reach for such a precise analysis.

μ	C_R	D_R
0	0.834 ± 0.058	1.542 ± 0.187
2	1.119 ± 0.091	1.718 ± 0.416
3	1.423 ± 0.026	1.499 ± 0.063
4	2.022 ± 0.075	1.965 ± 0.202
5	2.561 ± 0.033	1.975 ± 0.066

μ	C_F	D_F
0	0.825 ± 0.059	11 ± 0.7
2	1.125 ± 0.098	11.370 ± 2.939
3	1.457 ± 0.042	9.983 ± 0.677
4	2.088 ± 0.065	11.900 ± 1.061
5	2.663 ± 0.032	10.750 ± 0.344

Table 4.4: We fit ΔR^2 and ΔF^2 by using the two-parameter ansatz (4.90) and (4.91), respectively. The $\mu = 0$ value is the extrapolation of the fit to the $\mu \to 0$ limit.

BFSS values for two-parameter fits			
C_E	D_E	C_F	D_F
0.83 ±0.21	1.59 ± 0.51	0.73 ± 0.24	1.93 ± 0.65

Table 4.5: The available two-parameter fit data for the BFSS model taken from [138].

Moreover, the dependence of the exponential parameters (C_R, C_F) on μ is given in Fig. 4.48 and they seem to converge to their BFSS values [138] apart from D_F (see also Table 4.5). This is not a problem because there is no constraint between $C_{R,F}$ and $D_{R,F}$ so we do not know what happens at intermediate μ and the results of [138] regarding this are not conclusive. Thus, this provides additional evidence that the limit $\mu \to 0$ is smooth and consistent.

4.4.6 Hamiltonian splitting in perturbative regime

When we Legendre transform the Lagrangian of the BMN model, e.g equation (3.96) and take the large μ limit, the Hamiltonian splits into a free and an interacting part which decouple from each other

$$H = H_0 + H_{\text{int}}, \tag{4.93}$$

where

$$H_0 = \frac{N}{\lambda}\,\text{Tr}\left[\left(\frac{\lambda}{N}\right)^2 \frac{1}{2}\left(\Pi^M\right)^2 + \frac{\mu^2}{2}\left(X^i\right)^2 + \frac{\mu^2}{8}\left(X^a\right)^2 - \frac{3\mu}{4} i\bar{\psi}^\alpha \gamma_{123}\psi_\alpha\right], \tag{4.94}$$

$$H_{\text{int}} = \frac{N}{\lambda}\,\text{Tr}\left[-\mu i \epsilon_{ijk} X^i X^j X^k + \frac{1}{4}[X^M, X^N]^2 + \bar{\psi}^\alpha \gamma^M [X^M, \psi_\alpha]\right], \tag{4.95}$$

with $\Pi^M = \frac{\delta \mathcal{L}}{\delta \dot{X}^M}$ being the conjugate momenta for bosonic matrices. The H_0 terms construct the free $U(1)$ sector of the model while H_{int} denotes the interactive $SU(N)$ part. In the large μ limit, the interactive sector can be treated perturbatively while the free sector is claimed to be protected from contributions to all orders in μ (see e.g [112, 157, 268]). In addition we can introduce harmonic oscillators defined by the operators

$$A_i := \sqrt{\frac{1}{\mu}}\left(\frac{\lambda}{N}\frac{\Pi_i}{\sqrt{2}} - \frac{i\mu}{\sqrt{2}}\sqrt{\frac{N}{\lambda}}X_i\right), \tag{4.96}$$

$$B_a := \sqrt{\frac{2}{\mu}}\left(\frac{\lambda}{N}\frac{\Pi_a}{\sqrt{2}} - \frac{i\mu}{2\sqrt{2}}\sqrt{\frac{N}{\lambda}}X_a\right) \tag{4.97}$$

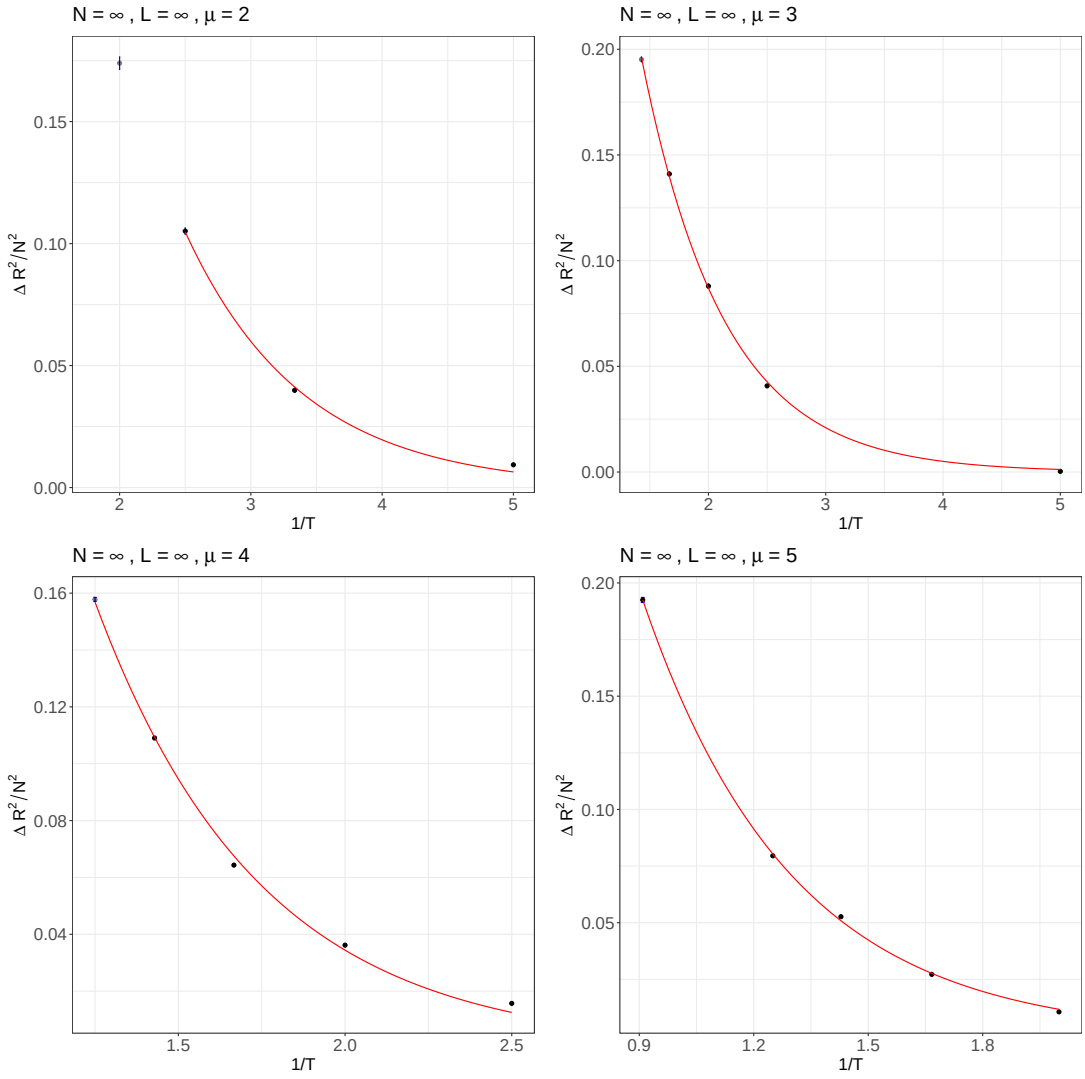

Figure 4.47: The large N and continuum exponential fits for ΔR^2 and different μ with error bars included but being small.

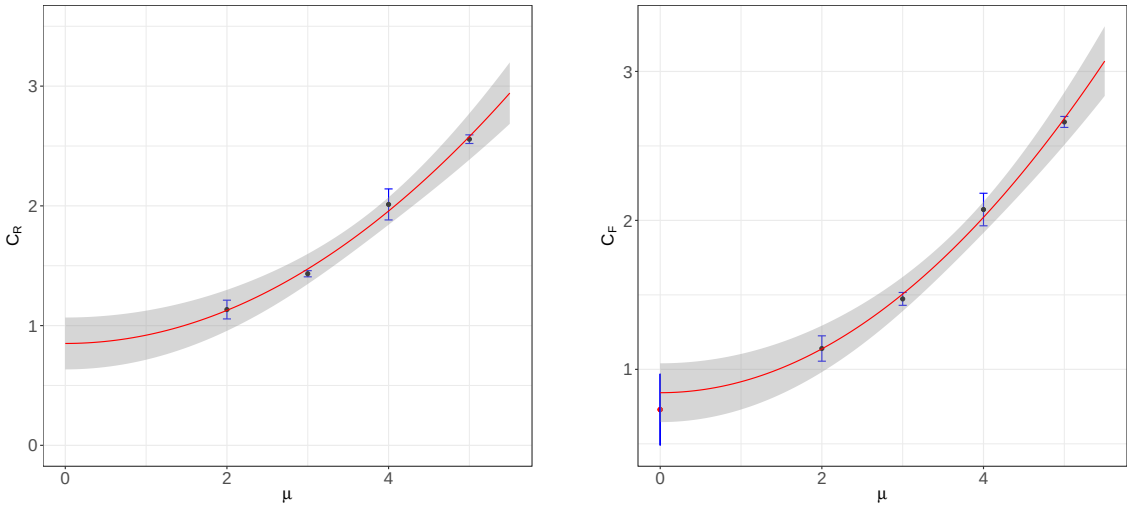

Figure 4.48: The behaviour of the exponential parameter ($C_{R,F}$) from (4.90), (4.91) with respect to μ. [Left]: the fit for C_R is given by the equation $C_R = 0.834(58) + 0.070(4)\mu^2$. [Right]: the fit for C_F is given by the equation $C_F = 0.825(59) + 0.074(4)\mu^2$. The left most point is the BFSS point taken from [138] (see also Table 4.5).

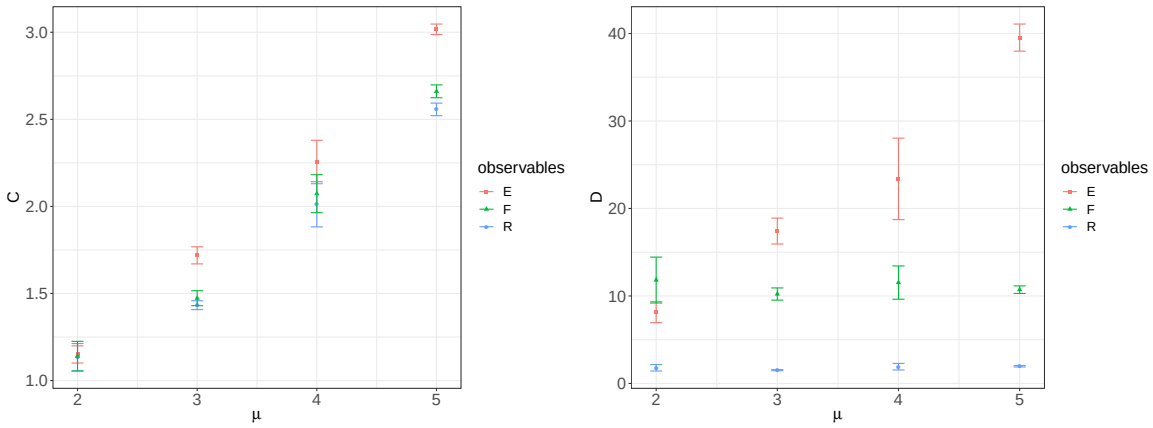

Figure 4.49: The change of parameters with respect to μ in the large N and continuum limit. [Left]: Values of C_E, C_F, C_R labelled as E, F, R respectively. We expect these values to be approximately the same when the partition functions of both models are exponentially close to each other. We see that this happens as $\mu \to 0$ and indeed we expect this to be the case in this limit as we can recall from eq. (4.81). [Right]: Values of D_E, D_F, D_R. We observe that D for $\mathrm{Tr}\, X_I^2$ and $\mathrm{Tr}\,[X_I, X_J]^2$ observables do not change with respect to μ but for energy does. This is probably due to different degeneracies of the energy eigenstate of the system.

which obey canonical commutation relations

$$[A_i, A_j^\dagger] = \delta_{ij} \quad , \quad [B_a, B_b^\dagger] = \delta_{ab}. \tag{4.98}$$

Then, the bosonic part of the free Hamiltonian results in

$$H_0^{\text{bosonic}} = \frac{N}{\lambda}\,\mathrm{Tr}\left[\mu A_i^\dagger A_i + \frac{\mu}{2} B_a^\dagger B_a\right] \tag{4.99}$$

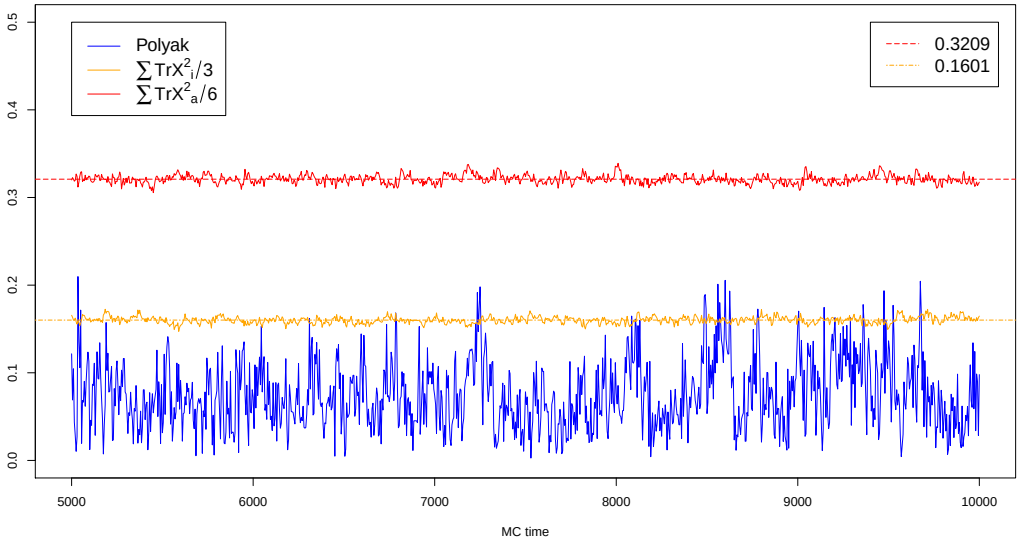

Figure 4.50: Another typical Monte Carlo history for gauged $N = 12, S = 48$ simulation at $\mu = 2, T = 0.2$. We observe the breaking of symmetries $SO(9) \to SO(3) \times SO(6)$ since the first three matrices are grouped together and have less expectation values than the rest six, which form the $\mathbf{S}^5$ sphere.

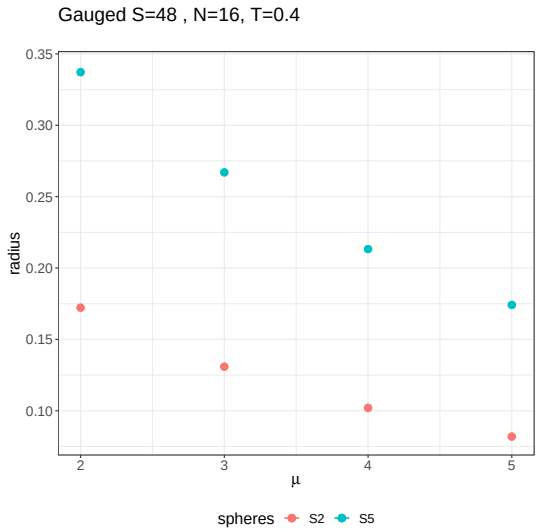

Figure 4.51: The radii of the two spheres $\mathbf{S}^2$ and $\mathbf{S}^5$ constructing $SO(3)$ and $SO(6)$ parts respectively. Recalling equations (4.96) and (4.97) we can deduce that in the weak coupling limit where we can interpret the D0-branes as a bunch of oscillators, the respective radii scale as $r_2 \sim 1/\mu$ and $r_5 \sim 2/\mu$.

Complexifying the real spinor matrices ψ_α using

$$\psi^\pm = \mathcal{C}^\pm \psi \quad \text{where} \quad \mathcal{C}^\pm = \frac{1}{2}\left(\mathbb{1} \pm i\gamma_{123}\right), \tag{4.100}$$

yields the anticommutation relations

$$\{\psi^{+\alpha}, \psi^{-\beta}\} = \frac{1}{2}\left(\mathcal{C}^{+}\right)_{\alpha\beta} \quad , \quad \{\psi^{+\alpha}, \psi^{+\beta}\} = 0 = \{\psi^{-\alpha}, \psi^{-\beta}\}. \tag{4.101}$$

We may now use the chirality property of the complexified fermions $(i\gamma_{123})\psi^{\pm} = \pm\psi^{\pm}$ accompanied with $(\mathcal{C}^{\pm})^2 = \mathcal{C}^{\pm}$ and $\mathcal{C}^{+}\mathcal{C}^{-} = 0$. Recalling the splitting $\psi = \psi^{+} + \psi^{-}$ the fermionic part results in

$$H_0^{\text{fermionic}} = -\frac{3\mu}{4}\,\text{Tr}\,\left[i\bar{\psi}^{\alpha}\gamma_{123}\psi_{\alpha}\right] = \frac{3\mu}{2}\,\text{Tr}\,\left[\psi^{+\alpha}\psi^{-\alpha}\right]. \tag{4.102}$$

Summing both results in the $U(1)$ free part of the Hamiltonian written in terms of bosonic and fermionic harmonic oscillators

$$H_0 = \frac{N}{\lambda}\,\text{Tr}\,\left[\mu A_i^{\dagger}A_i + \frac{\mu}{2}B_a^{\dagger}B_a + \frac{3\mu}{2}\psi^{+\alpha}\psi^{-\alpha}\right]. \tag{4.103}$$

In our conventions, the $SO(3)$ and $SO(6)$ sectors have mass μ and $\mu/2$ respectively while the fermions have mass $3\mu/4$ [33]. The zero-energy ground state of this free Hamiltonian is denoted as $|0\rangle$ and is annihilated by

$$A_i\,|0\rangle = 0 \quad , \quad B_a\,|0\rangle = 0 \quad , \quad \psi^{-\alpha}\,|0\rangle = 0. \tag{4.104}$$

The $U(1)$ free sector of the above Hamiltonian is spanned by excitations of operators of word-length one, e.g $\text{Tr}\,[A_i^{\dagger}]$, $\text{Tr}\,[B_a^{\dagger}]$, $\text{Tr}\,[\bar{\psi}^{\alpha}]$ while the $SU(N)$ free sector is spanned by operators of word-length two and larger. The lightest mode is given by the $SO(6)$ part of the free Hamiltonian with lowest energy

$$E_{SO(6)} = \frac{\mu}{2}. \tag{4.105}$$

For the gauged model this is the first excited state created by $\text{Tr}\,B_a^{\dagger}\,|0\rangle$, while the remaining excitations of the free sector are shown in Table 4.6. For the ungauged model, one can simply act with $B_a^{\dagger}$ on $|0\rangle$ which results in the same energy. There are six oscillators yielding a six-fold degeneracy of this sector. In addition there are $n = 3$ oscillators for the $SO(3)$ part with energy $E_{SO(3)} = \mu$ and $n = 8$ fermionic oscillators with energy $E_{\text{fermions}} = 3\mu/4$. The ground state energy vanishes since due to supersymmetry we have

$$3\mu - 8\cdot\frac{3\mu}{4} + 6\cdot\frac{\mu}{2} = 0. \tag{4.106}$$

The lowest adjoint mode of the gauged theory in the perturbative limit $\mu \to \infty$ is (4.105) and perturbation theory shows that it is protected at least to first order in μ [254, 267, 268].

The spectrum of the free Hamiltonian has been studied in perturbation theory (with perturbative parameter $\sim 1/\mu$, e.g (4.79)) in [267–269] and their energy, representations and degeneracy are given in Table 4.6. It was conjectured that the free spectrum does not receive any perturbative corrections to all orders in μ^{-1}. On the other hand short representations of the $SU(N)$ sector can, in principle, combine and form multiplets and indeed it is possible that they receive perturbative corrections. On top of that we may also note that there could be non-perturbative corrections [268]. A precise analysis of the form of non-perturbative and perturbative corrections for the construction of multiplets has not been done and, therefore, the energy correction can not be estimated precisely.

[33] We recall the splitting $\psi = \psi^{+} + \psi^{-}$.

state	$SO(6) \times SO(3)$ reps.	energy	degeneracy
$\|0\rangle$	$(\mathbf{1},\mathbf{1})$	0	1
$\mathrm{Tr}\, B_a^\dagger \|0\rangle$	$(\mathbf{6},\mathbf{1})$	$\frac{\mu}{2}$	6
$\mathrm{Tr}\, \psi_{M\alpha}^\dagger \|0\rangle$	$(\bar{\mathbf{4}},\mathbf{2})$	$\frac{3\mu}{4}$	8
$\mathrm{Tr}\, A_i^\dagger \|0\rangle$	$(\mathbf{1},\mathbf{3})$	μ	3
$\mathrm{Tr}\, B_a^\dagger\, \mathrm{Tr}\, B_b^\dagger \|0\rangle$	$(\mathbf{1},\mathbf{1})+(\mathbf{20},\mathbf{1})$	μ	1+20
$\mathrm{Tr}\left(B_a^\dagger B_b^\dagger\right) - \frac{1}{N}\mathrm{Tr}\, B_a^\dagger\, \mathrm{Tr}\, B_b^\dagger \|0\rangle$	$(\mathbf{1},\mathbf{1})+(\mathbf{20},\mathbf{1})$	μ	1+20

Table 4.6: Lowest energy states for the trivial background $X = 0$, their representations and degeneracy. The first five lines correspond to the $U(1)$ part of the model which is free.

4.4.7 Representation algebra of the BMN model

Finite μ corrections to n_{adj} are not known. We observed that they change with μ and here we can ask whether or not the works of [270] and [268] could provide some insight. On the other hand, finite μ corrections to C_{adj} depend on mixing of states, presumably coming from the interacting sector of the model whose precise form is unknown.

Let us highlight some of the results in the literature. The classification of the superalgebra in the plane wave limit of M-theory has been consider in [270]. Indeed, in this work and building on the results from Kac [271], it was shown that the complexification of the special unitary Lie superalgebras $\mathfrak{su}(2|4;2,0)$ (for $\mu > 0$) or $\mathfrak{su}(2|4;2,4)$ (for $\mu < 0$) results in $\mathbf{A}(1,3) \cong \mathfrak{sl}(2,5)$. However, here we are always in a scenario of positive μ, and hence the bosonic part of the algebra is given as $\mathfrak{su}(2,0) \oplus \mathfrak{su}(0,4) \cong \mathfrak{so}(3) \oplus \mathfrak{so}(6)$.

The peculiar supersymmetry of the BMN model manifests itself in a time dependence of the supersymmetry transformations. In the large μ limit the Hamiltonian splits into a free and interacting part (see Sec. 4.4.6). The commutator between the interacting Hamiltonian and the supersymmetric charge is proportional to the supersymmetric charge. This implies that the boson and fermion masses differ. In particular the energy level difference given by the commutator between the supercharges Q_α and the Hamiltonian in the interacting $SU(N)$ sector

$$[H_{\text{int}}, Q_\alpha] = \frac{\mu}{4} Q_\beta \gamma^{123}_{\beta\alpha} + \mathrm{Tr}\,(\psi_\alpha \mathcal{G}), \tag{4.107}$$

is $\frac{\mu}{4}$ in our conventions whenever the Gauss constraint is satisfied. The application of the supersymmetry charges $Q^\pm_\alpha$, where one performs a chirality split as

$$Q^\pm = \mathcal{C}^\pm Q \quad , \quad \mathcal{C}^\pm = \frac{1}{2}\left(\mathbb{1} \pm i\gamma_{123}\right), \tag{4.108}$$

can be applied at most eight times for Q^+ or eight times for Q^- changing the energy level by $Q^\pm |state\rangle = \mp \frac{\mu}{4} |state\rangle$. This results in a multiplet consisting of $2^8 = 256$ states with irreducible representations at each level. Thus, one can change irreducible representations by acting with $Q^\pm$ resulting in a shift of the energy at each level. This energy shift coincides with the difference of bosonic and fermionic masses $\mu - \frac{3\mu}{4} = \frac{\mu}{4} = \frac{3\mu}{4} - \frac{\mu}{2}$ in the $SO(3)$ and $SO(6)$ sectors respectively. The successful application of a supercharge Q_α on a state leads to changing one $u(1) \oplus su(2) \oplus su(4)$ irreducible representation to another [270]. The multiplets (energy levels) split into a specific positive integer given by m. The energy of each multiplet differs from the vacuum (E_0) as [270]

$$E = E_0 + \frac{\mu m}{4} \quad , \qquad \text{with} \quad m = 0, 1, \cdots, 8. \tag{4.109}$$

Each of the zeroth and highest level multiplets correspond to an irreducible representation of $u(1) \oplus su(2) \oplus su(4)$, while others are in general reducible representations. Therefore the maximum shift for the gauged theory comes from the highest energy level with $m = 8$ corresponding to eight applications of Q^-. For $\mu > 0$, $m = 0$ has the lowest energy $E = E_0$ representing the ground state. This is the situation for the gauged model.

On the other hand for the ungauged model, one can perform a shift in the Hamiltonian

$$H^{\text{new}} = H - \text{Tr}\left(X^1 \mathcal{G}\right), \tag{4.110}$$

accompanied by the condition $(\gamma^1 + \mathbb{1})\epsilon = 0$. This is a supersymmetric deformation of the ungauged theory and in [254] it was shown that this shift compensates the gauge condition in the superalgebra resulting again in

$$[H^{\text{new}}, Q_\alpha] = \frac{\mu}{4} Q_\beta \gamma^{123}_{\beta\alpha}. \tag{4.111}$$

We expect that in the ungauged model, extra degrees of freedom living on the boundary of the theory and interpreted as open strings [254] (which in principle can reach deep into the bulk) may contribute in the partition function. These degrees of freedom transform in the adjoint representation. Therefore, one is led to ask what is the adjoint representation of the superalgebra of the BMN model. This question has been answered in [270] and the result is given in Table 4.7

Energy	Representations
$+\mu/4$	$(\mathbf{2,4})$
0	$(\mathbf{1,1}) \oplus (\mathbf{3,1}) \oplus (\mathbf{1,15})$
$-\mu/4$	$(\mathbf{2}, \bar{\mathbf{4}})$

Table 4.7: Adjoint representation of $\mathbf{A}(1,3)$

4.4.8 Interpretations

As we explained, the model has two interesting regimes in low temperatures, the strong coupling regime (4.81) and the perturbative regime (4.84). We expect our results to reproduce the former as we take the limit $\mu \to 0$ remaining at small temperatures, while the latter case is reproduced for bigger values of μ. This is summarised in Fig. 4.42 which is our main result.

We stress again that the conjecture is made in the limit of eq. (4.81), yet numerically this limit for BMN is currently inaccessible. What we did instead is to check the behaviour of the system for finite values of μ keeping T small and the results to $\mu = 0$. Doing so, we were able to reproduce the already established BFSS results of [138]. The limit in which the conjecture is made is automatically satisfied for the BFSS model because $\mu = 0$ in this case. The drawback is that keeping our simulation at finite μ we introduced some complicated corrections in the energy. This is the case because turning on μ we create some massive modes $C_{adj}(\mu)$ which can in principle contribute non-trivially in the partition function even for the gauged model. Their precise contribution, is far from known, and there is not any relevant analysis available. The shift in the degeneracy is not clear to us, in particular which sector contributes the most and how. This shift indeed reminds the formula (4.109) for the energy shifts and hints that a similar formula could hold for the degeneracy of the energy states. We stress though that this is a speculative argument based on the fact that the

gauged interacting $SU(N)$ sector could receive finite μ contributions that could potentially contaminate the simulation due to massive (finite μ) modes. In other words, even though there is still an exponential decay on the partition functions, the energy and the degeneracy change non-trivially with μ.

Our results are also supported by the fact that they reproduce the perturbative result (4.84) as μ starts becoming larger and being at low temperatures. This is best seen in Fig. 4.42, where at finite μ and relatively low temperatures we show the contribution of the full $U(1)$ sector from Table 4.6. As we argued previously around (and gave a precise example in) Fig. 4.45 at very low temperatures the lightest mode (4.83) and the full $U(1)$ sector (4.84) are practically indistinguishable. We chose to use the $U(1)$ sector as perturbative result because there is no crossing with the data at finite values of temperature. This can be best seen from Fig. 4.45 where we demonstrate the situation for $\mu = 5$. In addition, in Fig. 4.42 indeed the perturbative result converge to the data produced by the non-perturbative data using the two-parameter fit (4.86) giving us more confidence about the results.

We studied the BMN model at intermediate μ values and relatively small temperatures, such that for the gauged model we remain in the confined phase. This was crucial to ensure that the energy does not depend on the Polyakov loop as it was shown in the deconfined phase [272]. We confirm the exponential decay of the partition functions with a Boltzmann weight $e^{-C_{\rm adj}/T}$ by studying the energy of the system, and the observables R^2 and F^2 defined by (4.88), (4.89) respectively. Our main result remains Fig. 4.42 which at higher μ values converges to the perturbative result (4.83), while the supergravity result is obtained even slightly beyond the supergravity prediction. At the same time extrapolating to $\mu = 0$ limit our results are also consistent with $C_{\rm adj} = 1$ and $n_{\rm adj} = 2$ within error bars obtained in [138]. The non-perturbative nature of the simulations allows us to probe both the perturbative result and the strong coupling/gravity results simultaneously. The change of the degeneracy with μ, as we elaborated, it is most likely because of finite μ effects whose form in the interacting gauged sector has not been studied extensively. We hope that this will initialise a more systematic study of the precise finite μ contributions to the partition function of the model, perturbatively and (if possible) also non-perturbatively.

In addition, the results above might have a twofold role. Apart from genuine physical interest where non-gauge theories could have very similar bulk duals with gauge theories at low temperature, great interest goes also into the development of the quantum computer. That non-singlet modes are exponentially suppressed can make quantum simulation based on the extended Hilbert space simpler. To demonstrate this, suppose that Hamiltonian time evolution is performed on a quantum computer, as $|\Phi\rangle \to e^{-i\hat{H}t}|\Phi\rangle$. If $|\Phi\rangle$ is gauge-invariant, $e^{-i\hat{H}t}|\Phi\rangle$ is also gauge-invariant, as long as the time evolution is exactly realized. If $|\Phi\rangle$ is a specific gauge fixed state, for example, a fuzzy sphere with a certain representation, then the gauge fixing will not be spoiled via the Hamiltonian time evolution. However, if there were light non-singlet modes, small simulation errors could easily excite non-singlet modes and lead to a large deviation from the exact result. Our findings in this paper are that we do not have to worry about such a possibility. In other words, instead of having a gauged matrix model that has a local $SU(N)$ symmetry, it might be easier to have a non-gauged matrix model that has a global $SU(N)$ symmetry, since in the former case $SU(N)$ gauge redundancy could emerge by a different model.

The main message of this project

In this project we studied the difference of gauged and ungauged matrix models and its relevance for gauge/gravity duality [273]. It added the following new insights that can be summarised in the list:

- We verify that the gauged and ungauged partition functions are exponentially close to each other at small temperatures hinting that in these particular examples the gauge singlet constraint might not playing a major role. It is indeed a non-gauge/gravity example of the duality.
- In fact, the partition functions of the gauged and ungauged BMN model are exponentially close to each other even at intermediate temperatures and at finite μ. In other words, we show that the conjecture is true even when the constraint $\mu/T \ll 1$ is not satisfied.
- There is a shift in the energies and effective degeneracies. It seems to be a finite μ effect, which in particular changes the energy of the gauged and ungauged sectors and the degeneracies in a non-trivial way.
- We reproduce both the supergravity results when we take $\mu \to 0$ and the perturbative results when we turn on larger values of μ, revealing the power of the non-perturbative nature of the simulations.
- The implication of these results on quantum computing may be crucial. Specifically the ungauged model could be used easier as we explained in the main text.

4.5 Low temperature supergravity and matrix models

One of the best test examples of gauge/gravity duality was carried out in [134], where the energy of the matrix model was compared with the gravitational energy

$$\frac{E(T)}{N^2} = \frac{\left(c_0 T^{\frac{14}{5}} + c_1 T^{\frac{23}{5}} + c_2 T^{29/5} + c_3 T^{32/5} + \cdots\right)}{N^0} + \frac{\left(d_0 T^{\frac{2}{5}} + d_1 T^{\frac{11}{5}} + \cdots\right)}{N^2} + \mathcal{O}\left(\frac{1}{N^4}\right). \tag{4.112}$$

The zeroth terms are available by exact calculations from string theory and are $c_0 = 7.41$ and $d_0 = -5.77$ respectively. Higher-order terms are not known analytically. The test was done for temperatures $T \geq 0.4$ and compared with the supergravity result containing the terms c_0, c_1, and c_2. The first term c_0 is dominant for extremely low temperatures where the supergravity result dominates, while higher order terms (c_1, c_2) include α' corrections. In this work, we would like to extend the results to lower temperatures. The difficulty with this is that the BFSS simulations start becoming unstable at small temperatures mainly due to the flat direction problem. However, in the previous sections, we argued that the advantage of simulating the BMN model manifests in the stability of the simulations even at small temperatures. The reason was explained earlier and in Appendix A. Hence we would like to take advantage of this and use the BMN matrix model and compare it with the gravity energy even using preliminary data since it is an ongoing project at this point. We shall

stress here as well as in the text that follows that we will report more statistics and preciser tests in [274], hence the comparison done here is preliminary yet it seems to converge in the right direction. The reason we are comparing with preliminary data is to check whether or not the large N and continuum trends approach the supergravity results. It is by no means a precision test but we hope with the production of more data shortly to become precise. In Sec. 3.5 we studied the effect of finite μ on the energy and we showed that at small μ the energy difference between the BMN model and the BFSS could be negligible and hidden inside the simulation error bars. Note, however, that we shall always have in mind that our simulating temperature should respect the bound[34]

$$T \gtrsim 0.318\mu \tag{4.113}$$

such that we are always in the deconfined phase and can compare with the gravity results. On the gauge side, being in the canonical ensemble, the energy is given via the temperature $E(T)$.

Let us remind a bit more the situation discussed in Sec. 3.5. We mainly want to compare with the supergravity energies for the BFSS and the BMN model. The energy of the former is given as

$$\frac{E(T,\mu=0)}{N^2} = 7.41\lambda^{-3/5}T^{14/5}, \tag{4.114}$$

while the energy of the latter contains the deformation terms $s(\hat{\mu})$ and $f(\hat{\mu})$ resulting in

$$\frac{E(T,\mu)}{N^2} = -4.11\lambda^{-3/5}T^{14/5}f(\hat{\mu}) + 11.52\lambda^{-3/5}T^{14/5}s(\hat{\mu}) \quad , \quad \hat{\mu} = \frac{7\mu}{12\pi T}. \tag{4.115}$$

The deformation parameters s, f are known only numerically up to a few orders as we saw in Sec. 3.5. In Fig. 4.52 we show the difference of energies between the BFSS model and the BMN model at low temperatures and $\mu = 0.5$. Motivated by the very small energy difference,

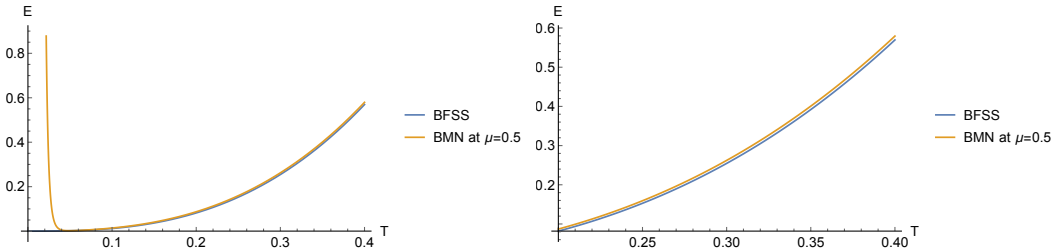

Figure 4.52: [Left]: The gravitational energies of the BFSS and BMN model at $\mu = 0.5$ in the temperature range $T \in [0, 0.4]$. The blowing up behaviour at small temperatures is due to the truncation of the expanding functions $f(\hat{\mu}), s(\hat{\mu})$. [Right]: The same energies zoomed in the range $T \in [0.2, 0.4]$. We see that the BFSS energy is slightly less than that of the BMN but in simulations we will not be able to distinguish the two.

we have simulated the BMN matrix model at various temperatures setting $\mu = 0.5$. We have checked that indeed the μ dependence on the energy is small as we see in Fig. 4.53. Based on this observation we did large N and continuum extrapolations to obtain the energies for small temperatures. Up to now, we have used $N = 16, 18, 24$ and $S = 30, 36, 48, 72$ to perform this. Several extrapolations were done using the ansatz (4.85) keeping up to $\varepsilon_{1,1}$, while the best fit

[34] The difference with the relation shown in Sec. 3.5 is a factor of three since $\mu \to 3\mu$ in our conventions.

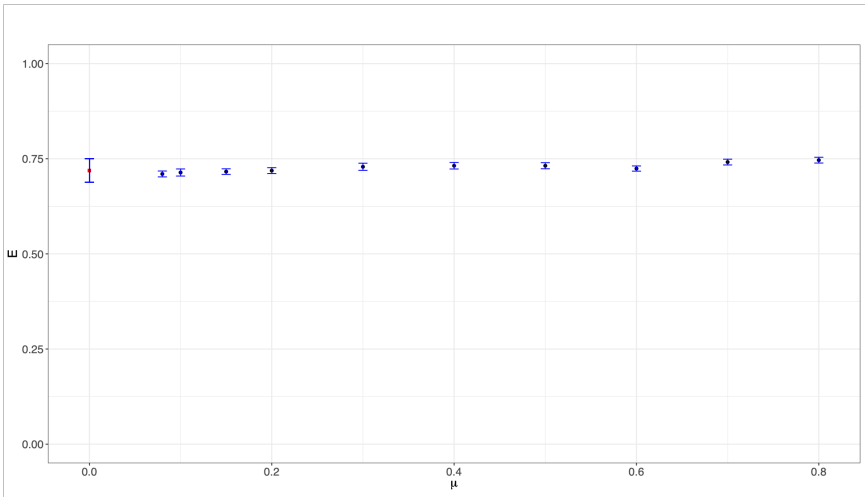

Figure 4.53: The mean value of energy is plotted for various values of μ for $N = 16, S = 24$ at temperature $T = 0.4$. We checked that at these small values of μ the energy difference between the BMN model and the BFSS model is negligible.

was represented by a simultaneous large N and continuum fit using the $\varepsilon_{1,0}$ and $\varepsilon_{0,1}$ terms. We shall refer to in what follows as a two-dimensional fit and compare it with more fits later on. Specifically, the two-dimensional fit is given by the equation

$$\frac{E(N,S)}{N^2} = \varepsilon_{0,0} + \frac{\varepsilon_{1,0}}{N^2} + \frac{\varepsilon_{0,1}}{S}. \tag{4.116}$$

The two-step fit, e.g doing first large N with the $\varepsilon_{1,0}$ term and then extrapolating to the continuum limit with the $\varepsilon_{0,1}$ term was giving larger error bars in the values of energy. Usually, the two-step fit contains the two-dimensional fit within its error bars. One more fit we tried was to include higher terms (quadratic) for the lattice as we shall comment.

The μ dependence at this level turned out to be small. The preliminary hint is shown in Fig. 4.53 while the large N and continuum results confirm this picture. In most cases, the BMN energy value was slightly higher than that of the BFSS results, and recalling Fig. 4.52 this is to be expected.

Let us now review a bit the work of [134] such that we will be able to understand the results which follow. The authors simulated the BFSS model for temperatures $T \in [0.4, 1.0]$ and took the simultaneous large N and continuum limit. The points are shown in Fig. 4.54. The latter were reproduced by a fit of the form of (4.112) with fitting parameters c_i. Being in the large N limit we can exclude finite N corrections and concentrate only on the N^0 term. The fit shown in Fig. 4.54 is reproduced by the following equation

$$\begin{aligned} \frac{E(T)}{N^2} =& c_0 T^{\frac{14}{5}} + c_1 T^{\frac{23}{5}} + c_2 T^{29/5}, \\ c_0 =& 7.4 \pm 0.5 \quad , \quad c_1 = -9.7 \pm 2.2 \quad , \quad c_2 = 5.6 \pm 1.8. \end{aligned} \tag{4.117}$$

These were the fitting parameters while in principle one can include also the c_3 term in (4.112) which indeed has a better behaviour also for the $T = 1.0$ point with the exchange though of increasing the uncertainties of the fit [134]. We shall adopt the scenario of the fitting parameters of (4.117) and assume, based on equation (4.115), that a similar deformation holds

for the situation of the BMN model. In particular, we may assume (at first approximation) that we do not have a strong mixing between finite μ and α' corrections that could potentially contaminate the simulations. If our guessing would be correct, then according to Fig. 4.52 the BFSS and the BMN results should not be that much different. Therefore, we expect the BMN gravity energy to be given by the function

$$\begin{aligned} \frac{E}{N^2} &= -4.11\lambda^{-3/5}T^{14/5}f(\hat{\mu}) + 11.52\lambda^{-3/5}T^{14/5}s(\hat{\mu}) + c_1 T^{\frac{23}{5}} + c_2 T^{29/5} \\ c_1 &= -9.7 \pm 2.2, \quad , c_2 = 5.6 \pm 1.8. \end{aligned} \tag{4.118}$$

This is the case in an ideal world where the finite μ corrections and α' corrections do not mix. The former are captured by the $T^{14/5}$ terms while the latter by c_1 and c_2 terms.

It could also be the case that the latter points are contained in the error bars of the former for small values of μ (specifically for $\mu = 0.5$) as we show in Fig. 4.52, and Fig. 4.53.

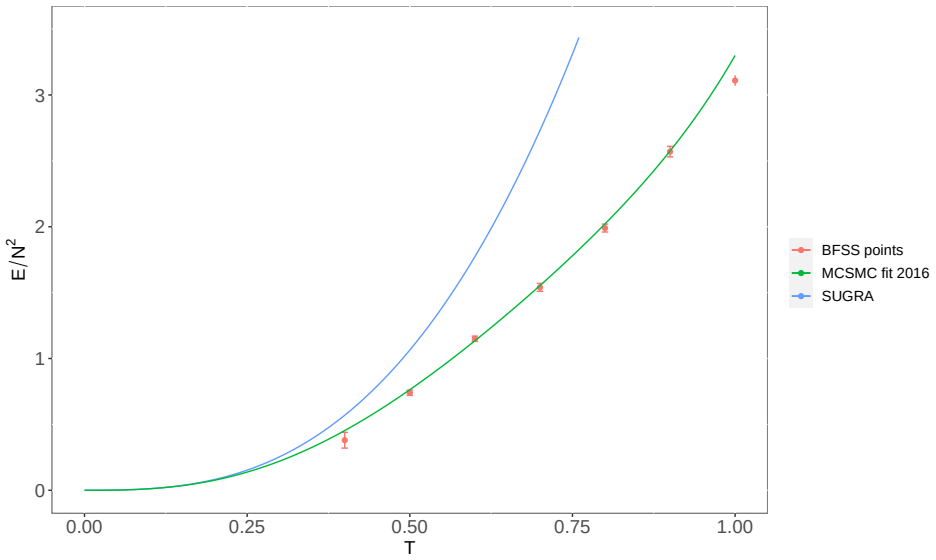

Figure 4.54: Comparison between the zero-brane energy (4.114) and the BFSS simulation points from [134]. The fit is given by (4.117). The discrepancy at higher temperatures between the simulation points and the supergravity result can be understood as α' corrections recalling that we set always $\lambda = 1$ in simulations and finite λ means that we take α' corrections into account.

This is a very interesting scenario in which, taking into account the better behaviour of simulation stability of the BMN model, we can put the gauge/gravity duality on test for temperatures $T < 0.4$. The main problem in the past that did not allow for simulating lower temperatures is the fact that the BFSS model is more sensitive to the flat direction problem in this small temperature region and the only way out of this was considered to be the usage of more resources. In this project, we are showing that we do not need incredible resources to attack this problem if we use the BMN model, which is more stable in this region.

This will be our main motivation, to exploit the above analysis, that the energies of the two models should not be that different for small μ and compare the simulation results with the supergravity results. This opens a serious possibility to better test the gauge/gravity duality, going to lower temperatures and comparing with supergravity since as we saw, some

analytic results are available. At this level of statistics we cannot claim that the above analysis is a precision test but what we can claim is that it can capture the supergravity behaviour in a way that is pointing in the right direction. One more assumption that we will make as we said above is that the α' corrections and finite μ corrections do not mix. As we saw from the supergravity (analytic) analysis for the energies of the gravitational systems, we do not have any indication that these corrections mix, and (at least to first order) this assumption is verified by our data at this level.

To this end, we were able to reach $T = 0.3$ and get stable configurations. In particular, the lowest temperature we have tested was $T = 0.24$ (see some preliminary data in Fig. 4.55), while $T = 0.2$ appeared to be out of reach at this level because of the confinement transitions at finite N and very slow growth of statistics in a sense Monte Carlo trajectories per job generation. In particular even for $T = 0.24$ there is a significant difficulty to collect enough data for good precision, but we present these preliminary results anyway in Fig. 4.55 stressing in the caption that should be taken with caution.

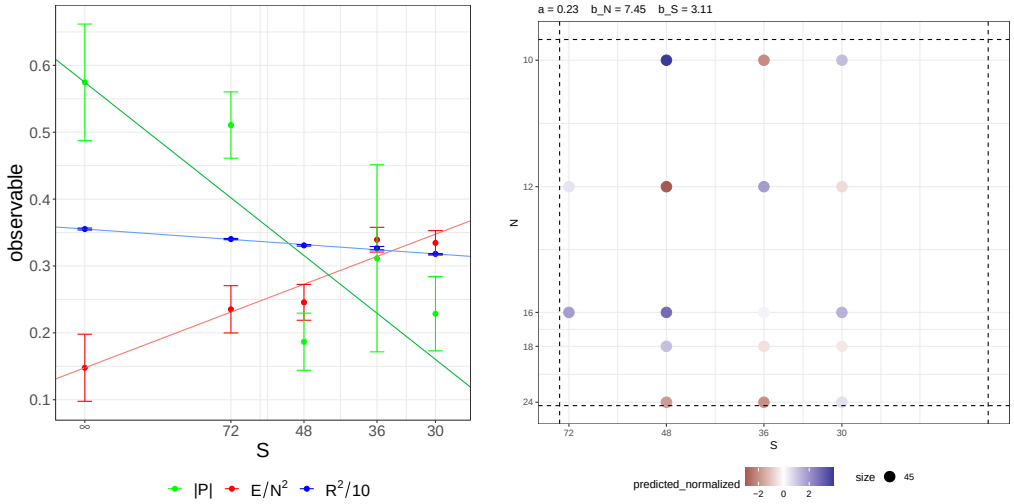

Figure 4.55: [Left]: Continuum extrapolation for $T = 0.24$ and $N = 16$. The transition to a confined state is showed from the Polyakov loop. [Right]: The results of the two-dimensional fit for the same temperature $T = 0.24$. x axis denotes $1/S$ term and y axis $1/N^2$ of the fit, while the small circles show the deviation from data and predictions from the fit. We stress that these are preliminary data with low statistics and should not be taken as precision data. In particular, at this level of statistics we are interested in capturing the leading behaviour of the system at this temperature using all our data available. For this we see that extrapolations are done using $N = 10, 12$ also while for higher temperatures these were ignored due to instabilities at higher statistics. There is also an instability occurring at this temperature but to capture the leading order it makes sense to use all sensible data before transitions (such as confinement/deconfinement) occur. The large N and continuum value is not conclusive. Note also that there is no obvious clustering of the data in a specific region which makes to some extend the fit trustable. We expect by including more lattice points, the energy to drop more and the errors to become smaller [274].

We started the investigations by double-checking the already known point for $T = 0.4$ using the BMN model at $\mu = 0.5$. A simple large N and then continuum extrapolation gives $E\big|_{\mu=0.5,T=0.4} = 0.39(3)$ which is indeed very close to the BFSS energy value from [134]

$E\big|_{\mu=0,T=0.4} = 0.38(6)$. Note that the authors of [134] always used a two-dimensional fit to find the energies over a different parameter (N, S) region. Our two-dimensional fit in this case gives $E\big|_{\mu=0.5,T=0.4} = 0.458(11)$. We report these two-parameter fits in Fig. 4.56 and the two-dimensional fits in Fig. 4.58. One important observation at this level is to consider higher-order lattice corrections and see whether the results change or not. The reason we are interested in these corrections is that we want to be sensitive in the level of precision. Therefore, we can include higher-order corrections in (4.85) and in particular the term $\varepsilon_{0,2}$ containing the $1/S^2$ term. In other words, we may perform first a large N analysis using the term $\varepsilon_{1,0}$ and then include lattice corrections as

$$\frac{E(S)}{N^2} = \varepsilon_0 + \frac{\varepsilon_1}{S} + \frac{\varepsilon_2}{S^2}. \tag{4.119}$$

This allowed us to verify the crude estimation of the simple one-dimensional and two-

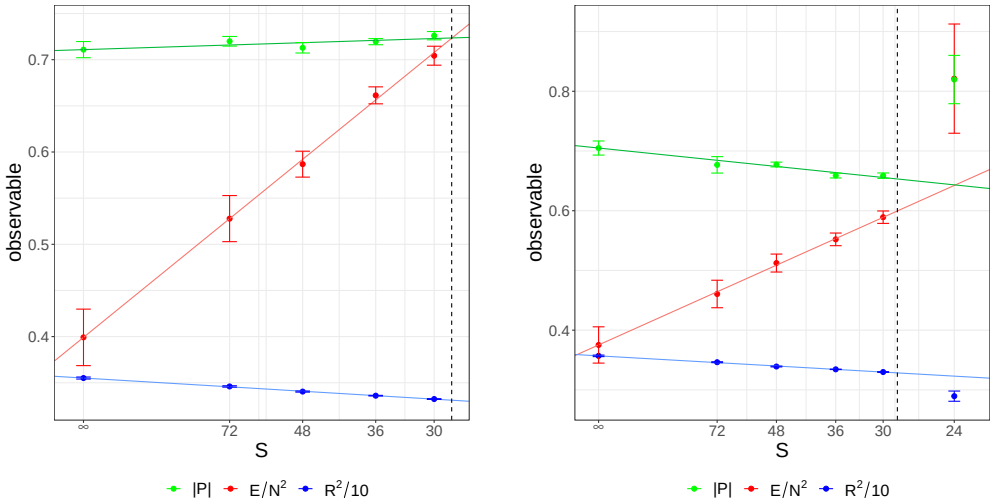

Figure 4.56: [Left]: Large N and then continuum extrapolation for $T = 0.4$. [Right]: Large N and then continuum extrapolation for $T = 0.35$. The vertical dotted line restricts the data taken into account for extrapolation.

dimensional fits including higher-order lattice corrections. One interesting point is that even at this level where the lattice points are relatively large, there is still a small curve passing over the finite S data as can be seen in Fig. 4.57. Although there is a curved trend for the finite S points, from the same figure it can be observed that the continuum extrapolations fall into the error bars of the one-dimensional large N and continuum extrapolations and the two-dimensional, simultaneous extrapolation. Therefore, even though the level of statistics is low since this is an ongoing project, the extrapolations of the data are pointing in the right direction, while for a more complete and more precise analysis we will refer to [274]. Recalling the discussion in Sec. 4.3.9 smaller temperatures correspond to bigger "time" circles and the way we parametrise the circle is crucial. In particular, at small temperatures, higher lattice points are of great importance to perform a precision test [274]. On the other hand, higher temperatures correspond to smaller "time" circles and hence fewer lattice points are indeed enough to draw safe conclusions.

However, at this level of statistics and trying to include a quadratic term also in the continuum extrapolation might cause some problems. In particular doing first a large N and

then a continuum fit using (4.119), the careful reader would probably observe that we are passing our four data points (see Fig. 4.57) through a three-parameter fit. Being optimistic, we expect that higher S data points will not alter the results by much but rather the error bars will be smaller and the precision will be better. Indeed, this is what we start to observe at smaller temperatures, the introduction of more lattice points slightly reduces the energy, constantly approaching the gravity curve [274]. We may also note that currently we are

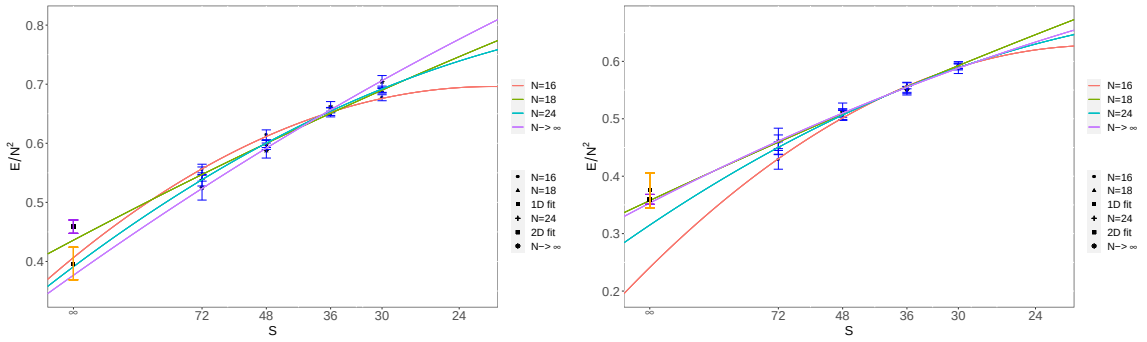

Figure 4.57: [Left]: Large N and then continuum extrapolation for $T = 0.4$ using (4.119). [Right]: Large N and then continuum extrapolation for $T = 0.35$ using the same equation.

not always in position to draw conclusions safely if we want a precision test. In particular, it would be very nice to reproduce finite N corrections in (4.112) and specifically the term containing the d_0 coefficient. For $T = 0.35$ three different kinds of fit reproduce the same value of energy for this specific temperature. In particular, the two-dimensional fit is contained in the two-step fit while including the quadratic term in the large N data coincides with quite good accuracy with the two-dimensional fit (see e.g right panel of Fig. 4.57). We cannot claim the same for the data at $T = 0.4$ as it can be seen from Fig.s 4.57 and 4.58, but let us point out that statistics at $T = 0.4$ are less than that of $T = 0.35$.

Some concluding remarks

Being at this level of statistics let us conclude now regarding this project. The aim was to understand, given the current resources, to what extent we can use the BMN model to push the simulations at low temperatures. At the technical level, this was not possible in the past due to the instability of the BFSS model at these low temperatures and the need for more resources to better attack the problem. Indeed, the latter starts manifesting even at these parameters we are using now and it begs for better simulation algorithms using improved lattice actions. On the other hand, we know now that the BMN model is more stable in this parameter region [194] (see also Appendix A) such that we were able to push all our resources to their ultimate limits. Therefore, using the BMN model with small μ and exploiting the fact that the energy difference, predicted by the supergravity duals of the BMN and BFSS models is very small, we can use the BMN model to better understand the thermodynamic features of the black-zero brane supergravity. The easiest example would be to verify the energy prediction of the black-zero brane using the BMN model at these low temperatures. In this small temperature regime, the stringy corrections are very small and the supergravity result dominates, thus verifying the energy prediction using the BMN model would lead to one strong verification of the gauge/gravity duality for these models.

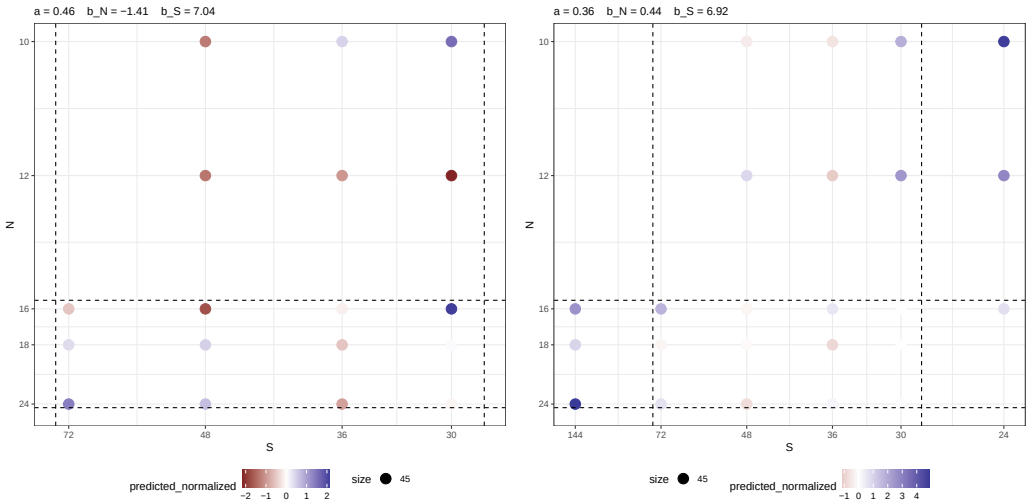

Figure 4.58: [Left]: Simultaneous large N and continuum extrapolation for $T = 0.4$ using (4.116). [Right]: Simultaneous large N and continuum extrapolation for $T = 0.35$ using the same equation. Note that data contained in the region spanned by vertical and horizontal doted lines are taken into account, while no obvious clustering is observed in the data we used so far. a, b_N and b_S are referred to $\varepsilon_{0,0}, \varepsilon_{1,0}$ and $\varepsilon_{0,1}$ of (4.116) respectively.

To this end, we firstly showed that the μ dependence is small in the parameter region we investigated. Then we switched to performing large N and continuum extrapolations aiming for high statistics. Unfortunately, we are still not at this level due to the finiteness of resources and the difficulty of simulating the model at these parameters. On the other hand, we have some preliminary data for $T \leq 0.4$ which was our main goal. In particular, we reached the point $T = 0.24$ capturing the leading energy value showing good agreement with the gravity results as we demonstrate in Fig. 4.59. In the same figure, we show the points for $T = 0.3$ and $T = 0.35$ which we are most confident with, while as we argued previously a considerable amount of statistics shows that the points $T = 0.35$ and $T = 0.4$ capture the same pattern as the $T = 0.3$ point as we observe in Fig. 4.57. This gives us more confidence about the preliminary results which we present here and as we currently observe including more lattice points changes the energy value by 5%. For more details regarding this point and more precision we shall refer again to [274].

We could use various fits to perform a two-dimensional fit getting an, equally good fit over our data. To show this, we can use a biased fit where we fix the coefficient $\varepsilon_{1,0}$ at each temperature which including stringy corrections is given by the sum of d_0 and d_1 terms in (4.112). The latter constants were obtained in [134] with quite high uncertainties though such as $d_0 = -5.8 \pm 3.0$ and $d_1 = -3.4 \pm 5.7$. Thus, we can use a fit of the form

$$\frac{E(N,S)}{N^2} = \varepsilon_{0,0} + \frac{\varepsilon_{1,0}(T)}{N^2} + \frac{\varepsilon_{0,1}}{S} + \frac{\varepsilon_{1,1}}{N^2 S}, \tag{4.120}$$

where we fix the coefficient $\varepsilon_{1,0}(T)$ to perform a two-dimensional large N and continuum fit. For example for $T = 0.4$ we have $\varepsilon_{1,0}\big|_{T=0.4} = -4.473$ resulting in $\varepsilon_{0,0}\big|_{T=0.4} = 0.399(28)$ which corresponds to a 6% change compared with the fit (4.116). The respective values for $T = 0.35$ read $\varepsilon_{1,0}\big|_{T=0.35} = -4.15$ and $\varepsilon_{0,0}\big|_{T=0.35} = 0.346(25)$, a difference of 1%. We see that being at this level of statistics it is not of particular importance which fit we are using, but to trust a specific fit and talk about precision measurements one should be careful.

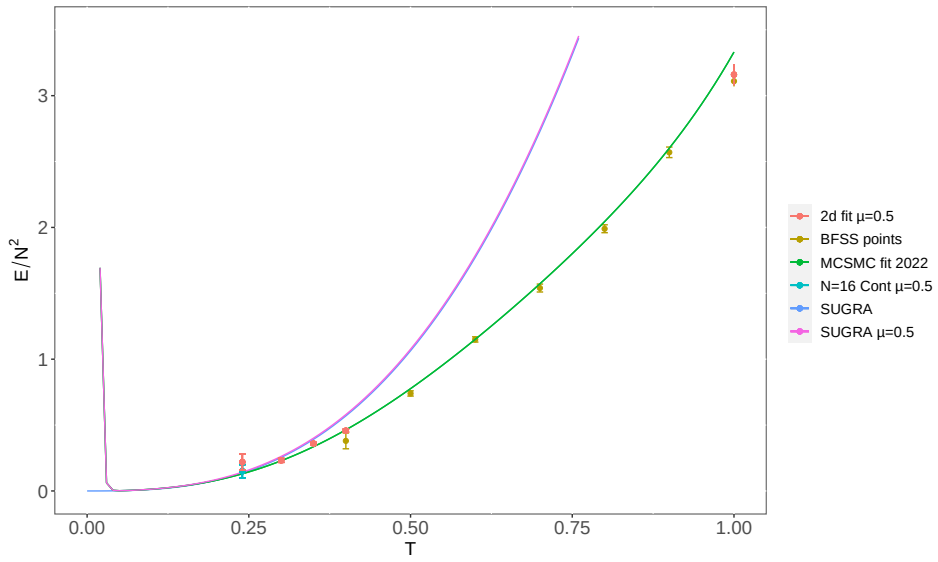

Figure 4.59: Our current results compared with the supergravity prediction from the BMN model at $\mu = 0.5$, the BFSS supergravity prediction and the data from [134] labelled as BFSS points. We are particularly interested in the low temperature regime having the most confidence for the $T \geq 0.3$ data. The MCSMC fit here is given by (4.118) while the two-dimensional fit is given by (4.116).

An equally important route is the fact that using the stability of the BMN model at low temperatures we can study the first-order phase transition which qualitatively would be very close to that of BFSS. In Fig. 4.22 we show the μ dependence of the transition temperature and for small enough μ this would be very close to the BFSS transition temperature. Then one important point would be to study with more precision the transition we discussed in Sec. 4.3 which according to the discussion there is related to the M-theory parameter region at small temperatures and small μ [194]. Indeed, the demonstration that the BMN model is thermodynamically very close to the BFSS at this small non-zero μ opens a possibility for such a detailed study and we hope to investigate more on this in the future.

What this project is going to add

When this project will be completed [274] we expect the following points to be addressed:

- The gauge/gravity duality will be put to better tests going at temperatures not accessible in the past
- Precision measurements will reveal what kind of fitting functions can be used in the large N and continuum limits more efficiently and with more trust in this parameter region
- A possibility to carefully study with precision the first order transition going from type IIA supergravity to the M-theory region in these small temperatures starts becoming significant

Part IV

Spin networks, polyhedra and matrix models

5

Polyhedra and Matrix models?

Αεί ο θεός γεωμετρεί.

Plato

The connection between different theories of quantum gravity is not so difficult to imagine since they all try to address the same question using different tools and perspectives. The idea of loop quantum gravity [275–286] manifests in four spacetime dimensions and treats the character of the diffeomorphism group of gravity and covariance seriously and rigorously keeping it as a key ingredient of the theory [287–294].

Since both loop quantum gravity and string theory try to understand the same problem, having different perspectives, it makes sense to investigate whether there exists some common ground between the two or not. Since string theory, as a theory itself is much broader than loop quantum gravity one can ask whether or not one can embed the latter into the former [295–297]. Apart from the attempt of embedding, there are also other, similar works trying to connect the two theories, each using different tools [298–301]

In this last chapter we are not presenting by any means a rigorous way to address similar connections between loop quantum gravity and string theory as in the previous works but we could not resist investigating some interesting analogies occurring between the matrix models we discussed previously and some specific (coarse-grained) spin network of loop quantum gravity formulation. In fact, this should not be taken as an established connection but merely as an interesting observation, at least to the eyes of the author. In particular, a striking analogy occurs for the case of a spin network consisting of a simple vertex in the bulk and N edges forming some sort of boundary. In this case, one can realise the gauge group $U(N)$ as the group of diffeomorphisms on the surface of this spherical spin network and the question asked in this chapter is whether or not there is a connection with a similar analysis for the fuzzy sphere, since in the latter case and in the matrix model framework one can imagine this fuzzy sphere as consisted of N D0-branes and the group of diffeomorphisms on the surface is again the gauge group $U(N)$ [106]. The connection between the fuzzy sphere

$*$-product and spin networks was firstly considered in [302]. One can see this analysis as revisiting an old idea [298–300, 303].

Convex Polyhedra

Polyhedra have an interesting role in spin networks [304]. A convex Polyhedron is a finite set of points constructing convex patches in the Euclidean $\mathbb{R}^3$ space

$$\mathbf{\Pi} = \{x \in \mathbb{R}^3 | \vec{\eta}_\alpha \cdot x \leq h_\alpha, \quad \alpha = 1, \cdots, N\}, \tag{5.1}$$

where $\vec{\eta}_\alpha$ are arbitrary vectors and h_α are real numbers. This arbitrary description is redundant and non-unique. On the other hand, we are interested in describing a Polyhedron with a fixed number of faces N and therefore we will use variables that have apparent geometric meanings, that is we will use the areas that are associated with each face (α) and the unit normals to the planes that support the faces.

Therefore, we construct a convex polyhedron by considering N patches of area $\vec{A}_\alpha$ and $\vec{\eta}_\alpha$ normals associated to each patch. A theorem due to Minkowski states that N (pairwise non-parallel) unit normals $\vec{\eta}_a$ and N areas $\vec{A}_\alpha$ satisfying $\sum_{\alpha=1}^N \vec{\eta}_\alpha \vec{A}_\alpha = 0$ together determine a unique (up to translations) convex polyhedron with face areas $\vec{A}_\alpha$ and outward pointing face normals $\vec{\eta}_\alpha$. In three dimensions, the space of polyhedra up to translations and rotations can be turned into the Kapovich-Millson phase space [305] by equipping the vectors $\vec{A}_\alpha$ with the $SU(2)$ Poisson bracket $\{\vec{A}^i_\alpha, \vec{A}^j_\beta\} = \epsilon^{ij}_k \vec{A}^k_\alpha \delta_{\alpha\beta}$ and the first class constraint $\vec{C} = \sum_{\alpha=1}^N \vec{\eta}_\alpha \vec{A}_\alpha = 0$. The latter being a first class constraint generates gauge transformations [102]. Indeed, by calculating the Poisson bracket one can prove that it generates $SO(3)$ rotations of the Polyhedron. At the classical level, the phase space has a structure of a symplectic manifold defined as

$$\mathbf{\Pi}_{KM} := \{\vec{\eta}_a \in (S^2)^N | \sum_{a=1}^N \vec{\eta}_\alpha \vec{A} = 0\}/SO(3). \tag{5.2}$$

The dimensionality of this phase space is $\dim_{\mathbf{\Pi}_{KM}} = 2N - 6$, and the Poisson structure is inherited via symplectic reduction of the natural $SO(3)$-invariant Poisson structure on each of the N spheres. In other words, one removes N degrees of freedom by fixing the same area for each patch such that the dimensionality becomes (even) $\dim_{\mathbf{\Pi}_{KM}} = 3N - 6 - N$.

5.1 Quantum Polyhedra and spin networks

When we consider the space of vectors in three-dimensional Euclidean space with norm j, we are constructing a phase space whose Poisson structure is rotationally invariant of a two-sphere of radius j. The quantization of this phase space is done in terms of representations $\mathcal{V}^{j_\alpha}$ of $SU(2)$.

The Poisson structure of $\mathbf{\Pi}_{KM}$ is obtained by symplectic reduction of the product of N spheres of a certain radius. Due to the Guillemin-Sternberg theorem, quantisation commutes with symplectic reductions only if the action generated by the constraint is free. Hence the process ordering in this particular case does not play an important role, see Fig 5.1.

The correspondence between polyhedra and spin networks is the following [304]

$$A_\alpha \eta_\alpha \quad \to \quad \hat{E}_\alpha = 8\pi\gamma l_p^2 J_\alpha \tag{5.3}$$

$$\sum_{\alpha=1}^{N} \vec{\eta}_\alpha \vec{A}_\alpha = 0 \quad \to \quad \sum_\alpha J_\alpha = 0 \tag{5.4}$$

$$\hat{A}_\alpha = \sqrt{\hat{E}_\alpha \cdot \hat{E}_\alpha} \quad \to \quad 8\pi\gamma l_p^2 \sqrt{j_\alpha(j_\alpha+1)}. \tag{5.5}$$

This correspondence tells us that we can promote the inner product of η with A to a quantum operator with a dimensionful constant, known in the literature as the Barbero-Immirzi parameter [43, 306–308], carrying a specific representation of $SU(2)$. In addition, the closure constraint of the Polyhedron reflects the vanishing of the sum of all $SU(2)$ representations. Moreover one can also choose a spectrum for the area operator, for which there is a priori no preferred choice because at the quantum level there is still the operator ordering problem persists [278].

In other words, the correspondence is that every area patch of the polyhedron carries a $SU(2)$ representation inherited by the link that punctures this area patch. The closure constraint could be interpreted as a vanishing total $SU(2)$ charge. This is due to the Gauss constraint, and a naive analogue is to consider it as a vanishing "$SU(2)$ charge" on a compact object in the spirit of conventional electromagnetism.

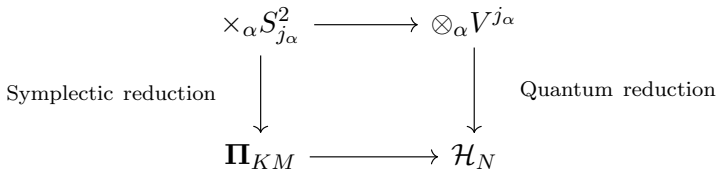

Figure 5.1: Commutative diagram of symplectic reductions and quantizations. Whether one first quantizes and then doing quantum reduction or first doing symplectic reduction and then quantizes results to the same Hilbert space $\mathcal{H}_N$.

5.1.1 Coarse-grained spin network

In general, an arbitrary spin network should be considered as a projective limit of graphs [309]. In a nutshell, one considers a graph as a geometrical object made out of all possible finer subgraphs and this allows to properly define a superposition of spin network states living (a priori) in different graphs. Here, however, we would like to study a simpler, specific, and coarse-grained spin network. To this end, let us consider a graph $\mathbf{\Gamma}$ that defines a bounded region of the embedding space, that is a finite set of vertices and edges linking them. Each edge $\mathbf{e}$ of the spin network is dual to an elementary patch (surface) and carries a half-integer spin representation $j_\mathbf{e} \in \frac{\mathbb{N}}{2}$ defining in this way a quantum of area in Planck units via the mapping (5.5). The vertices on the other hand define an intertwiner state, which furthermore could be interpreted as an elementary volume. We will consider the case in which the spin network has a topology of a sphere, specifically $\mathbf{S}^2$.

One can embed this spin network in $\mathbb{R}^3$

$$\mathbf{S}^2 \hookrightarrow \mathbb{R}^3, \tag{5.6}$$

where the interior of the $\mathbf{S}^2$ is a complicated graph with arbitrary, but in any case finite, edges and vertices. However, we will neglect the inside of the ball and focus exclusively on the surface and its dynamics. Essentially, we will see that dynamics are encoded exclusively on $\mathbf{S}^2$ [310]. A priori the bulk can contain non-trivial loops with many vertices. The closure constraint (5.4), enforces the bulk to contain just one single vertex. This is a gauge fixing procedure where one maps the holonomies inside the bulk to the identity and the non-trivial loops map to trivial ones, yielding in this way a bulk consisted out of just one vertex. The details of this construction can be found in [311, 312]. This results in a holographic construction of this particular spin network which consists of one single vertex (one intertwiner) inside connected with the physical degrees of freedom living on the surface. The latter is defined as the set of edges linked to vertices in the interior. For the case of just one vertex in the bulk these N edges are attached to this one vertex (see left panel of Fig. 5.3). The (dual) polyhedron picture with the closure constraint ensures that there are N elementary area patches which form the polyhedron. For a surface that encloses a generic number of vertices and is punctured by N links, the quantum Hilbert space is a tensor product of all spins

$$\mathcal{H}_{\rm sn} = \bigoplus_{\{j_{\mathbf{e}}\}} \left(\bigotimes_{\mathbf{e}=1}^{N} \mathcal{V}^{(j_{\mathbf{e}})} \right), \tag{5.7}$$

where $V^{j_{\mathbf{e}}}$ is the $SU(2)$ representation of dimension $d_{\mathbf{e}} = 2j_{\mathbf{e}} + 1$, associated to the spin-$j_{\mathbf{e}}$ representation. Imposing gauge invariance, the Hilbert space is given as

$$\mathcal{H}_{\rm sn} = \bigoplus_{\{j_{\mathbf{e}}\}} \mathrm{Inv}_{\mathrm{SU(2)}} \left(\bigotimes_{\mathbf{e}=1}^{\mathrm{N}} \mathcal{V}^{(\mathrm{j_e})} \right), \tag{5.8}$$

The fact that we have to sum over all possible spins $j_{\mathbf{e}}$ above is a direct consequence of the fact that the edges do not carry the same representation at this point. However, as we will see there is a way to make them carry, or transfer the same $SU(2)$ representation to the surface they puncture.

We are interested in a boundary surface that has a topology of a two-sphere. Then, the links will puncture the surface at N points. If moreover, we coarse-grain the bulk to a single vertex then we have a single vertex connecting all the links which belong to the same $SU(2)$ representation. This can also be viewed as a synchronization procedure of the edges which transfer the same representation on the surface and furthermore constructs a N punctured two-sphere. Through the procedure of coarse-graining, the degrees of freedom are realised on the boundary of this surface, the N punctures. The closure constraint forces

$$\sum_{i=1}^{N} j_i = 0, \tag{5.9}$$

where j_i is the spin of each link/puncture. However, we can imagine that we have a closure defect that is associated with non-trivial holonomies in the bulk related to curvature. This defect is realised as the spin $\mathcal{J}$ to which all j_e's recouple. In other words, we can define and

fix the total area of the sphere as the sum of all spins[1]

$$\mathcal{A} := \sum_{i=1}^{N} j_i, \tag{5.10}$$

and if the Casimir of each spin j_i is given as $c_i := \vec{j}_i^2 = j_i(j_i+1)$ then the total Casimir operator has as the norm the total spin $\mathcal{J}$, i.e

$$\mathcal{A} = \sum_{i=1}^{N} j_i \quad , \quad \mathcal{C} := \mathcal{A}^2 = \mathcal{J}(\mathcal{J}+1). \tag{5.11}$$

In this way, we have a global $SU(2)$ representation assigned with the surface. When we fix the total area and there exists a closure defect one can realise a $U(N)$ structure on the surface as we will see and as is explained in [312,313]. We will be particularly interested in surfaces of spherical topologies, while the generalization to arbitrary surfaces depends on the graph data and the Dirac operator [117,314].
Having a topology of a sphere and a surface representation of spin $\mathcal{J}$ and embedding now this structure in $\mathbb{R}^3$ constructs a fuzzy sphere [241]

$$X : \quad \mathbf{S}^2 \hookrightarrow \mathbb{R}^3, \tag{5.12}$$

where X are some matrix-valued embedding maps related to a specific $SU(2)$ representation.

Hence, with this procedure, a notion of holography emerges, since the patches on the surface that are physical, i.e gauge-invariant degrees of freedom, characterize the region inside, the bulk which consists of a single vertex. As we discuss next, one can precisely use matrices transforming in $U(N)$ on the surface because this is the gauge group appearing on the surface.

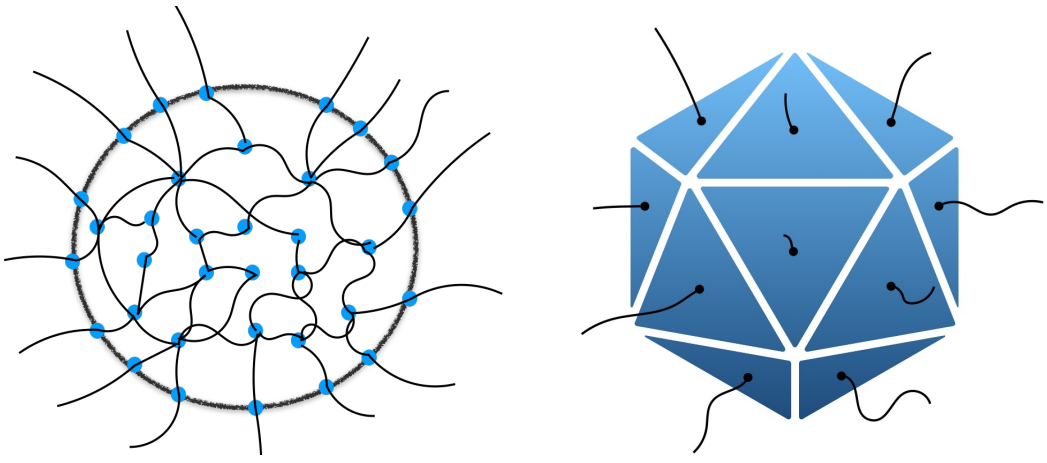

Figure 5.2: Artistic representations of spin networks and polyhedra. [Left]: A spin network bounded by a spherical surface. The links puncture the surface assigning a $SU(2)$ representation on each the N punctures. [Right]: Its' dual picture as a polyhedron. The edges on the left picture that puncture the surface are dual to area patches of the polyhedron.

[1]Note that due to the operator ordering ambiguity at the quantum level, there is a priori no preferred way to order the area operator.

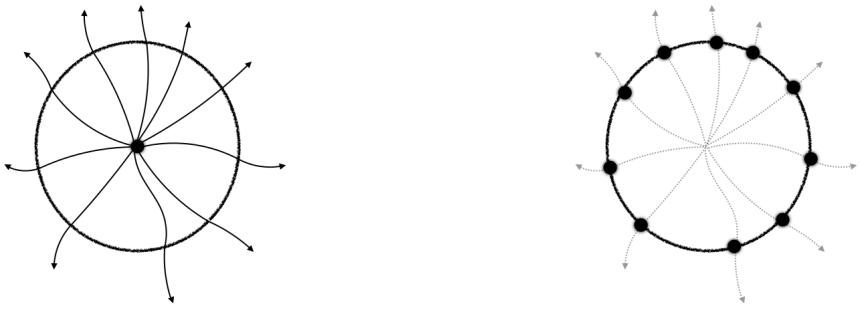

Figure 5.3: [Left]: The spin network picture, N links puncture the boundary and one vertex in the bulk. [Right]: In the D0-brane picture, N D0-branes are tethered on the surface. One can think that at each puncture we have an analog of a D0-brane.

5.1.2 Realizing $U(N)$ on the surface

Up to now, we are discussing an object with N elementary patches. At the same time, each patch is dual to an edge while the patches themselves are non-commutative hence in our case we have a fuzzy polyhedron. On each face of the polyhedron, and whenever the closure constraint is satisfied, there is a $SU(2)$ gauge symmetry. Thus, one can exploit this gauge symmetry on each surface patch and use the Schwinger representation of the $\mathfrak{su}(2)$ algebra, instead of using the basis of quantum vectors, their norms, and directions [311]. In addition, with this procedure, one can write operators on this basis. The two descriptions are equivalent [313] and one can imagine that each area patch is assigned to two harmonic oscillators and reformulate the problem using as a basis the elementary area. These harmonic oscillators represent $2N$ degrees of freedom and they have the usual commutation relations

$$[a_i, a_j^\dagger] = \delta_{ij}. \tag{5.13}$$

Moreover we can create operators with the normal ordering

$$\hat{E}_{ij} := \sum_{i,j} a_i^\dagger a_j \quad , \quad i,j = 1, \cdots, N, \tag{5.14}$$

which apart from being Hermitian also form a $\mathfrak{u}(N)$ Lie algebra

$$[\hat{E}_{ij}, \hat{E}_{kl}] = \delta_{jk}\hat{E}_{il} - \delta_{il}\hat{E}_{kj}. \tag{5.15}$$

The group on which these operators act is the $U(N)$ group. The same group is realized as the group of the diffeomorphisms on the fuzzy sphere in the large N limit [106, 241, 315] since it just moves around the degrees of freedom on the surface of the sphere. Hence, the question that naturally arises is whether or not the gauge-invariant physics is realized on the boundary of some (fuzzy) sphere. This was hinted in [302] and it was put into more solid grounds in [311, 313].

Before giving more details let us comment on the general structure. Let $\mathcal{V}_i^j$ be the subspace that defines each face of the polyhedron. Then one can construct a bigger subspace denoted as the space of intertwiners by tensoring products of the form

$$\mathcal{W}_\mathcal{A} = \bigotimes_{i=1}^{N} \mathcal{V}^{j_i}. \tag{5.16}$$

This is also the space of the whole quantum polyhedron with fixed area $\mathcal{A} = \sum_i j_i \in \mathbb{N}$ on which the $SU(2)$ invariant operators E_{ij} act and generate the $U(N)$ action on each such subspace $\mathcal{W}_\mathcal{A}$. The full Hilbert space of intertwiners is obtained by summing over all possible polyhedra with fixed areas

$$\mathcal{H}_\mathcal{I}^{(N)} = \bigoplus_{\mathcal{A}\in\mathbb{N}} \mathcal{W}_A^N. \tag{5.17}$$

In fact, this construction can be generalised to an arbitrary set of harmonic oscillators by

$$\hat{E}_{ij} := \sum_\rho \sum_{i,j} a_i^{\dagger(\rho)} a_j^{(\rho)} \quad , \quad i,j = 1, \cdots, N, \tag{5.18}$$

where the index ρ is the number of sets of oscillators that we are counting. For $\rho = 1$ we have one simple set of oscillators and this constructs the highest (only possible) representation of $\mathfrak{u}(N)$, while the $\rho = 2$ case is relevant for $SU(2)$ invariant intertwiners [313]. To allow all representations of $\mathfrak{u}(N)$ we have to consider $\rho = N$ sets of oscillators, that is $2N$ different oscillators that carry different $SU(2)$ representations.

We wish to understand what is the meaning of this construction, hence we demonstrate only the case $\rho = 1$ following Ref. [313]. This constructs the maximum representation of $U(N)$, that is one single copy of $SU(2)$, with the maximum dimension W. To see this, we are focusing on coherent states. The latter are characterised by the maximum weights of the group up to unitary transformations. In our case, the group is $U(N)$ and the operators that act on this are given as a single set of harmonic oscillators

$$\hat{E}_{ij} = \sum_{i,j=1}^{N} a_i^\dagger a_j. \tag{5.19}$$

Let us now use the conventions $E_i \equiv E_{ii}$ and $E \equiv \sum_{i=1}^N E_i$. These are (diagonal) elements of the Cartan subalgebra and it is possible to check the generators E_{ij} leave the total surface invariant

$$\forall i,j \quad \left[\sum_k \vec{J}^k, E_{ij}\right] = 0. \tag{5.20}$$

In addition using the diagonal elements above and the $\mathfrak{u}(N)$ algebra for E_{ij} leads to the following relation

$$\forall i, \quad \sum_j E_{ij}E_{ji} = E_i(E + N - 1). \tag{5.21}$$

Generalizing this more to arbitrary indices by summing also over i one gets

$$\sum_{i,j} E_{ij}E_{ji} = E(E + N - 1). \tag{5.22}$$

This equation relates the $U(1)$ Casimir and the (quadratic) Casimir of $U(N)$ which are E and $\mathcal{C}_2 \equiv \sum_{i,j} E_{ij}E_{ji}$ respectively. Now we wish to apply this equation to the highest weight vector v of the irreducible representation. Denoting by w_i the weights we have

$$E_i v = w_i v, \tag{5.23}$$

where $w_i \in \mathbb{N}$ with $w_1 \geq w_2 \geq \cdots \geq w_N \geq 0$ and $E_{ij}v = 0$ for all $i < j$. Thus before calculating the weights, we expand

$$\begin{aligned} \forall i \ \sum_{i,j} E_{ij}E_{ji}v =& E_i^2 v + \sum_{i<j}[E_{ij}, E_{ji}] \\ =& \left[w_i^2 + \sum_{i<j}(w_i - w_j) \right] v. \end{aligned} \tag{5.24}$$

Equating this with $E_i(E + N - 1)$ we get

$$\left[w_i^2 + \sum_{i<j}(w_i - w_j) \right] v = w_i(W + N - 1)v,$$

where $W = \sum_{i=1}^{N} w_i$ is the $U(1)$ Casimir. Now we may apply this $(N - i)$-times to get

$$\begin{aligned} \left[w_i^2 + w_i(N - i) - \sum_{i<j} w_j \right] v =& w_i(W + N - 1)v \\ \Rightarrow w_i^2 - w_i(W + i - 1) - \sum_{i<j} w_j =& 0. \end{aligned} \tag{5.25}$$

For $i = 1$ this yields one trivial solution and one non-trivial

$$w_1 = 0 \quad \text{or} \quad w_1 = W \quad \text{and} \quad w_j = 0, \quad j > 1. \tag{5.26}$$

This results in the coherent state with the highest $SU(2)$ representation. This can be denoted as $[W, 0, \cdots, 0]$ whose dimension is the weight and the spin is given as

$$j_{\max} = \frac{W - 1}{2}. \tag{5.27}$$

In a similar manner the case $\rho = 2$ gives rise to two copies of $SU(2)$ representation of equal dimensionality ($n_1 = n_2 = n$) and characterises a 2-valent intertwiner [313]. The latter condition is forced by the gauge invariance under $SU(2)$. Hence the representation of the highest weight in this case is $[n, n, 0, \cdots, 0]$, with spins

$$j_1 = j_2 = j_{\max} = \frac{n - 1}{2}. \tag{5.28}$$

When there is an overall (global) spin $\mathcal{J}$ the above construction becomes again the two copies of $SU(2)$ representation $[n_1, n_2, 0, \cdots, 0]$ with global spin

$$\mathcal{J} = \frac{|n_1 - n_2|}{2}. \tag{5.29}$$

The gauge constraint again collapses the overall spin to zero yielding $n_1 = n_2 = n$. This is an interesting feature that arises due to gauge invariance also in a different context as we shall see in Sec. 5.2. The most general construction is to consider $\rho = N$ sets of harmonic oscillators allowing in this way all the possible representations of $U(N)$. Their number is given via partitions of N.

For $\rho = 2$, in [313] it was argued that this construction describes a bi-valent intertwiner and geometrically corresponds to a squeezed sphere made out of two (possibly big) area

patches. Acting with E_{ij} on that coherent state should construct all N-valent intertwiners with the same total area. The only change occurs in the number of patches, and it seems that there is a $U(N)$ action on the space of intertwiners.

We have thus concluded that there is a rather natural way to use local $SU(2)$ operators to describe the system as a whole with operators creating a $\mathfrak{u}(N)$ Lie algebra and acting on the $U(N)$ group. Hence, to describe physics on the surface, one can use $N \times N$ matrices X interpreted as the embeddings and are invariant under the $U(N)$ action $X = UXU^T$. Therefore, asking the theory to be diffeomorphism invariant in this case means $U(N)$ invariant. The local operators E_{ii} are related to the diagonal elements of the matrix X, while the non-local E_{ij} to the non-diagonal ones.

We can construct a matrix X_{ij} based on this information acting on $U(N)$. We will focus on a Hermitian and symmetric matrix constructed purely from E_{ij}

$$X_{ij} = \begin{pmatrix} \hat{E}_{11} & \hat{E}_{12} & \cdots \\ \hat{E}_{21} & \hat{E}_{22} & \ddots \\ \vdots & \cdots & \hat{E}_{NN} \end{pmatrix}_{N\times N} . \tag{5.30}$$

As we saw diagonal elements act locally on the spin network (on the edges) while non-diagonal act non-locally (e.g from edge i to edge j). We can thus use this matrix to describe gauge-invariant physics on the surface of a polyhedron.

5.2 Fuzzy spheres and matrix models

We are interested in understanding and capturing the same features of the above construction using the intuition we built from matrix models of string theory. The common ground is the fuzzy sphere and in string theory, this construction is induced by a quite natural mechanism, a (higher dimensional) analogue of the electron polarization in presence of a magnetic field. We will use type IIA string theory whose fundamental objects are the string itself and the D0-branes. The latter are *non-perturbative* and dynamical [316] in their nature, zero-dimensional objects, and under the presence of fluxes, they can form higher dimensional structures. An interesting phenomenon is the Myers effect [84] (see also [104, 317–319] for reviews) where these D0-branes in the presence of a flux polarize and build a spherical D2-brane, creating in this way a structure that it is non-commutative, two-dimensional and have a spherical topology. It is actually a fuzzy sphere, as we encountered many times in the previous chapter.

This structure can originate in many different ways in string theory [320–322] and a general action is given via

$$S = T_0 \,\mathrm{Tr}\left(\frac{1}{2}\dot{X}_i^2 + \frac{1}{4}[X_i, X_j]^2 - i\kappa\epsilon_{ijk}X_i[X_j, X_k]\right), \tag{5.31}$$

where $X_i, i = 1, 2, 3$ are $N \times N$ matrices and $T_0 = \frac{\sqrt{2\pi}}{g_s}$ is the zero-brane tension with g_s being the string coupling. In fact we can also add a mass term for the bosonic matrices

$$S = T_0 \,\mathrm{Tr}\left(\frac{1}{2}\dot{X}_i^2 + \frac{1}{4}[X_i, X_j]^2 - i\kappa\epsilon_{ijk}X_i[X_j, X_k] - \frac{\kappa^2}{2}X_i^2\right), \tag{5.32}$$

such that we can complete the square in the potential. This action is not unfamiliar and recalling (A.1) we immediately see that this action is the same as the bosonic part of the BMN action constructing the $SO(3)$ part of the spacetime when $\kappa \to \mu/3$.

BMN from $\mathcal{N}=4$ SYM on $\mathbb{R}\times\mathbf{S}^3$

Another interesting construction of this model follows from $\mathcal{N}=4$ SYM on $\mathbb{R}\times\mathbf{S}^3$. This work was carried out originally in [112] where the BMN model was obtained by truncation of $SU(2)$ invariant configurations of the super Yang-Mills theory. The isometry group of the sphere can be decomposed as $SO(4)\cong SU(2)_L\otimes SU(2)_R$, this splitting is used in fact to perform a Kaluza-Klein reduction by expanding the four-dimensional fields in spherical harmonics. The $SU(2)_L$ invariant sector of this higher dimensional reduction gives the one-dimensional model (3.96). The couplings of both theories are identified, the X^i matrices arise from the gauge connection on $\mathbf{S}^3$ while the matrices X^a arise from scalars of the super Yang-Mills theory.

5.2.1 Mini bosonic BMN model

We return in the case of the BMN model and we focus on the bosonic $SO(3)$ sector[2]. We recall the corresponding piece of the action from (3.96)

$$S=\frac{1}{g_{YM}^2}\int \mathrm{d}t\ \mathrm{Tr}\sum_{i,j,k=1}^{3}\left(\frac{1}{2}\left(D_tX^i\right)^2+\frac{1}{4}[X^i,X^j]^2-\frac{1}{2}\left(\frac{\mu}{3}\right)^2(X^i)^2-i\frac{\mu}{3}X^iX^jX^k\epsilon_{ijk}\right). \tag{5.33}$$

We will call this model the mini BMN model. The equations of motion for the gauge field A_t impose the (bosonic) Gauß constraint

$$\mathcal{G}:=[D_tX^I,X^I]=0. \tag{5.34}$$

This constraint again restricts all the states of the theory to be singlets under the $U(N)$ symmetry and as we saw previously we have the choice to either use it or not. In other words, this constraint creates a gauge symmetry on the model being the $U(N)$ group.

It is easy to see that we can write the potential as

$$V=\frac{1}{4}\left(\frac{\mu}{3}\epsilon^{ijk}X^c+i[X^i,X^j]\right)^2, \tag{5.35}$$

which has again two different class of minima, for $X^i=0$ or

$$[X^i,X^j]=i\frac{\mu}{3}\epsilon^{ijk}X^k. \tag{5.36}$$

Furthermore, if we associate

$$X^i=\frac{\mu}{3}J^i, \tag{5.37}$$

with J^i being $SU(2)$ generators we represent the embeddings in terms of $SU(2)$ generators and hence the geometric description of this solution is a fuzzy sphere [241]. With this procedure, we give a global $SU(2)$ representation on the sphere, and this is the solution that from now onwards we will be interested in. In fact, these vacua contain also the trivial vacuum where $X^i=0$. The latter is realised as N copies of the trivial $SU(2)$ representation with spin $j=0$, namely N D0-branes.

[2]The reason we can focus on this subpart of the model is the fact that for a large fuzzy sphere the strings connecting the fuzzy sphere (living in $\mathbb{R}^3$) with the rest of D0-branes sitting at the center of $\mathbb{R}^6$ become heavy and the two descriptions decouple.

However, one important point is that the $SU(2)$ solutions of the potential result in a spontaneous symmetry breaking of the gauge symmetry $U(N)$. For the sake of simplicity suppose that we have one non-trivial $SU(2)$ representation with spin $j = \frac{1}{2}$ and the rest are singlets. This solution has less energy than the trivial solution and the $U(N)$ gauge symmetry breaks to $U(N-2) \times U(1)$. In general an arbitrary $SU(2)$ representation of spin j and dimension $d = 2j + 1$ breaks the gauge symmetry down to $U(N-d) \times U(1)$. This is the case for one irrep of $SU(2)$ or just one fuzzy sphere. If instead, we have several (m) non-trivial $SU(2)$ representations then the residual symmetry is

$$U(N - \sum_{a=1}^{m}(2j_a + 1)) \otimes U(1)^m. \tag{5.38}$$

The $U(1)$ symmetry is associated with each fuzzy sphere and in fact, gets enhanced if the reducible solution contains multiple copies of $SU(2)$ representations. Let us demonstrate this with one simple example. Suppose that we represent the reducible solution with 4×4 matrices. However, this can be well described also by two irreducible representations of spin $j = \frac{1}{2}$ which occupy the diagonal blocks of the matrix. Now, each representation gives rise to a fuzzy sphere and hence one $U(1)$ symmetry for each. There is also an additional symmetry that rotates these $j = \frac{1}{2}$ configurations to each other without any energy cost. This in fact enhances the gauge symmetry to $SU(2)$ and can be generalised for two $d-$dimensional representations of the same spin.

Suppose that initially, we have N coincident D0-branes that have a $U(N)$ gauge symmetry and suddenly (under polarizations and the Myers effect [128]) they polarize and form all of them a big fuzzy sphere. Then the initial $U(N)$ gauge group of N coincident D0-branes breaks to N $U(1)$'s, e.g $U(1) \times U(1) \times U(1) \times \cdots \times U(1)$ since we separate all the D0-branes [3]. The interpretation that these D0-branes actually construct the fuzzy sphere and each of them is tethered on an area patch[4], results in one D0-brane carrying a $U(1)$ phase per area patch. That is because just one arbitrary Dp-brane has a $U(1)$ gauge theory on its worldvolume.

If we fix the size of the matrices N, then the vacua are characterised by irreducible $SU(2)$ representations of dimension $d_a = 2j_a + 1, \;\; a = 1, \cdots, N$, and as we saw in the BMN analysis in Sec. 3.3 we can write all the extrema of the action as the sum over these representations

$$X^i = \bigoplus_i J^i_{(d_a)}. \tag{5.39}$$

Interestingly this is similar to the Hilbert space of spin networks (5.7) or the space of Polyhedra for a fixed number of faces N.

Also, the number of vacua of the mini BMN theory is given by partitions of N, i.e by a Young tableau of N rows and N columns, which again is the same classification of N pairs of harmonic oscillators for the case of spin networks.

In addition for coincident fuzzy spheres we have

$$N = \sum_a n_a(2j_a + 1), \tag{5.40}$$

with n_a being the degeneracy of the $d_a = (2j_a + 1)$ representation. Then, the gauge group partially breaks to $\bigtimes_a U(n_a)$.

[3] One can think that a D0-brane is a fuzzy sphere of zero dimension (i.e of spin $j = 0$).

[4] In fact their commutation constructs the area patch [53, 117].

For the simplest case of the highest $SU(2)$ representation with dimension $N = 2j + 1$, the (previously coincident) D0-branes polarize to form a single fuzzy sphere. This phenomenon results in the creation of two additional dimensions out of the initial zero-dimensional case with the exchange of breaking the gauge symmetry of the system from $U(N)$ to $U(1)$.

Suppose now that we have two copies of $SU(2)$ representation with arbitrary but equal dimension $n = 2j+1$. This corresponds to two fuzzy spheres of the same radius. In the Young table language, this corresponds to two rows of equal length represented as $[n, n, 0, \cdots, 0]$. This can actually be a vacuum of the mini BMN theory and employing the above rules the gauge symmetry breaks spontaneously to

$$U(N) \mapsto SU(2) \otimes U(1). \tag{5.41}$$

We have only one $U(1)$ with the exchange of having an extra $SU(2)$ gauge symmetry, reflecting the fact that for the same dimensionality two fuzzy spheres can be freely exchanged.

For the special case that these two fuzzy spheres carry all the degrees of freedom of the theory results in $n = \frac{N}{2}$, and the gauge symmetry becomes

$$SU(2) \otimes U(1), \tag{5.42}$$

that is one $U(1)$ for the fuzzy sphere and the freedom to interchange the two fuzzy spheres represented as $SU(2)$ [323]. In the case of N different fuzzy spheres of the trivial representation (i.e N D0-branes) the gauge group is

$$SU(N) \times U(1) = U(N). \tag{5.43}$$

The Hilbert space of the mini BMN model is the singlet sector

$$\mathcal{H}_{\text{singlets}}, \tag{5.44}$$

which represents states whose overall quantum number is zero. In the case of $SU(2)$ this refers to states with total spin zero. In string theory language, these states correspond to closed strings (see Fig. 5.4). Thus, the physical states are realised as the trace of a combination of matrix operators acting on the vacuum as we saw in Sec. 4.4 (see also Fig. 5.4).

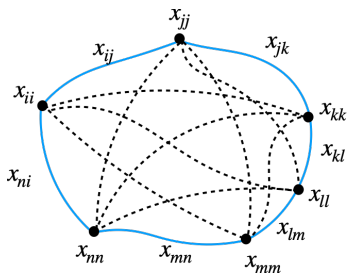

Figure 5.4: A gauge invariant state representing a closed string (blue/solid) and connecting six D0-branes.

Let us consider again the case when there are two fuzzy spheres of spins j_1, j_2 in the mini BMN model. Let us leave for the moment the spins and the dimensionalities n_1, n_2 arbitrary. When we consider an embedding on matrices, we have that the off diagonal block connecting

the block n_1 with block n_2 transforms as $j_1 \otimes j_2$ with respect to $SU(2)$ [323]. In other words, the matrices transform as

$$\bigoplus_{j'=|j_1-j_2|}^{j=j_1+j_2} j', \tag{5.45}$$

with respect to $SU(2)_L$. To consider gauge invariant scalars we should take the tensor product between them

$$\bigoplus_{\tilde{j}} \tilde{j} \otimes (j,j) \cong \bigoplus_{\tilde{j}} \bigoplus_{j'=|\tilde{j}-j|}^{\tilde{j}+j} (j',j). \tag{5.46}$$

In order to have $SU(2)_L$ singlets we require $j'=0$, leading to $\tilde{j}=j$, such that the singlet states are denoted as

$$\bigoplus_{\tilde{j}} \tilde{j} \otimes (j,j)\Big|_{\text{singlets}} \cong \bigoplus_{\tilde{j}} (0,\tilde{j}). \tag{5.47}$$

In fact, we see that the $SU(2)_L$ and $SU(2)$ should be the same such that they have singlet states for the scalars (X^i) of the theory. This can be motivated by the singlet constraint of vanishing spin [323]. In fact, gauge invariance forces the two representations to have the same dimensionality, in other words, two fuzzy spheres of the same radii. In addition, in this case, the gauge group is $SU(2) \times U(1)$ as we previously discussed.

5.3 Are the models connected by any means?

Intriguingly, the structures emerging from both models have completely different origins. Yet they both share some common features which we comment on below.

On one hand, the case of a spin network carries a $SU(2)$ representation on each of the edges. This representation gives an area patch and considering N representations constructs a polyhedron whose faces have different representations, and different areas and are thus desynchronised. On each of these individual faces, one can exploit the Swinger representation of $SU(2)$ in terms of two harmonic oscillators and thus the relevant operators $\hat{E}_{ij}$ constructed actually act on the $U(N)$ group. In addition, this $U(N)$ group is realised as the area-preserving diffeomorphism of the fuzzy sphere in the $N \to \infty$ limit. The latter is characterised by a specific $SU(2)$ representation, whose radius and hence area are related to the dimensionality of this representation. Therefore, it is tempting to speculate that each face of the polyhedron corresponds to a fuzzy sphere of a specific representation.

For the polyhedron, each face carries a $SU(2)$ representation, since it is assigned with a specific spin j_i. Let us consider N different faces/punctures, such that in general one has arbitrary representations. Since this representation labels also the area of each patch, it is understood that different representations lead to different areas such that the polyhedron is not made of equispaced patches of the same area. By the procedure of synchronization, [310,324] as we saw it is possible to give the same global representation on the boundary and fix the individual areas. In addition, it is also possible to assign a $U(1)$ phase per area patch of the polyhedron which is equivalent to giving a meaning of frame on each area patch [325]. Therefore our polyhedron will consist of patches that contain the same amount of area. One more ingredient is to consider small representations and take the number of patches to be large in order to obtain the classical limit. Specifically, one may consider the smallest spin (corresponding to the smallest representation) which gives the smallest area patch for each

face. This amounts to taking a large number of (same) spins in loop quantum gravity and not the limit of large spins [286]. This is the analogue of the usual preferable large N limit of quantum theories to recover the classical setting via a large number of quantum degrees of freedom and not via blowing up the norms of the quantum quantities. The same holds for the case of the BMN model where the large N limit corresponds to a large number of D0-branes.

The $SU(2)$ gauge symmetry plays an important role in loop quantum gravity after the work of [326]. The so-called intertwiners of loop quantum gravity in order to be $SU(2)$ invariant have to be subject to some constraints. In the language of polyhedra, we saw that this translates to the closure constraint (5.4). In [313] it was shown that the space of N-leg intertwiners for a fixed total area (fixed spin) carries an irreducible representation of $U(N)$. In fact, the space of N-leg intertwiners having a total fixed area (total spin) is shown to be isomorphic to $U(N)$. The highest-weight state consisting of 2-leg intertwiners is made of two irreducible representations carrying the same spin as we saw above. In the language of the polyhedron, this translates to a "twohedron" made out of two area patches. Then it is possible to act with the $\mathfrak{u}(N)$ operators E_{ij}'s to create all the rest N-leg intertwiners with the same area creating in this way a Polyhedron of the same area with N faces. It is also possible to assign the same area per face by equipping each face with a $U(1)$ phase. Then, this procedure enlarges the phase space and the gauge group to

$$\mathbf{\Pi}_{\text{fixed}} \times U(1)^N, \tag{5.48}$$

where $\mathbf{\Pi}_{\text{fixed}}$ is the space of polyhedra of fixed area (via fixing N) and its' quantum analogue is the $SU(2)$-invariant space of intertwiners (5.17).

Let us now turn to the respective picture of the $SO(3)$ BMN model. We saw that whenever we do have two copies of $SU(2)$ representation of the same spin, we essentially have two coincident fuzzy spheres made out of $N/2$ D0-branes each, such that the system has a $SU(2)\times U(1)$ gauge group as we explained. This would be the analogue of the highest weight state discussed for the intertwiners where it was concluded to be a 2-leg intertwiner which was interpreted as a flat "twohedron" made of just two squeezed area patches.

It would be interesting to ask whether we could construct the above space from the mini BMN model since all irreducible $SU(2)$ representations are realised as vacua of the bosonic potential. Therefore, we need N fuzzy spheres such that we construct the $U(1)^N$ part. The $SU(2)$ invariant part can be constructed by any pair of these fuzzy spheres since by interchanging them we get the same configuration. To this end, we remind that the D0-branes are in fact fuzzy spheres of vanishing radius (i.e of spin $j = 0$), and indistinguishable such that if we can interchange them pairwise we create a $SU(2)$ gauge symmetry. Then it might not be unnatural to interpret each minimal area patch in the polyhedron/spin-network configuration with fixed and coincident minimal areas as a single D0-brane at the same position, because also in this latter case the area patches have the same minimal values. Depending on whether we impose a $SU(2)$ gauge symmetry or not, we can get certain configurations between fuzzy spheres.

In the most general case where the faces (N) of the polyhedron do not have the same area but have rather different spins $j_i, i = 1, \cdots, N$, the analogue would be a single fuzzy sphere of radius j_i per area patch which is realised as a solution of the mini BMN potential. It seems that whenever we are considering different spins for each face of the polyhedron, these different configurations case can be classified by the mini BMN vacua.

It would be interesting to investigate more rigorously whether or not we can construct the space of intertwiners by considering the mini BMN vacua. We saw that even though the gauge groups of the two models are different, forcing gauge invariance for the case of the spin network creates a 2-valent intertwiner while for the mini BMN model creates two coincident fuzzy spheres. Different intertwiners can be classified by different vacua configurations of the mini BMN model, and in fact relaxing the gauge constraint(s) different fuzzy sphere configurations, namely different BMN vacua, which correspond to different polyherda and coarse-grained spin networks. Recalling that there is a natural $U(N)$ action on the space of these intertwiners [313] one could investigate what matrix model could be used meaningfully to grasp (at least effectively) the same characteristics. Indeed, the fuzzy sphere seems to be shared by the two models [302] and it certainly worths to be explored in more detail and in a more systematic way, especially now that fuzzy spheres can be studied also numerically.

Whether or not this is something useful for both models we do not know, but in any case, we could not resist pointing out this interesting similarity. As a matter of fact, it should be stressed that the above discussion is heavily speculative and by all means neither rigorous nor convincing, yet both a coarse-grained spin network and the mini BMN model share some similar features.

Part V

Epilegomena

6

Synopsis

Εάν μη έλπηται ανέλπιστον, ουκ εξευρήσει.

Heraclitus

In this final chapter, we come to the conclusion of the thesis, and, in a not-so-formal language, it could be considered the take-away of everything aforementioned. The main topic was the matrix models of superstring theories in general and specifically, the D0-matrix models, such as the BFSS [53] and the BMN [89] models as well as their bosonic variations. The initial goal was to understand how to use these matrix models with the current technology and knowledge available to better understand gravitational systems both analytically and numerically. One particularly important feature was to understand the behaviour of these models in the large N limit and at low temperatures, where a known gravitational dual is available. One could then verify or falsify the gauge/gravity correspondence. On equal footing were the finite N corrections, which, recalling now the idea of the thermodynamic limit of statistics, this kind of corrections could be regarded as quantum corrections on a gravitational theory. The idea was examined by using non-perturbative techniques and specifically in this thesis by using simulations.

As interesting as this sounds it remains an ambiguous undertaking because one has to ensure that this idea survives first in the large N limit where classical supergravity is known and then consider finite N. On the other hand, we were always in a position to first explore the finite N region and then extrapolate to the large N limit excluding all kinds of hidden parameters and occasions that could spoil trusting our results. In this way, we were not always in the position to appreciate the quantum corrected results until we concluded that indeed we get consistent large N limits. An important example showing this ambiguity is the fact that the simulation could be trapped in a region of the phase space which does not correspond to any physical quantity, and hence making interesting claims could lead to undesired results. On the other hand, the simulation could also be trapped in a region of the

phase space that indeed has a physical interpretation but not monitoring all the parameters and not analysing the observables could lead to undesired results. An obvious example is being in the fuzzy sphere background of the BMN model while trying to probe the trivial vacuum. As we repeatedly commented in the previous sections we were indeed very careful in analysing all small details and observables of the system to ensure that we actually probe what we were aiming for.

Motivated by this, we tried to push the idea of gauge/gravity duality to further tests. At the same time, most of the easily accessible ideas were already accurately tested in the past [134, 138, 146, 148, 149, 164, 193, 272, 327, 328]. Most of the previous works regarded the BFSS model while partially some works concerning the BMN model started to appear [194, 243, 273, 274, 329, 330].

In some cases, not even the analytic results were available and an interesting example was studied in Sec. 3.4 for the BMN model where at finite N we observed a repulsive force acting on a probe D0-brane. This was verified for the BFSS model in [164] following the work of [132], while here we chose a different way to study the bulk dual of the BMN model in a specific limit since it is not known analytically [159, 258, 331]. This behaviour might not be so unexpected since the gravitational physics of the BMN model are of the same nature as that of the BFSS model. For the latter, we can assume the black hole to be constructed by a collection of D0-branes sitting on top of each other. However, it is not entirely clear what the exact physical picture in the former case is, since one has to take the plane-wave limit of an eleven-dimensional metric. Note that we did not test this idea numerically for the BMN model but it would be interesting to do so in the future.

An equally interesting direction is to understand the large d limits of field theories, namely the large limit of spatial dimensions. As we discussed in Sec. 4.2 the near horizon limit of a Schwarzschild black hole in the generalised Einstein gravity in the large d limit is equivalent to a two-dimensional gravity with a specific dilaton profile in a string theory. In this large d limit, the entropy of the Schwarzschild black hole shows a Hagedorn behaviour, a feature that is shared with string theory. It seems, that the constituents constructing this higher-dimensional Schwarzschild are showing a stringy behaviour. It would be tempting to relate the constituents with partons living in a d-dimensional space which furthermore are represented by a large number (d) of matrices but this idea needs to be explored in a more rigorous and systematic methodology to draw any meaningful conclusions. We showed that by simulating the matrix model using bosonic statistics only, we were able to capture the behaviour of the confinement-to-deconfinement transition temperature predicted by the gauge theory in the large d expansion. We are referring to the pattern in Fig. 4.5 where the shift could be related to finite N and finite lattice steps. On a more speculative ground, we tried to see whether or not the above system could be related to a gravitational system. To this end, we considered a minimalistic gravitational theory, namely Einstein's gravity in d dimensions and we discussed a topology change of a Schwarzschild black hole in this theory. The motivation being that this kind of transition [131] is related to a transition in the gauge theory [175] which is also usually captured by a confinement-to-deconfinement transition. Of course, the connection of this gravitational theory with a gauge theory is not established but we just might have experienced some hint pointing towards this direction in specific limits. In any case, to either falsify or verify, a more systematic and well-defined methodology has to be employed to attack this problem. A similar discrepancy between the large N predictions and

finite N simulations was also observed in the next project we are about to discuss [194].

In the view of understanding and testing the gauge/gravity duality, whenever there is a discrepancy between the gauge theory and the gravitational side, one has to be extremely careful to relate this mismatch with a physical phenomenon because computational errors, especially numerical errors, can occur quite easily. The Polyakov loop is a very powerful tool used to investigate the behaviour of the system in different phases. One of these was the investigation of the confinement-to-deconfinement temperature transitions and the comparison between the gauge side, the gravity side, and the simulations. When two of these pillars coincide, then the remaining pillar should do the same otherwise there is an obvious problem. The gravity side of both BFSS and BMN is always deconfined because they are governed by some sort of a black hole, namely a black zero-brane. An apparent puzzle that arose during this analysis was the fact that we were able to obtain confined simulations at small temperatures, but confinement is not predicted from the type IIA supergravity dual where the black zero-brane lives. After excluding obvious numerical errors, and checking that we have confined simulations surviving in the large N limit, we turned to understanding this phenomenon physically.

The only available explanation was that this confined phase corresponds to a gas of supergravitons living in eleven dimensions which is available only in small temperatures, explained around Fig. 4.15 based on Fig. 3.4. An important feature that was used was the fact that there was a large hysteresis in this parameter region which for large enough N could be explained physically. As we show in Appendix D in the large N limit there is a big overlap between the two phases of the model(s). That of an eleven-dimensional, small Schwarzschild black hole and that of the ten-dimensional black zero-brane of type IIA supergravity. These are the two different gravitational phases separated by the diagonal line in Fig. 4.15 and it seems that the matrix model(s) can probe this separation. A more detailed discussion can be found around this figure. Yet this is not the end of the story but merely the beginning of a new era of simulations where more systematic tests have to verify this picture and even investigate other observables of M-theory such that the membrane and the fivebrane. It seems that we are just starting to investigate the phase of the M-theory and this theory will finally be verified to be a Matrix theory. As technology advances, simulating these kinds of models will be easier and more beneficial, since with the development of the quantum computer simulations will be performed more efficiently.

The latter might benefit from the question of whether the singlet constraint is important for a physical system or not. This is a legitimate physical question which was investigated in [133, 138], and recently in [273] confirming the intuition. At low temperatures, the gauge constraint that introduces gauge degrees of freedom in the matrix model system is not important to have a gravitational theory. This introduces another non-gauge/gravity example and generalizes the idea of the duality further. On the other hand it has a twofold interest because is also important for quantum computers. For the matrix models under consideration, the gauge symmetry is $SU(N)$. Trying to put these models in a quantum computer is not easy because it is difficult to realise the $SU(N)$ gauge symmetry [141]. On the other hand, it might be easier to consider a set of harmonic oscillators and Majorana fermions such that by fine-tuning the interactions between them one obtains the ungauged version of the models which has a $SU(N)$ global symmetry. $SU(N)$ non-singlet states have higher energy than the singlet states, hence we would expect that a small perturbation that

breaks the global $SU(N)$ symmetry will be irrelevant in the IR.

Some further ongoing work [274] tries to push the idea of gauge/gravity duality to the lowest possible temperatures until now by using a considerable amount of current resources. As data show at the current moment of writing, there is an overall good behaviour of the large N and continuum extrapolations in a sense that in the parameters we studied so far the fits, hint a convergence with the gravitational and the BFSS results. Of course, these are preliminary data to discuss for a precision test but the pattern, even at this low level of approximation, seems to point in the right direction. We will not be too enthusiastic about it, but if this possibility turns out to be true and trustworthy, by going to small temperatures and performing several tests we can learn about the black zero-brane and M-theory gravitational systems. In particular, because the finite μ corrections are small, we can study the features of the first order, confinement-to-deconfinement, transition at finite and small μ, and since these features are qualitatively very close to the BFSS features, we might also be able to investigate the M-theory region. This is because the, so far good, agreement with supergravity hints at such a possibility. Of particular importance would also be to investigate other contents of M-theory such as the membrane and the fivebrane, since the latter is believed to be the trivial vacuum of the BMN model [89].

The last part of our journey consisted of the exploration of a by now quite old idea [298–300, 332]. It was an interesting observation that similar structures appearing in specific coarse-grained spin networks from loop quantum gravity could be classified by the BMN non-trivial vacua. We are talking about the fuzzy spheres, and a crude approximation to relate area patches between the two formalisms was made. Of course, being at this level we cannot claim at all that there is a rigorous connection due to the different points of view of the two main theories, and again a more systematic approach is needed to verify or falsify this idea. In the miraculous case where there will turn out to be a connection between the two, the benefits would mainly be for the loop quantum gravity community, since the matrix models from string theory are well understood by now and can be simulated in a computer. The latter case might help to simulate specific spin networks similarly and study their dynamics in this way.

Finally, matrix models can be used to study a plethora of different physical systems, lower-dimensional and higher-dimensional. In particular, it seems extraordinary how a one-dimensional system containing nine matrices can describe a gravitational physical system in ten spacetime dimensions. To have d matrices which are $N \times N$ it is obvious that a lot of knowledge is stored in them and one of the primary goals is to carefully extract useful information from this. Indeed, some of these connections are known and others are under investigation. The non-perturbative nature of matrix models allows us to probe theories without expanding parameters. On the other hand, by tuning N we can study quantum corrections of classical systems, a feature which is of high importance for gravitational systems. It is the beginning of a new era, and especially taking advantage of the (hopefully soon operating) quantum computers one might use these non-perturbative tools to study very interesting physical systems in more depth extracting knowledge that was not accessible in the past. We could not resist pointing out that the brain is also a physical system whose synapses create geometrical structures in higher dimensions [333].

Part VI

Appendices

A

The potential barrier in the BMN model

We are interested in finding the potential barrier of BMN model, a feature that controls the probability for the trivial vacuum configuration to transition to a fuzzy sphere configuration. As we may proceed with the analysis, also some conceptual ideas about the model will become clearer.

Let us then concentrate on the bosonic action of the BMN model which has the following form

$$S = \frac{N}{\lambda}\int \mathrm{d}t\ \mathrm{Tr}\left[\frac{1}{2}(D_t X^i)^2 + \frac{1}{4}[X^i, X^j]^2 - \frac{1}{2}\left(\frac{\mu}{3}\right)^2 (X^i)^2 - i\frac{\mu}{3}X^i X^j X^k \epsilon_{ijk}\right]. \tag{A.1}$$

To find extrema of this potential let us consider an ansatz of the form $X^i(t) = r(t)J^i$ and substitute it into the Lagrangian. Using identities of ϵ_{ijk} and that for irreducible $SU(2)$ representations we have $\mathrm{Tr}\,(J^i)^2 = \frac{N}{3}(N^2-1)$, we find

$$\mathcal{L} = \frac{N^2(N^2-1)}{6\lambda}\left(\dot{r}^2 - r^2\left(r - \frac{\mu}{3}\right)^2\right), \tag{A.2}$$

with potential

$$V = \frac{N^2(N^2-1)}{6\lambda} r^2\left(r - \frac{\mu}{3}\right)^2, \tag{A.3}$$

whose profile is given at Figure A.1.

Asking stability of this potential, we differentiate with respect to r and we obtain three solutions

- $r = 0$ which is stable,
- $r = \frac{\mu}{3}$ which is stable,
- $r = \frac{\mu}{6}$ which is unstable.

The maximum of the potential is given by

$$V\left(r=\frac{\mu}{6}\right)=\frac{N^2(N^2-1)}{6\cdot 36\cdot 36\lambda}\mu^4. \tag{A.4}$$

In the large N limit, this potential barrier behaves like $\sim \mu^4 N^4$, which means that the combination μ, N is what matters such that we keep under control the system. Specifically in simulations it is of much importance to keep this combination large to avoid undesirable tunnellings from the trivial backgrounds to fuzzy backgrounds.

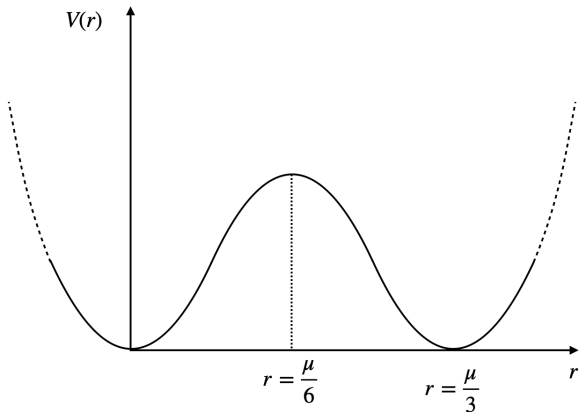

Figure A.1: The profile of the potential (A.3) showing also the respective extrema.

B

Effects of the BMN geometry on a D0-brane and a D2-brane

In this section we start by calculating the force that a D0-brane feels in a classical plane wave background in ten dimensions and then repeating the calculation for a D2-brane.

B.1 A D0-brane feels only the trivial vacua

The starting point the symmetry reduced metric (3.137). In the limit of small curvatures $Q^2/4 \ll 1$ one can expand as follows

$$e^{-\frac{2\Phi}{3}} \approx 1 + \frac{Q^2}{8} + \mathcal{O}\left(Q^4\right)$$
$$A_0 \approx -\frac{Q^2}{4} + \mathcal{O}\left(Q^4\right).$$

When we want to calculate the force, we have in mind a situation when we naively place a D0-brane probe in the spacetime and ask for its dynamical behaviour. To this end, we need to write down the DBI action for the D0-brane by choosing the gauge where the parameter of the worldline of the D0 coincides with the time component of the spacetime. In a general background, it is given by

$$S_{D_0} = -T_0 \int \mathrm{d}t e^{-\phi} \sqrt{-g_{\mu\nu} \frac{\mathrm{d}x^\mu}{\mathrm{d}t} \frac{\mathrm{d}x^\nu}{\mathrm{d}t}} + T_0 \int \mathrm{d}t A_0, \tag{B.1}$$

where $T_0 = \frac{M_s}{g_s}$ is the tension of the D0-brane and the expression inside the square root is the pull-back of the spacetime metric on the worldline of the D0-brane. We remind that a Dp-brane naturally couples with a p+1 form, thus the only form that couples (naturally) to

a single D0-brane is the one-form [1] potential A_0. Then, the action reads as

$$S_{D_0} = -T_0 \int \mathrm{d}t \left(1 + \frac{3Q^2}{16}\right) \sqrt{1 + \frac{Q^2}{8} - \left(1 - \frac{Q^2}{8}\right)\dot{x}^2} + T_0 \int \mathrm{d}t \left(-\frac{Q^2}{4}\right). \tag{B.2}$$

Moreover, after taking the non-relativistic limit we expand the action up to $\dot{x}^2$ and Q^2 terms leading to

$$S_{D_0} \approx -T_0 \int \mathrm{d}t \left[1 + \frac{Q^2}{2} - \frac{1}{2}\dot{x}^2\right] + \mathcal{O}(Q^4, \dot{x}^4, \dot{x}^2 Q^2). \tag{B.3}$$

One can read off the potential from this action:

$$V_{D_0}(x) = T_0(1 + \frac{Q^2}{2}). \tag{B.4}$$

Recalling (3.138) we write the potential as,

$$V_{D_0}(X^i, X^a) = T_0 \left[1 + \frac{1}{2}\left(\frac{\mu^2}{9}\sum_{i=1}^{3}(X^i)^2 + \frac{\mu^2}{36}\sum_{a=4}^{9}(X^a)^2\right)\right]. \tag{B.5}$$

We see an explicit dependence of μ in the potential. It is also worth noting that the trivial vacua ($X^i = 0$ and $X^a = 0$) are supersymmetric solutions of the potential after performing a shift, but the non-trivial $SU(2)$ vacua are not. The latter, geometrically are believed to correspond to concentric fuzzy spheres, however the single D0-brane in this background is agnostic if there are any fuzzy spheres at all. Had we consider a different probe, for example a D2-brane, then this would couple to higher forms and would give rise to the $SU(2)$ part of the potential. This is demonstrated in the next subsection.
Furthermore, we can write the terms inside the sum as the radii of an S^2 and S^5 sphere. In other words we can write the potential as

$$V_{D_0}(r_2, r_5) = T_0 \left[1 + \frac{1}{2}\left(\frac{\mu^2}{9}r_2^2 + \frac{\mu^2}{36}r_5^2\right)\right], \tag{B.6}$$

where r_2 denotes the radius of the S^2 sphere and r_5 the one of S^5.
From this potential one can obtain the force that the D0-brane feels by differentiating with respect to the radial coordinates. This is simply given by

$$F_{D_0}(r_2, r_5) = -T_0 \frac{\mu^2}{9}\left(r_2 + \frac{r_5}{4}\right). \tag{B.7}$$

However, this is a naive picture because the hole system is studied at the classical level. According to matrix model simulations, the matrices are never zero but they subject to quantum fluctuations independent of which vacuum one studies [164, 193, 334].

B.2 A D2-brane feels the $SU(2)$ vacua

In this section we calculate the force that a D2-brane probe feels in the weakly curved background (3.137). A similar discussion can be found in [159]. One can think this D2 probe

[1] We could of course consider a three-form flux and via this procedure the D0-brane would couple to also a three form, giving rise to a Myers effect. This would change the output of the discussion but we change in the first place the background by the introduction of the three-form.

as being made of (q) D0-branes where the number of D0's is taken to be large. However, in order to consider this as a probe, one has to require that the probe charge q is much less than the background charge N such that it does not backreacts to the geometry, i.e we are studying the limit $1 \ll q \ll N$. We can imagine this brane to have a S^2 topology embedded in a three dimensional space. In particular, one natural embedding would be along the $SO(3)$ part of the metric where the other six dimensions are transverse to it. For convenience, we place the D2-brane in the center of the the six transverse directions such that $X^a = 0$. Then the DBI and WZ action of the D2-brane will be of the familiar form

$$S_{D_2} = -T_2 \int \mathrm{d}^3\sigma e^{-\Phi} \sqrt{-\det\left(G_{ab} + 2\pi\alpha' \mathcal{F}_{ab}\right)} + T_2 \int \left(A_3 + 2\pi\alpha' \mathcal{F}_2 \wedge A_1\right), \quad q \ll N \tag{B.8}$$

where $2\pi\alpha'\mathcal{F}_2 = 2\pi\alpha' F_2 - B_2$. As in the case of the D0-brane, we have also chosen the static gauge here, which corresponds to identify the worldvolume dimensions with the three dimensional part of the subspace of the ten-dimensional spacetime. We can choose t, θ, ϕ coordinates parametrizing the S^2. The radius of S^2 is given by r, while the angles have the usual ranges $\theta \in [0, \pi]$, $\phi \in [0, 2\pi]$. For a compact D2-brane of arbitrary topology the total charge q is quantized and it is given as

$$\int_{S^2} F_2 = 2\pi q \quad \longrightarrow \quad F_2 = \frac{1}{2} q \sin\theta \, \mathrm{d}\theta \wedge \mathrm{d}\phi. \tag{B.9}$$

We note that the integer q is also related to the first Chern class of the U(1) bundle at a fixed point in time [335], [336] and moreover, it acts as a source for the R-R vector field and the interpretation of it is the number of D0-branes that are bound on the surface of the D2-brane. Analogously, the forms are given in the static gauge as

$$A_1 = \left(1 - \frac{Q^2}{4}\right)^{-1} \mathrm{d}t \tag{B.10}$$

$$A_3 = \frac{1}{3}\mu \, \mathrm{d}t \wedge S_2 \quad , \quad S_2 = \frac{1}{2}\epsilon_{ijk} x^i \wedge \mathrm{d}x^j \wedge \mathrm{d}x^k, \quad i, j, k = 1, 2, 3. \tag{B.11}$$

Furthermore, the pullbacks of the metric G_{ab} on the D2-brane are given as

$$\det g_{tt} = -\left(1 - \frac{Q^2}{4}\right)^{-\frac{1}{2}} \tag{B.12}$$

$$\det g_\perp = \det(g_{\theta\theta} g_{\phi\phi}) = \left(1 - \frac{Q^2}{4}\right) r^4 \sin^2\theta. \tag{B.13}$$

From these we have that

$$F_{\theta\phi} = \frac{1}{2} q \sin\theta \tag{B.14}$$

$$F_{ab}F^{ab} = \frac{q^2}{2\left(1 - \frac{Q^2}{4}\right) r^4} \tag{B.15}$$

$$\det F_2 = \frac{1}{2} F_{ab} F^{ab} \det g_\perp = \frac{q^2}{4} \sin^2\theta. \tag{B.16}$$

The DBI action can be written as

$$S_{DBI} = -T_2 \int \mathrm{d}^3\sigma e^{-\Phi} \sqrt{-\det g_{tt}} \left(\det g_\perp + 2\pi\alpha' \det F_2\right)^{\frac{1}{2}}, \tag{B.17}$$

and considering the main contribution coming from $\det F_2$[2], we can expand the action around this and get

$$S_{DBI} \approx -T_2 \int \mathrm{d}^3\sigma e^{-\Phi}\sqrt{-\det g_{tt}}\left(2\pi\alpha'\sqrt{\det F_2}+\frac{\det g_\perp}{4\pi\alpha'\sqrt{\det F_2}}\right). \tag{B.18}$$

Using the exact expressions this gives

$$\begin{aligned} S_{DBI} &\approx -T_2 \int \mathrm{d}t\,\mathrm{d}\theta\,\mathrm{d}\phi\left[\left(1-\frac{Q^2}{4}\right)^{-1}\pi\alpha' q\sin\theta+\frac{r^4\sin\theta}{2\pi\alpha' q}\right] \\ &\approx -T_2\int \mathrm{d}t\left[\left(1-\frac{Q^2}{4}\right)^{-1}4\pi^2\alpha' q+\frac{2r^4}{\alpha' q}\right]. \end{aligned} \tag{B.19}$$

Similarly the WZ action gives

$$S_{WZ} = T_2\int \mathrm{d}t\left[\frac{4\pi\mu r^3}{3}+4\pi^2\alpha' q\left(1-\frac{Q^2}{4}\right)^{-1}\right]. \tag{B.20}$$

We see that the leading terms cancel each other, the subleading terms that remain can be mapped to the commutator term $\sim \mathrm{Tr}\,[X^i,X^j]^2$ and the Myers term $\sim -\mathrm{Tr}\,\left(i\frac{\mu}{3}\epsilon_{ijk}X^iX^jX^k\right)$ in the BMN model. In addition, one could also be interested in the contributions coming from the B_2 field. However, as it is shown in [337] the contributions of B_2 coming from WZ and DBI action cancel each other. Nevertheless, we can add a term $\sim \mu^2r^2$ such that we complete the square in the action. This will make the interpretation more clear. By adding and substracting this term, we write the action as

$$S_{D_2} \approx -\frac{2T_2}{\alpha' q}\int \mathrm{d}t\left[\left(r^2-\frac{2\pi\mu\alpha' q}{3}r\right)^2-\frac{4\pi^2\mu^2\alpha'^2q^2r^2}{9}\right]. \tag{B.21}$$

The potential is simply

$$V_{D_2}(r) = \frac{2T_2}{\alpha' q}\left[\left(r^2-\frac{2\pi\mu\alpha' q}{3}r\right)^2-\frac{4\pi^2\mu^2\alpha'^2q^2r^2}{9}\right]. \tag{B.22}$$

This potential profile, reminds the one from the BMN matrix model discussed in (A.3). We see that apart from the trivial $r=0$ solution, there is a non-trivial equilibrium radius at

$$r = \frac{4\pi\alpha' q\mu}{3}. \tag{B.23}$$

This is understood as the radius in which the contraction that is caused by the r^2 and r^4 terms compensates with the expansion caused by the r^3 term in the potential. In fact one can generalize this and have a number (k) of concentric D2-branes instead of just one. Then for each D2-brane there is an equilibrium radius given by

$$r_i = \frac{4\pi\alpha' q_i\mu}{3}, \quad i=1,\cdots,k, \tag{B.24}$$

[2]This amounts to $\frac{q^2}{4}\sin^2\theta \gg 1$, reflecting the fact that the charge q is large but nevertheless we are in the limit $q \ll N$

with q_i being the charge of the i-th D2-brane. In the Matrix model side instead, this picture corresponds to a particular copy of the N dimensional representation of $SU(2)$ up to a non-commutative factor in the case of a single D2-brane and a partition $\{N1, \cdots, N_k\}$ of the N dimensional representation of $SU(2)$ in the case of k concentric D2-branes .

The force that the D2 feels from the background is given as

$$F_{D_2}(r) = -\frac{8T_2}{\alpha' q} r^2 (r - \pi q \alpha' \mu). \tag{B.25}$$

In fact, we see that it is independent of the configuration of the geometry, for example independent of the warp factor $e^{\frac{2\Phi}{3}}$, but it does depend on its own charge q and the flux parameter μ, in accordance with the D0-brane case. We also see that the force becomes repulsive for $r \in (0, \pi q \alpha' \mu)$. This results to an interpolation from a strong, attractive force to a slightly repulsive force after going through the minimum of the potential. In the minimum, we have a D2-brane freely sitting on a position in spacetime. So in this way, we can see that we probe and reveal different parts of the geometry since this picture in the D0-probe was absent.

C

Microcanonical and grandcanonical statistics

Here, we give more some complementary information and tools to better understand the statistical picture of the proposal in Sec. 4.3. In particular we discuss maxima and minima. In the microcanonical ensemble, the energy E is restricted to a small range $[E, E + \mathrm{d}E]$, and all states contribute with the same weight. The entropy $S(E)$ is related to the density of states $\Omega(E)$ as $S(E) = \log \Omega(E)$. Dual gravity solutions such as 11d Schwarzschild black hole correspond to typical configurations dominating the entropy. The microcanonical temperature T_{micro} is obtained from the entropy S as

$$\frac{1}{T_{\mathrm{micro}}} = \frac{\mathrm{d}S}{\mathrm{d}E}. \tag{C.1}$$

Therefore, the specific heat capacity $\frac{\mathrm{d}E}{\mathrm{d}T_{\mathrm{micro}}}$ is

$$\frac{\mathrm{d}E}{\mathrm{d}T_{\mathrm{micro}}} = -\frac{1}{T_{\mathrm{micro}}^2}\left(\frac{\mathrm{d}^2 S}{\mathrm{d}E^2}\right)^{-1}. \tag{C.2}$$

The Euclidean path integral of the matrix model describes the canonical thermodynamics. In the canonical ensemble, the temperature T is a controllable parameter. The partition function is given by

$$Z(T) = \int \mathrm{d}E \Omega(E) e^{-E/T} = \int \mathrm{d}E e^{-F(E,T)/T}, \tag{C.3}$$

where F is the free energy defined by

$$F(E, T) = E - TS(E). \tag{C.4}$$

For simplicity, let us assume that the maximum of entropy is uniquely determined at each E. (It is not the case if there are two or more separate local maxima and the first-order phase transition in the microcanonical ensemble takes place. We will consider such a case later.) Then, by taking the derivative with respect to the energy, we obtain

$$\frac{\partial F(E,T)}{\partial E} = 1 - T\frac{\mathrm{d}S(E)}{\mathrm{d}E} = 1 - \frac{T}{T_{\mathrm{micro}}(E)}. \tag{C.5}$$

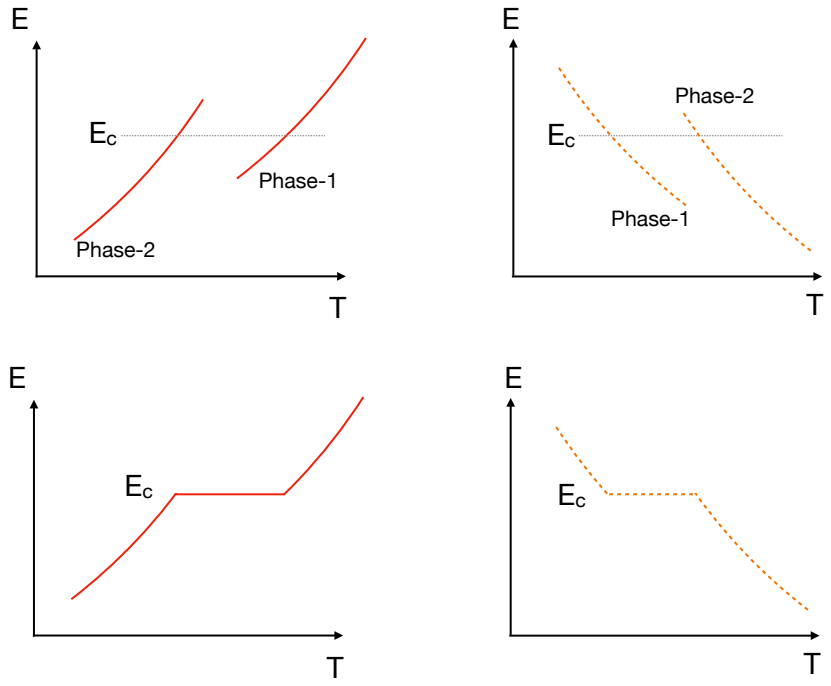

Figure C.1: [Top] Coexistence of two local maxima of entropy $S_1(E)$ and $S_2(E)$ corresponding to phase-1 and phase-2 in the microcanonical ensemble. We assume that $S_1(E) > S_2(E)$ at $E > E_c$ and $S_1(E) < S_2(E)$ at $E < E_c$. [Bottom] Corresponding canonical phase diagram; free energy minimum (left) and maximum (right).

Therefore, free energy is extremized at the value of E which corresponds to $T_{\rm micro}(E) = T$. The second derivative is

$$\frac{\partial^2 F(E,T)}{\partial E^2} = \frac{T}{T_{\rm micro}^2}\left(\frac{{\rm d}E}{{\rm d}T_{\rm micro}}\right)^{-1}. \tag{C.6}$$

Therefore, if the heat capacity in the microcanonical ensemble is positive (resp., negative), the free energy is minimized (resp., maximized) in the canonical ensemble.

The case of first order transition in the microcanonical ensemble

Suppose there are two local maxima of the entropy $S_1(E)$ and $S_2(E)$ corresponding to phase-1 and phase-2, as shown in the top row of Fig. C.1. We assume that $S_1(E) > S_2(E)$ at $E > E_c$ and $S_1(E) < S_2(E)$ at $E < E_c$, and hence a first-order transition takes place at $E = E_c$. The entropy $S(E)$ in (C.3) becomes $S = \log(e^{S_1} + e^{S_2})$. This is approximated well by S_1 and S_2 at $E > E_c$ and $E < E_c$, respectively. When E is infinitesimally close to E_c, we have to take into account both phases.

We have

$$\frac{{\rm d}S(E)}{{\rm d}E} = \frac{1}{e^{S_1} + e^{S_2}} \times \left(\frac{e^{S_1}}{T_{\rm micro,1}} + \frac{e^{S_2}}{T_{\rm micro,2}}\right), \tag{C.7}$$

where $\frac{1}{T_{{\rm micro},i}} = \frac{{\rm d}S_i}{{\rm d}E}$ is the microcanonical temperature of phase-i ($i = 1, 2$). When E is varied from slightly below E_c to slightly above E_c, it moves from $\frac{1}{T_{\rm micro,2}}$ to $\frac{1}{T_{\rm micro,1}}$. Therefore, the canonical phase diagram becomes like the bottom row of Fig. C.1.

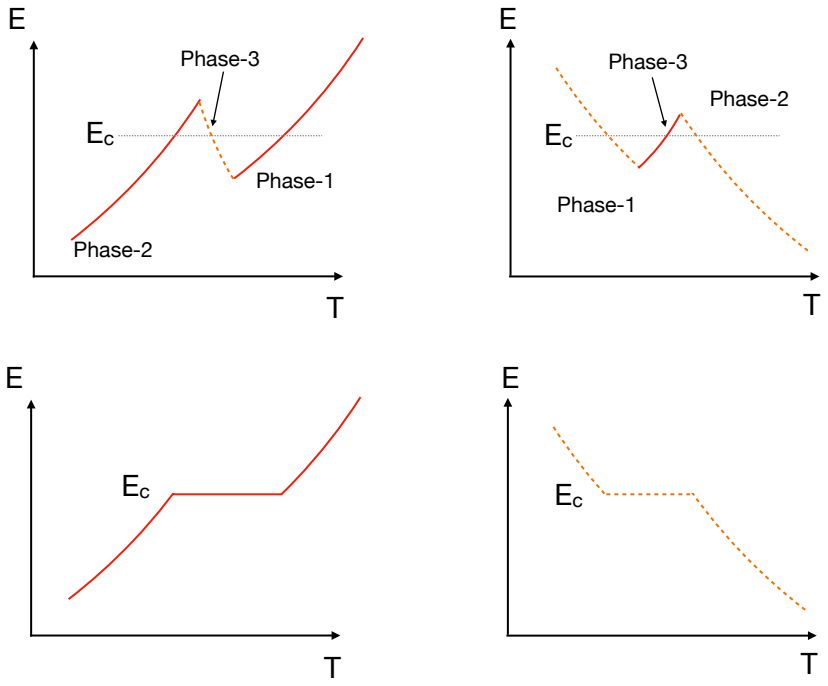

Figure C.2: [Top]: Coexistence of three local maxima of entropy $S_1(E), S_2(E)$, and $S_3(E)$ in the microcanonical ensemble. We assume that $S_1(E) > S_2(E)$ at $E > E_c$ and $S_1(E) < S_2(E)$ at $E < E_c$, and $S_3(E)$ is always smaller than $S_1(E)$ or $S_2(E)$. [Bottom]: Corresponding canonical phase diagram; free energy minimum (left) and maximum (right).

Suppose yet another maximum of the entropy $S_3(E)$ corresponding to phase-3 exists as shown in Fig. C.2, and $S_3(E)$ is always smaller than $S_1(E)$ or $S_2(E)$. Then phase-3 does not affect the canonical phase diagram at all; see the bottom row of Fig. C.2. Still, if other parameters than energy are taken into account, phase-3 may be visible in the canonical simulation.

D

The Schwarzschild black hole in 11 dimensions

One candidate to capture the behaviour of maximum (minimum) confinement (deconfinement) temperature for matrix model is the eleven-dimensional Schwarzschild black hole in the unboosted frame and non-compact space. This candidate is one of the possible choices but nevertheless not unique. In fact the boost does not play an obviously important role as we shall see. Assuming that the gravity correspondence is correct this can be achieved by studying this black hole with minimal mass, the Plank mass m_P. At small temperatures and large N we expect the matrix model to be described by a theory of gravity. In particular, for very low temperatures and strong coupling in the matrix model we expect to approach the M-theory limit in the gravity side [49]. That is because the 11-th dimension opens up since the radius of the compact dimension is in direct relation with string coupling $R = g_s\sqrt{\alpha'}$. In a sense, going to very low temperatures/energies we are approximating the non-compact spacetime. The generalization of a Schwarzschild black hole in eleven dimensions is straightforward (as we saw in (4.27) it is the Schwarzschild-Tangherlini metric [196] for $D = 11$)

$$\begin{aligned} \mathrm{d}s_{11}^2 &= -f(r)\,\mathrm{d}t^2 + f(r)^{-1}\,\mathrm{d}r^2 + r^2\,\mathrm{d}\Omega_9^2, \\ f(r) &= 1 - \left(\frac{r_0}{r}\right)^8. \end{aligned} \tag{D.1}$$

The horizon of this black hole is setted by

$$r_0^8 = \frac{16\pi G_{11} M}{9\Omega_9}, \tag{D.2}$$

where G_{11} is the 11-dimensional Newton's coupling and $\Omega_{d-1} = \frac{2\pi^{\frac{d}{2}}}{\Gamma\left(\frac{d}{2}\right)}$ is the surface of the $(d-1)$-dimensional sphere. The associated temperature is given as

$$T = \frac{8}{4\pi r_0}. \tag{D.3}$$

We recall that the relation between the 11-dimensional Planck length, string coupling and $\alpha' = \ell_s^2$ is [338]

$$\ell_P = (2\pi g_s)^{1/3}\sqrt{\alpha'}, \tag{D.4}$$

and from the above we can relate the string coupling with Planck's mass via the uncertainty principle[1] as

$$g_s^2 = \frac{2\pi R^3}{\ell_P^3} = 2\pi R^3 m_P^3. \tag{D.5}$$

In addition to those, we have the general conventions [166]

$$g_s = 4\pi^2 \ell_s^3 \frac{\lambda}{N}, \tag{D.6}$$

and

$$16\pi G_{11} = (2\pi)^8 g_s^3 \ell_s^9. \tag{D.7}$$

Thus we can solve (D.5) for m_P in terms of N,

$$m_P = \frac{N^{1/3}}{2\pi\sqrt{\alpha'}\lambda^{1/3}}, \tag{D.8}$$

while from (D.7) we get

$$G_{11} = \frac{(2\pi)^8}{16\pi}(4\pi^2)^3\lambda^3 N^{-3}\ell_s^{18}. \tag{D.9}$$

Now plugging all these in (D.2) and setting $\lambda = 1 = \alpha'$ we find that

$$r_0 = \kappa(d) N^{-1/3}, \tag{D.10}$$

where $\kappa(d)$ is a function that depends on the dimensionality of spacetime. For the 11-dimensional case we get $\kappa \simeq 10.5$.
Therefore via (D.3) this results into a critical temperature scaling as

$$T_c \sim N^{1/3}. \tag{D.11}$$

Carrying all constants for $D = 11$ we obtain

$$T_c \simeq 0.0634 N^{1/3}. \tag{D.12}$$

Hence this is the maximum(minimum) confinement(deconfinement) temperature we can probe related with the gravity side. Let us now see why the boost is irrelevant for physical quantities. The idea is that if the horizon of the black hole was an ordinary system upon boosting it would Lorentz contract leading in this way a decreasing area of the horizon yielding in addition a violation of the second thermodynamic law since the entropy assigned with the horizon would shrink. Fortunately, horizons do not Lorentz contract following from the fact that every cross section of the horizon has the same area, such that in every frame, the area of the horizon remains the same. Let us see an explicit example of this by writing a four-dimensional Schwarzschild black hole in isotropic coordinates using the transformation [37]

$$r \to r\left(1 + \frac{M}{2r}\right)^2. \tag{D.13}$$

[1] We are using units $c = 1 = \hbar$ such that $\ell_P m_P \sim 1$.

The metric reads

$$\mathrm{d}s^2 = -\left(\frac{r-r_0}{r+r_0}\right)^2 \mathrm{d}\tilde{t}^2 + \left(1+\frac{r_0}{r}\right)^4 \left(\mathrm{d}\tilde{z}^2 + \mathrm{d}\rho^2 + \rho^2\,\mathrm{d}\phi^2\right). \tag{D.14}$$

The coordinates are related via $r^2 = \tilde{z}^2 + \rho^2$ and they cover both asymptotically flat regions with the horizon at $r = r_0$. Let us suppose that we want to apply the boost along the $\tilde{z}$ direction but since it is not a symmetry direction, there is an ambiguity about how one defines the boost in the interior of spacetime. One natural choice would be to set

$$\mathrm{d}\tilde{t} \pm \mathrm{d}\tilde{z} = e^{\pm\gamma}\left(\mathrm{d}t \pm \mathrm{d}z\right), \tag{D.15}$$

where γ is the boosting parameter and the new horizon geometry is setted by $t = \text{const.}, r = r_0$ in the metric

$$\mathrm{d}s^2 = 16\left(\cosh^2\gamma\,\mathrm{d}z^2 + \mathrm{d}\rho^2 + \rho^2\,\mathrm{d}\phi^2\right). \tag{D.16}$$

The horizon is spanned by t, z and ρ via

$$r_0^2 = r^2 = (\cosh\gamma\cdot z + \sinh\gamma\cdot t)^2 + \rho^2, \tag{D.17}$$

and differentiating this equation at constant times ($\mathrm{d}t = 0$) yields

$$(\cosh\gamma\,\mathrm{d}z)^2 = \frac{\rho^2\,\mathrm{d}\rho^2}{r_0^2 - \rho^2}, \tag{D.18}$$

such that the static metric on the horizon is given as

$$\mathrm{d}s_h^2 = 16\left(\frac{r_0^2\,\mathrm{d}\rho^2}{r_0^2-\rho^2} + \mathrm{d}\phi^2\right) \tag{D.19}$$

which is indeed independent of the boost and describes a round sphere. This illustrates that the horizon of the four-dimensional Schwarzschild black hole does not Lorentz contract. On the contrary, the metric element (D.16) expands under a boost. This means that even though the black hole horizon does not Lorentz contract, the spacetime itself expands such that it can accommodate the black hole. Hence, by boosting black holes one can expand the spacetime such that even a large black hole fits in it. The same argument holds for higher dimensional black holes such the one in ten-and-eleven dimensions. In fact the reason for this analysis is because this scenario applies to black holes boosted along the x_{11} dimension to connect type IIA string theory with M-theory. As a consequence, this also applies to matrix models better depicted in Fig. 4.15.

List of Figures

Acknowledgments

As I am reaching one of my Ithakas it certainly worths stressing that I had the privilege of never being alone in this journey. I was accompanied by a generous number of co-travellers who made my journey more pleasant and easily accessible. To this end, I want to thank my family for their love, and support throughout the pursuit of my studies and research until now. A special thanks goes to my supervisor Norbert Bodendorfer who granted me the privilege to pursue high-end research showing me at the same time the importance of being impartial, and remaining true to the scientific beliefs and ethics. He is indeed a scientist that academia worths having. I also thank him for showing patience with my programming development and also exposing me to the ideas of loop quantum gravity. I acknowledge also the Elite Network of Bavaria for financial support during this time. The numerical simulations were performed on ATHENE, the HPC cluster of the Regensburg University Compute Centre.

I was fortunate to be in a stimulating office environment with high-qualified, open-minded colleagues who had also high-quality scientific ethics. To this end, I would also like to thank my colleagues at the beginning of my Ph.D. period and my current friends, Fabio M. Mele and Johannes Münch who warmly welcomed me into the office. In a retrospective analysis of an empty office, I realise now how much I enjoyed being a disturber of the piece in the office. I tried to teach an Italian that it is fine to put ice cubes in espresso to make a freddo espresso and I tried to convince a German that I.P.A is indeed a beer. Nevertheless, I thank them for being patient with my never-ending confusion and for sharing their thoughts and also their confusion with me. Phrases beginning with: "I have a question..." were creating a stimulating interchange of ideas on physics, such as the diffeomorphisms of general relativity, and ideas on the (non)physical world such as how many dimensions we see and experience, ending several hours later being on the blackboard or in a bar where usually we were more confused than in the beginning. It turns out that indeed we see two dimensions, while movement along the third dimension creates a 3D perception. There is, of course, research for this [339] (see also [340, 341] falling in the branch of Psychophysics [342]!) while for the 3D perception, more than one hundred years ago, not so unexpected, a giant of Mathematics discussed this [343]. Poincaré realised the importance of moving along the third dimension to produce a 3D perception and experience a three-dimensional world. In the same way, movement along the fourth dimension creates the illusion of time, the so-called perception of the fourth dimension. On the other hand, the latter issue, perhaps connected with spacetime diffeomorphisms and general covariance, remains still under investigation.

I am also grateful to Andreas Schäfer for providing guidance, experience and useful discussions during my academic life, and for collaborating on some projects. I am also grateful to Masanori Hanada for direct collaboration and useful discussions on Skype, about projects, more general topics in physics, and interesting stories. I benefited also from the MCSMC collaboration where, in addition, I had interesting discussions with its members.

I would also like to thank Bianca who appeared in my life and made it brighter in dark times.

The importance to have people on whom you can count and share and discuss issues of life and benefit from them is again a privilege. These people also include Christos and Konstantina for reminding me of the Greek culture in Germany. Moreover, Marco, Daniela, Saeed, Saeed, and Saba. In particular, I have enjoyed discussions on physical, sociological, philosophical, genetic, and mathematical matters, from German, Greek, Italian and Iranian people, cultures that emanate from the same ancient roots.

I would like to thank Günter and Susanne for providing me with a wonderful place to live and making my stay here in Regensburg more pleasant. I thank, in addition, my cousin Stratos and his girlfriend Maria for reading the introduction and conclusions of this dissertation and providing useful comments on my English skills.

I thank also my Greek friends who always believed in me and for asking interesting questions about physics, making me a better teacher. In particular, Giannis, Giannis, Giorgos, Fotis, Nikos, Savvas and my brother Thomas.

During my studies, I have met many interesting people, scientists, current friends, and colleagues. Spanning a (hyper)worldvolume, people interact with each other in many trivial and non-trivial ways. These interactions, whether we realise it or not, remain in our worldvolumes as information, conscious (such as memories), and subconscious. These interactions help us to become who we are, and how we think. To this end, I would also like to thank each one whom I have interacted with and improved the way I think, making me a better scientist, but most importantly a better human being.

Translations of epigraphs

These epigraphs are all taken from written words of ancient philosophers, either as part of a phrase or as a whole sentence. As such, one cannot really hope to understand their *philosophical* meaning if one reads them superficially and not adding important philosophical dimensions. For the convenience of the interested reader we are presenting here a crude translation from the author of the thesis while a deep exploration should be looked elsewhere.

- **Chapter 1** *Αρχή σοφίας της αγνοίας η γνώσις*: The beginning of wisdom is to understand what you do not know.
- **Chapter 2** *Ετεή δε ουδέν ίδμεν. Εν βυθώ γαρ η αλήθεια*: We know nothing. Because truth lies deep in the bottom.
- **Chapter 3** *Φύσις κρύπτεσθαι φιλεί*: Nature likes to hide.
- **Chapter 4** *Τα πάντα ρει*: Everything flows.
- **Chapter 5** *Αεί ο θεός γεωμετρεί*: God always geometrizes.
- **Chapter 6** *Εάν μη έλπηται ανέλπιστον, ουκ εξευρήσει*: If you do not hope for the hopeless you will never find it.

Bibliography

[1] B. Odom, D. Hanneke, B. D'urso and G. Gabrielse, *New measurement of the electron magnetic moment using a one-electron quantum cyclotron*, *Physical Review Letters* **97** (2006) 030801.

[2] G.t. Hooft, *The Holographic Principle*, in *Basics Highlights Fundam. Phys.*, pp. 72–100, WORLD SCIENTIFIC, apr, 2001, DOI.

[3] L. Susskind, *The World as a Hologram*, *J. Math. Phys.* **36** (1994) 6377 [9409089].

[4] S.W. Hawking, *Black hole explosions?*, *Nature* **248** (1974) 30.

[5] S.W. Hawking, *Gravitational Radiation from Colliding Black Holes*, *Phys. Rev. Lett.* **26** (1971) 1344.

[6] J.M. Bardeen, B. Carter and S.W. Hawking, *The four laws of black hole mechanics*, *Communications in Mathematical Physics* **31** (1973) 161.

[7] J.D. Bekenstein, *Black Holes and Entropy*, *Physical Review D* **7** (1973) 2333.

[8] J.D. Bekenstein, *Generalized second law of thermodynamics in black-hole physics*, *Physical Review D* **9** (1974) 3292.

[9] A. Strominger and C. Vafa, *Microscopic origin of the Bekenstein-Hawking entropy*, *Physics Letters B* **379** (1996) 99 [9601029].

[10] A. Strominger, *Black Hole Entropy from Near-Horizon Microstates*, Tech. Rep. (1998).

[11] S. Carlip, *Black Hole Entropy from Conformal Field Theory in Any Dimension*, *Physical Review Letters* **82** (1999) 2828 [9812013].

[12] A. Dabholkar, *Exact Counting of Supersymmetric Black Hole Microstates*, *Physical Review Letters* **94** (2005) 241301 [0409148].

[13] A. Sen, *Black hole entropy function, attractors and precision counting of microstates*, *Gen. Relativ. Gravit.* **40** (2008) 2249.

[14] S. Kloster, J. Brannlund and A. DeBenedictis, *Phase space and black-hole entropy of higher genus horizons in loop quantum gravity*, *Classical and Quantum Gravity* **25** (2008) 65008 [0702036].

[15] K. Krasnov and C. Rovelli, *Black holes in full quantum gravity*, *Classical and Quantum Gravity* **26** (2009) 245009 [arXiv:0905.4916 [gr-qc]].

[16] J.F.B. G. and E.J.S. Villaseñor, *The thermodynamic limit and black hole entropy in the area ensemble*, .

[17] E. Frodden, M. Geiller, K. Noui and A. Perez, *Black-hole entropy from complex Ashtekar variables*, *Europhysics Letters* **107** (2014) 10005 [arXiv:1212.4060 [gr-qc]].

[18] A. Ashtekar, J. Baez and K. Krasnov, *Quantum Geometry of Isolated Horizons and Black Hole Entropy*, *Advances in Theoretical and Mathematical Physics* **4** (2000) 1 [0005126].

[19] E. Frodden, M. Geiller, K. Noui and A. Perez, *Statistical entropy of a BTZ black hole from loop quantum gravity*, *Journal of High Energy Physics* **2013** (2013) 139 [arXiv:1212.4473 [gr-qc]].

[20] S.D. Mathur, *The VECRO hypothesis*, Tech. Rep. (2020).

[21] A. Ashtekar, J. Engle and C. Van Den Broeck, *Quantum horizons and black-hole entropy: inclusion of distortion and rotation*, *Classical and Quantum Gravity* **22** (2005) L27 [0412003].

[22] A. Ghosh and A. Perez, *Black hole entropy and isolated horizons thermodynamics*, .

[23] E. Bianchi, *Entropy of Non-Extremal Black Holes from Loop Gravity*, arXiv:1204.5122 [gr-qc].

[24] M. Bañados, C. Teitelboim and J. Zanelli, *Black hole entropy and the dimensional continuation of the Gauss-Bonnet theorem*, *Physical Review Letters* **72** (1994) 957 [9309026].

[25] A. Perez and D. Pranzetti, *Static isolated horizons: SU(2) invariant phase space, quantization, and black hole entropy*, *Entropy* **13** (2011) 744 [arXiv:1011.2961 [gr-qc]].

[26] T. Jacobson, *Black Hole Entropy and Induced Gravity*, 9404039.

[27] K.V. Krasnov, *On Quantum Statistical Mechanics of a Schwarzschild Black Hole*, 1998. 10.1023/A:1018820916342.

[28] E.R. Livine and D.R. Terno, *Quantum Black Holes: Entropy and Entanglement on the Horizon*, *Nucl. Phys. B* **741** (2005) 131 [0508085].

[29] R.K. Kaul and P. Majumdar, *Quantum black hole entropy*, *Physics Letters B* **439** (1998) 267 [9801080].

[30] J. Engle, K. Noui and A. Perez, *Black Hole Entropy and SU(2) Chern-Simons Theory*, *Physical Review Letters* **105** (2010) 31302 [arXiv:0905.3168 [gr-qc]].

[31] C. Rovelli, *Black Hole Entropy from Loop Quantum Gravity*, *Physical Review Letters* **77** (1996) 3288 [9603063].

[32] M. David, J. Nian and L.A.P. Zayas, *Gravitational Cardy Limit and AdS Black Hole Entropy*, 2005.10251.

[33] P. Mitra, *Area law for black hole entropy in the SU(2) quantum geometry approach*, 1107.4605.

[34] L. Modesto, *Space-Time Structure of Loop Quantum Black Hole*, *Int. J. Theor. Phys.* **49** (2008) 1649 [0811.2196].

[35] V. Husain, *Apparent horizons, black hole entropy, and loop quantum gravity*, *Physical Review D* **59** (1999) 84019 [9806115].

[36] A. Ghosh, K. Noui and A. Perez, *Statistics, holography, and black hole entropy in loop quantum gravity*, *Physical Review D* **89** (2014) 84069 [arXiv:1309.4563 [gr-qc]].

[37] G.T. Horowitz and E.J. Martinec, *Comments on Black Holes in Matrix Theory*, 9710217.

[38] Y. Nomura, J. Varela and S.J. Weinberg, *Black Holes, Information, and Hilbert Space for Quantum Gravity*, *Phys. Rev. D* **87** (2012) 84050 [1210.6348].

[39] T. Jacobson, *On the nature of black hole entropy*, in *Eighth Canadian conference on general relativity and relativistic astrophysics*, pp. 85–97, ASCE, aug, 1999, DOI [9908031].

[40] D. Oriti, D. Pranzetti and L. Sindoni, *Black holes as quantum gravity condensates*, *Physical Review D* **97** (2018) 066017 [arXiv:1801.01479 [gr-qc]].

[41] M. Domagala and J. Lewandowski, *Black-hole entropy from quantum geometry*, *Classical and Quantum Gravity* **21** (2004) 5233 [0407051].

[42] R.D. Sorkin, *Ten Theses on Black Hole Entropy*, 0504037.

[43] J. Barbero G., J. Lewandowski and E. Villasenor, *Flux-area operator and black hole entropy*, *Physical Review D* **80** (2009) 44016 [arXiv:0905.3465 [gr-qc]].

[44] P. Nicolini and E. Spallucci, *Holographic screens in ultraviolet self-complete quantum gravity*, *Adv. High Energy Phys.* **2014** (2012) 1 [1210.0015].

[45] J. Maldacena, *The Large N Limit of Superconformal Field Theories and Supergravity*, *Advances in Theoretical and Mathematical Physics* **2** (1998) 231 [9711200].

[46] J. Erdmenger, *Introduction to gauge/gravity duality*, *Lecture Notes in Physics* **851** (2012) 99.

[47] N. Engelhardt and G.T. Horowitz, *New insights into quantum gravity from gauge/gravity duality*, *International Journal of Modern Physics D* **25** (2016) 1643002 [arXiv:1605.04335 [hep-th]].

[48] M. Ammon and J. Erdmenger, *Gauge/Gravity Duality: Foundations and Applications*, Cambridge University Press (2015).

[49] N. Itzhaki, J.M. Maldacena, J. Sonnenschein and S. Yankielowicz, *Supergravity and the large N limit of theories with sixteen supercharges*, *Physical Review D - Particles, Fields, Gravitation and Cosmology* **58** (1998) 11 [9802042v3].

[50] O. Aharony, S.S. Gubser, J. Maldacena, H. Ooguri and Y. Oz, *Large N Field Theories, String Theory and Gravity*, *Phys. Rep.* **323** (1999) 183 [9905111].

[51] J. Polchinski, *Dirichlet Branes and Ramond-Ramond Charges*, *Physical Review Letters* **75** (1995) 4724 [9510017].

[52] C.V. Johnson, *D-Branes*, *D-Branes* (2002) .

[53] T. Banks, W. Fischler, S.H. Shenker and L. Susskind, *M theory as a matrix model: A Conjecture*, *Phys. Rev.* **D55** (1997) 5112 [hep-th/9610043].

[54] P. Horava and E. Witten, *Heterotic and Type I String Dynamics from Eleven Dimensions*, *Nuclear Physics B* **460** (1995) 506 [9510209v2].

[55] J. Polchinski, *String Theory, Vol. 1: An Introduction to the bosonic string*, Cambridge University Press, Cambridge (1998).

[56] J. Polchinski, *String Theory, Vol. 2: Superstring theory and beyond*, Cambridge University Press, Cambridge (1998).

[57] M.B. Green, J.H. Schwarz and E. Witten, *Superstring Theory, Vol. 1: Introduction*, Cambridge University Press, Cambridge (1988).

[58] M.B. Green, J.H. Schwarz and E. Witten, *Superstring Theory, Vol. 2: Loop Amplitudes, Anomalies and Phenomenology*, Cambridge University Press, Cambridge (1988).

[59] E. Kiritsis, *String theory in a nutshell*, *Book* 855.

[60] K. Becker, M. Becker and J.H. Schwarz, *String Theory and M-Theory: A Modern Introduction*, Cambridge University Press, Cambridge (2006), DOI: 10.1017/CBO9780511816086.

[61] B. Zwiebach, *A first course in string theory*, *Book* (2009) 673.

[62] H. Erbin, *String Field Theory*, *Book* **980** (2021) .

[63] J. Polchinski, *arXiv:hep-th/9611050v2 23 Apr 1997*, 9611050v2.

[64] J. Polchinski, *Dirichlet branes and Ramond-Ramond charges*, *Physical Review Letters* **75** (1995) 4724 [9510017].

[65] A. Sen, *An Introduction to Non-perturbative String Theory*, 9802051.

[66] E. D'Hoker and D.H. Phong, *The geometry of string perturbation theory*, *RvMP* **60** (1988) 917.

[67] R. Jackiw, *Another View on Massless Matter-Gravity Fields in Two Dimensions*, 9501016.

[68] W. Taylor and Y.N. Wang, *The F-theory geometry with most flux vacua*, *Journal of High Energy Physics* **2015** (2015) 1 [1511.03209].

[69] T. Kaluza, Kaluza and Theodor, *Zum Unitätsproblem der Physik*, *SPAW* (1921) 966.

[70] O. Klein, *Quantentheorie und fünfdimensionale Relativitätstheorie*, *Zeitschrift für Physik* **37** (1926) 895.

[71] E. Cremmer, B. Julia and J. Scherk, *Supergravity theory in 11 dimensions*, *Physics Letters B* **76** (1978) 409.

[72] M Huq and M A Namazie, *Kaluza-Klein supergravity in ten dimensions*, 1985. 10.1088/0264-9381/2/3/007.

[73] E. Bergshoeff, E. Sezgin, P.K. Townsend, E. Bergshoeff, E. Sezgin and P.K. Townsend, *Supermembranes and eleven-dimensional supergravity*, *PhLB* **189** (1987) 75.

[74] I. Bars, C.N. Pope and E. Sezgin, *Massless spectrum and critical dimension of the supermembrane*, *PhLB* **198** (1987) 455.

[75] M.J. Duff, P.S. Howe, T. Inami, K.S. Stelle, M.J. Duff, P.S. Howe et al., *Superstrings in D=10 from supermembranes in D=11*, *PhLB* **191** (1987) 70.

[76] M.J. Duff, K.S. Stelle, M.J. Duff and K.S. Stelle, *Multi-membrane solutions of D = 11 supergravity*, *PhLB* **253** (1991) 113.

[77] M.J. Duff, G.W. Gibbons and P.K. Townsend, *Macroscopic superstrings as interpolating solitons*, *Physics Letters B* **332** (1994) 321 [9405124].

[78] R. Güven, *Black p-brane solutions of D=11 supergravity theory*, *Physics Letters B* **276** (1992) 49.

[79] G.W. Gibbons, G.W. Gibbons, G.T. Horowitz and P.K. Townsend, *Higher-dimensional resolution of dilatonic black hole singularities*, .

[80] R.I. Nepomechie and R. I., *Magnetic monopoles from antisymmetric tensor gauge fields*, *PhRvD* **31** (1985) 1921.

[81] C. Hull, *Unity of superstring dualities*, *Nuclear Physics B* **438** (1995) 109 [9410167].

[82] W. Rarita and J. Schwinger, *On a Theory of Particles with Half-Integral Spin*, *Physical Review* **60** (1941) 61.

[83] P.K. Townsend, Townsend and P. K., *p-Brane Democracy*, *arXiv* (1995) hep [9507048].

[84] R.C. Myers, *Dielectric-Branes arXiv : hep-th / 9910053v2 11 Oct 1999*, 9910053v2.

[85] P.D. Francesco, P. Ginsparg and J. Zinn-Justin, *2D gravity and random matrices*, mar, 1995. 10.1016/0370-1573(94)00084-G.

[86] K.L. Zarembo and Y.M. Makeenko, *An introduction to matrix superstring models*, *Physics-Uspekhi* **41** (1998) 1.

[87] P. Ginsparg and G. Moore, *Lectures on 2D gravity and 2D string theory (TASI 1992)*, 9304011.

[88] M. Hanada, H. Kawai and Y. Kimura, *Describing curved spaces by matrices*, *Progress of Theoretical Physics* **114** (2005) 1295 [0508211].

[89] D. Berenstein, J. Maldacena and H. Nastase, *Strings in flat space and pp waves from Script N = 4 Super Yang Mills*, *Journal of High Energy Physics* **2002** (2002) 013 [0202021v3].

[90] V.A. Kazakov, *Bilocal regularization of models of random surfaces*, *Physics Letters B* **150** (1985) 282.

[91] J. Koplik, A. Neveu and S. Nussinov, *Some aspects of the planar perturbation series*, *Nuclear Physics, Section B* **123** (1977) 109.

[92] J. Ambjørn, B. Durhuus and J. Fröhlich, *Diseases of triangulated random surface models, and possible cures*, *Nuclear Physics B* **257** (1985) 433.

[93] F. David, *Planar diagrams, two-dimensional lattice gravity and surface models*, *Nuclear Physics B* **257** (1985) 45.

[94] A.M. Polyakov, *Quantum geometry of bosonic strings*, *Physics Letters B* **103** (1981) 207.

[95] V.G. Knizhnik, A.M. Polyakov, A.B. Zamolodchikov, V.G. Knizhnik, A.M. Polyakov and A.B. Zamolodchikov, *Fractal Structure of 2d—QUANTUM Gravity*, *MPLA* **3** (1988) 819.

[96] G. Hooft, *A planar diagram theory for strong interactions*, *Nucl. Phys. B* **72** (1974) 461.

[97] V.A. Kazakov, I.K. Kostov and A.A. Migdal, *Critical properties of randomly triangulated planar random surfaces*, *Physics Letters B* **157** (1985) 295.

[98] B. de Wit, J. Hoppe, H. Nicolai, B. de Wit, J. Hoppe and H. Nicolai, *On the quantum mechanics of supermembranes*, *NuPhB* **305** (1988) 545.

[99] E. Witten, *String theory dynamics in various dimensions*, *Nuclear Physics B* **443** (1995) 85 [9503124].

[100] W. Taylor and M. Van Raamsdonk, *Multiple D0-branes in Weakly Curved Backgrounds*, *Nuclear Physics B* **558** (1999) 63 [9904095].

[101] P.K. Townsend, *Four Lectures on M-theory*, 9612121.

[102] P.A.M. Dirac, *Lectures on Quantum Mechanics*, Belfer Graduate School of Science, Yeshiva University Press, New York (1964).

[103] Jens Hoppe, *Quantum Theory of a Massless Relativistic Surface and a Two-Dimensional Bound State Problem.*, *PhDT* (1982) .

[104] W. Taylor, *The M(atrix) model of M-theory*, 0002016.

[105] J. Madore, *The fuzzy sphere*, *Classical and Quantum Gravity* **9** (1992) 69.

[106] J. HOPPE, *DIFFEOMORPHISM GROUPS, QUANTIZATION, AND SU (∞)*, *International Journal of Modern Physics A* **04** (1989) 5235.

[107] M.J. Duff, *Supermembranes*, 9611203v2.

[108] B. De Wit, M. Luscher and H. Nicolai, *THE SUPERMEMBRANE IS UNSTABLE*, *Nuclear Physics* **320** (1989) 135.

[109] B. De Wit, K. Peeters and J.C. Plefka, *Supermembranes with winding*, *Physics Letters, Section B: Nuclear, Elementary Particle and High-Energy Physics* **409** (1997) 117 [9705225].

[110] L. Brink, J.H. Schwarz and J. Scherk, *Supersymmetric Yang-Mills theories*, *Nucl. Phys., B; (Netherlands)* **121:1** (1977) .

[111] E. Witten, *Bound states of strings and p-branes*, *Nuclear Physics B* **460** (1996) 335 [9510135].

[112] N. Kim, T. Klose and J. Plefka, *Plane-wave matrix theory from N=4 super-Yang–Mills on RxS3*, *Nuclear Physics B* **671** (2003) 359.

[113] M. Hanada, *Bulk geometry in gauge/gravity duality and color degrees of freedom*, 2102.08982.

[114] N. Ishibashi, H. Kawai, Y. Kitazawa and A. Tsuchiya, *A large-N reduced model as superstring*, *Nuclear Physics B* **498** (1997) 467 [9612115].

[115] A. Connes, *Gravity coupled with matter and the foundation of non-commutative geometry*, *Communications in Mathematical Physics* **182** (1996) 155 [9603053].

[116] C. Sochichiu, *M[any] vacua of IIB*, *JHEP* **05** (2000) 026.

[117] A. Connes, M.R. Douglas and A. Schwarz, *Noncommutative geometry and matrix theory: Compactification on tori*, *Journal of High Energy Physics* **2** (1998) [9711162].

[118] A. Konechny and A. Schwarz, *Introduction to M(atrix) theory and noncommutative geometry*, *Physics Report* **360** (2002) 353 [0012145].

[119] A. Konechny and A. Schwarz, *Introduction to M(atrix) theory and noncommutative geometry, Part II*, *arXiv* (2001) hep [0107251].

[120] J. Nishimura, *The origin of space-time as seen from matrix model simulations*, *Progress of Theoretical and Experimental Physics* **2012** (2012) [arXiv:1205.6870v1].

[121] J. Nishimura, T. Okubo and F. Sugino, *Systematic study of the SO(10) symmetry breaking vacua in the matrix model for type IIB superstrings*, 1108.1293.

[122] K.N. Anagnostopoulos, T. Azuma, Y. Ito, J. Nishimura, T. Okubo and S. Kovalkov Papadoudis, *Complex Langevin analysis of the spontaneous breaking of 10D rotational symmetry in the Euclidean IKKT matrix model*, *JHEP06* (2020) 69.

[123] K.N. Anagnostopoulos, T. Azuma, Y. Ito, J. Nishimura and S. Kovalkov Papadoudis, *Complex Langevin analysis of the spontaneous symmetry breaking in dimensionally reduced super Yang-Mills models*, *JHEP02* (2018) 151.

[124] K.N. Anagnostopoulos, T. Azuma, Y. Ito, J. Nishimura cd and S. Kovalkov Papadoudis, *Dynamical compactification of extra dimensions in the Euclidean type IIB matrix model: A numerical study using the complex Langevin method Dynamical compactification of extra dimensions*, 1906.01841v1.

[125] N. Seiberg, *Why Is the Matrix Model Correct?*, *Physical Review Letters* **79** (1997) 3577 [9710009v1].

[126] L. Susskind, *Another Conjecture about M(atrix) Theory*, 9704080.

[127] D. Kabat and W. Taylor IV, *Linearized supergravity from Matrix theory*, *Physics Letters, Section B: Nuclear, Elementary Particle and High-Energy Physics* **426** (1998) 297 [9712185v3].

[128] R.C. Myers, *Dielectric-Branes arXiv : hep-th / 9910053v2 11 Oct 1999*, 9910053v2.

[129] R.C. Myers, *Non-Abelian phenomena on D-branes*, *Classical and Quantum Gravity* **20** (2003) [0303072v2].

[130] J.M. Maldacena, *The Large N limit of superconformal field theories and supergravity*, *Int. J. Theor. Phys.* **38** (1999) 1113 [hep-th/9711200].

[131] R. Gregory and R. Laflamme, *Black strings and p-branes are unstable*, *Physical Review Letters* **70** (1993) 2837 [9301052].

[132] Y. Hyakutake, *Quantum near-horizon geometry of a black 0-brane*, *Progress of Theoretical and Experimental Physics* **2014** (2014) 0 [arXiv:1311.7526v3].

[133] J. Maldacena and A. Milekhin, *To gauge or not to gauge?*, *Journal of High Energy Physics* **2018** (2018) 0 [1802.00428].

[134] E. Berkowitz, E. Rinaldi, M. Hanada, G. Ishiki, S. Shimasaki and P. Vranas, *Precision lattice test of the gauge/gravity duality at large-N*, *Phys. Rev.* **D94** (2016) 94501 [1606.04951].

[135] E. Rinaldi, E. Berkowitz, M. Hanada, J. Maltz and P. Vranas, *Toward Holographic Reconstruction of Bulk Geometry from Lattice Simulations*, *JHEP* **02** (2018) 42 [1709.01932].

[136] M. Hanada, G. Ishiki and H. Watanabe, *Partial Deconfinement*, 1812.05494.

[137] N. Kawahara, J. Nishimura and S. Takeuchi, *Phase structure of matrix quantum mechanics at finite temperature*, *JHEP* **10** (2007) 97 [0706.3517].

[138] E. Berkowitz, M. Hanada, E. Rinaldi and P. Vranas, *Gauged And Ungauged: A Nonperturbative Test*, *JHEP* **06** (2018) 124 [1802.02985].

[139] D. Kadoh, *Precision test of the gauge/gravity duality in two-dimensional N=(8,8) SYM*, *PoS* **LATTICE201** (2017) 33 [1702.01615].

[140] S. Catterall, R.G. Jha, D. Schaich and T. Wiseman, *Testing holography using lattice super-Yang-Mills theory on a 2-torus*, *Phys. Rev.* **D97** (2018) 86020 [1709.07025].

[141] H. Gharibyan, M. Hanada, M. Honda and J. Liu, *Toward simulating Superstring/M-theory on a quantum computer*, 2011.06573.

[142] S. Catterall, J. Giedt, R.G. Jha, D. Schaich and T. Wiseman, *Three-dimensional super-Yang–Mills theory on the lattice and dual black branes*, 2010.00026.

[143] V.G. Filev and D. O'Connor, *The BFSS model on the lattice*, *JHEP* **05** (2016) 167 [1506.01366].

[144] D. Kadoh and S. Kamata, *Gauge/gravity duality and lattice simulations of one dimensional SYM with sixteen supercharges*, 1503.08499.

[145] S. Catterall and T. Wiseman, *Extracting black hole physics from the lattice*, *JHEP* **04** (2010) 077 [0909.4947].

[146] M. Hanada, A. Miwa, J. Nishimura and S. Takeuchi, *Schwarzschild radius from Monte Carlo calculation of the Wilson loop in supersymmetric matrix quantum mechanics*, *Phys. Rev. Lett.* **102** (2009) 181602 [0811.2081].

[147] M. Hanada, J. Nishimura and S. Takeuchi, *Non-lattice simulation for supersymmetric gauge theories in one dimension*, *Phys. Rev. Lett.* **99** (2007) 161602 [0706.1647].

[148] E. Berkowitz, M. Hanada and J. Maltz, *Chaos in Matrix Models and Black Hole Evaporation*, *Phys. Rev.* **D94** (2016) 126009 [1602.01473].

[149] E. Berkowitz, M. Hanada and J. Maltz, *A microscopic description of black hole evaporation via holography*, *Int. J. Mod. Phys.* **D25** (2016) 1644002 [1603.03055].

[150] S. Catterall and T. Wiseman, *Black hole thermodynamics from simulations of lattice Yang-Mills theory*, *Phys. Rev.* **D78** (2008) 41502 [0803.4273].

[151] K. Furuuchi, E. Schreiber and G.W. Semenoff, *Five-brane thermodynamics from the matrix model*, hep-th/0310286.

[152] D. Berenstein, *Submatrix deconfinement and small black holes in AdS*, *JHEP* **09** (2018) 54 [1806.05729].

[153] M. Blau, *Plane waves and Penrose limits*, *Lecture Notes for the ICTP School on Mathematics in ...* (2004) .

[154] R. Penrose, *Any Space-Time has a Plane Wave as a Limit*, *Differential Geometry and Relativity* (1976) 271.

[155] J. Kowalski-Glikman, *Vacuum states in supersymmetric Kaluza-Klein theory*, *Physics Letters B* **134** (1984) 194.

[156] M. Blau, J. Figueroa-O'Farrill, C. Hull and G. Papadopoulos, *Penrose limits and maximal supersymmetry*, *Classical and Quantum Gravity* **19** (2002) [0201081].

[157] K. Dasgupta, M.M. Sheikh-Jabbari and M. Van Raamsdonk, *Matrix perturbation theory for M-theory on a pp-wave*, *Journal of High Energy Physics* **6** (2002) 1333 [0205185v4].

[158] H. Lin, O. Lunin and J. Maldacena, *Bubbling AdS space and 1/2 BPS geometries*, *Journal of High Energy Physics* **8** (2004) 501 [0409174v2].

[159] H. Lin, *The supergravity dual of the BMN matrix model*, *Journal of High Energy Physics* **8** (2004) 1 [0407250v2].

[160] H. Lin and J. Maldacena, *Fivebranes from gauge theory*, *Physical Review D - Particles, Fields, Gravitation and Cosmology* **74** (2006) [0509235].

[161] H. Lin, *Instantons, supersymmetric vacua, and emergent geometries*, *Physical Review D - Particles, Fields, Gravitation and Cosmology* **74** (2006) 1 [0609186].

[162] J. Maldacena, M.M. Sheikh-Jabbari and M. Van Raamsdonk, *Transverse fivebranes in matrix theory*, *Journal of High Energy Physics* **7** (2003) 829 [0211139v2].

[163] J. Polchinski, *M-theory and the light cone*, *Progress of Theoretical Physics Supplement* (1999) 158 [9903165].

[164] E. Rinaldi, E. Berkowitz, M. Hanada, J. Maltz and P. Vranas, *Toward holographic reconstruction of bulk geometry from lattice simulations*, *Journal of High Energy Physics* **2018** (2018) [arXiv:1709.01932v2].

[165] K. Zarembo, *Coleman-Weinberg Mechanism and Interaction of D3-Branes in Type 0 String Theory*, .

[166] M.S. Costa, L. Greenspan, J. Penedones and J.E. Santos, *Thermodynamics of the BMN matrix model at strong coupling*, *Journal of High Energy Physics* **2015** (2015) 1 [arXiv:1411.5541v1].

[167] B. Sundborg, *The Hagedorn transition, deconfinement and N=4 SYM theory*, *Nucl. Phys.* **B573** (2000) 349 [hep-th/9908001].

[168] O. Aharony, J. Marsano, S. Minwalla, K. Papadodimas and M. Van Raamsdonk, *The Hagedorn/Deconfinement Phase Transition in Weakly Coupled Large N Gauge Theories*, *Comptes Rendus Physique* **5** (2003) 945 [0310285].

[169] A.M. Polyakov, *String theory and quark confinement*, *Nuclear Physics B - Proceedings Supplements* **68** (1998) 1 [9711002].

[170] G.t. Hooft, *Under the spell of the gauge principle*, .

[171] A.M. Polyakov, *Thermal properties of gauge fields and quark liberation*, *Physics Letters B* **72** (1978) 477.

[172] J.C. Collins and M.J. Perry, *Superdense Matter: Neutrons or Asymptotically Free Quarks?*, *Physical Review Letters* **34** (1975) 1353.

[173] C.B. Thorn, *Infinite Nc QCD at finite temperature: Is there an ultimate temperature?*, *Physics Letters B* **99** (1981) 458.

[174] G. 't Hooft, *On the phase transition towards permanent quark confinement*, *Nuclear Physics B* **138** (1978) 1.

[175] D.J. Gross and E. Witten, *Possible third-order phase transition in the large-N lattice gauge theory*, *Physical Review D* **21** (1980) 446.

[176] M. Hanada, *What lattice theorists can do for superstring/M-theory*, *International Journal of Modern Physics A* **31** (2016) 1643006 [arXiv:1604.05421 [hep-lat]].

[177] M. Hanada, *Markov Chain Monte Carlo for Dummies*, 1808.08490.

[178] J.M. Bardeen, B. Carter and S.W. Hawking, *The four laws of black hole mechanics*, *Communications in Mathematical Physics* **31** (1973) 161.

[179] E. Witten, *Anti-de Sitter Space, Thermal Phase Transition, And Confinement In Gauge Theories*, *Adv. Theor. Math. Phys.* **2** (1998) 505 [9803131].

[180] V. Cardoso and O.J.C. Dias, *Rayleigh-Plateau and Gregory-Laflamme instabilities of black strings*, Tech. Rep. (2006).

[181] G. Mandal and T. Morita, *Gregory-Laflamme as the confinement/deconfinement transition in holographic QCD*, *JHEP* **09** (2011) 73 [1107.4048].

[182] G. Mandal, M. Mahato and T. Morita, *Phases of one dimensional large N gauge theory in a 1/D expansion*, *Journal of High Energy Physics* **2010** (2009) [0910.4526].

[183] T. Morita and H. Yoshida, *Critical dimension and negative specific heat in one-dimensional large- N reduced models*, *Physical Review D* **101** (2020) [2001.02109v4].

[184] R. Emparan, *Blackfolds*, .

[185] B. Kol, *The Phase Transition between Caged Black Holes and Black Strings-A Review*, Tech. Rep.

[186] A. Almheiri, T. Hartman, J. Maldacena, E. Shaghoulian and A. Tajdini, *The entropy of Hawking radiation*, Tech. Rep. (2020).

[187] M. Hanada, J. Maltz and L. Susskind, *Deconfinement transition as black hole formation by the condensation of QCD strings*, Tech. Rep.

[188] D.B. Kaplan, *Supersymmetry on the lattice*, *The European Physical Journal Special Topics 2007 152:1* **152** (2007) 89.

[189] G. Bergner and S. Catterall, *Supersymmetry on the lattice*, *International Journal of Modern Physics A* **31** (2016) 1643005 [1603.04478].

[190] M.F. Golterman and D.N. Petcher, *A local interactive lattice model with supersymmetry*, *Nuclear Physics B* **319** (1989) 307.

[191] G. Curci and G. Veneziano, *Supersymmetry and the lattice: A reconciliation?*, *Nuclear Physics B* **292** (1987) 555.

[192] O. Aharony, J. Marsano, S. Minwalla and T. Wiseman, *Black-hole-black-string phase transitions in thermal (1 + 1)-dimensional supersymmetric Yang-Mills theory on a circle*, *Classical and Quantum Gravity* **21** (2004) 5169 [0406210].

[193] G. Bergner, N. Bodendorfer, M. Hanada, E. Rinaldi, A. Schafer and P. Vranas, *Thermal phase transition in Yang-Mills matrix model*, *Journal of High Energy Physics* **2020** (2019) 53 [1909.04592].

[194] G. Bergner, N. Bodendorfer, M. Hanada, S. Pateloudis, E. Rinaldi, A. Schäfer et al., *Confinement/deconfinement transition in the D0-brane matrix model – A signature of M-theory?*, *arXiv e-prints* (2021) arXiv:2110.01312 [2110.01312].

[195] E. Sorkin, *Critical dimension in the black-string phase transition*, *Physical Review Letters* **93** (2004) .

[196] F.R. Tangherlini, *Schwarzschild field in n dimensions and the dimensionality of space problem*, *Il Nuovo Cimento* **27** (1963) 636.

[197] R. Emparan, D. Grumiller and K. Tanabe, *Large D gravity and low D strings*, 1303.1995v2.

[198] G. Mandal, A.M. Sengupta and S.R. Wadia, *Classical solutions of two-dimensional string theory*, *Mod.Phys.Lett.A* **6** (1991) 1685.

[199] S. Elitzur, A. Forge and E. Rabinovici, *Some global aspects of string compactifications*, *Nuclear Physics B* **359** (1991) 581.

[200] E. Witten, *On string theory and black holes*, *Phys.Rev.D* **44** (1991) 314.

[201] J. Soda, *Hierarchical Dimensional Reduction and Gluing Geometries*, *Progress of Theoretical Physics* **89** (1993) 1303.

[202] D. Grumiller, W. Kummer and D.V. Vassilevich, *Dilation gravity in two dimensions*, *Physics Report* **369** (2002) 327.

[203] B. Kol and E. Sorkin, *Black-brane instability in an arbitrary dimension*, *Classical and Quantum Gravity* **21** (2004) 4793.

[204] B. Kol, *Topology change in general relativity, and the black-hole black-string transition*, *Journal of High Energy Physics* (2005) 1245.

[205] R. Emparan and H.S. Reall, *Black rings*, *Classical and Quantum Gravity* **23** (2006) R169 [0608012].

[206] R. Emparan and H.S. Reall, *Black Holes in Higher Dimensions*, *Living Reviews in Relativity* **11** (2008) [arXiv:0801.3471 [hep-th]].

[207] R. Emparan, R. Luna, M. Martínez, R. Suzuki and K. Tanabe, *Phases and Stability of Non-Uniform Black Strings*, 1802.08191v4.

[208] R.C. Myers and M.J. Perry, *Black holes in higher dimensional space-times*, *Annals of Physics* **172** (1986) 304.

[209] B. de Wit, J. Hoppe and H. Nicolai, *On the Quantum Mechanics of Supermembranes*, *Nucl. Phys.* **B305** (1988) 545.

[210] N. Itzhaki, J.M. Maldacena, J. Sonnenschein and S. Yankielowicz, *Supergravity and the large N limit of theories with sixteen supercharges*, *Phys. Rev.* **D58** (1998) 046004 [hep-th/9802042].

[211] D.E. Berenstein, J.M. Maldacena and H.S. Nastase, *Strings in flat space and pp waves from N=4 superYang-Mills*, *JHEP* **04** (2002) 13 [hep-th/0202021].

[212] E. Witten, *String theory dynamics in various dimensions*, *Nucl. Phys. B* **443** (1995) 85 [hep-th/9503124].

[213] E. Cremmer, B. Julia and J. Scherk, *Supergravity Theory in Eleven-Dimensions*, *Phys. Lett. B* **76** (1978) 409.

[214] K.N. Anagnostopoulos, M. Hanada, J. Nishimura and S. Takeuchi, *Monte Carlo studies of supersymmetric matrix quantum mechanics with sixteen supercharges at finite temperature*, *Phys. Rev. Lett.* **100** (2008) 21601 [0707.4454].

[215] J.D. Bekenstein, *Black holes and entropy*, *Phys. Rev. D* **7** (1973) 2333.

[216] S.W. Hawking, *Particle Creation by Black Holes*, *Commun. Math. Phys.* **43** (1975) 199.

[217] S. Catterall, A. Joseph and T. Wiseman, *Thermal phases of D1-branes on a circle from lattice super Yang-Mills*, *JHEP* **12** (2010) 22 [1008.4964].

[218] O. Aharony, S.S. Gubser, J.M. Maldacena, H. Ooguri and Y. Oz, *Large N field theories, string theory and gravity*, *Phys. Rept.* **323** (2000) 183 [9905111].

[219] E. Witten, *Anti-de Sitter space, thermal phase transition, and confinement in gauge theories*, *Adv. Theor. Math. Phys.* **2** (1998) 505 [hep-th/9803131].

[220] O. Aharony, J. Marsano, S. Minwalla, K. Papadodimas and M. Van Raamsdonk, *The Hagedorn - deconfinement phase transition in weakly coupled large N gauge theories*, *Adv. Theor. Math. Phys.* **8** (2004) 603 [hep-th/0310285].

[221] M. Hanada, A. Jevicki, C. Peng and N. Wintergerst, *Anatomy of Deconfinement*, 1909.09118.

[222] M. Hanada, H. Shimada and N. Wintergerst, *Color Confinement and Bose-Einstein Condensation*, 2001.10459.

[223] M. Hanada and B. Robinson, *Partial-symmetry-breaking phase transitions*, *Phys. Rev. D* **102** (2020) 096013.

[224] H. Watanabe, G. Bergner, N. Bodendorfer, S. Shiba Funai, M. Hanada, E. Rinaldi et al., *Partial Deconfinement at Strong Coupling on the Lattice*, 2005.04103.

[225] T. Banks, W. Fischler, I.R. Klebanov and L. Susskind, *Schwarzschild black holes from matrix theory*, *Phys. Rev. Lett.* **80** (1998) 226 [hep-th/9709091].

[226] T. Banks, W. Fischler, I.R. Klebanov and L. Susskind, *Schwarzschild black holes in matrix theory. 2.*, *JHEP* **01** (1998) 008 [hep-th/9711005].

[227] T. Banks, W. Fischler and I.R. Klebanov, *Evaporation of Schwarzschild black holes in matrix theory*, *Phys. Lett. B* **423** (1998) 54 [hep-th/9712236].

[228] G.T. Horowitz and E.J. Martinec, *Comments on black holes in matrix theory*, *Phys. Rev. D* **57** (1998) 4935 [hep-th/9710217].

[229] R. Gregory and R. Laflamme, *Black strings and p-branes are unstable*, *Phys. Rev. Lett.* **70** (1993) 2837 [hep-th/9301052].

[230] Y. Hyakutake, *Boosted Quantum Black Hole and Black String in M-theory, and Quantum Correction to Gregory-Laflamme Instability*, *JHEP* **09** (2015) 067 [1503.05083].

[231] T. Harmark and N.A. Obers, *Phase structure of black holes and strings on cylinders*, *Nucl. Phys. B* **684** (2004) 183 [hep-th/0309230].

[232] B. Kol, *The Phase transition between caged black holes and black strings: A Review*, *Phys. Rept.* **422** (2006) 119 [hep-th/0411240].

[233] G.T. Horowitz and T. Wiseman, *General black holes in Kaluza–Klein theory*, in *Black holes in higher dimensions*, G.T. Horowitz, ed., pp. 69–98 (2012) [1107.5563].

[234] M. Kalisch, *Numerical construction and critical behavior of Kaluza-Klein black holes*, other thesis, Jena U., 2, 2018, 10.22032/dbt.34074, [1802.06596].

[235] J.L. Hovdebo and R.C. Myers, *Black rings, boosted strings and Gregory-Laflamme*, *Phys. Rev. D* **73** (2006) 084013 [hep-th/0601079].

[236] M.S. Costa, L. Greenspan, J. Penedones and J. Santos, *Thermodynamics of the BMN matrix model at strong coupling*, *JHEP* **03** (2015) 069 [1411.5541].

[237] M. Spradlin, M. Van Raamsdonk and A. Volovich, *Two-loop partition function in the planar plane-wave matrix model*, *Phys. Lett.* **B603** (2004) 239 [hep-th/0409178].

[238] M. Hanada, *Bulk geometry in gauge/gravity duality and color degrees of freedom*, 2102.08982.

[239] H. Lin and J.M. Maldacena, *Fivebranes from gauge theory*, *Phys. Rev. D* **74** (2006) 084014 [hep-th/0509235].

[240] Y. Lozano, C. Núñez and S. Zacarías, *BMN vacua, superstars and non-abelian T-duality*, *Journal of High Energy Physics* **2017** (2017) [1703.00417].

[241] J. Madore, *The fuzzy sphere*, *Classical and Quantum Gravity* **9** (1992) 69.

[242] R.C. Myers, *Dielectric branes*, *JHEP* **12** (1999) 022 [hep-th/9910053].

[243] Y. Asano, V.G. Filev, S. Kovacik and D. O'Connor, *The non-perturbative phase diagram of the BMN matrix model*, *JHEP* **07** (2018) 152 [1805.05314].

[244] S. Choi, J. Kim, S. Kim and J. Nahmgoong, *Comments on deconfinement in AdS/CFT*, 1811.08646.

[245] A. Arabi Ardehali, J. Hong and J.T. Liu, *Asymptotic growth of the 4d $\mathcal{N} = 4$ index and partially deconfined phases*, *JHEP* **07** (2020) 073 [1912.04169].

[246] R. Hagedorn, *Statistical thermodynamics of strong interactions at high-energies*, *Nuovo Cim. Suppl.* **3** (1965) 147.

[247] D.J. Gross and E. Witten, *Possible Third Order Phase Transition in the Large N Lattice Gauge Theory*, *Phys. Rev. D* **21** (1980) 446.

[248] S.R. Wadia, *A Study of U(N) Lattice Gauge Theory in 2-dimensions*, 1212.2906.

[249] S.W. Hawking and D.N. Page, *Thermodynamics of Black Holes in anti-De Sitter Space*, *Commun. Math. Phys.* **87** (1983) 577.

[250] M. Hanada, Y. Hyakutake, G. Ishiki and J. Nishimura, *Holographic description of quantum black hole on a computer*, *Science* **344** (2014) 882 [1311.5607].

[251] G.T. Horowitz, *Comments on black holes in string theory*, *Class. Quant. Grav.* **17** (2000) 1107 [hep-th/9910082].

[252] O. Aharony, O. Bergman, D.L. Jafferis and J. Maldacena, *N=6 superconformal Chern-Simons-matter theories, M2-branes and their gravity duals*, *JHEP* **10** (2008) 091 [0806.1218].

[253] B. de Wit, M. Luscher and H. Nicolai, *The Supermembrane Is Unstable*, *Nucl. Phys. B* **320** (1989) 135.

[254] J. Maldacena and A. Milekhin, *To gauge or not to gauge?*, *JHEP* **04** (2018) 084 [1802.00428].

[255] G. Bergner, N. Bodendorfer, M. Hanada, E. Rinaldi, A. Schäfer and P. Vranas, *Thermal phase transition in Yang-Mills matrix model*, *JHEP* **01** (2020) 053 [1909.04592].

[256] D. Schaich, R.G. Jha and A. Joseph, *Thermal phase structure of a supersymmetric matrix model*, *PoS* **LATTICE2019** (2020) 069 [2003.01298].

[257] M.A. Clark and A.D. Kennedy, *The RHMC algorithm for two flavors of dynamical staggered fermions*, *Nucl. Phys. B Proc. Suppl.* **129** (2004) 850 [0309084].

[258] H. Lin, *The Supergravity Dual of the BMN Matrix Model*, *Journal of High Energy Physics* **2004** (2004) 001 [hep-th/0407250].

[259] C. Copetti, A. Grassi, Z. Komargodski and L. Tizzano, *Delayed Deconfinement and the Hawking-Page Transition*, 2008.04950.

[260] T. Yoneya, *Lectures on Higher-Gauge Symmetries from Nambu Brackets and Covariantized M(atrix) Theory*, 12, 2016 [1612.08513].

[261] S. Sachdev and J. Ye, *Gapless spin-fluid ground state in a random quantum Heisenberg magnet*, *prl* **70** (1993) 3339 [cond-mat/9212030].

[262] A. Kitaev, *A simple model of quantum holography, talks at kitp* , http://online.kitp.ucsb.edu/online/entangled15/kitaev/, http://online.kitp.ucsb.edu/online/entangled15/kitaev2/, .

[263] E. Witten, *An SYK-Like Model Without Disorder*, *J. Phys. A* **52** (2019) 474002 [1610.09758].

[264] C. Teitelboim, *Supergravity and hamiltonian structure in two spacetime dimensions*, *Physics Letters B* **126** (1983) 46.

[265] R. Gurau and J.P. Ryan, *Colored Tensor Models - a review*, *SIGMA* **8** (2012) 020 [1109.4812].

[266] E. Rinaldi, X. Han, M. Hassan, Y. Feng, F. Nori, M. McGuigan et al., *Matrix-Model Simulations Using Quantum Computing, Deep Learning, and Lattice Monte Carlo*, *PRX Quantum* **3** (2022) 010324 [2108.02942].

[267] N. Kim and J. Plefka, *On the spectrum of PP wave matrix theory*, *Nucl. Phys. B* **643** (2002) 31 [hep-th/0207034].

[268] K. Dasgupta, M.M. Sheikh-Jabbari and M. Van Raamsdonk, *Protected multiplets of M theory on a plane wave*, *JHEP* **09** (2002) 021 [hep-th/0207050].

[269] N. Kim, T. Klose and J. Plefka, *Plane wave matrix theory from N=4 superYang-Mills on R x S**3*, *Nucl. Phys. B* **671** (2003) 359 [hep-th/0306054].

[270] N. Kim and J.-H. Park, *Superalgebra for M theory on a pp wave*, *Phys. Rev. D* **66** (2002) 106007 [hep-th/0207061].

[271] V.G. Kac, *A sketch of Lie superalgebra theory*, *Communications in Mathematical Physics* **53** (1977) 31 .

[272] G. Bergner, N. Bodendorfer, M. Hanada, E. Rinaldi, A. Schäfer and P. Vranas, *Thermal phase transition in Yang-Mills matrix model*, *Journal of High Energy Physics* **2020** (2020) [1909.04592].

[273] S. Pateloudis, G. Bergner, N. Bodendorfer, M. Hanada, E. Rinaldi and A. Schäfer, *Nonperturbative test of the Maldacena-Milekhin conjecture for the BMN matrix model*, 2205.06098v1.

[274] G. Bergner, N. Bodendorfer, M. Hanada, S. Pateloudis, E. Rinaldi and A. Schäfer, *Precision lattice test of the gauge/gravity duality at low temperature*, *to appear* (2022) .

[275] T. Thiemann, *Lectures on Loop Quantum Gravity*, in *Lect. Notes Phys. 631*, pp. 41–135 (2003), DOI.

[276] T. Thiemann, *Introduction to Modern Canonical Quantum General Relativity*, 0110034.

[277] T. Thiemann, *Loop Quantum Gravity: An Inside view*, *Lect.Notes Phys.* **721** (2007) 185 [0608210].

[278] T. Thiemann, *Modern Canonical Quantum General Relativity*, Cambridge University Press, Cambridge (2007).

[279] T. Thiemann, *Lectures on loop quantum gravity*, *Lecture Notes in Physics* **631** (2002) 41 [0210094].

[280] C. Rovelli, *Zakopane lectures on loop gravity*, arXiv:1102.3660 [gr-qc].

[281] C. Rovelli, *Quantum Gravity*, Cambridge University Press, Cambridge (2004).

[282] C. Rovelli, *Ashtekar formulation of general relativity and loop-space nonperturbative quantum gravity: a report*, *Classical and Quantum Gravity* **8** (1991) 1613.

[283] C. Rovelli, *Notes for a brief history of quantum gravity*, 0006061.

[284] A. Ashtekar, *An Introduction to Loop Quantum Gravity Through Cosmology*, *Nuovo Cim.* **122B** (2007) [0702030].

[285] A. Ashtekar and R.S. Tate, *Lectures on Non-Perturbative Canonical Gravity*, World Scientific (1991).

[286] N. Bodendorfer, *An elementary introduction to loop quantum gravity*, 1607.05129.

[287] J. Lewandowski, A. Okołów, H. Sahlmann and T. Thiemann, *Uniqueness of Diffeomorphism Invariant States on Holonomy-Flux Algebras*, *Communications in Mathematical Physics* **267** (2006) 703 [0504147].

[288] M. Bojowald, S. Brahma and J.D. Reyes, *Covariance in models of loop quantum gravity: Spherical symmetry*, *Physical Review D* **92** (2015) 045043 [arXiv:1507.00329 [gr-qc]].

[289] A. Ashtekar, L. Bombelli and O. Reula, *Covariant Phase Space of Asymptotically flat Gravitational Fields*, in *Mechanics, Analysis and Geometry: 200 Years after Lagrange*, M. Francaviglia and D. Holm, eds., (Amsterdam), North Holland, 1990.

[290] M. Bojowald and H.A. Kastrup, *Symmetry reduction for quantized diffeomorphism-invariant theories of connections*, *Classical and Quantum Gravity* **17** (2000) 3009 [9907042].

[291] C. Rovelli and S. Speziale, *Lorentz covariance of loop quantum gravity*, *Physical Review D* **83** (2011) 104029 [arXiv:1012.1739 [gr-qc]].

[292] M. Bojowald and R. Das, *Canonical gravity with fermions*, *Physical Review D* **78** (2008) 64009 [arXiv:0710.5722 [gr-qc]].

[293] M. Bojowald, S. Brahma and D.-h. Yeom, *Effective line elements and black-hole models in canonical loop quantum gravity*, *Physical Review D* **98** (2018) 046015 [arXiv:1803.01119 [gr-qc]].

[294] A. Ashtekar, J. Lewandowski, D. Marolf, J.M. Mourão and T. Thiemann, *Quantization of diffeomorphism invariant theories of connections with local degrees of freedom*, *Journal of Mathematical Physics* **36** (1995) 6456 [9504018].

[295] N. Bodendorfer, T. Thiemann and A. Thurn, *Towards Loop Quantum Supergravity (LQSG) I. Rarita-Schwinger Sector*, *Class. Quantum Gravity* **30** (2011) 45006 [1105.3709].

[296] N. Bodendorfer, T. Thiemann and A. Thurn, *Towards Loop Quantum Supergravity (LQSG) II. p-Form Sector*, *Class. Quantum Gravity* **30** (2011) 45007 [1105.3710].

[297] N. Bodendorfer, T. Thiemann and A. Thurn, *Towards Loop Quantum Supergravity (LQSG)*, *Phys. Lett. B* **711** (2011) 205 [1106.1103].

[298] L. Smolin, *A candidate for a background independent formulation of M theory*, *Phys. Rev. D* **62** (1999) 86001 [9903166].

[299] L. Smolin, *Covariant quantization of membrane dynamics*, *Physical Review D - Particles, Fields, Gravitation and Cosmology* **57** (1998) 6216.

[300] L. Smolin, *The cubic matrix model and a duality between strings and loops*, *arXiv* (2000) 32 [0006137].

[301] T. Thiemann, *The LQG – String: Loop Quantum Gravity Quantization of String Theory I. Flat Target Space*, *Class. Quantum Gravity* **23** (2004) 1923 [0401172].

[302] L. Freidel and K. Krasnov, *The fuzzy sphere *-product and spin networks*, *Journal of Mathematical Physics* **43** (2002) 1737.

[303] L. Smolin, *A quantization of topological M theory*, *Nuclear Physics B* **739** (2006) 169 [0503140].

[304] E. Bianchi, P. Dona and S. Speziale, *Polyhedra in loop quantum gravity*, *Physical Review D* **83** (2011) 44035 [arXiv:1009.3402 [gr-qc]].

[305] M. Kapovich and J.J. Millson, *The symplectic geometry of polygons in euclidean space*, *Journal of Differential Geometry* **44** (1996) 479.

[306] J. Barbero, *Real Ashtekar variables for Lorentzian signature space-times*, *Physical Review D* **51** (1995) 5507 [9410014].

[307] G. Immirzi, *Quantum gravity and Regge calculus*, *Nuclear Physics B - Proceedings Supplements* **57** (1997) 65 [9701052].

[308] G. Immirzi, *Real and complex connections for canonical gravity*, *Classical and Quantum Gravity* **14** (1997) L177 [9612030].

[309] A. Ashtekar and J. Lewandowski, *Projective Techniques and Functional Integration*, *J. Math. Phys.* **36** (1994) 2170 [9411046].

[310] F. Girelli and E.R. Livine, *Reconstructing quantum geometry from quantum information: spin networks as harmonic oscillators*, *Classical and Quantum Gravity* **22** (2005) 3295 [0501075].

[311] F. Girelli and E.R. Livine, *Reconstructing quantum geometry from quantum information: Spin networks as harmonic oscillators*, *Classical and Quantum Gravity* **22** (2005) 3295 [0501075].

[312] E.R. Livine, *Deformation Operators of Spin Networks and Coarse-Graining*, 1310.3362.

[313] L. Freidel and E.R. Livine, *The fine structure of SU(2) intertwiners from U(N) representations*, *Journal of Mathematical Physics* **51** (2010) [0911.3553].

[314] B. Iochum, T. Krajewski and P. Martinetti, *Distances in finite spaces from noncommutative geometry*, *Journal of Geometry and Physics* **37** (2001) 100 [9912217].

[315] G. Ishiki and T. Matsumoto, *Diffeomorphisms on the fuzzy sphere*, *Progress of Theoretical and Experimental Physics* **2020** (2020) [1904.00308].

[316] T.P. Singh, *String theory, quantum mechanics and noncommutative geometry: A new perspective on the gravitational dynamics of D0-branes*, *International Journal of Modern Physics D* **15** (2006) 2153 [0605112].

[317] A. Sen, *An Introduction to Non-perturbative String Theory*, 9802051.

[318] W. Taylor, *Lectures on D-branes, Gauge Theory and M(atrices)*, 9801182.

[319] W. Taylor, *M(atrix) theory: Matrix quantum mechanics as a fundamental theory*, 2001. 10.1103/RevModPhys.73.419.

[320] E. Witten, *Non-abelian bosonization in two dimensions*, *Communications in Mathematical Physics 1984 92:4* **92** (1984) 455.

[321] J. Wess and B. Zumino, *Consequences of anomalous ward identities*, *Physics Letters B* **37** (1971) 95.

[322] A.Y. Alekseev, A. Recknagel and V. Schomerus, *Brane dynamics in background fluxes and non-commutative geometry*, *Journal of High Energy Physics* **4** (2000) .

[323] D. Berenstein and D. Trancanelli, *Dynamical tachyons on fuzzy spheres*, Tech. Rep. (2011).

[324] A. Feller and E.R. Livine, *Quantum surface and intertwiner dynamics in loop quantum gravity*, *Physical Review D* **95** (2017) [1703.01156].

[325] E.R. Livine, *Deformations of Polyhedra and Polygons by the Unitary Group*, *Journal of Mathematical Physics* **54** (2013) [1307.2719].

[326] A. Ashtekar, *New Variables for Classical and Quantum Gravity*, *Physical Review Letters* **57** (1986) 2244.

[327] G. Bergner and S. Catterall, *Supersymmetry on the lattice*, *Int. J. Mod. Phys.* **A31** (2016) 1643005 [1603.04478].

[328] T. Wiseman, *On black hole thermodynamics from super Yang-Mills*, *Journal of High Energy Physics* **2013** (2013) 101.

[329] N.S. Dhindsa, A. Joseph, A. Samlodia and D. Schaich, *Non-perturbative phase structure of the bosonic BMN matrix model*, 2201.08791.

[330] D. Schaich, R.G. Jha and A. Joseph, *Thermal phase structure of dimensionally reduced super-Yang-Mills*, 2201.03097.

[331] M.S. Costa, L. Greenspan, J. Penedones and J.E. Santos, *Thermodynamics of the BMN matrix model at strong coupling*, *Journal of High Energy Physics* **2015** (2015) 1 [arXiv:1411.5541v1].

[332] L. Smolin, *The cubic matrix model and a duality between strings and loops*, 0006137.

[333] M.W. Reimann, M. Nolte, M. Scolamiero, K. Turner, R. Perin, G. Chindemi et al., *Cliques of neurons bound into cavities provide a missing link between structure and function*, *Frontiers in Computational Neuroscience* **11** (2017) 48.

[334] S. Catterall and T. Wiseman, *Extracting black hole physics from the lattice*, *Journal of High Energy Physics* **2010** (2010) [0909.4947].

[335] J.M. Figueroa-O'Farrill and S. Stanciu, *D-brane charge, flux quantisation and relative (co)homology*, *Journal of High Energy Physics* **5** (2001) [0008038].

[336] S. Stanciu, *A note on D-branes in group manifolds: Flux quantisation and D0-charge*, *Journal of High Energy Physics* **4** (2000) .

[337] W. Taylor, *D2-branes in B fields*, *Journal of High Energy Physics* **4** (2000) 1.

[338] K. Becker and M. Becker, *Quantum gravity corrections for Schwarzschild black holes*, *Physical Review D - Particles, Fields, Gravitation and Cosmology* **60** (1999) .

[339] N.J. Finlayson, X. Zhang and J.D. Golomb, *Differential patterns of 2D location versus depth decoding along the visual hierarchy*, *NeuroImage* **147** (2017) 507.

[340] H. Davson, *Physiology of the Eye*, Macmillan Education UK, London (1990), 10.1007/978-1-349-09997-9.

[341] H. Davson, *The perception of depth*, *https://www.britannica.com/science/human-eye/The-perception-of-depth* .

[342] G.A. Gescheider, *Psychophysics : The Fundamentals*, Psychology Press (jun, 2013), 10.4324/9780203774458.

[343] H. Poincare, *Science and Hypothesis.*, Read Books Ltd (2016).